UNIVERSITÀ
DEGLI STUDI
DI PADOVA

Università degli Studi di Padova

Dipartimento di Astronomia

SCUOLA DI DOTTORATO DI RICERCA IN ASTRONOMIA

CICLO XXII

METHODOLOGIES OF CLIMATIC INVESTIGATIONS: HISTORICAL SERIES IN ITALY AND SKY-QUALITY FROM SATELLITE DATA

Direttore della Scuola : Ch.mo Prof. Giampaolo Piotto

Supervisore :Ch.mo Prof. Dario Camuffo

Supervisore :Ch.mo Prof. Sergio Ortolani

Dottorando : Chiara Bertolin

Misura ciò che è misurabile,
e rendi misurabile ciò che non lo è

Galileo Galilei

A Francesco

Riassunto

La tesi è strutturata in due parti ben distinte: la prima, riguarda i metodi di indagine applicati alla climatologia storica, mentre la seconda parte riguarda i metodi di indagine atti alla ricerca, su scala globale, di siti che possiedano le migliori condizioni per le osservazioni astronomiche. Nella prima parte si trattano i metodi per l'analisi e la ricostruzione delle serie storiche di temperatura e si espongono i risultati ottenuti sia localmente, per l'Italia, che su scala globale, per l'area Mediterranea. Nella ricostruzione del clima storico si utilizzano due tipologie di dati: i 'proxy' di tipo documentario e gli strumentali. I dati di tipo documentario vengono utilizzati per ricostruire la frequenza di eventi termici estremi nel periodo di tempo antecedente l'invenzione dei primi termometri trasformando le informazioni contenute nei documenti scritti in indici numerici. Tali indici sono definiti sulla base della valutazione della causa fisica e dell'effetto riportato sulla cronaca e statisticamente, con la calibrazione e validazione su un comune periodo di dati strumentali di temperatura. Allo stesso modo, la ricostruzione di una serie strumentale di temperatura necessita di un lungo ed attento lavoro di ricerca, validazione ed analisi statistica delle osservazioni che assicuri l'eliminazione di errori e discontinuità. I risultati ottenuti da queste serie strumentali, statisticamente omogenee e di alta qualità anche dal punto di vista dello studio dei metadati, offrono un notevole miglioramento sia per la qualità del dato presentato sia in termini di copertura temporale che, superando i 360 anni, diviene la più lunga esistente al mondo. Il miglioramento nella conoscenza dell'andamento termico in Italia e nell'area del Mediterraneo risale quindi al 1654, nel mezzo della piccola età glaciale (LIA) ed è notevole se confrontato con l'intervallo temporale presentato nel noto report dell'Intergovernmental Panel on Climate Change (IPCC 2007) che si arresta al 1850. Inoltre, se si aggiungono i risultati ottenuti dall'analisi dei dati documentari, i risultati riguardanti l'andamento di temperatura nel Nord-Centro Italia, presentati in questa tesi, arrivano a coprire gli ultmi 500 anni. Questo intervallo temporale plurisecolare aggiunge nuova luce alle attuali conoscenze soprattutto se analizzato in termini di riscaldamento globale. Grande attenzione rivestono in questa prima parte della tesi anche le prime osservazioni strumentali, effettuate dai discepoli di Galileo con

il piccolo termometro fiorentino che fu il primo strumento della storia in grado di registrare in modo fisicamente attendibile la temperatura dell'aria. Queste osservazioni, analizzate e presentate qui per la prima volta, nacquero all'interno della Rete Medicea (1654-1670) che fu la prima rete meteorologica esistente al mondo, nata sotto l'egida del Granduca di toscana Ferdinando II. Infine, aggiungendo altri 60 anni di dati di temperatura (1716-1774) alla ricostruzione della serie strumentale storica di Padova, si è ottenuto un risultato particolarmente importante per la storia della nostra specola. Questa serie strumentale, ad oggi ininterrotta, è infatti una delle più lunghe e complete d'Italia, e ci è giunta grazie alle osservazioni effettuate da astronomi quali Toaldo, Chiminello, Santini succedutisi come direttori dell'osservatorio astronomico di Padova.

La seconda parte della tesi riguarda l'analisi di dati satellitari e della tecnica in remote sensing per la ricerca di siti che presentino condizioni ottimali per osservazioni astronomiche. Dal punto di vista climatico, l'uso di piattaforme satellitari di tipo sun-syncronous, grazie alla copertura quasi totale della superfice terrestre sono il mezzo attualmente più efficace per il monitoraggio di parametri atmosferici di aree in cui sono presenti osservatori astronomici già attivi da anni e divengono al contempo un mezzo molto potente per rilevare nuovi siti che possiedano le condizioni ottimali richieste dalle osservazioni. Lo scopo di questa seconda parte, è in primis quello di esplorare l'uso di altri rivelatori diversi dal Total Ozone Monitoring Spectrometer a bordo del satellite Earth Probe (Bertolin, 2005), con una miglior risoluzione spaziale, per studiare la correlazione tra il contenuto di aerosol e l'estinzione atmosferica all'osservatorio Roque de Los Muchachos nell'isola di La Palma (Canarie, Spagna). In secondo luogo, il fine è quello di valutare quanto la risoluzione spaziale degli strumenti satellitari influenzi la qualità del dato utilizzato e conseguentemente i risultati ottenuti per la caratterizzazione di un sito astronomico. Per questo intento si sono utilizzati due tipi di dati: dati di livello 2 ad alta risoluzione e dati di livello 3 a più bassa risoluzione spaziale. Importanti risultati si sono ottenuti dall'analisi di questi ultimi dati. Questo tipo di studio in remote sensing è stato rivolto, parallelamente, su quattro tra i siti astronomici di eccelenza al mondo: La Silla e Paranal in Cile, La Palma e Tenerife nelle isole Canarie ed analogamente è stato testato anche per studiare le caratteristiche di un sito completamente nuovo indicato per poter ospitare il futuro extremely large telescope: Tolonchar. I risultati hanno portato a definire per ogni area presa in esame le principali

caratteristiche del contenuto aerosol (profondità ottica degli aerosol, altezza dello strato di particelle aerosol, albedo della singola interazione di diffusione con la particella aerosol) e della copertura nuvolosa. Lo scopo di tale confronto è stato quello di verificare se le caratteristiche di qualità del cielo fossero rimaste inalterate negli anni e di cercare tecniche di analisi appropriate a rivelare le proprietà climatiche delle aree in esame. A questo proposito, per la prima volta è stato effettuato un attento monitoraggio da satellite, su un database di 6 anni per il sito di Tolonchar. I risultati ottenuti hanno presentato conclusioni molto importanti. Sopra quest'area la presenza di nubi infatti si è dimostrata molto limitata e per la prima volta è stato possibile studiare e specificare la presenza e le caratteristiche degli aerosol.

I maggiori risultati riguardanti lo studio della nuvolosità sono stati ottenuti sia da un punto di vista climatico, in termini di percentuale di copertura nuvolosa, che da un punto di vista astronomico come trend a lungo termine del numero di notti fotometriche. La ricerca di periodicità, effettuata con la wavelet analysis, su oltre un trentennio di dati satellitari, ha messo in evidenza, per il sito astronomico di La Silla, un'anticorrelazione tra l'aumento medio della frazione di nubi e la diminuzione media del Southern Oscillation Index e viceversa. Un risultato analogo si è raggiunto anche studiando la relazione che intercorre tra la variazione del numero di notti fotometriche ed i picchi positivi e negative del SOI. Come dimostra il caso esemplificativo di La Silla, la differenza percentuale tra le peggiori e migliori condizioni in termini di numero di notti fotometriche è rilevante per le osservazioni astronomiche. Questo fatto ha portato a correlare l'anomalia di copertura nuvolosa (cioè la deviazione relativa del numero medio di notti fotometriche) ottenuto dalle misure in situ con un valore analogo recuperato da misure satellitari. L'obiettivo di tale analisi è la ricerca di una possibile correlazione tra queste due variabili per utilizzare i dati satellitari di percentuale di nuvolosità come mezzo per ricostruire una statistica di dati fotometrici su una scala temporale più ampia. Il metodo testato sull'area di La Silla e Paranal ha alcune limitazioni che non permettono di estenderlo ad altri siti astronomici con informazioni fotometriche per ricostruire in modo più completo l'andamento delle loro condizioni osservative negli anni.

Abstract

The thesis is structured into two parts: the first is concerning with the methodologies of climatic investigations applied to the historical climatology, while the second part is concerning with methodologies of climatic investigations applied to the site testing for astronomy. The purpose of the first part is to develop methodology guidelines for investigating temperature data to provide a high quality historical reconstruction of present and past climatic conditions locally in Italy and globally in the Mediterranean basin. The potentials and limitations of both documentary proxy data and instrumental observations available for such reconstruction, together with the methodologies used to analyze them, have been presented. Documentary proxies allow to study climate prior to the availability of early instrumental observations allowing the reconstruction of the extreme events. They must be transformed from written documents into numerical index through a calibration and validation approach to exctract the climatic signal related to the temperature variable. In the same way, high quality instrumental time series are achieved only after an enduring and long work of collection, validation, homogenization that makes clear the climatic signal stored into the data. This is the big challenge that we have presented in the first part of the thesis: the methodology to obtain high quality and statistically robust observations supported by the results obtained performing these careful analysis. The obtained results offer an improvement in the Italian and Mediterranean area of both data quality and instrumental data coverage. The reconstructed instrumental observations go back in time up to 360 years ago at the heart of the Little Ice Age, immediately after the invention of the first meteorological instruments covering a time twice respect the results reported in the Intergovernmental Panel on Climate Change (IPCC 2007) report. Moreover, the reconstructed series based on documentary data, extends our knowledge on temperature over the last 500 years. This longer temporal range adds new light especially in relation with the recent global warming.

Great attention has been conferred to the early instrumental observations carried out by several Galileo's followers, that, unexploited over the centuries, are presented here for the first time. This study is concerning with the invention of the first thermometer

exploitable for reliable instrumental observations performed under the guidelines of the first meteorological Network existing at world known as 'Rete Medicea'. Moreover another study that extends back to 1716 the long daily temperature series in Padua with the addition of newly recovered data and the transformation of initially obscure indoor readings into outdoor observations in terms of modern units and observational methodology, is presented here. This early temperature reconstructon is particularly interesting for our Padua's astronomical observatory because it is the continuation, back in time, of the temperature series carried out at the specula by Toaldo, Chiminello, Busatta, Conti, Santini and Lorenzoni that were directors of the Padua's astronomical observatory.

The second part of the thesis is focused on satellite data and remote sensing technique useful for climatic investigation applied at site testing for astronomy. The use of satellite platforms, at present, is the more effective mean to perform a worldwide survey of different climate parameters because they provide a global coverage useful to monitor the climatic situation around the world in the already active astronomical sites and above all they can reveal new sites appropriate for building astronomical observatories. The aim of this second part is from one hand, to explore the use of other detectors than TOMS-EP (Bertolin, 2005) with improved spatial resolution on board of different satellites for studying the relationship between the aerosol content monitoring and the visual atmospheric extinction in the Roque de Los Muchachos (ORM) astronomical site (Canary Islands, Spain). From the other hand, it is to test and quantitatively evaluate the weight that the satellite spatial resolution hold in site testing analysis. For this reason we handle both high spatial resolution level 2 data and lower resolution level 3 data. Important results are obtained working own with level 3 data, from their analysis in fact we were able to define the main aerosol content features (e.g. aerosol optical depth, height of aerosol layer and single scattering albedo) and the cloud coverage and free-cloud scenes. We performed such analysis on four among the top world's sites (i.e. La Silla, Paranal (Chile), La Palma and Tenerife (Spain)) and in particular we tested this methodology to study a new exploitable ELT site: Tolonchar. The aim of these comparisons is to verify if the sky quality characteristic are unchanged over time and to search for appropriate techniques able to reveal climatic properties exploitable when looking at new future very large telescopes sites.

Here, for the first time a careful satellite monitoring has been performed on a 6-years database on Tolonchar in order to obtain as information as possible from OMI level 3 data for this area that is actually under evaluation as possible ELT site. Our results show very important conclusions. Over this area in fact the cloud presence is extremely limited and for the first time we have detected and studied the aerosol presence.

The major evidences concerning with cloud climatology have been achieved both from the climatic point of view of cloud cover percentage and from the astronomical point of view of long-term trend in number of photometric nights. The Wavelet Analysis to search periodicities, performed over a cloud cover satellite dataset of more than 30-year, highlights for La Silla an evident anti-correlation between the increasing in cloud mean fraction and the decreasing in mean Southern Oscillation Index and vice-versa. A similar result is carried out also studying the relationship between change in number of photometric nights occurring between a negative SOI peak and a positive one. The difference in percentage between the best and the worst condition in term of number of photometric nights for La Silla is relevant for the observational purposes. For this reason a further analysis has been carried out to compare the cloud coverage anomaly (i.e. relative deviation of the mean number of photometric nights) in-situ measurements, with the satellite Cloud Cover Anomaly (sat CCA). The objective of such analysis is to analyse the correlation of CCA (in-situ) with the satellite CCA (remote-sensing) in order to assess the usefulness of satellite cloud cover values as a tool to reconstruct a larger time series in term of photometric data. If applicable, this method could be useful to reconstruct longer series of photometric data to best define the observational conditions of those astronomical sites around the world with photometric series of measurements at the beginning.

Publications

I carried out my PhD activity on historical climatology at the Italian National Research Council (CNR) - Institute of Atmospheric Sciences and Climate (ISAC), section of Padova, thanks to the Research Fellow provided by the European project MILLENNIUM EUROPEAN CLIMATE. During these years a number of national and international conference-papers and scientific papers on international peer-review Journals have been submitted, accepted and published. They are at the base of the work presented in this thesis.These papers are listed here for reference:

International referred publications:

- Varela, A. M., Bertolin, C., Muñoz-Tuñón, C., Ortolani, S. and J.J. Fuensalida. 2008. Astronomical site selection: on the use of satellite data for aerosol content monitoring MNRAS 391 (2) : 507-520 (14).

- Camuffo, D., Bertolin, C., Jones, P., Cornes, R. and E. Garnier. 2009. The earliest daily barometric pressure readings in Italy: Pisa, 1657-8 and Modena, 1694 and the circulation index over Europe, 1694. The Holocene 20(3) 1–13, doi: 10.1177/0959683609351900 http://hol.sagepub.com.

- Camuffo, D. and C. Bertolin. 2010a Recovery of the Early Period of Long Instrumental Time Series of Air Temperature in Padua, Italy (1716-2007). Physics and Chemistry of the Earth Journal (in print).

- Luterbacher, J., Koenig, S.J., Franke, J., van der Schrier, G., Zorita, E., Moberg, A., Jacobeit, J., Della-Marta, P.M., Küttel, M., Xoplaki, E., Wheeler, D., Rutishauer, T., Stössel, M., Wanner, H., Brázdil, R., Dobrovolný, P., Camuffo, D., Bertolin, C., van Engelen, A., Gonzalez-Rouco, F.J., Wilson, R., Pfister, C., Limanówka, D., Nordli, Ø., Leijonhufvud, L., Söderberg, J., Allan, R., Barriendos, M., Glaser, R., Riemann, D., Hao, Z., Zerefos, C.S. 2010. Circulation dynamics and its influence on European and Mediterranean January-April climate over the past half millennium: results and insights from instrumental data, documentary evidence and coupled climate models. Clim Change, doi:10.1007/s10584-009-9782-0

- Camuffo, D., Bertolin, C., Barriendos, M., Dominguez, F., Cocheo, C., Enzi, S., Sghedoni, M., della Valle, A., Garnier, E., Alcoforado, M. J., Xoplaki, E., Luterbacher, J., Diodato, N., Maugeri, M., Nunes, M. F. and R. Rodriguez. 2010. 500 year temperature reconstruction in the Mediterranean Basin. Climatic Change (Accepted).

- Glaser, R., Riemann, D., Schönbein, J., Barriendos, M., Brazdil, R., Bertolin, C., Camuffo, C., Deutsch, M., Dobrovolny, P., Engelen van, A., Enzi, S., Halićhová, M., Koenig, S., Kotyza, O., Limanowka, D., Macková, J. and M. Sghedoni. 2010. 500 years variability of European floods. Climatic Change (in review).

- Camuffo, D. and C. Bertolin. 2010b. The dawn of Meteorology in Italy and the earliest Meteorological Observations (1654-1670). The Holocene (submitted).

International Conference proceedings:

- Varela, A.M., Bertolin, C., Munoz-Tunon, C., Fuensalida, J.J. and S. Ortolani. 2007. Use of satellite data for astronomical site characterization. SPIE proceedings, 6745, 674508, doi:10.1117/12.737346.

- Varela, A.M., Bertolin, C., Munoz-Tunon, C., Fuensalida, J.J. and S. Ortolani. 2007. In situ calibration using satellite data results. RevMexAA (Serie de Conferencias), 31, 104-110.

- Camuffo, D. and C. Bertolin. 2009. The Climate Change at the European and Global scale over the last Millennium: methodologies and results.Centro Universitario Europeo per i beni culturali (Roger-Alexandre Lefevre Ed.), Ravello, Italy. (In print).

National Conference proceedings:

- Camuffo, D., Bertolin, C. and A. della Valle. 2008. Cambiamenti climatici, microclima storico, climatizzazione e. . .quale conservazione? Atti convegno 4820 Vb-IP-5 Società Italiana di Fisica (SIF)

- Camuffo, D., della Valle, A., Bertolin, C., Leorato, C. and A. Bristol. 2010. Umidità e Diagnostica Ambientale in Palazzo Grimani, Venezia.
  1-2 Aprile 2010, Workshop Edifici Storici e Destinazione Mussale

Index

Introduction: 21

I Part Methodology of Climatic investigation: Documentary proxy data and historical instrumental series in Italy 25

Chapter 1 How are climate variables studied over the last millennium? 27

1.1 Which data are useful to? 28
1.1.1 Instrumental data: the close past recorded with precision 28
1.1.2 Proxy Data: ways to reconstruct past climate more back in time 30
1.1.3 Satellite data: the future toward an earth information system 36

1.2 Data quality on which the actual knowledge are based on 40

Chapter 2: Documentary Proxy Data: potential and limitations to reconstruct climate variability 53

2.1 The sources and the characteristics of documentary proxy data 55

2.2 Potential and limitation of documentary proxy 64

Chapter 3: Methodology of Climatic Analysis based on Documentary Proxy: a Case Study 69

3.1 Site selection and data collection 71

3.2 Indexing and Dating 72

3.3 Calibration and Verification 76
3.3.1 Calibration and Verification: open questions and their statistical background 77
3.3.2. Calibration and Verification: our methodology 82

3.4 Reconstruction and uncertainties 85

3.5. Large-Scale Surface Temperature Reconstruction: the case study results 88

Chapter 4: Early Instrumental Data: potential and limitations to reconstruct climate variability 101

4.1 Potential and limitations of early instrumental temperature observations 103

4.2 The thermometer birth: from the thermoscope to the air thermometer 110

4.3 Early temperature observations: a case study 116
4.3.1 The first liquid thermometer: the Little Florentine 116
4.3.2 The first European meteorological network the Rete Medicea (1654-1670) 124

Chapter 5: Methodology of Climatic Analysis based on Early Instrumental Data: a Case Study 147

5.1 The Amontons air thermometer 148

5.2 Recovery of the Early Period of Long Instrumental Time Series of Air Temperature in Padua: a case study 159
5.2.1 Data recovery, discussion and analysis 160

II Part Methodology of Climatic investigation: Sky quality from satellite data 179

Chapter 6: Climatology applied to the astronomical site testing....181

6.1 General description of Atmosphere 182
6.1.1 Classification of the atmospheric regions based on temperature distribution 187

6.2 Seeing and atmospheric turbulence in Astronomy 189

6.3 Parameters to test site quality 200

6.3.1 Overview on concepts and instruments for site testing....203

Chapter 7: Atmospheric Extinction and Aerosol Physics 211

7.1 The Tropospheric Aerosol....211

7.2 Atmospheric extinction 215

7.3 Optics of individual aerosol particles 222
7.3.1 Rayleigh scattering....222
7.3.2 Mie scattering 225

7.4 Optics of the atmospheric aerosol....229
7.4.1 Reflection, transmission and absorption radiation change 231

Chapter 8: OMI aerosol remote sensing and in-situ atmospheric extinction retrieval: the Roque de Los Muchachos astronomical site case study....237

8.1 The Ozone Monitoring Instrument 239
8.1.1 OMI measuring principles 240
8.1.2 OMI aerosol algorithm 241

8.2 High spatial resolution OMI aerosol data: comparison with in situ atmospheric extinction records over the ORM site 248

8.3 Lower spatial resolution OMI aerosol data: height of aerosol layer comparison in world's top astronomical sites....261

8.4 Evidences and conclusions....281

Chapter 9 A Thirty-year satellite records of cloud climatology from TOMS and OMI observations 285

9.1 The Impact of clouds on UV/visible measurements: cloud effects and measurement technique....287

9.2 A thirty-year satellite record of cloud climatology from TOMS and OMI observations....289
9.2.1 Cloud cover over the world's top astronomical site and its possible correlation with atmospheric and oceanic circulation 292
9.2.2 Photometric nights pecentage on La Silla and Paranal: comparison between in situ and satellite measurements 304

9.3 Evidences and conclusions....318
Conclusions....325
Figure List....333
Table List....339
Acronymous List....341
Acknowledgments....345
Bibliography....347

Introduction:

The thesis is structured into two parts: the first is concerning with the methodologies of climatic investigations applied to the historical climatology while the second part is concerning with methodologies of climatic investigations applied to the site testing for astronomy. The purpose of the first part: **'Documentary Proxy data and historical instrumental series in Italy'**, conducted mainly in the Italian geographical area, is to develop baselines of methodologies for investigating climate data and relating variables to provide an historical reconstruction of present and past climatic conditions. In the study of temperature reconstruction over the last 500 years, we are going to present different data typologies (i.e. proxy, and early instrumental data) with their strength points and limitations followed by the introduction of different case studies. The results from case-studies presented here, in some cases accepted and published in climatic peer reviewed Journals, will facilitate the understanding of the importance to improve the climatic data quality. Moreover they will help to follow the huge work required for increasing the data quality that necessitate of careful and necessary steps ranging from data collection up to data validation and homogenization in order to extract the best possible results. Reading the different sections of this first part, it will be clear as not always the present data availability on local and global scale is based on such high quality. High quality climate data, although local, in fact, plays a major role in advancing climate science respect to a global coverage of scarce quality data. In this first part, a big effort toward this direction is made to lay the foundations for a methodology of climatic investigation that could improve the early instrumental data quality as well as the documentary proxy quality during the pre-instrumental period and to understand the major climate variations prior to the 21th century, developing the longest possible high quality consistent record of past climate conditions.

The results obtained during the research work in these last three years are presented in form of case-studies, focused mainly on the analysis of temperature. Results will show as this climatic variable has already changed during the past centuries, locally in Italy, and globally in the Mediterranean basin, bringing new light on the widely accepted views that global warming is occurring and increasing for anthropogenic forcing. As

explained before, the main aim of this part is not to report the primary evidences for the global warming but to track steps for improving quality both of instrumental and documentary proxy data. However the choice of focusing our work mainly on the surface temperature reconstructions, going back up to the last 500 years, will answer also to the nowadays main question concerning global warming in the area taken in exam. The surface temperature reconstruction in fact has the potential to provide independent information about climate sensitivity and about the natural variability of the climate system. In particular, the indication that recent warmth is un-previous on the last centuries and potentially on the last millennium, support the conclusion that human activities are responsible for much of the recent warming. However, the uncertainties in reconstructions of surface temperature for the period prior to the instrumental record make this evidence less conclusive. It should also be noted that the human-induced global warming would not be substantively altered if, for example, the global mean surface temperature 500 years ago was found to be as warm as it is today.

The first Chapter provides a brief description of the data available to study climate variables in the last millennium and the data quality on which are based the actual climatic knowledge. The subsequent chapters are instead focused on the different types of data used in our research work: Chapter 2 and the following case study in Chapter 3 deal with the sources and characteristics of the proxy datasets used in our analysis i.e. documentary proxies on the timescale that range from 1500 to 1800. Concluding the first part concerning the data available for climatic investigations, Chapters 4 and 5, are focused mainly on early instrumental observations ranged in the period immediately after the invention of the first meteorological instruments, i.e. 1654-1750. Great attention is given at the problems met with these first instruments and light is thrown on case studies on the basis of observations sites in Italy.

The second part of the thesis: **'Methodology of Climatic Investigation: sky quality from satellite data'** are focused on another type of data, useful for climatic investigation applied at site testing for astronomy: satellite data. The use of satellite platforms, at present, is the more effective mean to perform a worldwide survey of different climate parameters related to astronomy site testing for three main reasons: i) using sun-syncronous satellite it is possible remote sensing monitoring climate parameters adopting the same method, algorithm, spatial and vertical resolution with an

homogeneous worldwide coverage that make us able to daily compare ground sites with different climatic and orographic characteristics. ii) At present time the satellites databank extend back to more than thirty years. A climate analysis over this whole temporal range is possible thanks a chain of platforms that partly have maintained, in recent time, a heritage with similar algorithm used for the pioneer instruments. iii) From satellite data we can obtain a wide spectrum of climatic values over both oceans and lands. Therefore these data are actually the only one to provide a global coverage useful to reveal sites appropriate for building astronomical observatories and above all to monitor the climatic situation around the world in the already active astronomical sites. Along all this second part, we deal with remote sensing technique for site testing application in astronomy. We study both the aerosol content monitoring in comparison with the visual atmospheric extinction for the case study of Roque de Los Muchachos (ORM) astronomical site (Canary Islands, Spain) and some other aerosol content features (e.g. aerosol optical depth, height of aerosol layer, and single scattering albedo) in comparison with cloud coverage and free-cloud scenes in several most important astronomical sites in the world. We highlight strengths and faults of performing good preliminary site testing campaigns in order to choose the site with best conditions for astronomy and, in the same way, we stress the importance of keeping a constant monitoring also for sites already active. In order to test and quantitatively evaluate the weight of satellite spatial resolution in site testing analysis, we handle two different levels of data. Taking into account the Roque de Los Muchachos Observatory case study, analysed in our paper published in MNRAS, we explain the methodology to investigate the photometric sky quality using satellite data properly and we deal both with satellite high spatial resolution level 2 data and with lower resolution level 3 data. This is a good test to show that the correlation between aerosol content and atmospheric extinction is led rather than the satellite field of view by other spurious effects that enter in the algorithm theoretical basis of the satellite instrument. Moreover we make sky quality comparison between the most famous astronomical sites of La Silla, Paranal in Chile and Roque de los Muchacos and Izana in Spain performed over the last three decades. The aim of these comparisons is from one to verify if the characteristics of sky quality are unchanged over time, from the other to search for appropriate techniques to reveal astronomical sites climatic properties exploitable in looking at new sites hosting

future extremely large telescopes. This kind of comparison now is getting available thanks the year by year larger satellite data series and several interesting results are obtain in this thesis already using low resolution satellite data.

In Chapter 6 we present a general description of the atmospheric regions and an overview of the key parameters that must be evaluated in astronomical site quality determination together with a brief description of the most used instruments and technique for their monitoring. In particular we deal in depth with the concepts of atmospheric turbulence in astronomy. In Chapter 7 we present a brief description of atmospheric extinction of aerosol components with the theoretical concepts on the optics of individual particles, as the Rayleigh and Mie scattering and an example of two streams treatment of transfer of radiation into a plane parallel atmosphere. In Chapter 8 we first analyse high spatial resolution aerosol content data from the Ozone monitoring Instrument (OMI) onboard of AURA satellite platform in comparison with in situ atmospheric extinction measurements for the case study of Roque de Los Muchachos (ORM). Secondly we use six-year smaller spatial resolution level 3 records to compare the height of aerosol layer in free-cloud scenes for different top astronomical sites around the world. Here, for the first time a careful analysis has been performed on the aerosol presence in Tolonchar area in perspective of hosting the site of future ELT. Finally in Chapter 9, using one of the longest dataset retrieved from satellite, i.e. an archive of more than 30 years level 3 data, coming from different platforms, we analyse cloud climatology making a comparison of the cloud coverage over different astronomical sites around the world in order to verify if these sites, standing into the area of influence of El Nino – La Nina, get a direct and visible connection with these phenomena. Important conclusions will be give concerning these teleconnection and the periodicity of these events that may affect the percentage of the photometric night, possibly deteriorating the sky quality of these sites.

I Part

Methodology of Climatic investigation:

Documentary proxy data and historical instrumental series in Italy

Chapter 1

How are climate variables studied over the last millennium?

Contents

1.1 Which data are useful to?
1.1.1 Instrumental data: the close past recorded with precision
1.1.2 Proxy Data: ways to reconstruct past climate more back in time
1.1.3 Satellite data: the future toward an earth information system
1.2 Data quality on which the actual climate knowledge are based on

Observations of current and past climates play an important role in improving the characterization of processes in the ocean, atmosphere, land surface and polar regions and in validation of climate models. The climate record is a time series of key variables, such as temperature, precipitation, and pressure, at monitoring sites or aggregated at local and regional levels. These data are essential input to climate models and therefore key to meeting the complex challenge of predicting future climate. The need for refining, extending (both backwards and forwards), and analyzing the long-term climate record to better discriminate natural variability from human-induced global change is particularly important to be identified, quantified, and understood on the decade-to-century time scales that are of most concern to human beings. Recently, space based and in situ observations, often associated with weather networks, have provided the data for the detection and attribution of causes of climatic change on global scale. However to assess the importance of modern climate change it is essential to place recent observed change in a longer-term context to correctly evaluated it. This approach requires records of much longer duration i.e. centennial and millennial scale rather than decadal scale as available basing only on modern instrumentations. For this reason, it is

necessary a search for, and recovery of, existing early instrumental data (17th-18th Centuries) and proxies data going back to the pre-instrumental time.

We need to integrate the historical and modern records as far as possible into the past to best calibrate the nowadays climate trend estimates through a very careful reanalyze of past instrumentations, calibrations and performed readings methodologies. Understanding the magnitude and impact of past climate variations and changes is the key to developing confidence about how climate is changing at the present time and how may it will change in the future. This requires comprehensive documentation about the full spectrum of all the time series involved.

1.1 Which data are useful to?

1.1.1 Instrumental data: the close past recorded with precision

Nowadays, widespread, reliable instrumental records are available mainly for the last 150 years as reported in the IPCC wp1 2007. The novelty produced in this thesis is the description of the methodology followed to analyze and study the historical instrumental series and the problems solved for making reliable the instrumental records up to the invention of the very first meteorological instruments in 17th Century. Italy in fact has the longest instrumental temperature records of any region of the world, so the natural variability of climate could be assessed for more than 100 years before any anthropogenic influences can be expected to have occurred. The intrinsic value of these early instrumental data can be revealed only with a deep analysis. A careful study must be performed for understanding how the instruments worked, how and which kind of calibrations were performed by the observers as well as their working methods to take meteorological readings. Only through all these steps it is possible to present exceptionally long instrumental series of high quality. More than a hundred years old instrumental series are necessary first of all to fit this recent warming in a most exact context of natural climate variability taking advantage, for a comparison, of the wider temporal range, secondly the lesson learned from studying past climates can also be applied to improve projections of how the climate system will respond to future changes in climate forcing.

Climate before the invention of the meteorological instruments must be deduced from proxy (i.e. non-instrumental) records. While proxy data tell us much about a large temporal window in past climate, they do not have the accuracy or resolution to support statements about a specific decade or year being the warmest in the millennium. They however provide a basis for comparing the climate of the 20th century to the climate of the preceding years within individual locations. A survey of the scientific literature offers strong evidence that the climate of the 20th century was not unusual, but fell within the range experienced during the past 1,000 years. The proxy data also offer strong support for the existence of the Medieval Warm Period (MWP), a period of warmer temperatures, which lasted from about 800 to 1300 and the Little Ice Age (LIA), a period of colder temperatures, which lasted from about 1400 to as late as 1900 in some regions.

Despite the possibility to extrapolate long tern trend or confirmation of warmer and cooler period than today, the direct temperature measurement record, although the concerns about their quality analysis that will be discussed later, represents the best information available about local and global climate variables analysis since 17th century.

However between these different typology of data as proxy, early instrumental and modern instrumental, it exists a strong connection among them, in which one is necessary to the other in order to improve their own vision of climate trend.

Analysis of modern weather station data for example indicates that a global warming trend occurred during the 20th century, it cannot tell us whether this warming was unusual or unnatural respect the past. A longer record is needed to answer this question. It is essential therefore we turn to other lines of evidence to evaluate the longer-term changes over the past centuries. One line of evidence, as explained before, is the early instrumental data, another one is provided instead by so-called proxy climate data, natural or historical archives of information that describe, although imperfectly, climate variations in prior centuries. Those proxy data with relatively high (decadal or better) resolution, such as tree rings, corals, ice cores, historical records, and in some cases lake and marine sediments can be used to reconstruct climate variations over past centuries and, in some cases, as far back as the past millennia. In addition, it is possible to use

independent proxy and historical sources to estimate the actual external "forcings" of climate over this time interval (specifically, volcanic and solar natural radiative forcing, and anthropogenic greenhouse gas, aerosol, and land-use forcing). These estimates can be used to drive theoretical climate model simulations of the past millennium or longer (Jones and Mann 2004).

Among all the possible choices of proxy data study and analysis, in this thesis, we deal with documentary and historical proxy because our research group has a long experience in this field, with present and past publication works. However, here to follow, it is reported a brief description of the proxy data available for studying climate variables in order to give an idea from one hand about the huge amount of possible natural data reservoirs present on global scale to retrieve the past climatic signal and from the other hand about the big work that is necessary made to create a data analysis methodology as much as possible similar among the big amount of research groups.

1.1.2 Proxy Data: ways to reconstruct past climate more back in time

Documentary and Historical Records

For centuries people have recorded the change of climate and in particular the extreme and not well understood events and their impact on human life and culture. In many parts of the world, but above all in Europe, archaeological inscriptions and historical documents such as chronicles, annals, logbooks, journals, court records diaries, ship's logs, etc. are a valuable source of climate information.

In the next two chapters we deal with these kind of historical sources, we start with underlying their strengths and limitations to retrieve climatic variables and then we follow with the methodology to extract reliable climatic signal. In particular documentary proxy permit to extend back in time for several centuries, the knowledge of surface temperature, rainfall amount, flood and drought events. In this type of data can be also included the phonological historical records as the wine harvest or the wheat sowing and harvest time and also the analysis of the rogation events pro pluvia and pro serenitate asked from people to the clergy or to the administrative authorities in case of long drought or very intensive precipitation periods. These documentary evidences shows for example that several regions were relatively cool from about 1500 to 1850, a period referred to as the Little Ice Age (Figure 1.1).

Figure 1.1: A painting representation of Venice lagoon frozen over during the Great Winter in 1709.

Historical evidences also suggests that Europe, in particular, experienced periods of relative warmth during the medieval interval from roughly A.D. 1000 to 1300.

In areas where writing was not widespread or preserved, archeological evidence such as excavated ruins can also sometimes offer clues as how climate may have been changing at certain times in history and how human societies may have responded to those changes. However, the interpretation of historical, documentary, and archeological evidences is not easy because often the documentary evidence is not directly and strongly related to the climatic variable that we want to take in exam (i.e. temperature or precipitation). Documentary proof in fact can be mixed with factors such as particular historical, health and environmental situation (respect to nowadays situation) as famine or war event that can affect the description of the climatic event made by the chronicler at that time. Hence, climatologists must use these data after a careful analysis and thick historical checks with the help of some archeologists or historians.

Tree Rings

Dendroclimatology is the science that study the climate variables as could be temperature and precipitation from the analysis of tree rings. This discipline is based on the fact that trees experience an annual growth cycle (see Figure 1.2).

This growth, and hence the width and density of tree rings, for each year, depends on many local factors. Clearly it depends on the own tree characteristic as the species, the age, the availability or less of nutrients in the soil or stored food in the tree, but, and this is the point interesting for the study of climate, the tree growth depends also on the full range of atmospheric variables as sunshine, precipitation, temperature, humidity and their distribution throughout the calendar year. The dependence of the wood density in individual tree rings is a good indicator for example of average temperature in the growing season and give the possibility to create a temperature time series that can be matched with overlapping records from other trees to produce longer time series. Annual records from tree rings typically go back 500 to 700 years.

Figure 1.2: Each year, a tree that is growing produces a layer of new cells beneath the bark and this appears as a series of ring.

The analysis methodology use multiple samples taken as core of wood in each tree and then use a sample of a certain number of trees to minimize the variation within and between trees. The calibration between the tree ring width and/or density data and the climate variables, typically temperature and precipitation is made comparing these data with the instrumental time series for the period of superposition, usually coincident with

the length of the instrumental series. For that common period, standard regression analysis techniques can be used to separate the effects of annual (or growing season) average temperature and precipitation on tree growth. The resulting information can be used to estimate annual (or growing season) average temperature and precipitation for the remaining range of time covered by proxy dendro data.

The limitation of this type of proxy data is first, for the same weather conditions, young trees grow faster than older trees. The effects of this early growth must be removed statistically, but this approach tends to smooth the year-to-year variability or lost some signal. Second, the necessity to collect multiple samples per tree and multiple trees in the study and then the necessity to average all these values can further decrease the size of year-to-year variability in the final results. Third, it is difficult to interpret the tree ring data in particular at the light of non-climate factors as changing atmospheric CO_2 concentration. In fact at higher concentration it makes the plants grow better but we know also that in these last decades carbon dioxide (CO_2) concentration is steady rise in atmosphere so it is difficult to separate the natural condition of growing from this forcing of anthropogenic nature. Finally, the statistical techniques used to combine data filter out the century-scale climate variability.

The effect of all these limitations make tree growth studies to take with care. However their major point of strength is that tree ring records permit a wide geographic availability for climate reconstruction, including, annual to seasonal resolution, ease of replication, and internally consistent dating. In particular they permit to evaluate the climatic signal also in environment with low or no urbanization and with less influence of anthropogenic forcings.

Ice Cores

The ice sheets that cover the tops of some mountainous areas, as well as large zone in the world as Antarctica, Greenland, northern Canada and Russia represent the accumulation of several hundred thousand years of snow fall. The ice cores drilled out in particular in very cold, dry areas such as the interior of Greenland and Antarctica, yield a big amount of information. In these zones in fact the records are particularly good because there is little year-to-year evaporation or melt and the snow remains compressed into annual layers of ice. The thickness of these layers is an indication of

the amount of precipitation that fell at that location during the year when the layer was deposited (Fiure 1.3), and the isotopic analysis of the water in the ice can provide a proxy for temperature.

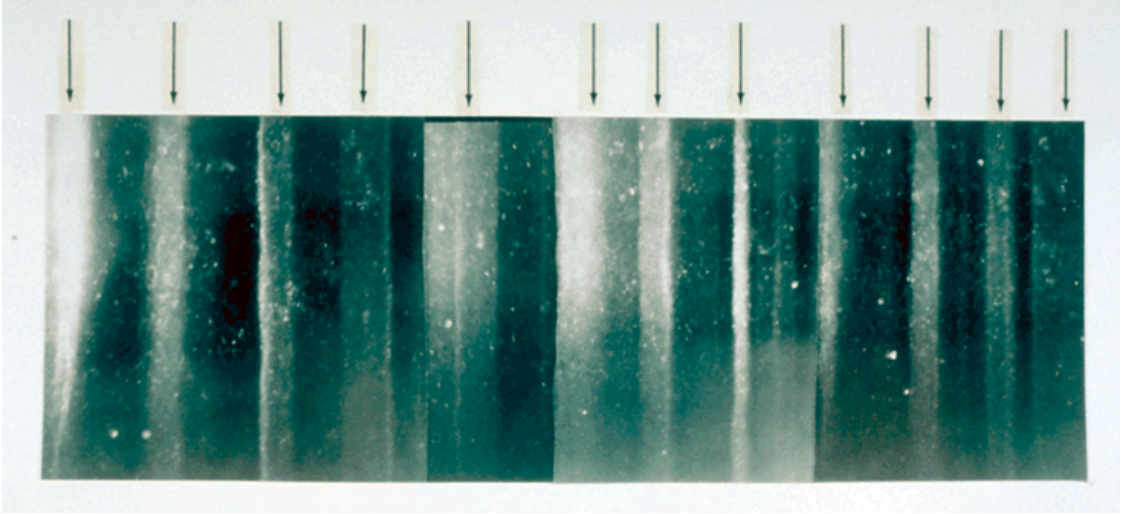

Figure 1.3: 19 cm long section of GISP 2 ice core from 1855m showing annual layer structure illuminated from below by a fiber optic source. Sections contains 11 annual layers with summer layers (arrowed) sandwiched between darker winter layers.

It is possible to reconstructed a past temperature time series making the oxygen isotope analysis. We know that 99% of the oxygen on Earth is the isotope ^{16}O; most of the rest is ^{18}O. Because water molecules containing the different isotopes (i.e. $H_2\ ^{16}O$ and $H_2\ ^{18}O$) have slightly different physical properties, it turns out that the $^{18}O/^{16}O$ ratio in ice locked up on land is affected by the ambient temperature at the time when the when the snow was originally deposited. Thus, fluctuations in the oxygen isotope ratio in an ice core provide a proxy for temperature changes back through time. The cores also include atmospheric fallout such as wind-blown dust, volcanic ash, pollen or bubbles of air. In fact as glacier ice is formed bycompaction of successive layers of snow, small bubbles of air become trapped. When a sample of ice is drilled out, these air bubbles can be dated quite accurately, and when analysed, provide an archive of past atmospheric composition – including the levels of CO_2, CH_4 and N_2O.

Marine and Lake Sediments

Layered sediments on lake and ocean floors are another rich source of paleoclimate data that can be analyzed to provide evidence of past climatic change taking cores from the bottoms of sediment regions.

Marine annually resolved sediment layers (varves) offer potential archives of information on past interannual climate variability, but they are in most cases, discontinuous. Laminated (layered) sediments are common in marine sedimentary basins of the continental margin because ocean and lake sediments typically accumulate slowly, hence it is only in regions where sedimentation rates are extraordinarily high (e.g., the Bermuda Rise, the northwest coast of Africa) or in a few oxygen-deprived areas (e.g. in deep crater lakes) that sediments can be dated accurately enough to provide information on climate changes during the last millennia.

Distinct sediment layers form in response to changes in the composition and flux of particles to the sediment-water interface. They are preserved either due to very rapid accumulation rates or because of the absence of post-depositional disturbance by physical or biological mechanisms. Sediment cores can be analyzed to determine the temperature of the water from which the various constituents of the sediment were deposited.

Records relevant to temperature include oxygen isotopes, the ratio of magnesium to calcium, and the relative abundance of different microfossil types with known temperature preferences (such as insects) or with a strong temperature correlation (e.g., diatoms and some other algae) that can be used to study seawater temperature, salinity (salt content), atmospheric CO_2 and ocean circulation as the ENSO variability, particularly using sediment cores from areas strongly affected by ENSO-forced changes in rainfall or water temperature.

Glacier Length Records

Glacier length records are proxy data useful to record long term trends, because their movements reflect average climate conditions over decades or longer, in fact mountain glaciers grow and advance during colder (and moister) periods, instead they shrink and retreat during warmer periods. There are two zones along a glacier: the accumulation zone and the ablation zone. The accumulation zone is where the mass of the glacier accumulates. Ice is lost, in the ablation zone, through melting, sublimation and, where glaciers enter lakes. The amount of income, in the form of snow, equals or exceeds the amount of outgoings, in the form of melting, sublimation and calving. If the addition of new snow doesn't keep up with the rate at which ice is lost, as a result, the glacier loses

ice volume, which is usually expressed as the retreat of the glacier's terminus or tongue (Figure 1.4). A significant period of time is necessary for a glacier to respond to a change in climate because of the large mass of ice. It is this lag in climate response that make the glacier movements not useful to determine annual changes in temperature but only an indicator of temperature trend. The rate of movement of glaciers can be determined from historical records, painting representation or from dating the moraines (rock deposits) they leave at their furthest point of advance. Because their characteristics, glacier movements provide only a qualitative information and not a quantitative measures of century-scale climate variability.

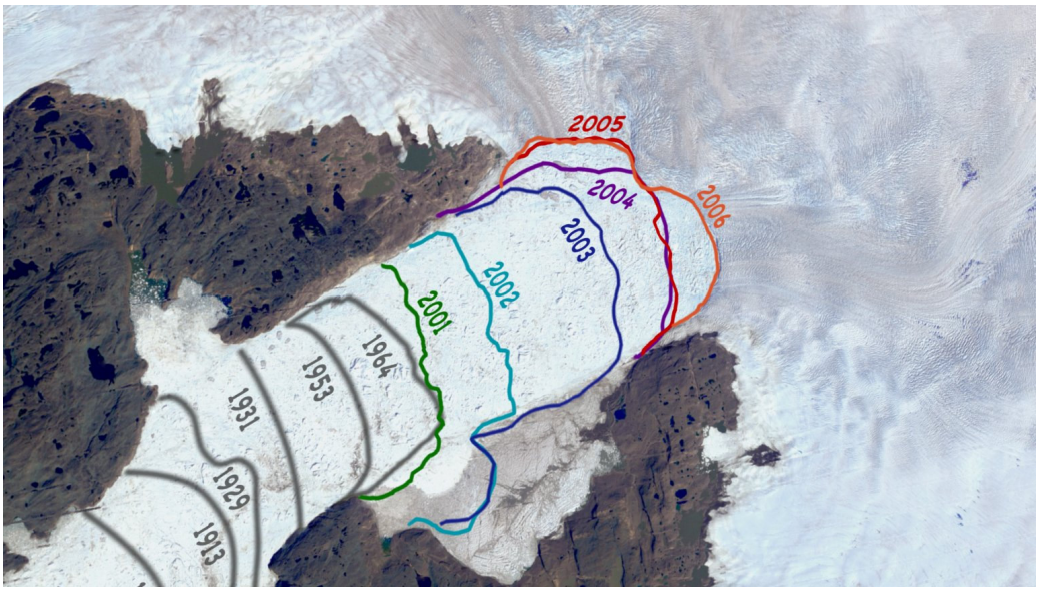

Figure 1.4: retreat of Jakobshavn glacier calving front (Greenland), ice cap on the right, Atlantic to the left.

1.1.3 Satellite data: the future toward an earth information system

In this thesis, near the effort to explain the methodologies for increasing temporal series of temperature back in time trough proxy and early and modern instrumental data, we put the attention also in the actual and future vision of climate data usage more and more based on the use of satellite data for climate researches.

Today, the WMO (World Meteorological Organisation) promotes properly taken observations from a worldwide network of land and marine monitoring stations, including moored buoys and fixed platforms at sea (e.g. oil rigs). The map in Figure 1.5 shows the distribution of these various surface stations.

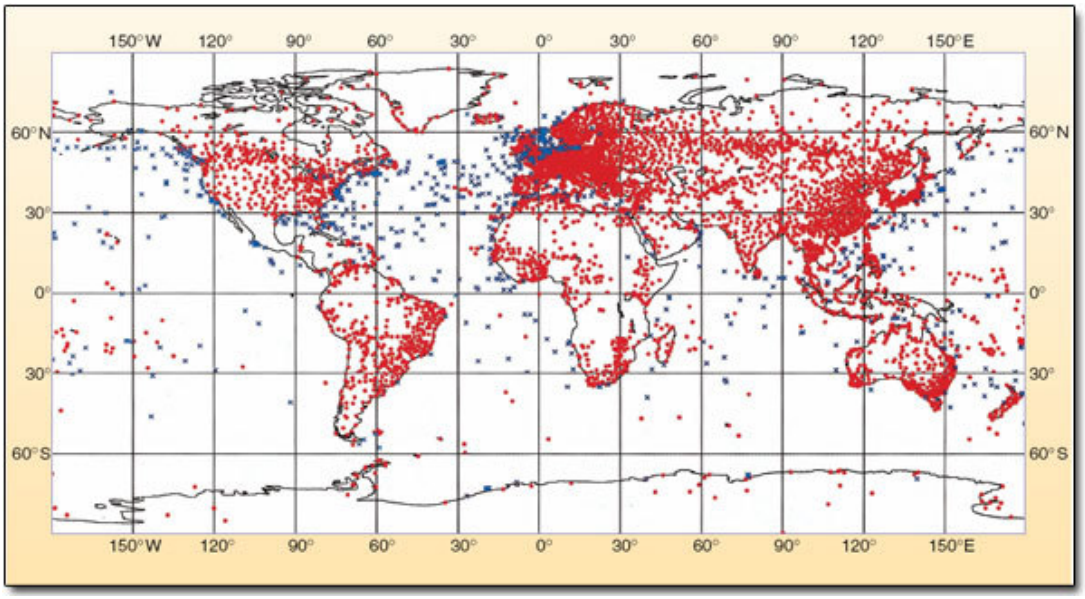

Figure 1.5: Worldwide map of daily coverage surface observations accepted by the WMO (World Meteorological Organization) made at meteorological stations (red) and from ships (blue).

The state of the climate is determined from the global climate observing network. This network is also used to examine the current state relative to the past, often in the form of anomalies (differences respect a reference period usually 1961-1990) relative to a mean state, and to examine long-term trends of climate-sensitive variables, such as sea level rise, air and sea temperatures, sea ice concentration and extent, and upper ocean heat content. The future state of the climate is predicted by starting from the present state of the climate. The importance of observations for producing an accurate assessment of the present state of the climate is recognized as a central objective by a lot of meteorological organizations.

Satellite data, in this view, offer an unprecedented potential for climate research because they supplement and improve the measurements and observations from traditional in-situ and remote sensing networks, such as weather stations, weather radars or weather balloons. Providing full area coverage from space, they can help to fill the 'white spots' on the meteorological map, oceans, for example, where far too few weather data are collected, or the upper layers of the atmosphere where data collection is only possible with weather balloons at specific points. Another important aspect is the measuring of atmospheric conditions that otherwise could not be recorded from the Earth's surface, e.g. the radiation conditions at the top of the atmosphere. Nowadays environmental

satellite data have grown to be the most important source of information for daily global weather forecasting (see Figure 1.6).

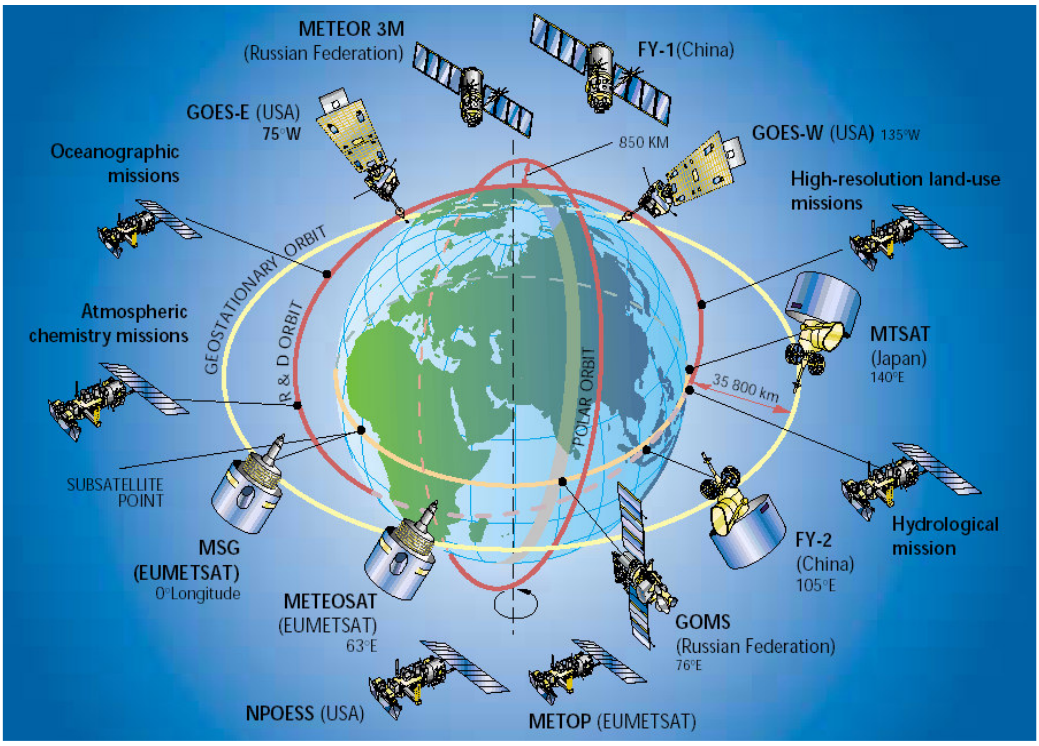

Figure 1.6 The present day environmental satellite orbiting around the Earth

In addition, these data are now also used by a large heterogeneous users community as instruments to obtain data for a large spectrum usage that ranges from oceanic, atmospheric, terrestrial and climate research to environmental monitoring; aviation safety, science education; and moreover also to obtain a rapid-response for decision support concerning security, as the case of tornado and hurricane alarms to the population.

In this thesis we deal with satellite of the National Aeronautics and Space Administration (NASA) of the United States. This choice was in part determined by a need of continuity with the past degree report and in part determined by the good correspondence between our requests of some precise environmental variables together with the necessity of high space and time resolution and the data provided by NASA satellites. In the next chapters 8 and 9 we explain the strengths and the limitations of scientific research performed with data satellite pointing the attention on the case study of the selection of an astronomic site through aerosol content monitoring from data satellite.

In the nearly 50 years of meteorological satellite observations, NOAA's satellite data have increasingly been used to complement research satellite data for purposes of observing climate processes and monitoring change. However, many of the early research and meteorological satellites were either not designed for climate-quality measurements or were not succeeded at the end of their lifetimes. The resulting patchwork of satellite measurements has required extraordinary scientific effort to yield credible climate information. In recent years, many robust and validated satellite algorithms have been developed both through NASA's Earth Observing System (EOS) science teams and NOAA's Center for Satellite Applications and Research (STAR). The algorithms at the beginning were developed to work and to quantitatively retrieve key earth system parameters of a single satellite instrument, but now these algorithms are appropriate for generalization and application to a longer time series of observations, see Figure 1.7.

Many algorithms must be executed within weeks of the observations to provide ongoing inputs to intra-seasonal applications and research. However, these "initial production" climate products typically do not meet the more rigorous uncertainty of climate data analysis. Only in a second step more accurate and precise climate products are generated but these data reprocessing follow significant time lapses (typically years).

The value of environmental satellite data derives from the unique, near-real-time, continuous global coverage from space of Earth's land and ocean surfaces and its atmosphere value that increases significantly as we accumulate satellite records that provide a historical perspective. In addition, probably, in the near future, in a more and more technologic world with a large use of telecommunication, environmental satellite data will be employed by a much wider spectrum of users and the agencies responsible for archiving and distributing environmental satellite data will have to develop the essential visions, plans, and systems in order to permit a stored high quality data product that will hold, in a future, the same chair to study climatic change, that now is due to instrumental data.

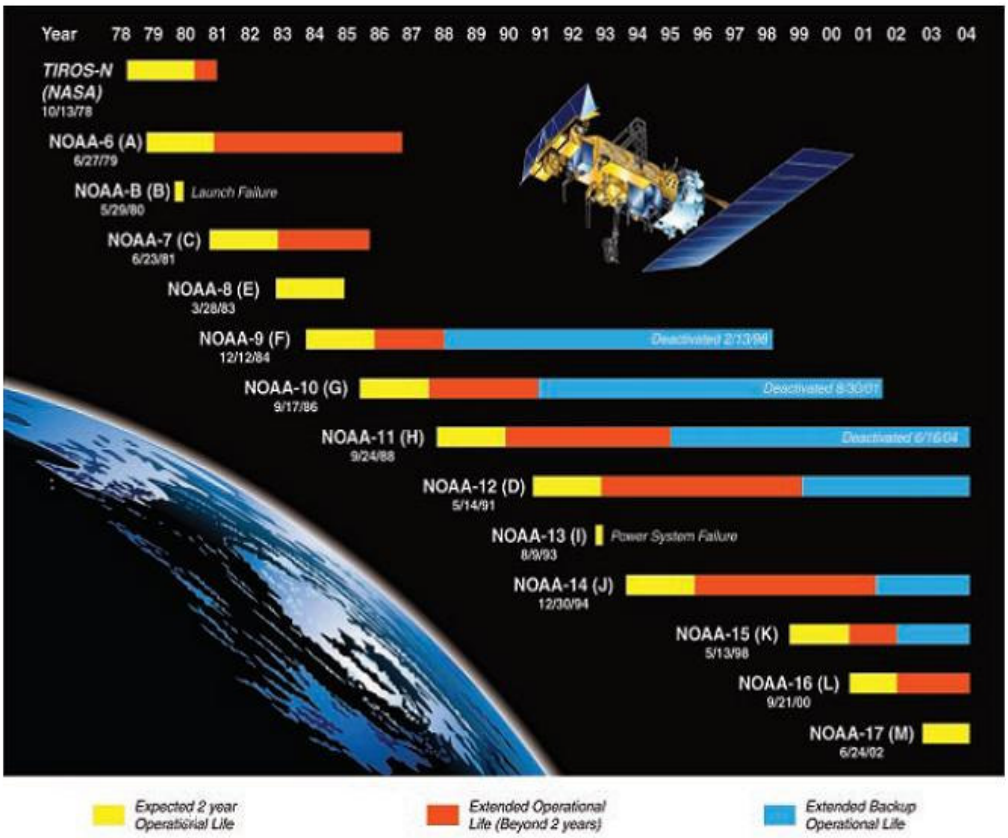

Figure 1.7 CDRs (Climatic Data Records) constructed from series of NOAA overlapping satellites.

1.2 Data quality on which the actual knowledge are based on

In this section we try to understand the current state of the science through the exam of a specific climate variable, i.e. the large-scale surface temperature reconstruction.

A description, from different sources, of the present state of art concerning with the surface temperature of the last millennium, is illustrated in Figure 1.8. In this figure it is possible to have an idea of the different approaches drove and results obtained from the use of several different kinds of data to study a climate variable.

In separate pictures, from the top to the bottom are shown respectively:

1. instrumental record retrieved from traditional thermometer readings,
2. large-scale surface temperature reconstructions based on different kinds of proxy evidence as changes in length of many mountain glaciers, and borehole temperature measurements

3. compilation based on several recent multiproxy and tree-rings to reconstruct the Northern Hemisphere surface temperature,
4. two climate model experiments forced with time-varying estimates of natural climate forcings over the last 1,000 years plus anthropogenic forcing since the start of the Industrial Revolution.

As we described more in detail, each elaboration and result is here derived by a different paleoclimate research group that use its own approach to the selection of proxies, calibration and validation protocols. This can create some inconsistency or problem when a comparison between the temperature reconstruction is searched for First of all because each curve in Figure 1.8 has different uncertainties due to different geographical sampled area and different temporal data description. Some series in fact present more seasonal or more annual emphasis due to the proxy own intrinsic correlation with the temperature. No one curve can be said to be the best representation of the actual variations in Northern Hemisphere or global mean surface temperature during the last 1,000 years. However, despite these limitations, from these reconstructions some common features are visible: the relatively cool period between 1500 and 1850 (the Little Ice Age) and the growing surface temperature from about 1900 to present. In the reconstruction based on tree-rings and multiproxy shown in panel C also a relatively warm period around A.D. 1000 is visible, where at least one reconstruction shows surface temperatures comparable in warmth to the first half of the 20th century.

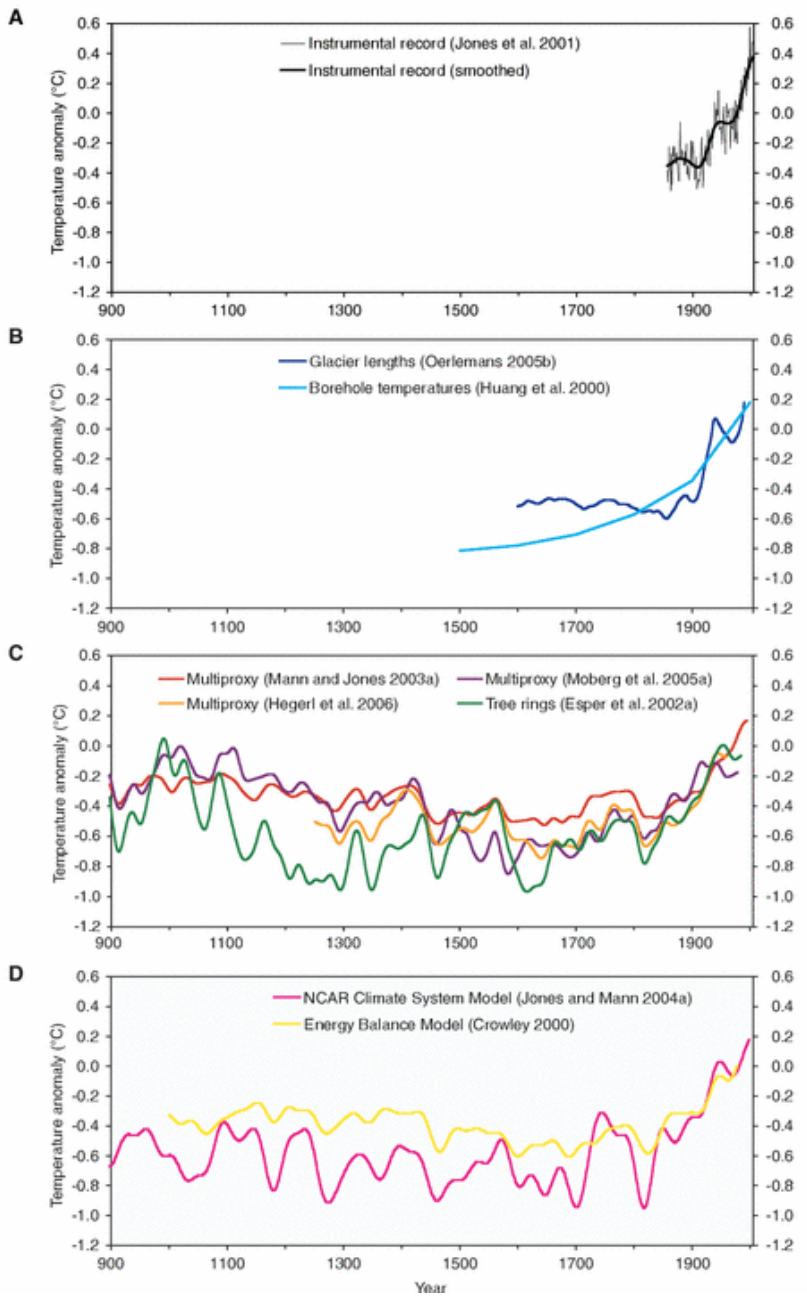

Figure 1.8: Northern Hemisphere surface temperature reconstruction since A.D. 900 derived from several sources. (a) smoothed and unsmoothed yearly instrumental temperature (Jones et al. 2001). (b) reconstructions based on glacier length records (Oerlemans 2005b) and borehole temperatures (Huang et al. 2000). (c) three multiproxy reconstructions (Mann and Jones 2003a, Moberg et al. 2005a, and Hegerl et al. 2006) and one tree-ring-based reconstruction (Esper et al. 2002a, scaled as described in Cook et al. 2004). (d) two estimates of NH temperature variations produced by models that include solar, volcanic, greenhouse gas, and aerosol forcings, as described by Jones and Mann (2004). All curves have been smoothed using a 40-year low-pass filter (except for the unsmoothed instrumental data), each curve has been aligned vertically such that it has the same mean as the corresponding instrumental data during the 20th century, and all temperature anomalies are relative to the 1961–1990 mean of the instrumental record.

Starting from different Northern Hemisphere surface temperature proxy reconstruction of Figure 1.8, we ask how can it be possible to put together these results to reconstruct a single most reliable 1,000 years long temperature reconstructed series? And moreover which is the reliability for each proxy series that goes to build the single overlapped reconstructed temperature series? What will be the confidence level of the final series representing our present knowledge on surface temperature reconstruction of the last millennium?

To answer at all these questions we analyse the generally accepted results for the NH temperature variability (Figure 1.9) presented at the world wide community both of scientists, policymakers and common people in the 4th Assessment Report of the Intergovernmental Panel on Climate Change IPCC made by the contribution of working group 1 concerning the physical science basis of climate change (IPCC-WG 1, 2007).

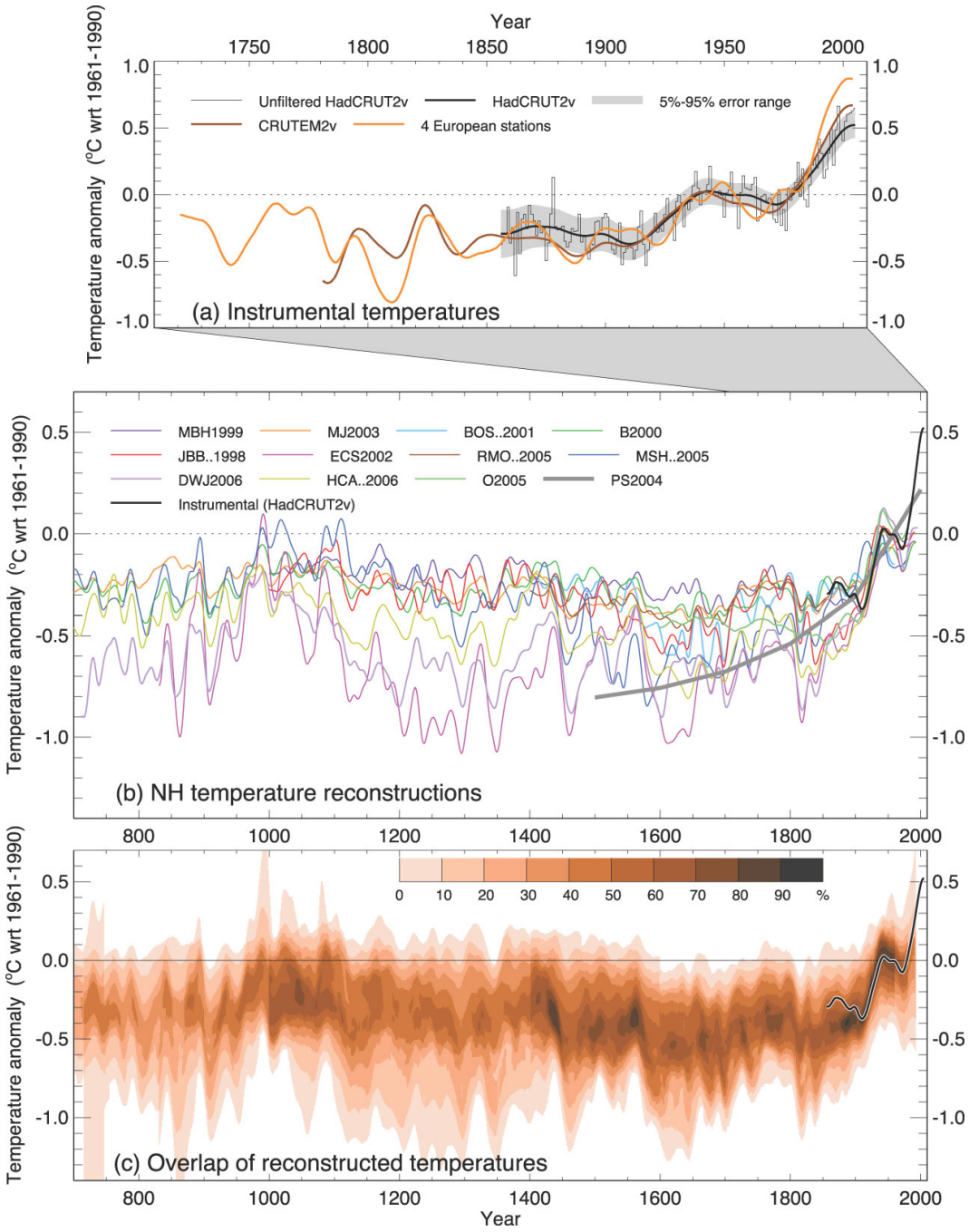

Figure 1.9 Plot performed by IPCC WG1 (2007) on NH temperature variation during the last 1.3 kyr. (a) Annual mean instrumental temperature records, (b) Reconstructions using multiple climate proxy records, including three records (JBB..1998, MBH..1999 and BOS..2001) and the HadCRUT2v instrumental temperature record in black. (c) Overlap of the published uncertainty ranges of all temperature reconstructions identified in Table 1, with temperatures within ±1 standard error (SE) of a reconstruction 'scoring' 10%, and regions within the 5 to 95% range 'scoring' 5% (the maximum 100% is obtained only for temperatures that fall within ±1 SE of all 10 reconstructions). The HadCRUT2v instrumental temperature record is shown in black. All series have been smoothed with a Gaussian-weighted filter to remove fluctuations on time scales less than 30 years. All temperatures represent anomalies (°C) from the 1961 to 1990 mean.

In Table 1.1 are summarized all records (name of the series in the plot legend, time cover period, reconstructed season, data description and work published references) of Northern Hemisphere temperature shown in Figure 1.9 (IPCC-WG1, 2007) with separation between different type of instrumental and proxy data sources.

Table 1.1 Records of Northern Hemisphere temperature shown in Figure 1.9. Table published in IPCC-WG1 2007 report.

Instrumental temperatures

Series	Period	Description	Reference
HadCRUT2v[a]	1856–2005	Land and marine temperatures for the NH	Jones and Moberg, 2003; errors from Jones et al., 1997
CRUTEM2v[b]	1781–2004	Land-only temperatures for the NH	Jones and Moberg, 2003; extended using data from Jones et al., 2003
4 European Stations	1721–2004	Average of central England, De Bilt, Berlin and Uppsala	Jones et al., 2003

Proxy-based reconstructions of temperature

Series	Period	Reconstructed Season	Region	Location Of Proxies[c] H	M	L	O	Reference
JBB..1998	1000–1991	Summer	Land, 20°N–90°N	◢	◢	□	□	Jones et al., 1998; calibrated by Jones et al., 2001
MBH1999	1000–1980	Annual	Land + marine, 0–90°N	■	■	◢	◢	Mann et al., 1999
BOS..2001	1402–1960	Summer	Land, 20°N–90°N	■	◢	□	□	Briffa et al., 2001
ECS2002	831–1992	Annual	Land, 20°N–90°N	◢	◢	□	□	Esper et al., 2002; recalibrated by Cook et al., 2004a
B2000	1–1993	Summer	Land, 20°N–90°N	◢	□	□	□	Briffa, 2000; calibrated by Briffa et al., 2004
MJ2003	200–1980	Annual	Land + marine, 0–90°N	◢	◢	□	□	Mann and Jones, 2003
RMO..2005	1400–1960	Annual	Land + marine, 0–90°N	■	■	◢	◢	Rutherford et al., 2005
MSH..2005	1–1979	Annual	Land + marine, 0–90°N	◢	◢	◢	◢	Moberg et al., 2005
DWJ2006	713–1995	Annual	Land, 20°N–90°N	■	◢	□	□	D'Arrigo et al., 2006
HCA..2006	558–1960	Annual	Land, 20°N–90°N	◢	◢	□	□	Hegerl et al., 2006
PS2004	1500–2000	Annual	Land, 0–90°N	◢	■	□	□	Pollack and Smerdon, 2004; reference level adjusted following Moberg et al., 2005
O2005	1600–1990	Summer	Global land	◢	■	□	□	Oerlemans, 2005

Notes:
[a] Hadley Centre/Climatic Research Unit gridded surface temperature data set, version 2 variance adjusted.
[b] Climatic Research Unit gridded land surface air temperature, version 2 variance corrected.
[c] Location of proxies from H = high-latitude land, M = mid-latitude land, L = low-latitude land, O = oceans is indicated by □ (none or very few), ◢ (limited coverage) or ■ (moderate or good coverage).

Starting from the analysis of Figure 1.9a, to construct this kind of climatological time series it is not a simple step because 'aggregating' weather observations from different geographical area into global averages can arise uncertainties. The uncertainty typology immediately evident, found in both early and modern instrumental records is the sampling error. In fact today as in the past, weather stations or place where in the past instrumental observations were performed tend to be concentrated in heavily populated regions of the industrialised world as is clearly visible in Figure 1.5. More remote areas are often poorly monitored, and this was even more true in the past. An uneven spatial coverage effectively 'samples' the Earth's temperature non-uniformly. As this spatial coverage becomes more and more complete over time, spurious trends and biases can become embedded in the historical record. For this reason the check of data reliability

becomes of fundamental importance before to overlap instrumental series that could be inhomogeneous both for their different temporal range and spatial coverage. Apparent jumps or trends in the record from a particular station may be an artefact of some local effect. Changes in instrumentation, observing times, or in precise location or in the local environment, can all affect the reliability of the data. An important example that will be deal in the last chapters here is the spurious warming effect associated with the growth of towns and cities around (or near) a weather station, the so-called 'urban heat island effect'. The instrumental series presented in Figure 1.9a lack of strongly space homogeneity, their bigger uncertainty arise from an incomplete spatial coverage of records through time (Jones et al., 1997). For example the series that consider only land-based network, labelled in the plot as CRUTEM2v, for the early instrumental readings (1781-1820) have a less consistent spatial coverage respect the 20th century, being composed only from 23 European stations, 1 North American station and no station in Asia. Likewise the series of 4 European stations instrumental data (Central England, De Bilt, Berlin and Uppsala) permit of going back more in time but, due to their very low number, the climatic indication remain with a regionally nature rather than global. Therefore the instrumental series presented by the most influent source at scientific and political level on which great part of present knowledge and political intervention are based on have an increasing biased towards Europe geographical area during the earlier periods, only with the increasing number of stations obtained during the 20th century their coverage become really global. The results evident in this picture show that the warming observed after 1980 is unprecedented compared to the levels measured in the previous 280 years, even considering a greater variance in an average of so few early data compared to the much greater number in the 20th century. Although we know that it is difficult to collect, analyse and validate a greater number of early instrumental data to fill the blank area, above all in zone of the world in which the climatic instrumental measurements started late, in our opinion, a number of stations quite uniform in time and space remain an unavoidable step to improve the quality of the Northern Hemisphere surface temperature reconstruction.

After several critical studies that attacked the proxy 'hockey stick' reconstruction of NH global temperature performed by Mann et al. (1999), the effort produced by the IPCC 2007 report was that one to give an higher quality paleoclimate reconstruction of the

last millennia in quantitative term (Figure 1.9b) and not more in qualitative one as occurred in the previous years. In order to understand the nowadays available proxy data quality for reconstructing temperature series, it is necessary to start with analysing some important points that highly affect both their quality and bring factors limiting our confidence in these reconstructed climate variables series.

1. *The statistical methods used to calibrate* different original proxies into different estimates of mean NH temperatures. In the absence of a consensus as to which methods or statistical formulas are most appropriate for calibrating and validating these reconstructions, different choices made by different investigators and research groups also contribute to the differences between them. One method used is that to compare the single series obtained by the average of all the regional proxy data, with the instrumental readings over an overlapping period, and to assume the same average and standard deviation between the matched series. (Jones et al., 1998; Crowley and Lowery, 2000, Camuffo et al 2010). A second one is concerning with a complex climate field reconstruction, where large-scale modes of spatial climate variability are linked to patterns of variability in the proxy network via a multivariate transfer function that provides estimates of the spatio-temporal changes in past temperatures, and from which large-scale average temperature changes are derived by averaging the climate estimates across the required region (Mann et al., 1998; Rutherford et al., 2003, 2005). Other reconstructions are considered intermediate applications between these two approaches, in that they involve regionalisation of much of the data prior to the use of a statistical transfer function (Briffa et al., 2001; Mann and Jones, 2003; D'Arrigo et al., 2006).

2. *Temporal and Climatic correlation between records and physical/biological proxy properties*: in order to detect which climatic variable best fit with the measured variation of proxy properties and quantify the statistical uncertainty associated with scaling proxies to describe this specific climatic variable, it is necessary to calibrate the proxy records over a number of years with available instrumental data. However, this comparison for searching the climatic correlation is not so simple because changes in physical and biological proxy properties as it is for example the case of tree rings growing do not respond

directly to the changes of a specific climate parameter or uniquely to it, such is the dependence for tree rings to both mean temperature and total rainfall at the same time. All series in Figure 1.9b, therefore show differences in temperature reconstructions that spread them. This is due mainly to the choice of different predictor series, different way to process proxies, different choice for the calibration period data, different statistical scaling approaches and to the compromise adopted to the choice of the correlation between proxy property and climatic dependent variable.

3. *Spatial-Temporal coverage samples*: another limitation to the reconstructed temperature, using proxy data is due to the not homogeneous spatial coverage, in the NH in fact we have only few long and well-dated climate proxies reconstructions that moreover contain inside the limitation to have a greatest sensitivity to summer rather than winter or annual conditions. Using summer-sensitivity proxies therefore, also the conclusions drawn regarding annual temperature reconstruction can own a limitation (Jones et al., 2003). The reliability of large-scale temperature time series derived from observations at a small number of sites and with varying levels of chronological precision is still unresolved. It is widely agreed that fewer sites are required for defining century-to-century fluctuations than year-to-year fluctuations, but errors in the reconstructions that are specifically attributable to the limited spatial sampling are difficult to be quantify.

4. *Instrumental record length*: the relatively short length of the instrumental record, in most case reaching only about 150 years is another important point to take in account. In fact it only provides a few pieces of independent information to both calibrate and validate surface temperature reconstructions over large spatial scales and multidecade time periods. In this approach, it could be also implied a bias because instrumental records, used for calibration and validation of proxy data, have also been collected during a period when both global mean temperatures and human impacts on the environment have increased substantially.

There are instead some points of strength for using proxy data in large-scale surface temperature reconstructions:

1. Proxy records are meaningful recorders of environmental variables because they are sampled on the basis of established criteria well justified in terms of physical, chemical, and biological processes.
2. Most surface temperature reconstructions incorporate proxy evidence from a variety of sources and wide geographic areas, and the resulting temperature estimates are often robust with respect to the removal of individual records.
3. The same general temperature trends emerge from different reconstructions.

Taking into account the points described above, by the light of the data quality on which our knowledge is based on, we wonder if the Northern Hemisphere surface temperature reconstruction present on IPCC 2007 could be consistent with the natural climatic signal and if this climatic change is real or less. To answer to this question we analyse the last panel in Figure 1.9. This last panel (c) is the most likely course of hemispheric mean temperature change during the last 1,300 years based on all of the reconstructions shown in Figure 1.9b, and taking into account their associated statistical uncertainty. The figure has been created enveloping the two standard error confidence limits that bracketed each reconstruction together to show where there is most agreement between the various reconstructions.

To analysed and understand the final overlapped series in Figure 1.9c, it is necessary to have clear the way of representation that IPCC made of these data.

Where IPCC scientists were unable to estimate and quantify the uncertainties in their conclusions, they adopted a ‘likelihood’ language. This was intended to convey their level of confidence in the validity of a conclusion. Probabilistic statements are based on a statistical analysis of observational data that here are translated from observational data and represented in term of confidence level. Given the ‘likelihood’ language adopted and the information in Figure 1.9c, What are the possible reasonable conclusions stored in this long term temperature reconstructed series? For example it seems ‘very likely’ (90–99% probability) that since the beginning of 20th century a warmest tendency in the reconstructed global superficial temperature is present until nowadays, as well as the evidence of a cooler period ranged from 1450 to 1800, going

back in time the probability that the confidence level of this series could be coincident with the real observational data goes down at the definition of 'medium likelihood' interval (33-66% probability), only the period around 1,000-1,100 is defined from the reconstruction 'likely' (in the of 66-90% probability range). The major differences in Figure 1.9c are concerning with the magnitude of past cool events as provided by different proxy reconstructions relating to the period 12th - 14th, 17th and 19th centuries. Concerning with the description of the Medieval Warm Period, the differences stand on fact that several reconstructions exhibit only a short-lived maximum just prior to AD 1000 but only one (Moberg et al., 2005) shows persistent conditions (i.e., during AD 990 to 1050 and AD 1080 to 1120) that were as warm as those in the 1940s and 50s. As only this reconstruction shows an early period that is noticeably warmer than the mean for the calibration period, the possibility of a bias does not affect the weight of current multi-proxy evidence that generally conclude about the relative warmth of the 20th century based on these data. Nevertheless, not all individual proxy records indicate that the recent warmth is unprecedented, although a larger fraction of geographically diverse sites experienced exceptional warmth during the late 20th century than during any other extended period from A.D. 900 onward. The substantial uncertainties currently present in the quantitative assessment of large-scale surface temperature changes prior to about A.D. 1600 that ranges mainly in 40-50% in probability, lower our confidence in this conclusion on a 21th century unprecedented warming period compared to the past millennium.

In this section we have spoken of the data quality on which our actual knowledge is based. Taking advantage of the results presented for the Northern Hemisphere superficial temperature for the last millennium in the IPCC 2007 report, we described how a reconstruction is carried on with which data and through which methods, underlying in particular the factors that actually make worse their quality. Our analysis on the data quality was focused in particular on the instrumental and proxy data, here below we want tell something else about the quality of the modern networks including ground stations and satellites.

As already told the nowadays climate research and monitoring includes both in situ and remote sensing platforms. An adequate global climate observing system is made up of instruments on various platforms, including aircraft and satellites, ground stations, ships

and balloons. The existing network however is in need of repair and maintenance, and many elements must be brought up to modern standards. One of the more pressing needs to maintain high the data quality for a climate monitoring perspective is the identification and correction of time-dependent data biases in observation systems as early as possible. Too often, in fact time-dependent biases have been discovered ten or more years after the fact, often through data reanalysis efforts. This degrades the climate record, even if adjustments can be developed to correct the errors. In addition, a system must be put in place so that when biases are found, network operators can be notified and corrective action taken above all for satellite instruments otherwise the risk is to invalidate great part of mission results. These biases are sometimes due to sensor degradation, but frequently result also from changes in algorithms or spatial and temporal sampling methods that at first appear not relevant.

Over land, the great spatial heterogeneity requires extremely detailed measurements and presents a major challenge to obtain a sort of "unification". A truly global observing system is only possible through international cooperation and coordination that could give support and standardization dictates to a so large number of observing networks. This is a big challenge to obtain since now, high quality, statistically robust and broad global observations in order to project the present state of the climate knowledge into the future.

There are two efforts that we want to carry on in this thesis: the first is to improve the quality of both instrumental and proxy data we use to reconstruct the past 1,000 year surface temperature series for Northern-Central Italy and 500 year temperature reconstructions for the Mediterranean basin and the second is to improve the measure of the climate natural variability, especially on multi-century long timescale for the area taken in exam. Both these aspects, till nowadays, are badly or not completely solved issues of climate science. The data quality, for the present persistent problems expressed above, and the climate natural variability as it is the only 'reading key' to solve the question if the climate of the 20th-21th century is unusual. Nevertheless, the usually almost 160 year-long global direct temperature instrumental record is still too short to perform an high quality calibration versus the proxy data and to reconstruct in this way the natural variability of temperature in its full millennial dynamic range. With regards these issues, the results obtained in this thesis offer an improvement of both data quality

and instrumental data coverage, back in time, to 360 years just immediately after the invention of the first meteorological instruments.

Chapter 2:

Documentary Proxy Data: potential and limitations to reconstruct climate variability

Contents

2.1 The sources and the characteristics of documentary proxy data
2.2 Potential and limitation of documentary proxy

The increasing interest to understand the present climate change has increased also the interest in past climate variability. It is the base in order to have a term of comparison for estimating the anthropogenic effects on climate by providing an accurate reconstruction of the natural climate variability, evaluating in this way, the last century situation. In the first chapter we gave a picture of the proxy data used in paleoclimatology to reconstruct and analyse the climatic signal going back in time. Here, we continue our route to describe the different data and methodologies used for the analysis of climatic variables in the last millennium. This Chapter will focus on the historical climatology branch that represents the temporal link between the paleoclimatology and the instrumental climatology and that it will be described in detail in the next chapters. The distinction among these three disciplines is not only based on their respective temporal windows, being paleoclimatology concentrated in the study of the whole Holocene period, the historical climatology on the period with documentary archives mainly ranged on the last 1,500 years and the instrumental climatology developed since the invention of the first meteorological instruments in the 1654 up to the present. The distinction is instead related to the type of evidence they store inside and in the methodological approach they need to extract it.

The historical climatology is based on the study of written proxies that consist mainly in documentary sources, i.e. written historical documents to give a picture of weather and

climate for the range of time previous of the invention of the first Meteorological Network. For their nature, documentary proxy give more information above all for the reconstruction of Historical Climate Variability and Useful for identification of impacts of extreme events as river flood-over or frozen over, storms or drought events as well as events that had a big impact on the society as scarcity of harvest related to bad and continuative weather condition or historical and social events that affected the people life and economic condition at that time as in the cases of wars and epidemic illness.

Written sources therefore are used to reconstruct past climate in the absence of direct instrumental data; roughly at a first analysis, the former could appear to be vague, imprecise, highly subjective, qualitative, hardly transformable into quantitative indexes; the latter, on the other hand, precise, objective, with high resolution. However who considers documentary proxies as poorer than instrumental data has not a clear idea about them. Proxies are not a duplicate or equivalent to instrumental records. The information they provide is simply different, sometimes with the above-mentioned limits, but sometimes including much more information than instruments can do. Instruments provide a quantitative measurement of a certain selected atmospheric variable and at a given time instant. Written proxies provide a wide picture of what happened in a certain area and for a certain time, sometimes pointing out cause-effect relationships, and from the gravity of the effect we could establish the severity of the cause, with an objective indexing. In general, written proxies provide a qualitative or a semi-quantitative synergistic effect of one or more atmospheric variables (Enzi and Camuffo, 1995). Written proxies describe some effects e.g. a river in flood, a water body frozen over, a famine derived from o prolonged aridity, which derive from the short-, medium- or long-term action of some atmospheric variables acting on a region. It needs, however, some interpretation. Let us consider for instance a water body freezing over. In the case of a lake with a little exchange of waters, slabs of ice form when enough heat has been lost, either a long-term slight cooling, e g. a long chilly winter, or short-term intense cooling, e.g. a very severe cold, with fresh wind for a few days. Briefly, a closed water body has a long-term memory, but may respond equally well to short, strong pulses. In the case of a lagoon, i.e. an open water body with continuous exchange with the sea, the atmospheric cooling is cancelled in a short by the tidal exchanges; the lagoon has a short-term memory and responds to two or three weeks of

very intense cooling, possibly worsened by cold wind. In conclusion, the proxy has a reaction that depends on the relaxation time of the considered item, and not all the apparently similar items suffer the same effect: in the above example slabs of ice may be formed on some water bodies, not in others. Not all the most severe winters had simultaneously frozen over both lakes and the Venice Lagoon (Camuffo and Enzi, 1992b).

Concerning with the **Reliability of the sources**, documentary proxies can be divided into three main subgroups: (i) the 'first class', includes reliable contemporary manuscripts; (ii) the 'second class' reliable but not contemporary collections; (iii) the 'third class' less reliable sources that should be rejected (Alexandre,1987; Pfister et al., 1998; Brazdil et al. 2005). It is generally assumed that the dating of contemporary chroniclers who lived the events they describe is reliable. However, it is reasonable and useful to verify the dating accuracy with cross comparison with independent factors, e.g. similar descriptions, historical analysis of social events found in the manuscript, cross checking with astronomical features (e.g. passage of comets, solar and lunar eclipses) whose dating is known after astronomy (Camuffo and Sturaro, 2004). This step allowed in the past to prevent the spurious multiplication of extreme events. According to Camuffo and Enzi (1992a), non-contemporary material (second class) was not completely rejected if it was possible to validate them. Validated second-hand reports have been included in this work when able to provide a sound contribution to the understanding of past climate.

2.1 The sources and the characteristics of documentary proxy data

The proxy evidences in which historical climatology is based on consist of different kinds of first and second-hand written sources, i.e. narrative, administrative and daily weather logs, with different reliability levels (Enzi and Camuffo, 1995; Pfister et al., 1999). Dealing with description of climate events or information on their impact upon the society. These documentary data are subdivided in direct and indirect data by the way in which meteorological variables are observed. The first are documentary data containing description of weather events born from the direct witness of the observer. The second are indirect documentary data because they describe the impact of weather on the environment that is however easily translatable on climatic information thanks to

the recurring in time of the event at the same natural and physical conditions (i.e. the time of freezing of rivers and lakes, observation of plant phenology with the time of wine harvest or epigraphic sources as the floods-marks in). The direct descriptive documentary can be further subdivided in narrative and administrative if we consider the range in which they were span in time and the reason for which they were produced.

- **Narrative sources**: Narrative sources are generic descriptions of events, such as chronicles, annals, diaries, early scientific treatises, poems, correspondence, and compilations of remarkable events, usually known as "Mirabilia" (i.e. Latin word for "extraordinary events"). Narrative sources can be manuscripts or printed, while their characteristics follow the literary genres on fashion during the various historical periods; they were often produced for divulgation aims. They typically report exceptional climatic events with some impact on the society, e.g. extreme cold or hot, periods of inactivity of mills, drying up of fountains for shortage of water supply, lack of water to sail in rivers, over abundant rains and rivers in flood, large water bodies completely frozen over an unusually frigid winter (Camuffo et al 2010). The narrative documents usually were born by observer's own initiative for recording exceptional more impressive weather events in his personal life experience. These sources, for their nature, are therefore not continuous in time with minor or major gaps, and they are limited by the life-span of the observer, with the risk also that the environmental perception by the chronicler is affected by his cultural, social, professional and personal background. However this risk is mitigated by the cross-comparison of the meteorological information as described in different chronicles. In fact more extreme is an events more in detail is described and more than one chronicle is compiled from different observers. Narrative sources exist on the whole Italian territory and most of them are printed in modern collections. In Northern Italy, for example, there is a gap in information regarding the early Middle Ages, followed by a progressive increase in data frequency.
- **Administrative sources**: Administrative sources are documents written by public officers usually to discuss a problem, its impact and the course of action to undertake in order to solve it. Administrative sources are quite objective,

reliable, precisely dated and often forming series of events exactly placed in a space and time context and above all are available over period of several centuries as long as the social, religious or economic authority life. The registers that were kept under authority's aegis involved more or less similar procedures and these often were written in the same way for centuries until the institutions were changed or abolished. In this way, the result is the possibility to collect a more than one century long and quasi-homogenous records (e.g. Leijonhufvud et al. 2009). For these reasons administrative sources are the most convenient archive sources: they mainly consist of manuscripts, originated for different aims as memory-self documentation of their authors (the concept of archives as public place of conservation and consultation goes back just to the end of 18th century). This kind of records largely increased in number with the development of national states (14th-16th centuries), when all over Europe specific departments were created to control the territory, sometimes with a special eye for the environment. In some cases the Royal Power established a centralised control of document in opposition to the clergy. This happened e.g. in France (Garnier, 2007) with the Royal Administrative Archives. Starting from the 16th century, the king of France created a number of public services with specific tasks (the Forestry Commission, the Department of Civil Engineering Navy). Scattered in the provinces, governmental officers noted all the main weather events and assumed that risk of atmospheric hazards was randomly distributed in opposition to the determinism supported by the Church. Several Mediterranean towns produced local records, in France called "Mercuriales", which included rather than note for documenting climate, note for documenting accounting activities concerned with the control of food prices and timing of the harvest. For example it is possible to find documentations related to the date of receipts (e.g. beginning of vine harvest) or expenditures (e.g. related to the payment of day laborers for field work or to maintenance operations such as ice cutting on waterways) that yield valuable evidence in the form of plantphenological or ice-phenological proxy data. French harvest bans and dates were one of the first used proxies (Chuine et al., 2004). The public administration evolved over time into great complexity, in Europe and also America, Africa and Asia.

Ecclesiastical sources are a particular type of administrative sources. The Catholic Church had a strong control over the territory, thanks to parish registers reporting weather injuries, mortality caused by natural hazards (famines, droughts, snow, floods, pestilences) and other relevant phenomena. The Church organization reached the same level of complexity of the State in economic, fiscal, institutional, judicial, educational and health matters. Clergy recorded liturgical services and rogation ceremonies commissioned by local communities or authorities in case of adverse weather conditions. "Pro pluvia" were the rogations i.e. religious rituals for rain to alleviate drought, while "Pro serenitate" were to stop precipitation in case of flood. Especially in Spain, but also in Portugal and the whole Mediterranean area, rogation ceremonies were generated within a completely institutional and bureaucratic setting and were submitted to both civil and ecclesiastic control. The standardization of items concerning rogations against environmental risks permitted their detection, exact dating, and simple quantification depending on the duration and severity of the dryness or rain (Martín-Vide and Barriendos, 1995; Barriendos, 1997, 2005; Alcoforado et al., 2000; Piervitali and Colacino, 2001; Barriendos and Llasat, 2003; Dominguez-Castro et al., 2008; Rodrigo and Barriendos, 2008).

- **Daily weather logs sources**: Daily weather logs were kept by some early meteorologists or other scholars, e.g. astronomers, nature philosophers, chronicle writers, always authors with a scientific background. This is a particular kind of documents, mainly started from the 16th century and encouraged by the advent of the Academies and other scientific Societies in the 18th Century (Camuffo and Enzi, 1992a, 1994). The chronological distribution of documentary proxies varies widely over the centuries. Information from early Middle Age is quite rare, followed by a progressive increase in data frequency. Administrative sources, usually handwritten, can be mostly found starting from the 15th century (Camuffo et al. 2010). The logbooks are also the most important institutional source yielding direct observations on wind direction, wind force and weather. They usually adopt a standardized vocabulary and system of recording. The documents provided the only official record of the voyage and they were needed also to assist in safe navigation. Their keeping was

an almost universal requirement of the military or merchant undertaking to which the ship belonged and many tens of thousands of logbooks are preserved in European archives, mostly in the UK (Wheeler et al. 2006).

Spatial and temporal data availability

The *spatial availability* of historical documents is strongly linked to the presence of well developed society with some interesting for written documents used by institutions to witness commercial exchanges, to report economic activities as the proceeds of the sale of agricultural goods or documents born to answer at the claims of a strong bureaucracy both civil than religious. However these institutions were not the only incentive to compile written documents, great part of the material came also from regions with long literary traditions, where it is easier to find works of single men of letters, that, drove by their personal initiative, due to the curiosity of knowing the natural and physical environment or due to the will to leave something of tangible to posterior, tested themselves writing chronicles or keeping the memory of extraordinary events based on eyewitness observations in annals or diaries. Clearly these conditions to have a good and active cultural substratum was not easy to find all around the world, above all going back in time. Great part of the documents nowadays available for this kind of climatic reconstruction studies come from Europe where cultures that followed one to another left always a rich soil for the development of documentary evidences. An homogeneous reconstruction of European climate is however difficult because, up to the present day, only a certain number of useful documentary evidences has been used in systematic historical-climatological investigations, these being mainly located in central-northern Europe and on South in Italy and Spain. This imbalance on spatial reconstruction is a problem that could be partially solved carry on a hard work to identify, validate and promote documentary sources in area still unexploited. A global coverage it will be however an hard task to solve because the geographical range and availability of documentary evidences is spread moreover in urban zones where institutional, cultural, framework or men of letters were present since the ancient times. For historical climatology an important role is also hold by the ship's logbook source that permit to enlarge the area taken in exam. The ship's loogbooks span the world's ocean and seas wherever trade and imperial interests took the ships of the age (Wheeler

et al. 2006) and extend the geographic range globally, penetrating even into the high latitudes for whaling and trade.

The potential of Italy. The spatial coverage of documentary sources in Italy is unprecedented because it is a huge, and in great part still unexploited mine of documentary sources, scattered in public and private archives and libraries: documentation here collected amounts to about one million parchments and eight million units of files, volumes, registers, logs etc., forming a incalculable number of pergamenaceous and papery single documents. The whole material takes up more than 1.200.000 linear meters on shelves. The most ancient pergamenaceous document dates back to 721; the earliest papery one dates back to 12th century. According to Alexandre (1987), 35% of all documents available for the Middle Ages in Central Europe are from Italy. Although documentary data are collected by CNR-ISAC since thirty years, only a minor part of written proxy has been gathered (Figure 2.1).

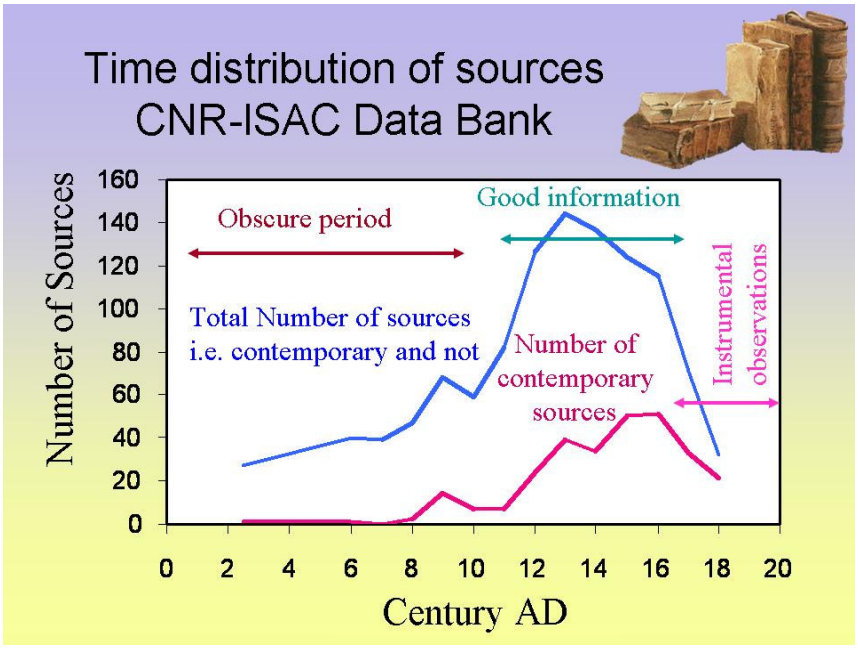

Figure 2.1: Time distribution of documentary sources data bank gathered in more than 30 years work performed by the CNR-ISAC Padua group (presented at Summer school, Catania 2009).

These are stored into a Data Bank including all information concerning usual and unusual weather (e.g. high or low temperature, dryness, rain, snow, hail, dry and wet fogs, winds), natural hazards (e.g. tornadoes, river flooding, large water bodies frozen over, earthquakes), climate features, strange phenomena (e.g. haloes, polar auroras) as

well as some astronomical observations (e.g. passage of comets, solar or lunar eclipses) useful to establish or to check a precise dating.

The way in which documentary proxy have been stored in the data bank contains more than the climatic information alone, it contains also a great preliminary work performed to analyse the sources and author reliability. The stored file contains the following information:

- Date of the event(s) as deduced from the document
- Revised and validated or likely date when different information concerning date were present
- Key words describing event(s)
- Bibliographical quotation
- Integral text describing events in original language (Latin,local variety of old Italian)
- Critical notes about the reliability of the author, the source, the dating style, the dating accuracy and other elements.

The documentary Data Bank is mainly concentrated on Northern and Central Italy, and includes 855,000 words, or 5 Million characters.

Concerning with the *temporal availability* of European documentary data, it is necessary to understand if sources are distributed continuously over centuries or only related to special events and to establish when documentary sources became reliable. Documentary data offer good potential for very long climate reconstructions in the time scale of one millennium. Earlier documents may extend back our knowledge, but with two main problems: they are rare and obscure, because going back in the time only the memory of major events has survived and this proxy is often mixed with interpretation, legends and myths. After AD 1000 the data became reliable and their accuracy and resolution increased over the centuries as evident in CNR-ISAC data bank too (Figure 2.1).

At *European scale* the documentary data starts with some records from the Byzantine Empire and the Carolingian Empire prior to AD 1000. In the temporal range AD 1000

to 1200 the documents are individual reports, in Italy for example numerous sources are in form of diaries, chronicles and annals and come from monasteries or areas with a strong religious presence (e.g. from Cassino or Orvieto). The reported information are focused mainly on astronomic items (solar and lunar eclipses, comets, aurora borealis), catastrophic items as descriptions of earthquakes and plague and in minor part concerning meteorological significant anomalies as floods, droughts, storms, frosting and snowing events. Analysing this predominant attention on celestial and catastrophic events it is possible to read the medieval spirit based on a theocentic vision of physical and natural phenomena (the chronicler's attention was focused on this kind of events because they were considered as an interpretative key of the God's wishes and understand them meant understand the environmental happening). During the temporal range from AD 1200 to 1500, continue the individual reports mainly on summer and winter with some reference to average conditions. In Italy during these three centuries there is an increasing interest for the climatic items that is inversely proportionate to the astronomic items that, going ahead in time, become more and more scarcely described. This change is due to the development of the man new renaissance mind. Already from the 14th century in fact, the thought becomes anthropocentric and the attention is moved on the man, author of his own history and therefore also able to understand himself the surrounding natural and environmental events. For this reason the renaissance man starts to describe and write down the climatic events with a real historical interest (Figure 2.2). The chronicles now become more reach of descriptions and from the 15th century, in Italy, there is also an increasing availability of institutional sources as the "Archivio Gonzaga" in Mantova.

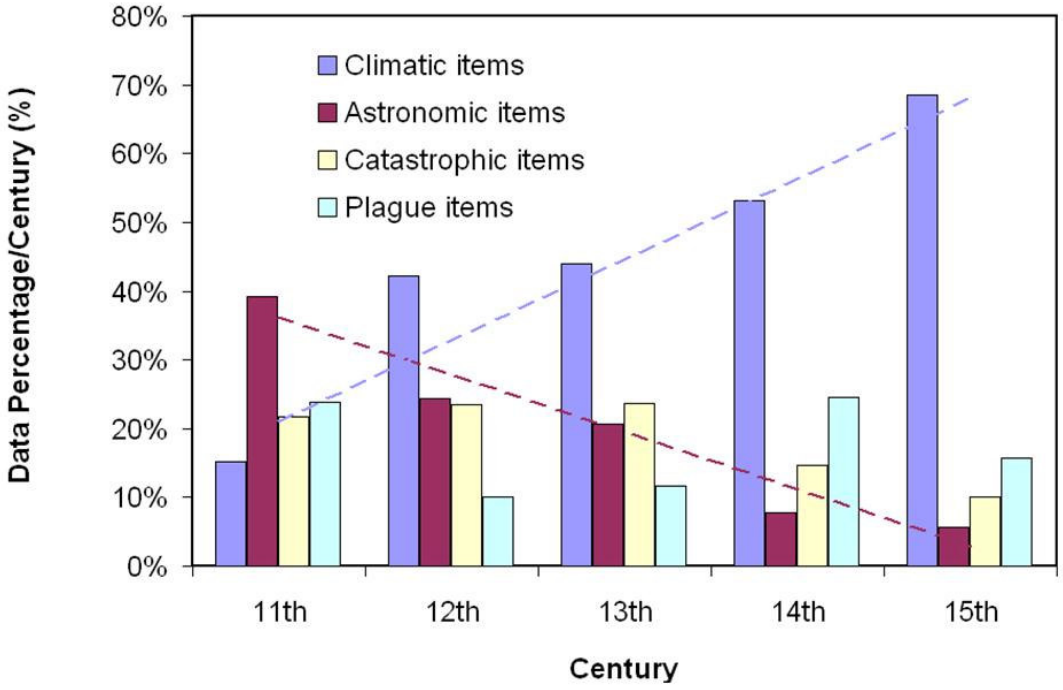

Figure 2.2: Interest for different items describing climatic, astronomic, catastrophic and plague events as reported in the chronicles during the Middle Age (11th-15th centuries). The data show an increasing interest toward climatic items to disadvantage of astronomic and catastrophic phnomena (presented at the Medieval workshop, Bern, Switzerland 6th-7th February 2009).

Since AD 1500 to 1800, there is an abundance of institutional sources and moreover the climatic descriptions in some area, reach the monthly and also the daily frequency (e.g. the Gennari's diary in Padua for the 18th-19th centuries).

Concerning with the temporal coverage for the areas of the Atlantic and Indian oceans where took place the commercial and economic interests of European conquerings, in literature it is possible to find works based on reports, letter and notes from the Spanish conquest in the early 16th century sent to the Crown, containing information on economically adverse extreme hydro-meteorological events. Finally the first ship's logbook of the Atlantic and Indian ocean crossings are dating from the mid-17th century (Wheeler at al. 2006).

The temporal availability of documentary sources needs to be understood in a cumulative way, i.e. older kinds of climate observations are not replaced but superposed by more recent ones. In sum, the quality of the data improves, their density and their time resolution increases and their spatial coverage extends over time.

2.2 Potential and limitation of documentary proxy

The first step to describe the potential and the limitation of documentary proxy is to define what is a good documentary proxy and what can be the uncertainties on such data. If we consider the classical natural archives, i.e. the classical proxy data, they are considered 'good' if:

- A proxy (e.g.. tree-ring width, stable isotope composition of ice) is *sensitive* to changes in environmental conditions (e.g.: temperature, precipitation, radiation, water table). A proxy dependent on many forcing factors is however difficult to be understood. It is necessary to select the cases in which a proxy can be more easily interpreted when the environmental dependence is reduced to only one limiting factor that may vary from site to site, e.g. for tree rings precipitation is the key factor on the border of a desert; air temperature is the key factor at high latitudes.
- A proxy should ideally be easy to find and naturally widespread (e.g. pollens, trees and sediments).
- A proxy can be calibrated (i.e. establish studies that provide *calibration* of the proxy in contemporary settings or across environmental gradients).
- A proxy "records or finger prints" climatic or biological information and preserves it for long periods of time (microbial life, ice, minerals, organic matter)

For potentially useful documentary data these criteria as well as the 'uncertainty' criteria (sampling, calibration uncertainty) are complemented or replaced by others. The exploitable due to the sensitive and the calibration of documentary proxy will be dealt in detail in the next chapter when it will be presented the methodology to analyse documentary proxy. Instead, here we stress attention on the difficult task of 'preservation'. To preserve a climatic information for a documentary proxy, means to preserve the whole written document. However, the information may survive even in the case the original document is destroyed. Document preservation results difficult first of all because over the centuries, many of them have been destroyed by fires, wars, floods, earthquakes, roditors and many others natural catastrophes or social-political

events. In second place the material in which handwritten documents were made, paper or parchment, that for their nature are easily perishable. A priori, it is difficult to know how many 'first hand' ancient documents have been lost during the centuries, an idea of some precious documents lost is however gave thanks to the witness of following chroniclers and men of sciences that sometimes wrote about ancient books looked up, read, or even, at best, copied giving us the possibility to know, date and cross-compare the most extreme climatic events of our primary sources during the last millennium. Since the Middle Age, in fact, this habit of copying in a same document, both an older, non contemporary, part deriving from ancient chronicles and a recent one written by the author himself, was deeply rooted. However, no information were given by the contemporary author about the document of his predecessor. In order to avoid the risk of spurious multiplication of meteorological extreme events it is important to take care and time for verifying if the documentary proxy taken in exam is a first hand source (i.e. contemporary, where the author, during his lifetime, could have been a witness of the meteorological event), or a second hand source quoted a posteriori with uncertain information.

Documentary Proxy Limitation:

The following drawbacks should be mentioned in documentary data respect to natural proxy data:

Most past attempts to climate variations in past centuries have used proxy data to reconstruct time series representing global or hemispheric mean temperatures or selected climate indices of phenomena such as the North Atlantic Oscillation (NAO) In some cases, the series, retrieved by low-resolution (decadal or centennial-scale) proxy records (Huang et al. 2000, Moberg et al. 2005) and used to reconstruct long-term trends, suffered of biases for the difficulty in properly calibrating proxy records against instrumental data (Mann et al. 2003, 2005b). Therefore it is preferable to reconstruct not just single time series but a spatially distributed set of local reconstructions of past climate variation, which can provide better insights of climate variability or the signatures of responses to particular climate forcings (Mann et al. 1998; Delworth and Mann 2000; Briffa et al. 2001; Shindell et al. 2001, 2003, 2004; Braganza et al. 2003; Luterbacher et al. 2004; Schmidt et al. 2004; Rutherford et al. 2005).

Another drawbacks is the extremely time consuming work related to extracting the climatic information from different documentary sources. The first step is looking for, finding and checking a substantial amount of documentary sources and to collect all the possible information to be sure of their high quality. This usually means to restrict ourself of working only with contemporary source ('first hand' source) where authors witnessed the events they describe or the events at least occurred during their life-time. Unlike, handling 'second hand' observations, which were copied from other documents or compilations, we have a certain probability to run against transcription errors especially misdating errors. In fact, before the printing invention, books were copied by hand (in particular during the Middle Ages this task was done by the monks). For this purpose manuscripts were frequently exchanged and as consequence, chronicles may have survived in a certain number of copies. Other uncertainties can derived also from the data (climatic information) extraction. This kind of limitations derives from the real difficult to read and understand the old handwritten document. This could be due to the bad state of preservation of the manuscripts (worn-out paper, fade inch,…) or to the difficult met to decode words meaning. In this last case the main difficulties could be the ancient language used as Latin, old French and English or the interpretation of the numerous regional dialects spread also in quite small area as the case of Italy. In this interpretative step of data extraction, the help of an Historian or an Archeologist is very important.

In this phase of data extraction one limitation could be due also to a wrong chronological interpretation. This aspect is the strongest potential point regarding documentary proxies, because, while other proxies as tree rings, ice core or terrestrial sediments have an hard-working process to date samples, e.g. through the carbon 14 dating, documentary data instead are dated by the authors themselves for the necessity to leave a reliable description and a temporal comparable proof of the extreme event just observed and present in some cases also an high temporal resolution. The limitation from which take care regards mainly the different calendars used in the past. The most known example is the difference of ten days that passed between the Julian style calendar and the Gregorian one that was reconciled in 1582 by Pope Gregory XII adopted in different time, so the 'old' and the 'new' style coexisted in Europe for many years. Furthermore, it is necessary to give attention at the beginning day of the year

because, in the Middle Ages, they were in use different calendars, linked to religious festivity and lunations. However these are not the only limitations. In order to transform the climatic information stored in written documents in an exploitable series with a good analysed signal, we must also solve bias concerning the discontinuous structure of the records e.g. descriptive documentary data limited by the observer life-length or documents produced by administrative routine during more than a hundred years old corporation life-length or bias given by the selective perceptions of different observers.

Documentary Proxy Potential

Documentary data has the following advantages in relation to natural proxy data:

The first strength of documentary proxy is the opportunity they offer to study climate prior to the availability of early instrumental observations as temperature and precipitation and they are the only evidence that is directly related to the socio-economic impacts of rare but significant disasters such as intense storms, severe floods, and long-lasting droughts in this period. The ancient climatic records obtained by documents are particular interesting because they are best dated and most sampled over the last thousand years, when the climatic change were driven into the range of natural climatic variability prior to the influence of the antropogenic activities.

The second strength point is that documentary data are the only kind of palaeoclimatic data that are based on direct observations of different meteorological parameters as air temperature, precipitation, snow-cover, sea ice distribution, cloudiness, wind and lake levels. Instead natural proxy, as tree rings, respect to documentary proxy, not always yield a distinct separation of the effects of temperature and precipitation (Bradley, 1999) and cannot be broken down to seasonal or monthly resolution. The high resolution advantage, needed for investigating climatic impacts on societies, is instead naturally given by documentary proxy that have a good chronological cover that spread from seasonal resolution until monthly and in some cases also daily resolution.

Moreover, for their nature, documentary proxy are focused on anomalies and natural disasters because, being written by men, they quoted all the most impressive events which they were present.

Chapter 3:

Methodology of Climatic Analysis based on Documentary Proxy: a Case Study

Contents

3.1 Site selection and data collection
3.2 Indexing and Dating
3.3 Calibration and Verification
  3.3.1 Calibration and Verification: open questions and their statistical background
  3.3.2 Calibration and Verification: our method
3.4 Reconstruction and uncertainties
3.5. Large-Scale Surface Temperature Reconstruction: the case study results

In the previous chapter we told that a proxy is potentially useful when is sensitive to changes in environmental conditions and when it can be calibrated in contemporary settings or across environmental gradients.

In this chapter we present and analyse the methodology mostly in use in the Scientific Community to perform climatic analysis based on documentary proxy data (DP). We introduce the methods of analysis bringing forward a case study born by the research work of our group. During these years of PhD, in fact, a big work based on large scale temperature reconstruction in the Mediterranean Basin by means of documentary data and instrumental observations (IO) was performed. The results presented in this chapter have been submitted in a Special Issue on the European climate at the Climate Change international Journal and now are in the review phase. This special issue has involved all the scientific community of the 'instrumental and documentary archives' of the European project Millennium. The Millennium project, financed by European funds, is a multidisciplinary consortium of more than 39 European Universities and Research Institutes with the Single Objective of quantifying whether the magnitude and rate of

20th Century Climate Change exceeds the natural variability of European Climate over the last Millennium (Figure 3.1).

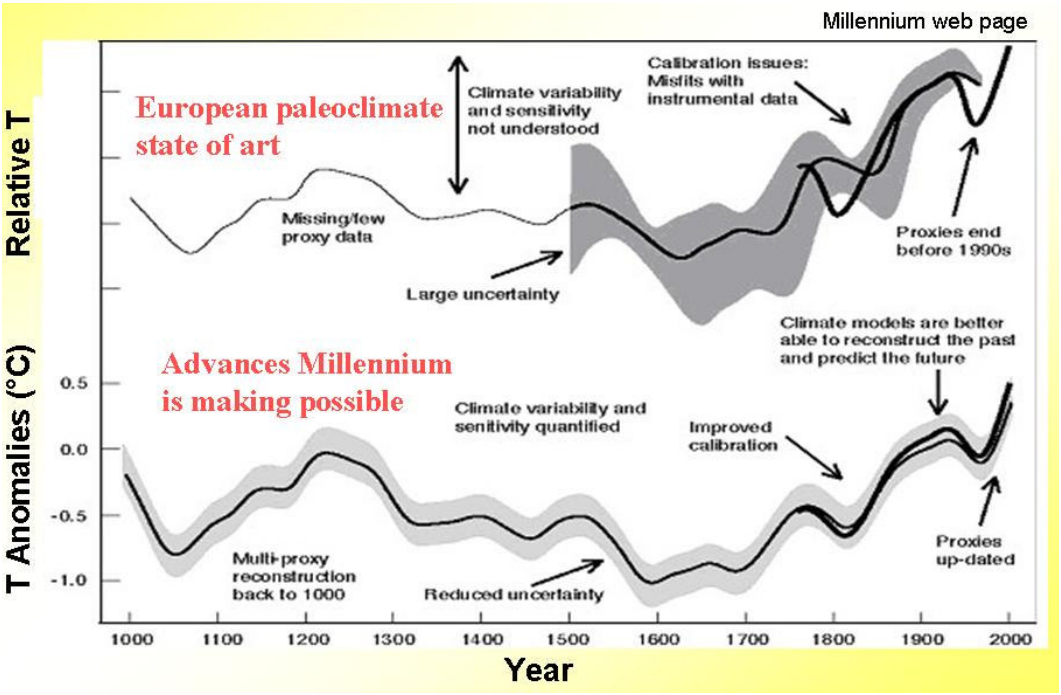

Figure 3.1: The quantificable advancements that European Millennium project is making possible in term of multiproxy reconstruction, reduced uncertainty and improved data calibration.

The project is organised in eleven sub-groups. Each sub-group will make significant advances beyond the state of the art in their own competence. Italy takes part in this project through our institute: the Institute of Atmospheric Sciences and Climate (ISAC) of the National research Council (CNR). Our work into the project is under the sub-group concerning with 'Instrumental and documentary archives' in the time scales 100, 500 and 1000 yr for the Italian and Mediterranean Area.

The process of reconstructing climate records from proxy data is essentially a statistical one. Statistical techniques are used to define the relationship between the proxy measurements and the concurrent instrumental record. Then this relationship is used to reconstruct past temperature or precipitation variations from the remaining proxy data (Fig.3.2). There could be variations in the way in which these methods are applied to different proxies and variations in the way that different research groups apply these methods. Although these different methodologies give different statistical weight

results, the method to reconstruct climatic variables, as temperature, over the last millennium follows the same necessary steps as described below:

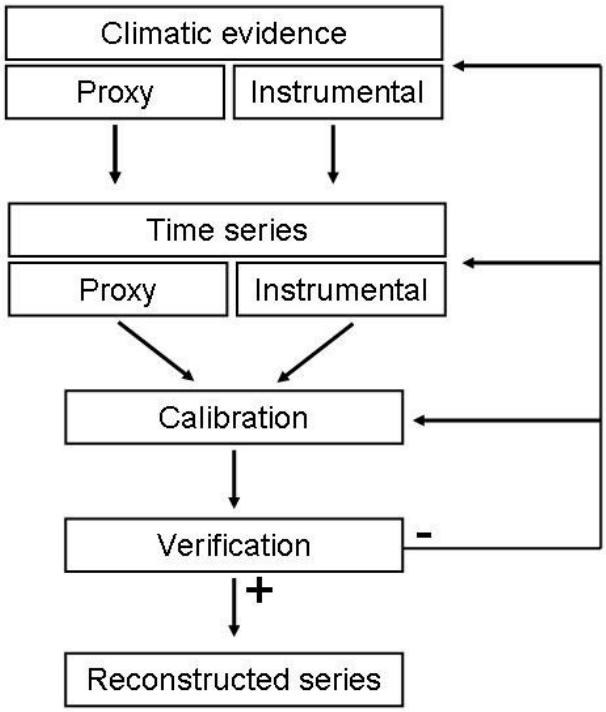

Figure 3.2 Schematic diagram of the general methodology used to reconstruct past climates (Brazdil, Springer-Verlag 2002).

3.1 Site selection and data collection

This preliminary phase regards the choice and the sampling of the particular site and documentary proxy to be used for the reconstruction work. In principle, DP and site selection should be based on an understanding of the physical (DP with information concerning snow fall and cover, freezing of water bodies, etc.), socio-economical (DP as plant phenology, with information on time of grain and vine harvest, etc.) or man observed processes (DP with descriptions of anomalies, natural hazards, weather situations, etc.) that determine how the chronicler that wrote documents reacted to local environmental conditions. In practice, the relationship between the proxy and the climate variable of interest is not exactly known but it must to be established taking into account both the mentality and the popular misconception of that time and the normal and extremes local environmental conditions of the sites taken in exam in order to evaluate the DP with an objective and valuable technique. While looking for sites the

choice is driven by places where proxy records are as long, continuous, and representative of the target climatic variable as possible.

3.2 Indexing and Dating

Once the long preliminary phase of site selection and data collection is concluded, a second phase of proxy dating and indexing starts. A big effort is required to transform DP into numerical indexes and obtain a quantitative evaluation of the local trends in temperature over the last 500 years. All DP series produced within Millennium, have been classified following the same procedure, i.e. each documentary proxy has been transformed into a numerical value x_i that has been then refinished by comparing it with the variability that is known from the instrumental observations.

The intensity of the numerical value attributed to the proxy is assessed on the ground of some effects that may help to understand the severity of the events. However, in the pre-calibration phase, two kinds of difficulties were found when indexing DP. The first was qualitative, i.e. to establish a clear correlation between this index and a meteorological variable; the second was quantitative, i.e. to transform the DP into a numerical index. Concerning the quality, data were selected only when the link was clear. For instance, the thickness of the ice slab exceptionally formed in the cold season on large water bodies helped to classify winters into severity classes, but this needs a careful interpretation for the context is changing with space and time. As example, let us consider a water body freezing over. A closed water body –e.g. a lake with small exchange of waters – has a cumulative effect and it may form slabs of ice after water has lost enough heat. It cannot freeze simply because the winter was long, but it needs two or three weeks of very intense cooling, possibly worsened by fresh wind, to freeze over. Not all the most severe winters had simultaneously frozen over both lakes and the Venice Lagoon. Figure 3.3 shows the result on the freezing of Venice Lagoon over the last Millennium as obtained studying documentary proxy data (Camuffo and Enzi, 1992b).

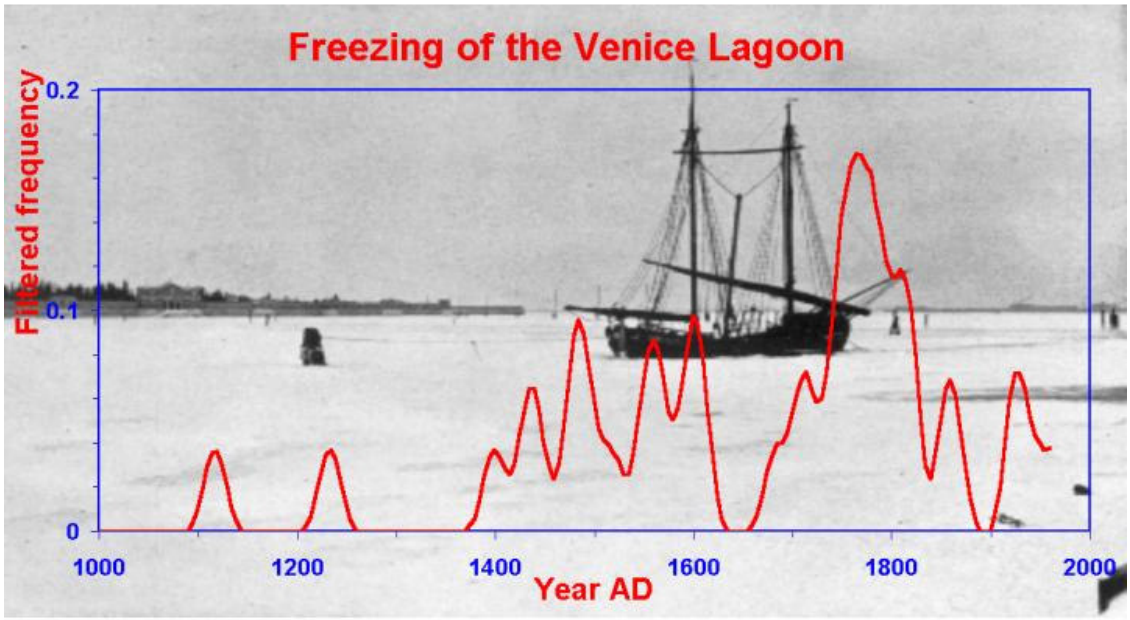

Figure 3.3: Example of extreme cold quantitative assessment, lasting for weeks on the Venice Lagoon. In the picture the 1928/29 winter: the most severe Great Winter in the past century

In the old times rivers flowed along the countryside forming marshes of stagnant water where ice slabs were easily formed and later transported by the current until they were eventually stopped at some bend, forming an ice bridge that soon extended from an embankment to another. This mechanism disappeared after regular riversides were cared to remove marshes and provide a better flow and protection. In practice, in the course of years, the same river needed a different cold threshold to freeze over. In conclusion, not always the same cause generates the same effect. DP provide information that depends on the particular nature of each phenomenon and its environmental context, variable over the course of time. The DP classification may differ a bit from country to country, depending on the critical thresholds that make exceptional or recognizable each event.

A list of numerical indexes and the relative description of event severity for temperature is given in Table 3.1.

Table 3.1. Temperature indexing from qualitative descriptions of Documentary Proxy (DP). This index has been used for all the Mediterranean localities.

Index	Comments
+3	Extremely hot – Not applicable for winter, very hardly for summer. Not easy to establish on a objective ground, often mixed and confused with dry and arid, especially in the summertime.
+2	Hot – Not applicable for winter, hardly for summer. Many people die, but possibly for epidemics; reduced yield or damage to crops probably connected with aridity.
+1	Warm. Applicable for hot summer: index established after (subjective) complaints from a number of witnesses. For mild winter: early plant growing and flowering, early migratory bird arrival.
0	Normal. Situation as usual, no special comments; sometimes, declared "normal" in the sources
-1	Cold. Complaints for unusual cold and need for heating or heavy clothing; some damage to local agriculture.
-2	Severe cold. Applicable for severe winters, hardly applicable for summer. winter: People, animals and plants killed for cold. Slab of ice cover large water bodies (including the Venice Lagoon) usually free. summer: continuous cloud cover and rains, almost never sunshine.
-3	Extremely severe cold. Applicable for great winters, not applicable for summer. In addition to the above descriptions, wine freezes into the barrels, springs and wells frozen over, rivers, lakes and other large water bodies completely covered with a thick slab of ice, supporting carriages and people walking on it.

This tables help to transform each DP into a numerical level xi, in quantitative terms, which ranges from -3 to +3, 0 being the normal. This is the first-order individual classification made by reading the descriptions and judging from the effects and called indexing. An example of this first order indexing classification for Winter in Northern-Central Italy over the last 1000-year is given in Figure 3.4.

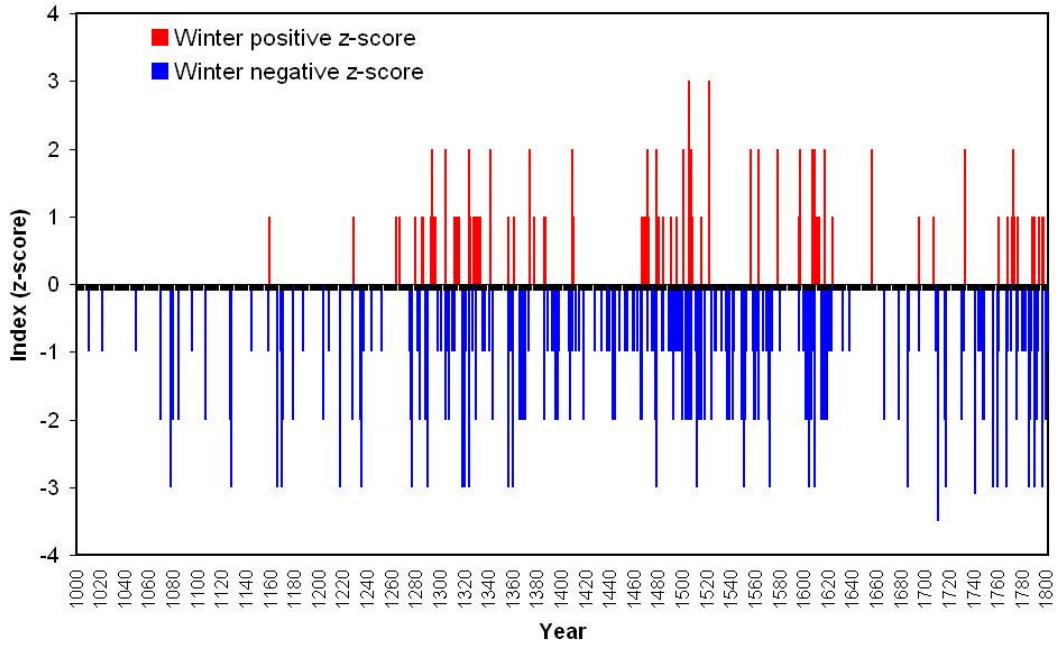

Figure 3.4: Indexing reconstruction of Winter temperature anomaly from documentary proxy data for Northern-Central Italy. Conceptually, this figure in terms of index reconstruction is equal to a temperature anomaly plot during the centuries. Indexing is based on the scale reported in Table 1, where zero is referred to a "normal" situation as observed by that time chronicler, in a similar way, the zero used in temperature anomaly plots refers to a arbitrary period, standardized assumed as the thirty-year period 1961-1990. The Mediaeval period 1000-1500 shows an increased density of information starting from 1200-1300.

In the pre-calibration phase another important step is to synchronize the individual proxy records for plotting them on a common time axis. Time histories derived from documentary proxy from different author describing the same area may also be averaged or spliced together to construct longer and more representative proxy records. To obtain a good and well representative proxy series of a certain period and geographical area, it is necessary first of all to establish how much the documentation is complete and how many events are missing. These tests on the data completeness, at the same time, help to perform a good dating of the proxy taken in exam. The way to proceed can involve different fields of action as follows:

- **History**: An observable, more probably exceptional event should be repeated by a number of independent observers. Although not always we can establish if the observers were really independent or if some event was not recorded for an unknown reason, cross comparison of contemporary chronicles are very useful both for dating the events and check the fullness of the material taken in exam.

- **Instrumental records**: Cross comparison with regular instrumental records, when available, are a useful mean to verify if some extreme events were lost or not recorded by chroniclers or to correctly date the year of the proxy.
- **Astronomy**: Celestial events (e.g. eclipses, comets) are another useful chance to test both the completeness of our database and to help us to give the correct temporal dimension at the proxy. Sun, lunar eclipses, or comet entry can be calculated and then check if they have been actually observed (Figure 3.5). The possibility of a lack of observations due, for example, to adverse sky condition, is however hard to evaluate a posteriori.

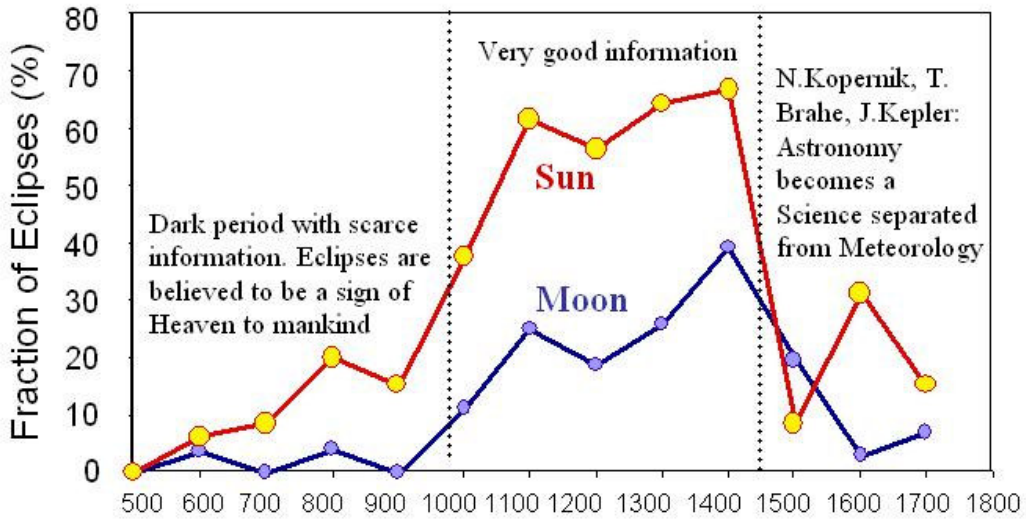

Fig.3.5: Check of precision and completeness of our data bank, controlling information of partial and total, Solar and Lunar Eclipses. Comparison is made between our proxy and the Canon of Eclipses. In the period AD 1000-1499 the percentage of observed Solar eclipses with exact and complete dating is extremely high, if we consider the fraction of time the sky could be obscured by clouds or the difficulty to observe partial eclipses at naked eye.

3.3 Calibration and Verification

In documentary proxy analysis, the bound step is typically to separate the period of instrumental measurements into two segments: a calibration period and a verification period. The statistical relationship between proxy data (expressed in form of index) and instrumental measurements of a climate variable (e.g., in our case the surface temperature) is determined over the calibration period. Past variations, including those during the validation period, are then reconstructed using this statistical relationship to predict the climatic variable from the proxy data.

Resolving the numerous methodological differences and criticisms of documentary proxy reconstruction is beyond the purpose of this chapter, but we will address some key issues related to temporal correlation, the use of principal components, and the interpretation of validation statistics. As a concrete example, the case study presented in this chapter will focus on seasonal and annual mean surface temperature reconstruction for the Mediterranean basin. However, the basic principles can be generalized to other meteorological variables.

Calibration - The aim of calibration is to determine the relation (transfer function) between the proxy index (predictor) and the instrumental observations (predictand) for the overlapped calibration period in which both values (proxy and instrumental) of the meteorological element are available. For reconstructing a series of temperature from proxy data, the Calibration is the same of placing a temperature scale on the "proxy thermometer." This step typically involves the use of independent data and a statistical technique called linear regression.

Verification – The role of a verification period is to provide an independent assessment of the accuracy of the reconstruction method. The linear regression coefficients derived from the calibration are used to reconstruct the temperature time series from the proxy data during a different verification period, and the reconstructed temperatures estimated from the documentary data are compared with the corresponding instrumental temperature record. An inherent difficulty in validating a climate reconstruction is that the verification period is limited to the historical instrumental record, so it is not possible to obtain a direct estimate of the reconstruction skill at earlier periods. Because of the autocorrelation in most geophysical time series, a validation period adjacent to the calibration period cannot be truly independent; if the autocorrelation is short term, the lack of independence does not seriously bias the validation results.

3.3.1 Calibration and Verification: open questions and their statistical background

In order to focus the attention on the importance of calibration to perform a good temperature reconstruction it is necessary to analyse some open questions concerning

documentary proxy and the way to translate them in term of a statistical problem that help us of searching for a best calibration approach.

1. In documentary proxy, it is difficult to find a statistical way to evaluate the value 0 of the index scale (see Table 3.1) and place it in a scale of temperature values. This difficult arises with the definition itself of the index 0 that is "normal" situation or event and so it is strictly related to the way of perceiving an extreme event or the cold and hot sensation of the chronicler and above all being normal it is less documented too. The question that remains unsolved is: The "normal" way of perceiving meteorological parameters in 11th century, for example, is the same of 14th century and above all is comparable with nowadays zero in anomaly? Looking at Figure 2.2 in previous chapter it is clear as mentality, beliefs and man interests have changed during century, and the perception of meteorological events.
2. From a statistical point of view it seems correct to calibrate documentary proxy with instrumental observation in the overlapped period, however, while this is correct for natural proxy where the environmental dependence is reduced to only one key factor that varies and can be measured, for documentary proxy, some doubts remain. In fact though documentary data are the only paleoclimatic data based on direct observations of meteorological parameters in terms of narrative description, they are strictly dependent to chronicler life experience and interpretation. The focal point is to understand if it can be right to use the transfer function obtained from the calibration, made at best with proxy deriving from 17th-18th centuries writing, to reconstruct the temperature series beginning from indices obtained by 11th-16th centuries chroniclers. Is it the same thing that apply the way of thinking of a Renaissance men to a Medieval one?
3. A similar bias is difficult to recognize because the verification period that had to define the statistical goodness of the calibration, in fact it is based on a time period bordering with that of calibration and therefore with the higher probability to have documentary proxy coming from a same cultural substratum. Moreover the rather short lengths of both calibration and verification period

respect the full period of proxy data reconstruction is another problem that must be solved.

When the linear regression is used to calibrate and validate proxy, the first two open key questions, summarized as: (1) How is the proxy related to the climate variable? And (2) Is this relationship consistent across both the instrumental period and at earlier times? can be addressed, from a statistical point of view, with the assumptions of linearity and stationarity. The definition of these two assumptions is the following:

Linearity is the assumption of a linear statistical relationship between the proxies and the expected value of the climate variable exists.

Stationarity is the assumption that this statistical relationship between the proxies and the climate variable remains the same throughout the calibration period, validation period, and reconstruction period.

An illustration of methodology based on linear regression with linearity and stationarity conditions, to reconstruct temperature from proxy, is given in Figure 3.6. In this graph are plotted a hypothetical annual series of proxy data and corresponding instrumental surface temperature measurements over a 100-year calibration period. The solid black line is the linear fit to these data, or the calibration, which forms the basis for predictions of temperatures during other time periods. Here the prediction of temperature based on a proxy with value A is T_A and the proxy with value B predicts the temperature T_B. The curved blue lines in Figure 3.6 present the calibration error, or the uncertainty in predictions based on the calibration which is a standard component of a regression analysis. In this illustration, the uncertainty associated with temperature predictions based on proxy data is greater at point A than it is at point B. This is because the calibration errors are magnified for predictions based on proxy.

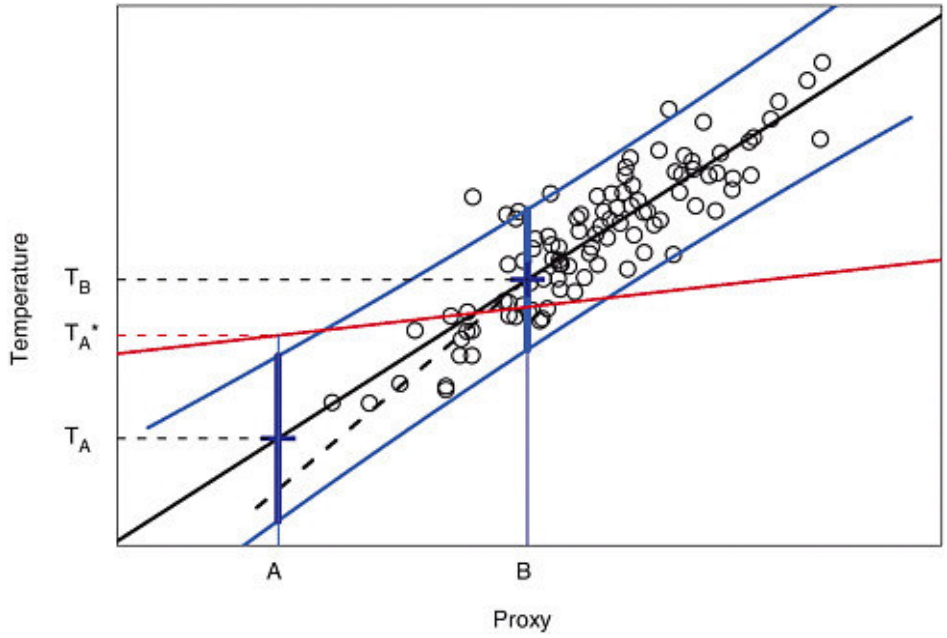

Figure 3.6: An illustration of using linear regression to predict temperature from proxy values. Plotted are points of a hypothetical dataset of proxy observations and temperature measurements. The solid black line is the linear regression line and the blue lines indicate 95 percent prediction intervals for temperature using this linear relationship. The dashed line and the red line indicate possible departures from a linear relationship between the proxy data and the temperature data. The figure also illustrates predictions made at proxy values A and B and the corresponding prediction intervals (wide blue lines) for the temperature.

We describe some possible errors that could be made during the calibration period if linearity and stationarity assumptions are not strictly kept and we describe the open question 3 from a statistical point of view. All the examples of departures are made looking at Figure 3.6.

Variability in the Regression Predictions. Strictly speaking, linearity assumption gives a straight-line relationship between the average value of the climate variable, given the proxy, and the value of the proxy. This detail has the practical significance of potentially reducing the variability in the reconstructed series. For example, in Figure 3.6 it is possible to note some variability in the instrumental temperature measurements at the proxy value B (i.e., near point B, there are multiple temperature readings, most of which do not fall on the calibration line). However, estimates of past temperatures using proxy data near B will always yield the same temperature, namely T_B, rather than a corresponding scatter of temperatures. This difference is entirely appropriate because T_B is the most likely temperature value for each proxy measurement that yields B. In general, the predictions from

regression will have less variability than the actual values, so time series of reconstructed temperatures will not fully reproduce the variability observed in the instrumental record.

Departures from the Assumptions. they can be of two types, a departure from linearity or from stationarity. The first case, is presented in Figure 3.6 with dashed line that represents a hypothetical different linear correlation between proxy and instrumental data. This illustrates a violation of the linearity assumption because, for lower values of the proxy, the relationship is not the same as given by the (straight) linear regression line. Therefore, if the dashed line describes a more accurate representation, following this different linear relationship, it will be obtained a different reconstructed temperature series. The second case, the departure from stationarity is illustrated instead by the red line in Figure 3.6. Supposing that in a period other than the calibration period, the proxy and the temperature are related on average by the red line, that is, a different linear relationship from the one in the calibration period. For an accurate reconstruction, it should use this red line and its estimate, at the proxy value A, for the temperature (i.e. T_A* in the figure).

Regression with Correlated Data: we address the last open question described before as: (3) Is the calibration linear equation, based on proxy and instrumental data sequential in time, statistically useful for the reconstruction in no adjacent periods?

In most cases, calibrations are based on proxy and temperature data that are sequential in time. However, geophysical data are often autocorrelated, which has the effect of reducing the effective sample size of the data. This reduction in sample size decreases the accuracy of the estimated regression coefficients and causes the standard error to be underestimated during the calibration period. To avoid these problems and form a credible measure of uncertainty, the autocorrelation of the input data must be taken into account.

From a statistical point of view, now, we want to address the last open question on the idea and the statistical background that was useful to us to find a new approaching method for calibration and verification. The focal point to take into account, is that

linearity and stationarity hypothesis, assumed in the linear regression approach, to a proxy reconstruction, do not fit during the temperature reconstruction step because both temperature and proxy values, out of the calibration and verification period, are not controllable. In our opinion, a more useful model to solve this problem is instead to consider the index obtained by documentary proxy and the temperature data as a bivariate observation. Now the statistical solution to the reconstruction problem is to state the conditional distribution of the unobserved part of the pair, temperature, given the value of the observed part, the proxy. If the bivariate distribution is Gaussian, then the conditional distribution is itself Gaussian, with a mean that is a linear function of the proxy and a constant variance.

3.3.2. Calibration and Verification: our methodology

In this section we describe the calibration and verification steps followed in the 500 years of temperature reconstruction of the Mediterranean area. In the climate of the Mediterranean in general, and of Italy in particular, indexing, i.e. the first-order individual classification made by reading the descriptions and judging from the effects for usual temperature variability, is an hard task. The problem is that temperature does not constitute a serious risk for agriculture, sailing or other social activities, so that there is no special reason to mention in historical documents that this variable have exceeded its usual range. In this way, modest and less modest departures from the average pass unobserved, except for some very exceptional events, the most typical of them being e.g. winter severity killing people and freezing over water bodies or unusual snow killing flocks of sheep. Extreme meteorological events in form of natural hazards are much better documented and constitute the best information in this context. However, within the EU project Millennium, an effort was made to transform the narrative descriptions and the documentary sources concerning temperature into numerical indexes in order to obtain a quantitative evaluation of the climate change that has occurred up to the last 1000-year period. After this first-order classification is concluded (see Figure 3.4 for Winter season in Northern-Central Italy as example), in order to make stronger the calibration and verification phases we search for a second-order ensemble classification. As told before, we consider the index obtained by documentary proxy and the temperature data as a conditional distribution, approximated to a Gaussian. This last hypothesis is quite reliable because the population of each class of

indexes, theoretically, should reflect the Gaussian distribution as well as the temperature distribution. The Gaussian distribution for documentary proxy is classified in Table 3.2 and is visible in Figure 3.7, with frequent normal events, less frequent severe, and very rare exceptional ones.

Table 3.2. Classification in terms of Standard Deviation (SD) obtainable from the scatter of data.

Index	Type	Classification	Population (% of total data)
+3	Extremely high	x_i > 2 SD	2.1
+2	Very high	1 SD< x_i <2 SD	13.6
+1	High	0.5 SD< x_i <1 SD	15
0	Normal or no comments	-0.5 SD< x_i <0.5 SD	38.3
-1	Low	-0.5 SD< x_i <-1 SD	15
-2	Very low	-1 SD< x_i <-2 SD	13.6
-3	Extremely low	x_i < -2 SD	2.1

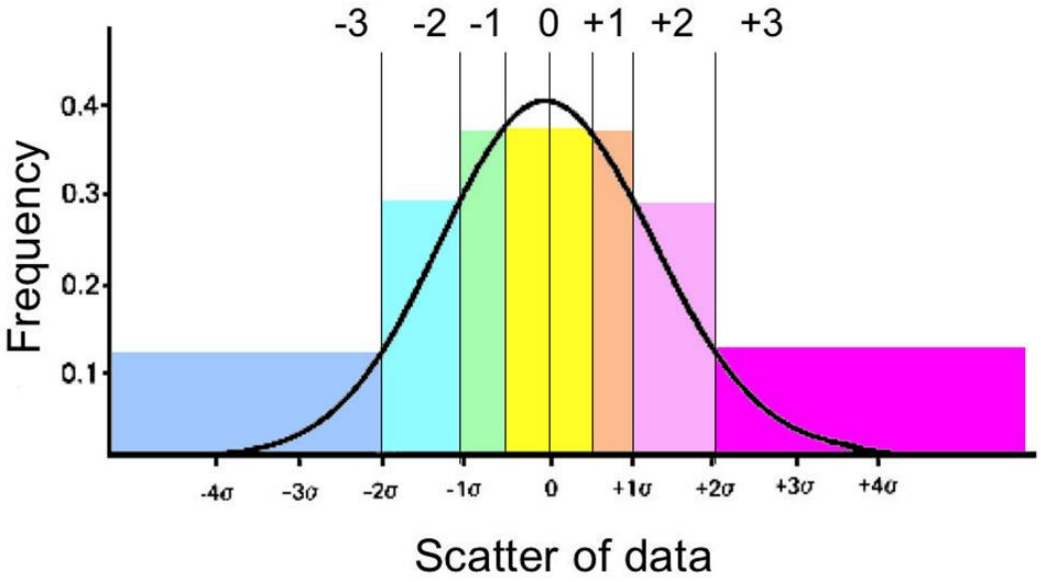

Figure 3.7: The climatic fluctuations are subdivided by classes to obtain indexes. Example for a Gaussian Distribution and quantitative indexing.

Events are classified in terms of standard deviation (SD) into 7 intervals, bound by + 0.5 SD, +1 SD, +2 SD or external (see Table 3.2). If we impose that the frequency distribution of numerical level x_i (derived by DP indexing) should be the same as instrumental observations, this leads to a further improvement of the indexing levels (x_i). Now, it is possible to express the index, in terms of temperature (°C). As told

before, when a period is simultaneously covered with both DP and IO, it can be used for calibration and verification. Following our working method, it is sufficient to impose that both DP and instrumental observations have the same distribution, i.e., the same range, mode and standard deviation following in this way the key assumption of linearity and stationarity.

In a Gaussian distribution, the mode coincides with the average and the 50 percentile and may become the Zero reference of some selected periods (e.g. 1961-1990) when computing the anomaly. This is simple with instrumental observations, less easy with DP. The mode is the typical, most frequent value that contemporary witness considered "normal"; therefore, in documentary proxy it is also the less documented level and cannot be coincident with our 1961-1990 averages. Temperatures below the "normal" were perceived as negative (e.g. cold), above positive (e.g. warm) and this situation is reflected in the numerical values of indexes too. Per each proxy, our aim was to establish a scale that give back the correct distribution of the indexed variable, as we know it today, in modern units. The distribution of temperature is generally Gaussian. A problem is with DP, because the human factor may increase skewness, making emphasis towards the most dangerous events. In summertime too much hot may be the problem, in winter too much cold. These extremes have been quite well documented for their negative impacts on the territory and the society; on the other hand, their opposites (i.e. mild summers or winters) are less dangerous and less documented. Unfavourable extreme events, which have caused severe damage or social trouble, have a higher probability of being recorded compared with less relevant events that had a minor impact. For this reason we proceeded as follows. First we tentatively applied a temporary index based on the documentary text. Then we ordered all of these indexes from the smallest to the largest one and expressed them in a percentile form. In the case of a Gaussian distribution, the 2.1 percentile corresponds to -2 SD, 13.6 percentile to -1 SD, 50 percentile to the average, 86.4 percentile to +1 SD and 97.9 percentile to +2 SD. The application of Table 2 makes easy classification. As positive and negative values, e.g. hot and cold, are derived from different phenomena and suffer a different perception, it was useful to operate separately for positive and negative values.

The unknown level of the SD of documentary proxy was associated to the known one from instrumental readings. In this way we calibrated our series and passed from

arbitrary values to an evaluation in °C for temperature. In the case the local instrumental observations had the same SD for both positive and negative values, i.e. a symmetrical distribution, the same was kept for the DP; in the case the instrumental observations was skew, the same skewness was applied to the DP too. By applying to DP the standard deviation observed with instrumental observations per each geographical area, the indexed data were corrected for the bias of the old time writer.

3.4 Reconstruction and uncertainties

The regression algorithm developed in previous step (i.e. Calibration and Verification) is applied to the proxy data that are available prior to the instrumental record (in the paper presented here, the span is 1500-1653) to extend temperature reconstruction back in time. Error bars are assigned to the reconstruction based on how well it matches the observed surface temperature variations during the validation period. In general, the width of the error bars will vary in time according to the quantity and quality of available proxy evidence. From the previous sections, we know that standard proxy reconstruction, based on linear regression, is generally reasonable statistical method for estimating past temperatures but may be associated with substantial uncertainty. There is a need for more rigorous statistical error characterization for proxy reconstructions of temperature that includes accounting for temporal correlation. The variability of proxy reconstructed temperatures in fact will be less than the variability of the actual temperatures and may not reproduce the actual temperature pattern at particular timescales. This is due to some intrinsic drawbacks:

Length of overlapped period: The length of the overlapped period between proxy and instrumental data sets limits on a statistical assessment of the uncertainty in the reconstruction. Most critically, the relatively short instrumental temperature record provides very few degrees of freedom for verifying the low-frequency content of a reconstruction.

Index subdivision scale: The assumption concerning the subdivision of documentary proxy evaluation in an index scale of seven unit, will return the predictions from regression with less variability than the actual values, so time series of

reconstructed temperatures will not fully reproduce the variability observed in the instrumental record.

Adjacent time period: Within the calibration period, the fraction of variance of temperature that is explained by the proxies naturally decreases as the noise level of the proxies increases. If the regression equation is then used to reconstruct temperatures for another period during which the proxies are statistically similar to those in the calibration period, it would be expected to capture a similar fraction of the variance.

An indication of the uncertainty of a reconstruction is an important part of any display of the reconstruction itself. The prediction mean squared error is the square of the standard error and is the sum of two terms. One is the variance of the errors in the regression equation, which is estimated from calibration data, and may be modified in the light of differences between the calibration errors and the validation errors. This term is the same for all reconstruction dates. The other term is the variance of the estimation error in the regression parameters, and this varies in magnitude depending on the values of the proxies and also the degree of autocorrelation in the errors. This second term is usually small for a date when the proxies are well within the range represented by the calibration data, but may become large when the equation is used to extrapolate to proxy values outside that range.

In order to make some practical example, we describe the reconstruction steps of our analysis performed on the Mediterranean area.

In our work, proxies and instrumental observations have been homogenized with each other thanks to a calibration and verification made on a overlapped common period (i.e. 1654-1780) following the methodology described in the previous sections. DP have been adjusted to instrumental observations and benefit of the same standard deviation found for instrumental data, either symmetrically or skewly distributed. In the latter case two standard deviation are used, i.e. one for positive and one for negative values. However, despite all our efforts, a DP noise level persist respect to instrumental observations. An example is shown in Figure 3.8 where indexed DP and IO winter temperature are reported from 1716 to 1800 together with their Hamming filters.

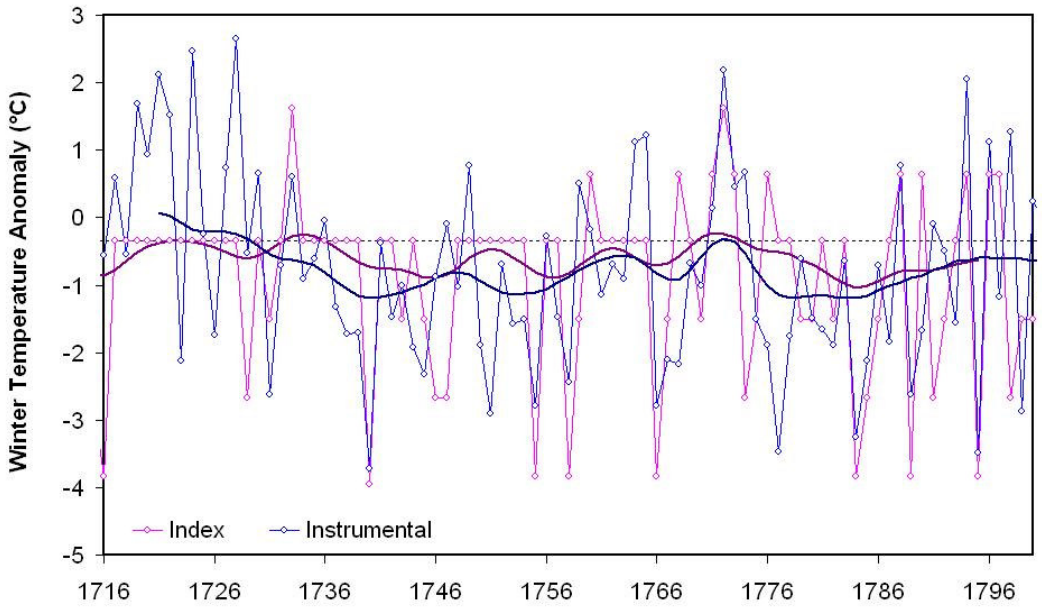

Figure 3.8: Difference in climatic signal reconstruction by the comparison between Proxy reconstructed signal and Instrumental temperature anomaly in Northern-Central Italy for the overlapped period: 1716-1800. Pink thin line is signal reconstruction coming from index and blue thin line represents the temperature anomaly coming from instrumental observations; thick lines represent the hamming filters.

In Figure 3.8 both Hamming filters are almost parallel with each other showing that the signal is reasonably provided, with 0.5°C average difference. Most of the individual points provide similar information, but in some cases, e.g. 1768, 1776 and 1777, the DP departs too much from the instrumental observations. When a period is not documented, this is considered a gap in knowledge, i.e. no information. However, when a period is generally well documented and the old time authors missed to report relevant weather information, the index is automatically interpreted as a zero, i.e. a normal situation, as shown in Table 3.1. This justifies the high number of “normal” events in the indexing. In general this is a correct procedure, but sometimes it may be misleading. As told before, another problem is the true zero DP level. DP cannot be expressed in terms of absolute quantitative level, which means no possibility of establishing trends or expressing them in terms of anomaly with respect to a given period as 1961-1990. In the case of instrumental observations continuing till nowadays this is very simple. However, things are different for DP because the writer living centuries ago noted some events because he judged them 'anomalous' or 'exceptional' making reference to his experience and time. DP are intimately referred to their contemporary period, with a floating zero reference level. In our graphs the DP zero has been established to be

coincident with the average of the whole available period of instrumental data (i.e. the average anomaly of all available instrumental observations). This choice, although arbitrary, avoids unjustified jumps in level when passing from DP to instrumental observations. So, the records that we got superimposing DP and IO are useful to improve our knowledge about the Little Ice Age (LIA) but remain not completely homogeneous. From the mathematical point of view, a filter should be applied to strictly homogeneous and continuous series. Whatever effort of calibration and validation we can do, DP and instrumental observations preserve some differences in nature and have a slightly different confidence level (e.g. DP potentially missing or contradictory data, as discussed above). For this reason we prefer to keep distinguished DP from instrumental observations showing them, in the graphs, with different colours because the nature of each signal is slightly different. Moreover we assign to DP, as estimated error, the mean of the signal difference between instrumental observations and proxy, besides the estimated instrumental error. All these error bars are quoted on the graphs.

3.5. Large-Scale Surface Temperature Reconstruction: the case study results

Several surface temperature reconstructions carried out since the mid-1990s involve the synthesis of data from many different locations, often coming from disparate documentary sources. Chronicles, diaries, annals or administrative and cultural documents as the rogation ceremonies commissioned by local communities to the Church infer patterns of temperature variations over large geographic areas. The methodology used to carry out these large-scale surface reconstructions is broadly similar to the methodology described in the preceding section, but modified in the following ways. There are two general approaches that are commonly used to perform the calibration, validation, and reconstruction steps (see Figure 3.1) for large-scale surface temperature reconstruction. In the first approach, proxies are calibrated against the time series in the instrumental temperature record and the results are combined to yield a time series of large-scale average temperature. In the second approach, the individual proxy data are first composite and then this series is calibrated directly against the time series of large-scale meteorological variables variations. In our work

we have followed the second large scale reconstruction approach as we explain in detail later.

Both the number and the quality of the proxy records available for reconstructions decrease dramatically moving backward in time. At present very few annually resolved proxy time series are available for A.D. 1000. Although it is true that fewer sites are required for example, for defining long-term (e.g., century-to-century) variations in hemispheric mean temperature than for short-term (e.g., year-to-year) variations, the coarse spatial sampling limits our confidence level in hemispheric mean or global mean temperature estimates prior to about A.D. 1600. Moreover, the instrumental record is shorter than some of the features of interest in the preindustrial period, so there are very few statistically independent pieces of information in the instrumental record for calibrating and validating long-term temperature reconstructions. In our opinion this is just the focal point and it is for this reason that the PhD work is based on the analysis of a few number of instrumental series but each one careful studied and homogenised. In particular, many efforts were made to obtain instrumental series of high quality, statistically robust and independent above all in the Early instrumental period when the anthropogenic forcing were almost completely absent. In this way the calibration and verification is performed both on a longest period respect others taken in exam in previous study and on a time window drove above all by the natural component of the climatic signal. Efforts in this direction, in our opinion, produce more substantial results in large scale climatic reconstruction than the use of a larger number of minor quality proxy or more instrumental series but recent in time.

The results on the climatic reconstructions on Mediterranean area obtained in these years, with the co-operation of a large Group constitute by Research institutes and Universities from Portugal, Spain, France, Italy and Greece has been summarized into the paper “500-year temperature reconstruction in the Mediterranean Basin by means of documentary data and instrumental observations” accepted for a Special Issue of the International Climatic Change Journal.

Here are presented for the first time, some unknown instrumental temperature series, checked for problems, discontinuities and errors and extend back up to 1654. Although they originated at the dawn of meteorological observations, their quality has been

carefully assessed. A schematic view of instrumental series used for this work is presented in Table 3.3 together with indications concerning: place of origin, temporal range covered, observer initiator of the instrumental series, new period made available within Millennium European project and references of past and present works concerning each single series. A Mediterranean dimension, of the climate variability over the last five centuries, is reached by combining all together the individual proxy and instrumental series coming from places indicated in the map of Figure 3.9 to obtain only one large-scale temperature comprehensive series.

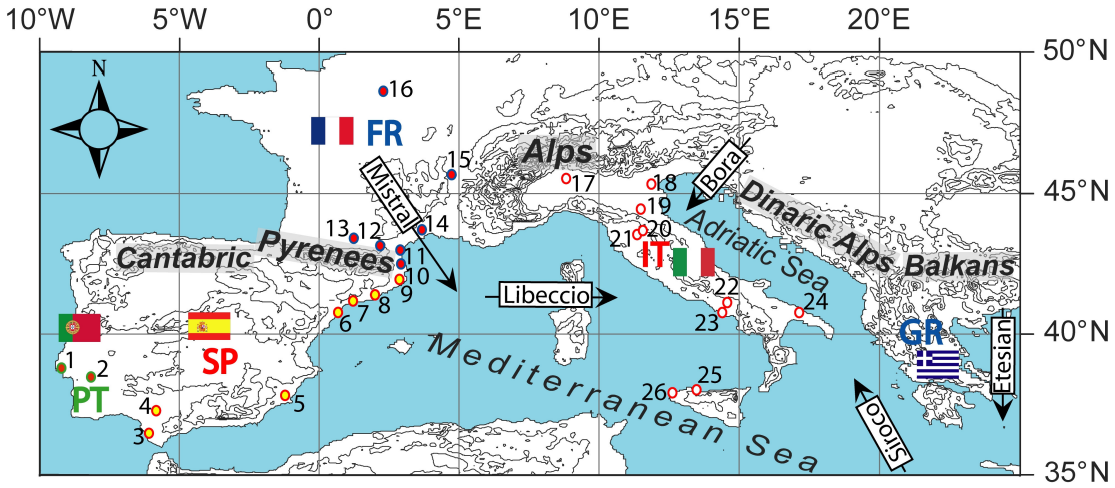

Figure 3.9: The Mediterranean Basin taken in exam in the paper:"500-year temperature reconstruction in the Mediterranean Basin by means of documentary data and instrumental observations" with indicated the localities (circles with progressive number label and flag colour code) where documentary proxies and/or instrumental observations have been retrieved for use in this paper, divided by countries: Portugal (PT), Spain (SP), France (FR), Italy (IT) and Greece (GR). The stations are: 1: Lisbon (PT), 2: Évora (PT), 3: Cadiz (SP), 4: Seville (SP), 5: Murcia (SP), 6: Tortosa (SP), 7: Tarragona (SP), 8: Barcelona (SP), 9: Girona (SP), 10: Perpignan (FR), 11: Narbonne (FR), 12: Carcassonne (FR), 13: Toulouse (FR), 14: Montpellier (FR), 15: Lyon (FR), 16: Paris (FR), 17: Milan (IT), 18: Padua (IT), 19: Bologna (IT), 20: Vallombrosa (IT), 21: Florence (IT), 22: Benevento (IT), 23: Naples (IT), 24: Locorotondo, 25 (IT): Palermo (IT) and 26: Erice (IT)

Table 3.3: Instrumental Series produced within Millennium European project and/or used in this paper. The series are presented in chronological order i.e. from the earliest observation to the more recent together with the bibliographic references of each series studied.

Country	Location	Length	First Observer	MILLENIUM new period	References
Italy	Florence	1654-2007	Rete Medicea	1654-1670	Maracchi 1991; Crisci et al, 1998; Camuffo and Bertolin 2010b
Italy	Vallombrosa	1656-2003	Papeschi and Casini	1656-1670	Gandolfo and Sulli, 1970; Camuffo and Bertolin 2010b
France	Paris	1676-2007	Morin	1676-1712	Legrand and Le Goff, 1992; Slonosky, 2002
Italy	Padua	1716-2008	Poleni	1716-1769	Camuffo, 1984; Camuffo et al, 2000b; Camuffo and Bertolin 2010a
Italy	Bologna	1716-2007	Beccari	1716-1774	Baiada, 1986; Brunetti et al, 2001
Italy	Naples	1727-2003	Cirillo	1727-1754	Cyrillus, 1731-1732
France	Lyon	1740-2007	Jesuits Fathers	1740-1780	
France	Toulouse	1750-2007		1750-1850	
Italy	Milan	1763-2007	Lagrange		Maugeri et al, 2002
Spain	Barcelona	1780-2007	Salvá	1780-1825	
Portugal	Lisbon	1783-2007	Velho		Maheras et al 1994 and 1995; Alcoforado et al., 2000; Taborda et al., 2004
Spain	Cadiz	1787-2004	de Mazzaredo		Barriendos et al, 2002; Rodrigo, 2002; Gallego et al, 2007
Italy	Palermo	1791-2006	Piazzi	1791-1853	Chinnici et al, 2000; Micela et al, 2001

To perform the calibration, validation, and reconstruction steps we have first of all subdivided the sites under examination in sub-region with similar climatic characteristics. Most of them in fact are situated in the three large European peninsulas (Iberian Peninsula, Italian Peninsula, and Balkan Peninsula), which extend inside the Mediterranean area.

The Mediterranean region is an area of great climatic interest because it is influenced by some relevant mechanism affecting the global climate system. It represents, in fact, a transitional zone between the deserts of North Africa, situated within the arid zone of the subtropical high and Central and Northern Europe, which is influenced by the westerly flow during all the year. The Mediterranean is shielded from the continental regions of Western and Central Europe by a system of folded mountains, including Pyrenees, Alps and Balkans (see Figure 3.9), and its Climate is characterized by the polarward (summer) and equatorward (winter) shift of the Azores subtropical high pressure cell. As a consequence, during summer, Western Mediterranean is almost invariably dominated by anti-cyclonic circulation, with dry sinking air capping a surface marine layer of varying humidity. During summer, the situation is with no rain in central Mediterranean but thunderstorms in the northern belt. On the contrary, in winter, the polar jet stream and the associated periodic storms reach frequently the Mediterranean region, bringing heavy rain.

In order to take into account all these climatic features, in a first phase, for each sub-region, we composite together both proxy data and instrumental series coming from individual stations. Once obtained these composite 'regional' proxy and instrumental series, we calibrate directly the composite series one with the other on an overlapped period. To make an example, we create the Northern-Central series both for proxy and instrumental data taking together all the documentary information coming from this geographical area from 1500 until 1780 and all the oldest and continuous instrumental series (more than three hundred years-old) in the same area (i.e. Padua, Milan, Bologna, Florence and Vallombrosa), in order to obtain an overlapping period, useful for calibration, as long as possible. In a second phase, once a local 500-years reconstructed series of temperature is made available for each Mediterranean sub-region, we create the whole Mediterranean larger surface reconstruction composing together the individual zonal series.

The result of the large scale temperature anomalies seasonally reconstructed from 1500 till nowadays for the Mediterranean basin is reported in Figures 3.10a, b, c, d. In the plots, we maintain different colours for the different data types used for the reconstruction (pink color for DP, blue color for IO). Moreover to examine the change through time, in all plots, temperature time series are converted into anomaly time series

by subtracting out the mean temperature from a base period, such as the 30-year 1961–1990. This choice has been made for a precise reason: unlike actual temperatures, station anomaly values can be averaged together without adversely impacting the time series when a particularly warm or cold location has some observations missing, because temperature anomalies are much more geographically coherent than actual temperatures. Because the analysis presented here only examines changes in temperature over time, all of the results will be using anomaly time series.

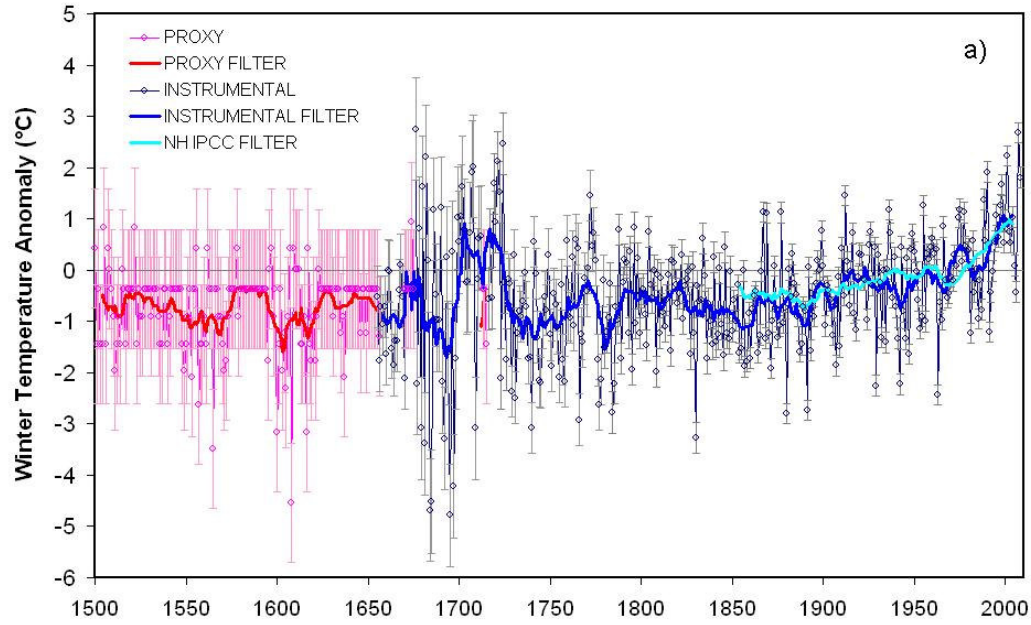

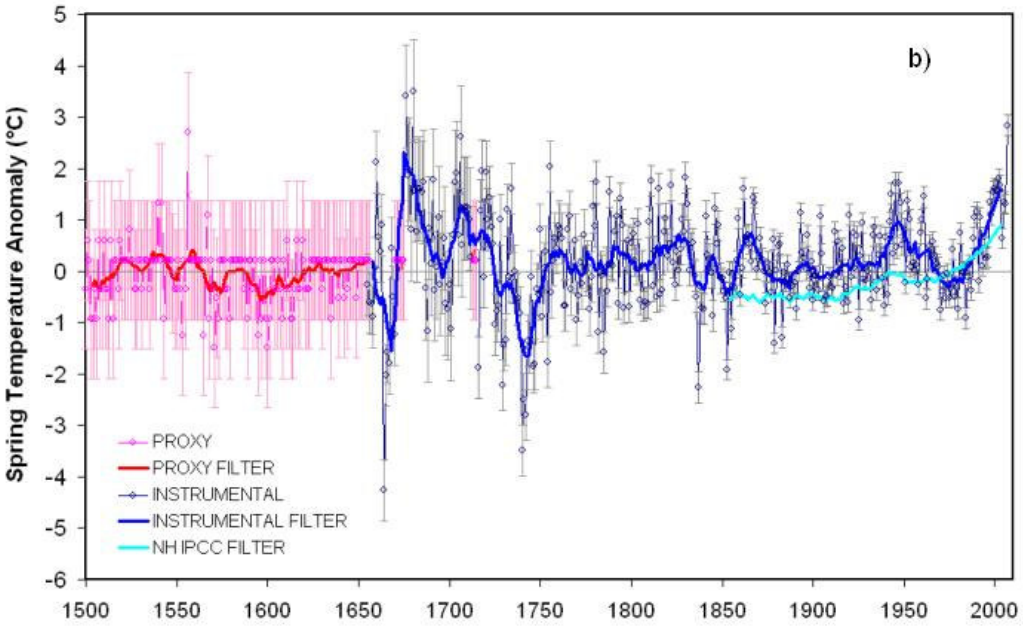

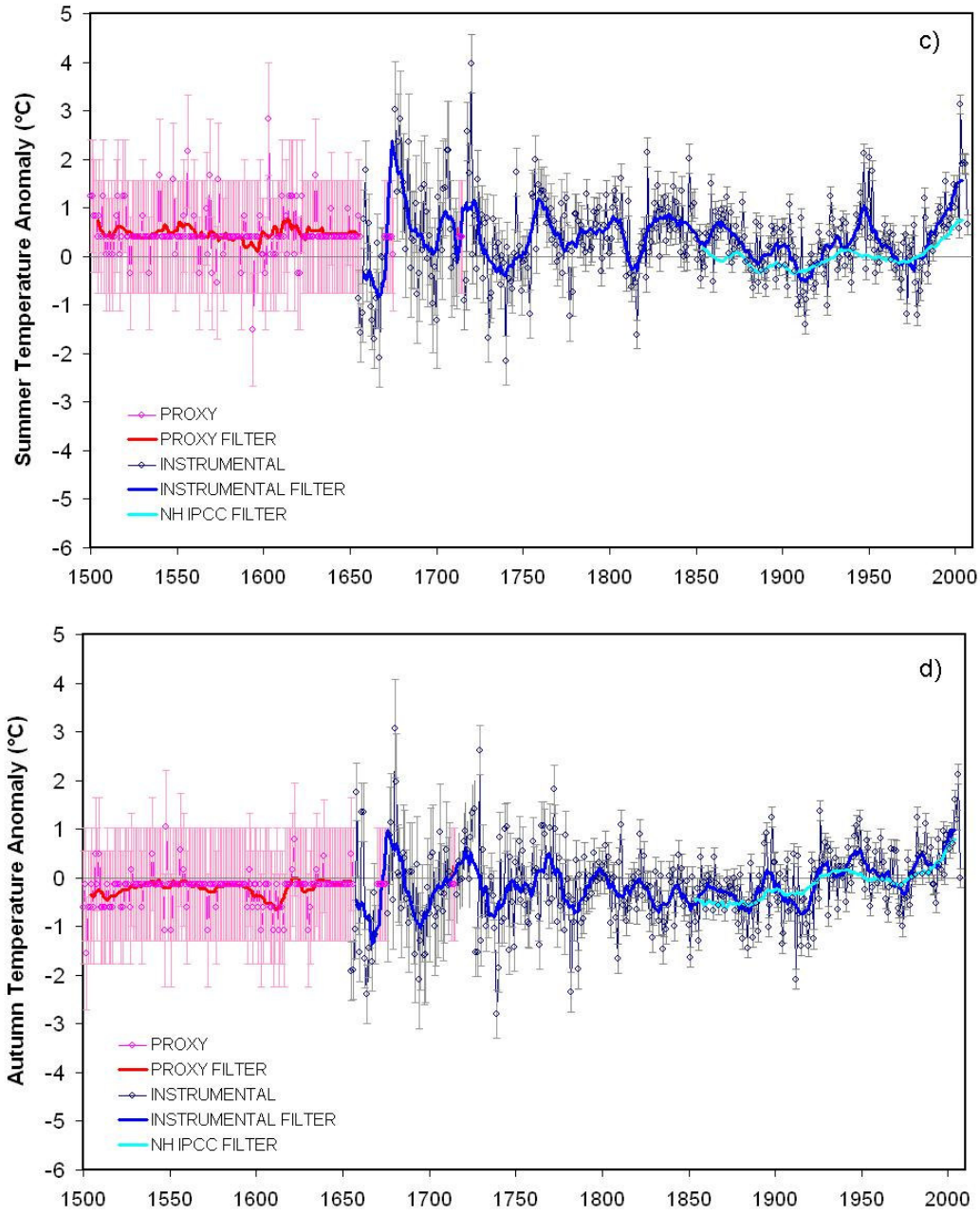

Figure 3.10: From top to the bottom temperature anomaly over the last 500-years in the Mediterranean basin: a) Winter, b) Spring, c) Summer and d) Autumn. In each window is shown the Mediterranean Basin reconstructed series from documentary proxy (DP) (open circle and thin pink line) and from instrumental observations (open circle and thin blue line) with their filters thick red and blue line respectively. The IPCC 2007 results for the Northern Hemisphere have been overlapped for comparison (thick cyan line). DP 'normal or average' level is arbitrarily moved at the average level of the whole instrumental period.

In these figures extreme events and some periods with increased frequency of anomalous weather are visible. However, in the pink line series, reconstructed from documentary proxy, no trends can be established although we remember for example that the values of winter severity derived from DP are established after the main

climatic effects, e.g. people killed or large water bodies frozen over. From the other hand, in the seasonal averages of instrumental observations (blue line series), extreme events well documented from DP, as years famous for the most severe winters, i.e. 1709, 1789 and 1929 are not well characterized because they are average by the lowest seasonal value. The great winters, in fact, were determined by spells of very cold air persisting for two, three, or more weeks. The impact was tremendous, but the peak of the cause was generally limited to a short period, for this reason the comparison between DP famous year and instrumental observations averages seems contradictory, except if we consider, instead of the seasonal averages, the more detailed monthly averages in which cold spells are recognizable. Therefore, we should keep in mind that if we change the way of presenting data, e.g. by passing from daily, monthly or seasonal averages, also the top years characterized by the most severe hot or cold will change.

Works that made comparison between regional and hemispheric/global past trends in surface temperature during the last millennium shown dramatic differences (Jones and Mann, 2004) and local to global comparisons are hardly justified. However, it is interesting to see the sensitivity of the Mediterranean, i.e. to what extent the Mediterranean responded to the climate forcing factors in comparison with the Northern Hemisphere, i.e. the well-known IPCC 2007 graph (Le Treut et al., 2007). For this reason, in Figure 3.10, the IPCC 2007 results with the filter obtained for the Northern Hemisphere (thick cyan line), have been overlapped to the obtained Mediterranean filtered temperature (thick blue line).

To express our results, exactly in the same form used in the IPCC 2007 graph for the Northern Hemisphere temperature reconstruction and to go more in detail, in the comparison of the common period 1850-2007, we represent, in Figure 3.11, only the part of instrumental data of our Mediterranean temperature series with a yearly resolution. In the upper part of Figure 3.10 we report the Northern Hemisphere IPCC graph. The result for the Northern Hemisphere, in the upper window, shows minor oscillations until 1909, then a net warming from 1910 to 1940, followed by a stationary period that preceded the recent warming since 1970, attributed to anthropogenic forcing. On the other hand, the Mediterranean had more regular oscillations around the same average level, followed by the same warming phase after 1970. If we analyse the longer time scale, i.e. 1650-today, for the Mediterranean series, we show several warming-

cooling cycles, and the present-day warming is evident, but not dissimilar from previous ones. Of course, before to express some rash judgements regarding the results in Figure 3.11 we should keep in mind three factors: first, the number of Mediterranean stations used in this work are much less than the number used by IPCC 2007 for the Northern Hemisphere and, therefore, less representative; however, the quality of individual series is higher; second, even at the Mediterranean scale, the number of operative stations in the early period was much less than today, but the same problem holds for IPCC too; third, at the global scale we see that at high and at low latitudes the tendency to warming or cooling is opposite, and the Mediterranean is in the belt between these opposite tendencies: any oscillation of this belt may have a large impact on the Mediterranean scale, thus justifying the observed cycles, remarkable on the Mediterranean, but small on the global scale.

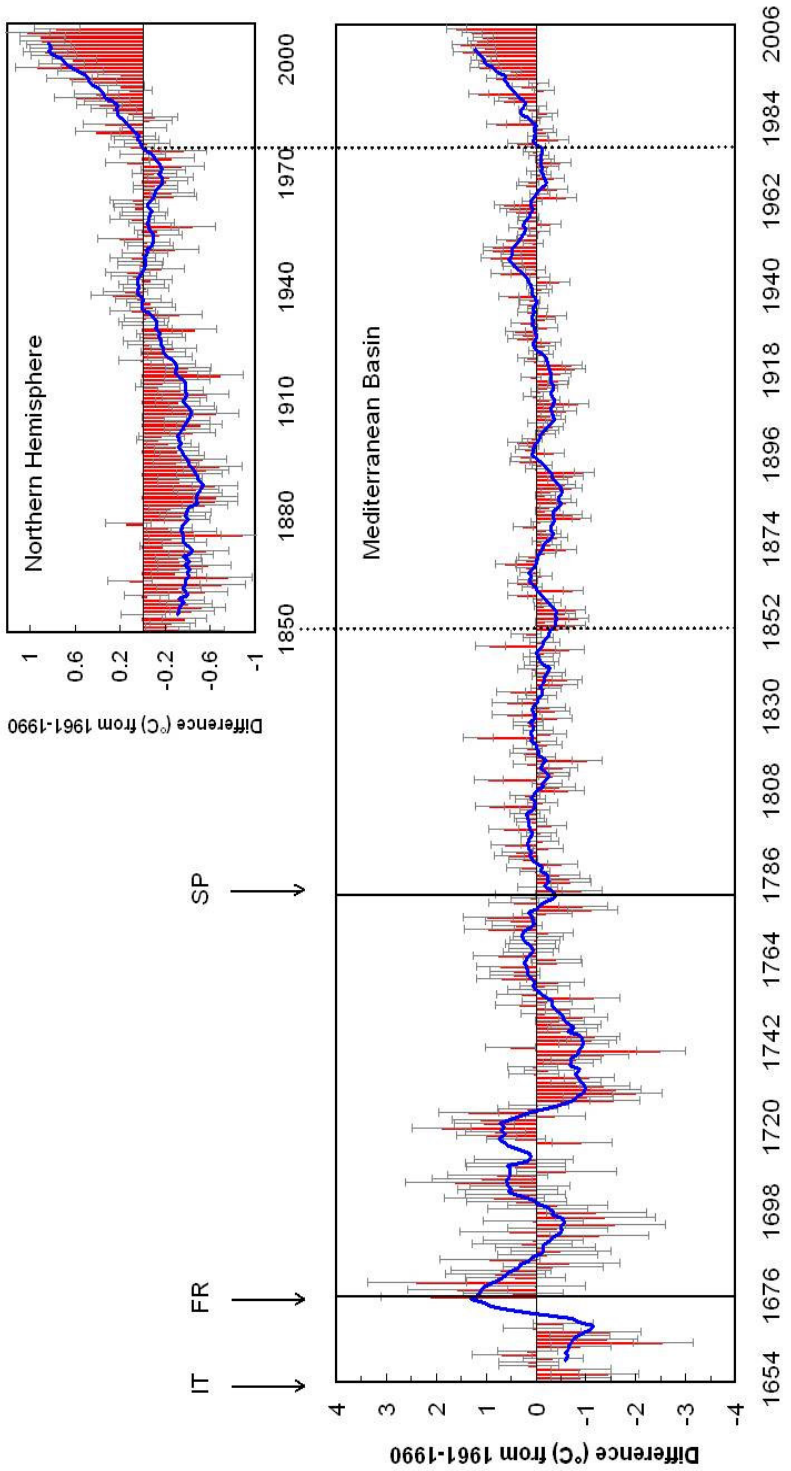

Figure 3.11: Comparison between the annual temperature anomaly form instrumental observations in the Mediterranean Basin and the Northern Hemisphere. Top: IPCC 2007 Northern Hemisphere temperature difference for 1850 to 2006 relative to 1961-1990 mean (Le Treut et al., 2007). Bottom: Annual temperature difference in the Mediterranean Basin for 1655 to 2007 relative to 1961-1990 mean. Labels IT, FR and SP indicate the starting point of series from Italy, France and Spain, respectively. Vertical thin lines: yearly averages; thick continuous line: 11-year moving average

Moreover the Power Spectrum Analysis have been performed on the whole Mediterranean temperature series for searching some periodicity. Annual cycles at 57.3 yr, 34.4 yr (Bruckner), 26.5 yr, 12.7 yr (Schwabe) and 2.2 yr (quasi-biennial) at 95% confidence level have been found (see Figure 3.12). In spring the same cycles are visible; in summer only Bruckner; in autumn 26.5 yr, 4.1 yr and other shorter ones; in winter 78 yr, 3.5 yr and shorter. Wavelet Analysis confirmed the same cycles.

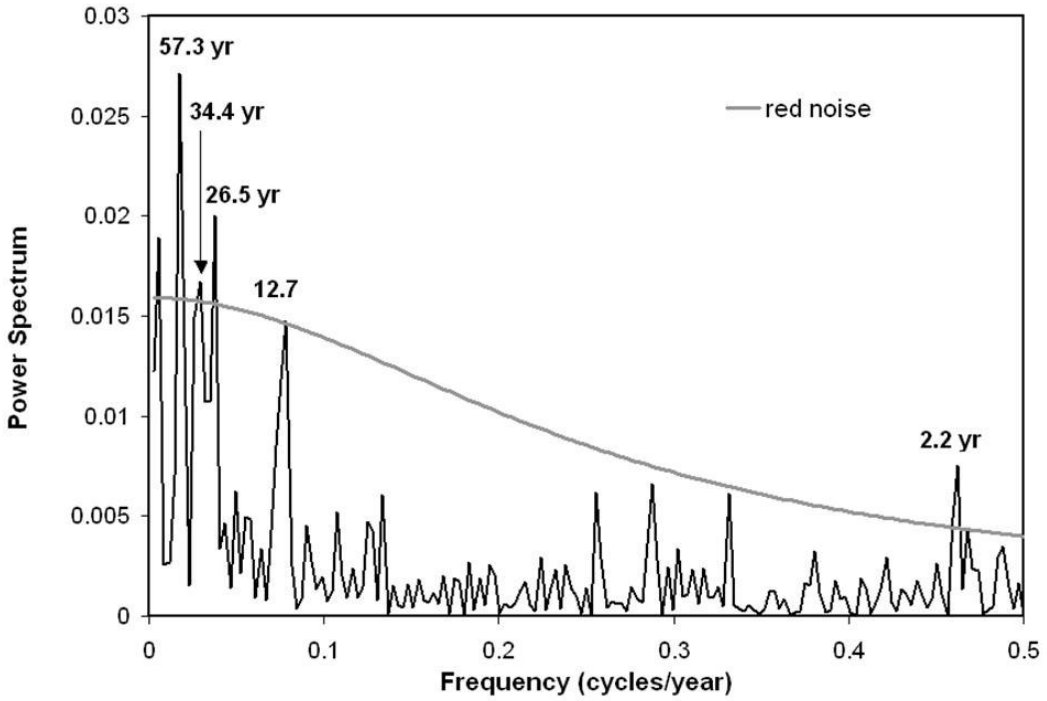

Figure 3.12: Power Spectrum analysis of yearly temperature for the whole set of Mediterranean series of instrumental observations. Gray line: red noise at 95% confidence level. Significant annual cycles at 57.3 yr, 34.4 yr (Bruckner), 26.5 yr, 12.7 yr (Schwabe) and 2.2 yr (quasi-biennial).

These results performed on the base of documentary data and instrumental observations concur to extend our knowledge on the temporal behaviour of temperature and in this area over the last 500 years (see Figure 3.10), especially in relation with the recent global warming (Figure 3.11). The tremendous effort made to gather, combine and homogenize both a huge stuff of documentary sources and a limited number of extremely long instrumental series, provide now a long-term general view of the climate features and their variability in the Mediterranean Basin. However in analysing these results it is important to keep in mind that extreme features in chronicles or annals may appear under a different light when compared with instrumental readings, depending on

the averaging time selected in data processing. While documentary proxy (DP) are convenient to establish the occurrence of extreme events, year-by-year variability, the existence of some time periods in which cold or warm situations were repeated, are not useful to pinpoint long-term trends. The latter point can be assessed only with instrumental observations (IO). For the first time, in these plots (Figure.3.10, 3.11) we can see the climate variability from purely instrumental observations (blue color data in Figure 3.10) since approximately 350 years that is a range that covers a time twice as long as the IPCC 2007 span and this longer context adds new light. In the recent time, i.e. the last 40 years, warming is evident over all the Mediterranean stations, in line with the well-known global warming. However, looking on the long-term time scale, warm and dry periods are not exceptional for the Mediterranean, which was characterized by a sequence of warming and cooling cycles depending on the relative influence of the Atlantic, the Eastern side and Africa. In the future, it will be interesting to see if such oscillation modes will persist and how they will combine with global warming.

Chapter 4:

Early Instrumental Data: potential and limitations to reconstruct climate variability

Contents

4.1 Potential and limitations of early instrumental temperature observations
4.2 The thermometer birth: from the thermoscope to the air thermometer
4.3 Early temperature observations: a case study
4.3.1 The first liquid thermometer: the Little Florentine
4.3.2 The first European meteorological network the Rete Medicea (1654-1670)

In this chapter we continue the first part of the PhD thesis concerning methodologies of investigations applied to historical climatology. In particular here and in the next chapter, we deal with early instrumental temperature observations performed by first scientific Academy immediately after the inventions of the air and liquid thermometers. As mentioned before, this first period of meteorological observations made by few precursors with the just invented new instruments called thermoscopes or thermometers is a branch of climatology still controversial. The reason is simple, early instrumental records made before the beginning of systematic meteorological observations in 19th century, in most cases cover only short periods or have a split character. The lack of detailed knowledge of the instruments and of their locations makes linkage to the modern reference period difficult and many efforts to retrieve information on instruments, locations, observation's methodology and to perform careful homogenisation, are required. The huge amount of work that the analysis of these data requires and the uncertain results they provide with a superficial approach, sometimes induce researchers to renounce the idea of analysing them. Rather than solve all doubts to transform early instrumental observation from incomprehensible readings to

comparable instrumental observations, some researchers prefer to consider them as a sort of proxy direct data.

Generally data quality and homogeneity are very capital factors in any climate-change-related issue, however, in our opinion, the data quality work performed on early instrumental observations is still most relevant than other instrumental periods because most surface temperature reconstructions use these records for both calibration and validation. In the following sections, we are going to describe at first the main features of instrumental data in terms of potentials and limitations respect the documentary proxy data previously analysed, and then the thermometer birth, following and analysing step by step the historical and scientific background that gave rise to this instrument.

In the last section of this chapter we will show as these early temperature data, if correctly handled, are completely comparable with the modern reference period and therefore for their real scientific value can not be considered as proxy direct data. In particular, we will expose the results obtained in our paper titled: "The dawn of Meteorology in Italy and the earliest meteorological observations (1654-1670)" and performed on the first international meteorological network called Rete Medicea, on the basis of the invention of the termoscope by Galileo Galilei (1564-1642), the barometer invented by his pupil Torricelli and other meteorological instruments built by his followers in Italy.

This work is concerning with a topic of great importance for different reasons:

- it deals for the first time, with the analysis performed on the data of the first Meteorological Network of the history carried out, on European scale, from 1654 to 1670 (i.e. the Rete Medicea)
- it deals with the use of the first meteorological instruments invented for this scope by the followers of Galileo, that under the Grand Duke aegis, continued to work and participate at the scientific life in Tuscany, also after the Inquisition sentence and the dead of their mentor.

- it deals with some discoveries and Galileo's invention in the field of climatology that remains quite unknown respect the picture of the big astronomer and big scientist that usually is painted

In the 2009 international year of astronomy (Iya) and in particular for the 400-year celebrations from the first observations made by Galileo with his telescope exactly here in Padua, we want present this work on the dawn of meteorology in Italy in order to complete the portrait of this big scientist from the meteorological point of view too. In particular we put the attention on the importance that the Galileo's "lessons" had on a new concept of Experimental Sciences. The experimental method that Galileo and his pupils followed gave the input for the birth of Meteorology. This discipline started when the man, feeling the necessity to understand the changes in Natural events and their physical mechanisms, invented the first scientific instruments to take measurements of these properties.

4.1 Potential and limitations of early instrumental temperature observations

The early instrumental temperature records are derived from the readings of first invented thermometers and provide the basis for generating calibration and verification on a larger temporal range than the usually devoted last 150-years, improving in this way, the surface temperature reconstruction and best estimating the actual climate changes.

Potential of Early instrumental temperature observations. To deal with potential of early instrumental temperature data is to deal with the History of Science and in particular with the birth of Meteorology as scientific discipline. Interest and curiosity of few men of Sciences devoted in discovering and understanding the Physical laws that ruled the natural phenomena gave the input to invent the instruments for measuring the 'Hot and Cold'. Since that moment the 'Hot and cold' were considered as sensations and not as different levels of a same physical concept. In the 17th century, different steps had to be based to cover the route that brought to perform systematic instrumental temperature observations. First, it was necessary to understand

- the physical quantity of measuring

- the gas expansion physical law that drove the mechanism
- the scale to graduate the quantity of measure
- the necessity to take at least a fixed point to refer the measuring and in particular the necessity to establish two fixed points to make the instruments replicable.

After these main concepts were carried out with the invention of the first air and liquid thermometers, the possibility to perform systematic observations of temperature become reliable.

Respect to documentary proxy data, early instrumental observations, are therefore real scientific measurements not more depending to observer's subjective sensations of 'Hot and Cold' but depending from objective values that are estimated on a scale. The readings in most cases were *carefully performed* by observers, however this last point, in the data analysis, remains a tricky passage as source of bias that must be evaluate 'a posteriori' taking into account a lot of information concerning the way in which the observations were performed (e.g. the location of the instruments, the reading time, the observer's methodology, the calibration made on the thermometer, possible errors made during the observations). Another big difference respect documentary proxy data is that instrumental observations have a *direct dependence* with the physical parameter that measure and not from some other spurious variables. This is not completely true for the first invented instruments called thermoscopes, or in the 18th century large spread Amontons thermometer that being itself a thermoscope, had to added the value of measurement read on its scale, with the dependence of the atmospheric pressure. However this was not a problem because taking contemporary the two measurements from the Amontons thermometer (i.e. the thermoscope) and from the barometer, it was possible to evaluate correctly the value of temperature alone as we show in the case study presented in the next Chapter 5.

Other main characteristics, as a sort of peculiar fingerprint of instrumental observations, are the *comparability* of instrumental observations among themselves and the *repeatability* of instruments fabrication and performed observations. These two characteristics are of primary importance. In fact, if temperature values could not be comparable among different thermometers and place where measurements were taken, all actually efforts carried out by researchers to study different local temperature

conditions or mean global temperature behaviour would be meaningless. In particular, it is interesting to stress the difference between these last instrumental peculiarities and the correspondent characteristics for documentary proxy data. As described in detail in Chapter 3, comparability and repeatability are hard to evaluate in documentary proxy. Comparability among documentary proxy is difficult because descriptions of climatic and natural events, being recorded by chroniclers lived in different historical time, could include some biases drove by the subjective way of thinking of chroniclers lived for example during the Renaissance or during the Middle Age. Secondly, for their nature, documentary proxy, are not strictly reproducible as instrumental observations because the scale is linked to the chronicler subjective sensations respect to the natural phenomena that he describes. Moreover the potential of early instrumental temperature observations stay also on the *information* stored in the data themselves. Early measurements of temperature in fact were recorded by observers since the second half of 16th century, just in the the Little Ice Age (LIA). This period of cooling and minima in the sunspots number (see Figure 4.1), occurred after a warmer North Atlantic era known as the Medieval Warm Period (MWP). It was not a true ice age, the LIA brought colder winters to portions of Europe and North America, the term was introduced into scientific literature by François E. Matthes in 1939. Climatologists and historians working with local records no longer expect to agree on either the start or end dates of this period, which varied according to local conditions to approximately the 16th century to the mid 19th century.

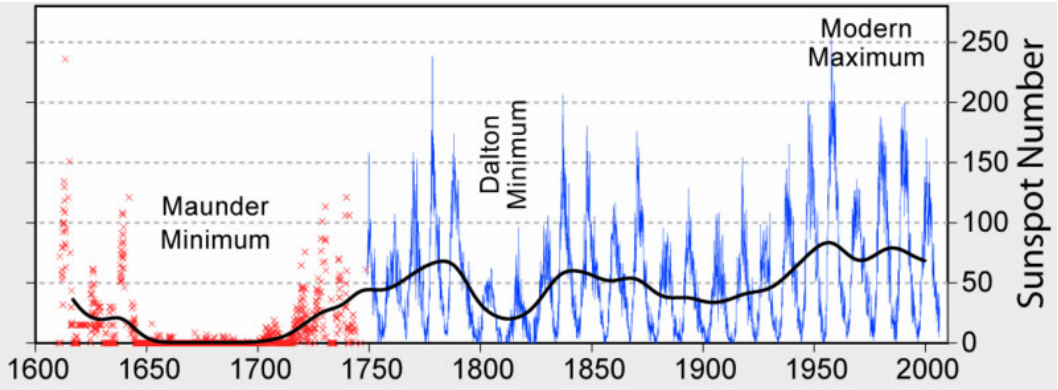

Figure 4.1: The sunspot number during the last 400 years of sunspot observations. In red the absolute minimum, known as Maunder minimum, another relative minimum during the LIA was in 1815 called Dalton minimum.

It is generally agreed that there were three minima of temperature, beginning about 1650, about 1770, and 1850, each separated by slight warming intervals, however analysis of new earliest temperature observations, as presented in this chapter with data of the Medici Network, could confirm these assumptions with more confidence. Moreover it is important remember that the climatic signal stored in these early data is the nearest to the natural variability. In more recent periods, after the 19th century, in fact the signal of observed climatic variables is spuriously confused with anthropogenic forcing difficult to distinguish from the natural one.

In the case study dealt in the last section of this chapter, we show as these data, after a correct handling to solve problems of instrumental scale, calibration and homogenisation, have the value to be *comparable* with the modern temperature observations adding high quality useful information to better understand the actual global warming.

Limitations of Early instrumental temperature observations. To deal with limitations of early instrumental data is to deal with a greater and widely debated topic of data quality and homogeneity. The scientific community, in fact, is well aware that any reconstruction of the past climate variability and change must rely on the most solid, reliable and homogeneous data-sets. For this reason, when studying past climate variability it is impossible to consider any record of climatic data as entirely reliable and homogeneous.

For definition, a temperature time series is considered homogeneous if variations are caused only by variations in weather and climate (Conrad and Pollak, 1950). Unfortunately, most long-term temperature time series, and in particular data coming from the early period, have been affected by a number of non-climatic factors that make these data unrepresentative of the actual climatic variation occurring over time and required quality checks and homogenization. Generally these limitations include *changes in instruments*, changes in *observing practices*, *unknown calibration* of instruments (an example of these limitations is reported in Figure 4.2), *sparse geographic and temporal sampling* as different station locations or different formulae used to calculate means, and in more recent time change in *station environment* (e.g., urbanization) too.

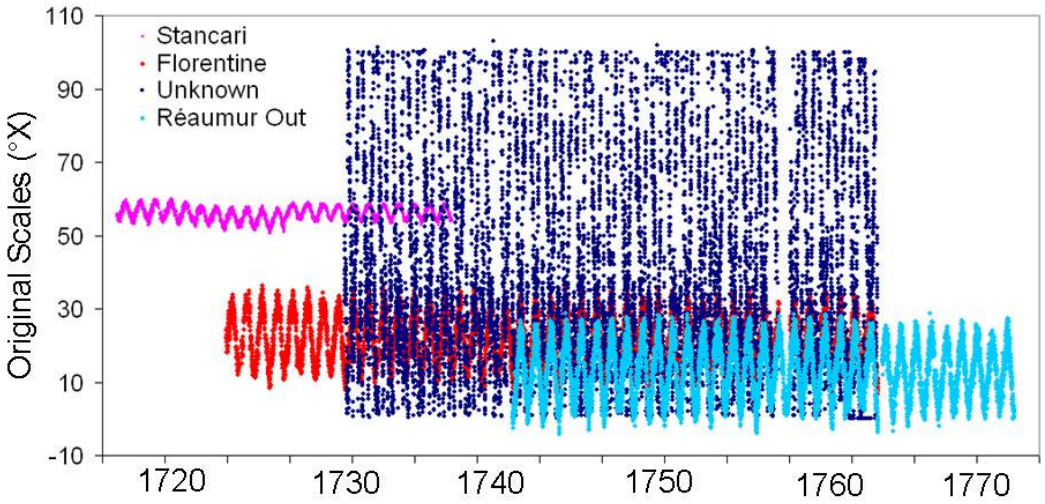

Figure 4.2: Example of raw thermometer readings as retrieved from the ephemeredes with meteorological instrumental observations performed by Jacopo Bartolomeo Beccari and his pupils in Bologna since 1716 to 1774. Each dataset is carried out with a different thermometer (i.e.different scale and instrumental calibration) and in some cases with different observing practice. Pink colour represents the Stancari thermometer, red colour the Florentine thermometer, Blue colour an completely unknown thermometer and the cyan colour the Réaumur thermometer.

Some changes cause sharp data discontinuities, while other changes, particularly change in the environment around the station, can cause gradual biases. All of these inhomogeneities and errors caused by faulty transcription, digitization, or transmission of the data can bias a time series and lead to misinterpretations of the studied climate unless they are accounted for by adjusting or "correcting" the data.

While all erroneous data points cannot be removed from a data set without the risk of removing a great deal of good data as well, biases due to large isolated errors can be eliminated (an example is reported in Figure 4.3).

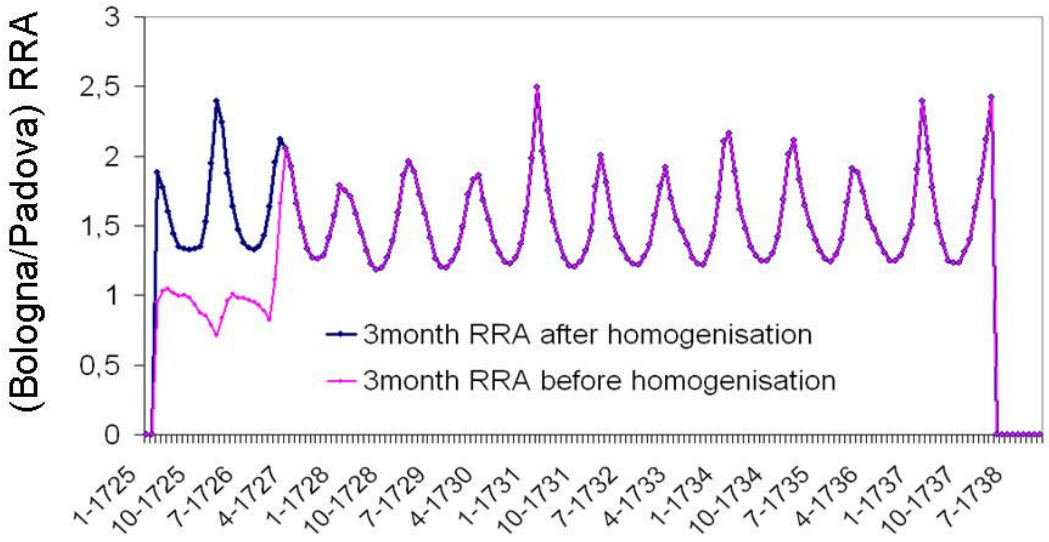

Figure 4.3: Example of bias due to large isolated error. This error can be estimated using statistical test where is performed a comparison among a reference (e.g. the Padua series) and a candidate series (e.g. the Bologna series). From the test, a drift of the Stancari thermometers in the Bologna series is evident (see pink line) and a opportune correction was necessary to make homogeneous the Stancari values (blue line).

Biases due to discontinuities in the observing network are a much more difficult problem to resolve. However, a great deal of work on homogeneity problems was done by our group in each instrumental series taken in exam in our work. Some examples of problems met with early instrumental series and then solved after a careful analysis will be presented in the case study concerning the 'Recovery of the Early Period of Long Instrumental Time Series of Air Temperature in Padua', in next Chapter 5. In this work we estimated and corrected bias caused by observers transfers with change in location, use of different instrumentations and changes in observing practices such as different observing time.

As told before the *uneven spatial distribution* of in instrumental data, and the change in their *distribution over time*, can potentially create biases. Some of the approaches to addressing this problem are: (a) acquiring more data through digitization of historical records, (b) improving international continue exchanges and (c) reconstructing full global grids using some spatial interpolation to fill in data sparse areas. However, global coverage of in situ tempeature data can never be achieved, particularly going back in time when the availability of early instrumental data become more and more difficult to find.

Another limitation mentioned before, related more to modern instrumental observations than early data, is to assess the impact of small, gradual changes in the *environmental* of observing network. Urbanization (and land-use changes in general) and the resultant urban warming is the most commonly cited example of this type of problem. Recent efforts to assess this bias focus on identifying which stations are rural and which are urban or poor and good site in agreement with the WMO indications, using map-based metadata (i.e. information that describes the environment in which a measurement is made and/or the methods and/or tools used to make the measurement (Peterson and Vose, 1997)) or night-lights derived metadata (Owen et al., 1998). Long-term global temperature trends calculated both from the full land surface network, and from rural stations only, turn out to be very similar, the same conclusion is obtained studying the effects of poor siting. In this study, Peterson tested if the homogeneity adjustments were appropriately accounting for all artificial changes at the stations or less. In the first hypothesis an adjusted temperature time series from the poorly sited stations should have been very similar to the time series from the stations with good siting and the trends should have still been about the same. Instead, in the second case, if poor current station siting produces an artificial bias in the temperature record that is not being addressed by homogeneity adjustments, temperature trends at the poorly sited station would be significantly different than the temperature trends at the stations with good siting, and these differences would most likely be that the poorly sited stations are warming relative to nearby stations with good siting. The analysis performed shows similarity between the homogeneity adjusted time series from the good and poorly sited stations supporting the view that even stations that do not appear to be spatially representative can, with proper homogeneity adjustments, produce time series that are indeed representative of the climate variability and change in the region (Peterson et al., 1998b).

Taking into account a general view with both potential and limitation for early instrumental observations, it is important to remember that the possibility to found biases and errors is almost constant during the time, nowadays as well as in the past. When the first temperature readings were performed, the possibility to make mistakes or biases was driven by inexperience or due to a vague knowledge of the best measuring conditions, at present time, this possibility is instead linked to incorrect daily sampling,

to the use of a variety of sensors not all having the same quality, or to the use of Stevenson Screen and other meteorological purposes solar screens that introduce bias. At last but not least the urbanization with its heating island and the land use change that could introduce some bias toward warming values as schematically reported in Figure 4.4.

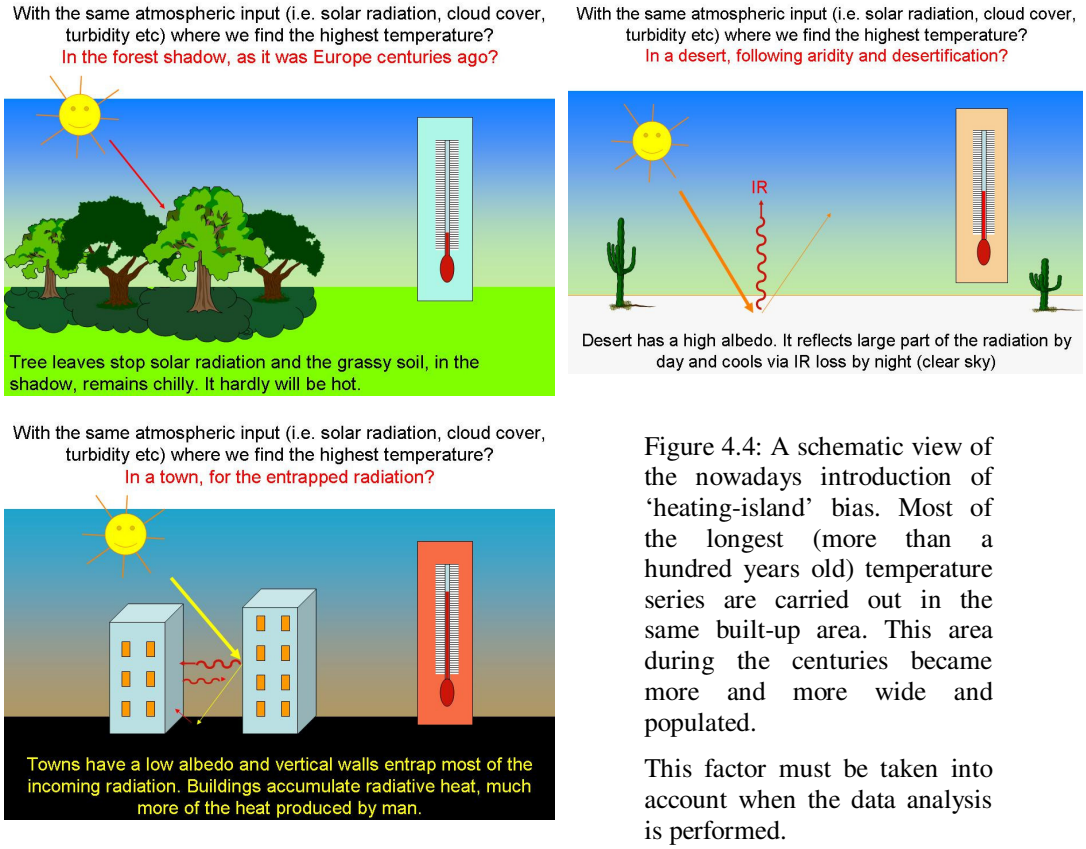

Figure 4.4: A schematic view of the nowadays introduction of 'heating-island' bias. Most of the longest (more than a hundred years old) temperature series are carried out in the same built-up area. This area during the centuries became more and more wide and populated.

This factor must be taken into account when the data analysis is performed.

In the next sections we deal with the technologic, scientific and cultural context in which the first air thermometer and the first spirit-in-glass thermometers were developed, not only to reconstruct an important page of the history of science, but to provide a holistic interpretation of the case study that we are going to present.

4.2 The thermometer birth: from the thermoscope to the air thermometer

In this section we will concentrate on the history of the thermometer before to analyse the earliest observations made with the newly invented instruments. We would better

understand the long path from the first Galileo's experience with the thermoscope in Padua (1593) to the development of this device into a gas thermometer.

During the ancient time, disciplines based on mind and direct observation of the sky as Logic, Geometry, Mathematics and Astronomy were very advanced, instead, products requiring manual work and technological skills were disregarded. For this reason many excellent ideas or prototypes, e.g. the steam machine or the thermoscope of Philo of Byzantium and Heron of Alexandria, were not correctly estimated and slept per millennia totally immersed in the dark until they were woke-up or re-invented in the turn between the 16th and 17th century of the modern era. It was with Giovanni Battista Della Porta (1535-1615) and his multi-volume book, first appeared in 1558, "Magiae Naturalis sive de Miraculis Rerum Naturalum" (i.e. "Natural Magic"), considered an early encyclopaedia of science and technology with advanced ideas, that the scientific interest was woke up. Della Porta, Paolo Sarpi and Galileo Galilei met in Padua in 1593, the year of the invention of the first experience with the thermoscope, assumed as the date of the invention of the thermometer. Della Porta, Sarpi and Galileo in 1593, probably talked about science and new instruments, possibly including the newly appeared translation of Heron by Giorgi (1592). No matter who first launched the idea or started to discuss about thermoscopes, or how a fruitful synergism was developed. The difference was between a pale idea of an amazing device and the comprehensive understanding of the whole problem including the behaviour of gases and the application for temperature measurements.

The aims of Galileo and the theory of gas expansion. Galileo thought to adapt the ancient experience of Heron to point out how much an air pocket expands when is warmed in some way and in 1593 he made the first experience at the University of Padua, probably to explain gases to his students. The experiment was based on the expansion of air and had a liquid as a pointer just to detect the change of air volume. At beginning he used water, later red wine to make more visible the column. The experiment shown a qualitative dependence of the height of the liquid column as a response to the heat supplied to the ampulla, when the ampulla was heated, the air expanded and the liquid column lowered; when cooled, the liquid column uprose until it reached equilibrium. Nevertheless, the instrument built by Galileo (see Figure 4.5) and the supporting theory had to be developed and interpreted. At that time Giovanni

Francesco Sagredo (1571-1620) was a young pupil and then became a good friend of Galileo. From the letter of Sagredo to Galileo dated 11/04/1615 we know that Galileo had precisely explained the theory of the expansion of the air pocket in the ampulla when heated. Heat (later "caloric") entered the ampulla, warmed the air and air expanded. A large amount of heat means a large expansion of air and a large displacement of the water meniscus inside the tube. In practice he had qualitatively recognized the first law of perfect gases, i.e. variation of volume at constant pressure, later better expressed and quantified by Joseph Louis Gay-Lussac (1778-1850).

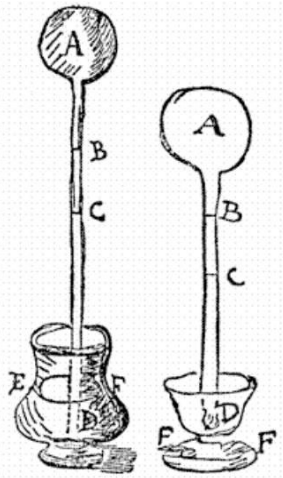

Figure 4.5: Thermoscope invented by Galileo in 1593 as described by Benedetto Castelli in the 20th September 1638 letter send to Mons. Cesarini. Extracted by 'Le opere di Galileo Galilei Edizione Nazionale' Ed. Barbéra, Firenze 1890 (B.X.)

Galileo was satisfied after having clarified the physical mechanism because his main interest was merely speculative and leaved his pupils to continue with practical developments and tests. Many details were cared by Sagredo who lived in Venice, in strict contacts with glass makers, and applied the instrument to microclimate (e.g. from a room to another) and meteorological purposes. In practice, Galileo made a beautiful demonstrative prototype but left to his pupils the air thermometer imperfect. The response of the instrument was dependent on the size of the ampulla, the internal radius of the tube and the air pocket entrapped into the ampulla. However, the main problem was that he did not pass from qualitative to quantitative. Probably, in his mind this was not a practical problem because it was possible to measure with a compass the displacements of the liquid in the tube, without needing a scale. For him the problem was solved and closed and passed to other inventions: the military compass (1597) and the telescope (1609).

The next step from the thermoscope to the thermometer: the scale by Santorio. It was necessary convert the thermal expansion of air into a readable value, i.e. from qualitative to quantitative. This development was made by Santorio Santorio (1561-1636), physiologist and physician, professor of Medicine at the University of Padua. Santorio was appointed to the University one year after Galileo left Padua to Florence (1610). Santorio was interested to measure everything concerning the physiology of the human body as people with or without fever and learn about the difference by measuring the heat released by expired air. At beginning, Santorio used a compass to measure the column of water (Santorio, 1612; Sagredo, letter 30 June 1612); then he graduated the tube of the thermoscope, making quantitative evaluation easier.

The addition of the scale was not sufficient to bridge the difference between a thermoscope and an air thermometer because the main problem was that readings were still affected by atmospheric pressure. This was unknown to Santorio, but he should have been in some way aware of the problem and solved it all the same. In fact, he made reference to the expansion of the air during a short, fixed time, by counting the oscillations of a pendulum. In such a time the variation in atmospheric pressure was absolutely negligible, and he considered only the difference between the final and the initial position of the liquid. Whatever the influence of the air pressure to the first reading, it was subtracted with the second one. In practice, he invented the differential measurements as an indication of a temperature change, always sampling per the same time duration, i.e. the same fraction of the time constant of the instrument. This happened in the period around 1612-1615.

Santorio was the first scientist interested to a specific practical application different from the local climate. He claimed having directly derived this idea from Heron, without ascribing any merit to Galileo. Santorio operated with a conflict of interest with Galileo, although the Galileo's experiences made some ten years before should certainly have been useful to inspire and reach his goals. It is difficult to distinguish merits and establish priorities. We should consider that Galileo and Santorio lived in the same cultural and geographical area, and that the Galileo findings were presented and discussed at the University lessons, where nothing remains confidential. In addition, Sagredo and Sarpi had frequent and precious cross-fertilising synergisms to improve the instrument and all of them were working at the same time on the same subject. Della

Porta might have provided further input. Santorio added the scale. However, Galileo was the first to give scientific dignity to a thermoscope and for this reason he affirmed to be the inventor of the thermometer. This was confirmed by direct witnesses: Sagredo (30 June 1612), Father Benedetto Castelli (1577/1578-1643) (1638) and Vincenzo Viviani (1622-1703) (1717 posthumous). Galileo died convinced of having invented the air thermometer, because he was not fully aware of the existence of the atmospheric pressure and all its consequences, although he was approaching this conclusion. Atmospheric pressure will be discovered in 1643, fifty years after the first experience with the thermoscope, one year after the death of Galileo.

The last step from the thermoscope to the thermometer, how to remove the influence of atmospheric pressure. The major fault of the thermoscope was that it also responded to changes in atmospheric pressure because the latter was exerted on the free surface of the water in the vessel and opposed the air expansion inside the ampulla. It was difficult to realise that small and slow changes in level in the Thermoscope tube were due to barometric pressure and not to a small change in temperature, because there was not an independent way to measure temperature. At that time the atmospheric pressure was unknown and the official science after Aristotle was that vacuum does not exist because it is immediately filled by air and that air has not weight.

However, Galileo's pupils realised that a problem existed, and it was as the air had an own weight. Finally, Evangelista Torricelli (1608-1647) arrived to the theoretical conclusion that air had a weight (1643). This was a revolutionary thought and required tests to be demonstrated. Vincenzo Viviani (1622-1703) set up the experimental device (the barometer) and made the first experience on behalf of Torricelli. This was successful and the device was called "Barometer" i.e. an instrument to measure the "weight" of the atmosphere. They demonstrated that the atmosphere has a weight and that it is possible to create vacuum without air in the upper part of the tube, above the column. This was not exactly true because this space had vapour of mercury, but it was too early to clarify this item.

After the atmospheric pressure was discovered in 1643, some obvious solutions to improve the thermoscope have been possible. A solution that solved some problems typical of air thermometers was to use mercury. Early thermometers in fact were open

and the evaporation of the liquid was a problem, mercury had a negligible evaporation and did not adhere to the glass tube and for these reasons per centuries was, with spirit, the favourite for thermometers. Another advantage provided by mercury was that the sensitivity of the instrument dh/dT, where dT is the change in temperature and dh the change observable in the capillary, is directly proportional to the number of moles entrapped in the air pocket, and inversely to other factors (Camuffo, 2002b). Mercury provided sufficient compression (about doubled) to the air pocket with a reasonable dimension of the thermometer, about one meter long. The third advantage of mercury is the small departure from linearity. This was clear soon (eg. Toaldo, 1775) but this was impossible to detect with accuracy until the progress in thermodynamics made evident this feature from comparison with precise constant-volume gas thermometers. Another advantage of mercury was that it is easy to have it purified at the same level, in order to get always the same behaviour, and this was impossible to obtain with spirit because of the uneven amount of water in solution.

Nevertheless the first main solution to improve the thermometer, was to add the barometric column to the thermoscope readings and to obtain the thermal expansion of the air inside the ampulla deprived of the contribution of the atmospheric pressure. This solution was adopted by the French scientist Guillaume Amontons (1663–1705) many years later (Amontons, 1702). The Amontons air thermometer was popular in the 18th century and it was used in Padua by Giovanni Poleni and his son Francesco from 1716 to 1718 and then from 1725 to 1769 (Camuffo, 2002a; Camuffo and Bertolin, 2010a) as we will present in the next Chapter. The second main solution, inspired to the Florentine Thermometers (presented in the next section) was to seal the upper end of the tube in order to make the air thermometer independent from the barometric pressure. The Italian scientist Vittorio Francesco Stancari (1678-1709) around 1707 adopted this solution building his own thermometer. He sealed the longer arm of the tube, thus leaving a vacuum (the saturation tension of Hg) between the surface of the mercury and the end of the tube thus stopping any pressure exchange with the atmosphere. The Stancari air thermometer had a limited diffusion and was used in Bologna by Jacopo Bartolomeo Beccari for the period 1716 to 1737.

Some fifty years before the air thermometer was able to operate with pressure compensated in some way, a third, genial solution was found before the discovery of

atmospheric pressure. This was the spirit-in-glass thermometer, born in Florence and renamed as Florentine Thermometer. This was not an evolution of the air thermometer but a totally different solution with a radical change of both the instrument and expanding fluid. As a matter of fact, the earliest true temperature readings were made with this spirit-in-glass thermometer as now we go to present.

4.3 Early temperature observations: a case study

The first aim of this case study is to investigate the instrument characteristics in their technological and scientific context. The fundamental question is: are these readings reliable or just a mere curiosity? At the dawn of the meteorology, have been the early scientists able to do a good job? Can we establish if they have correctly operated from the scientific point of view? The second aim is to present and interpret the daily observations taken with the little Florentine spirit-in-glass thermometer in a number of sites coordinated within the Medici Network for the time span of 16 years from 1654 to 1670. These are the earliest instrumental meteorological observations in the world. Although a number of studies was made to know and reconstruct the observations made in Florence and Vallombrosa (Boffito, 1926; Cantù, 1985 ; Gandolfo and Sulli, 1990; Maracchi, 1991; Vergari, 2006; Borchi 2009), which are the two main stations of the Medici Network, nobody has up to now recovered and analysed the earliest period 1654-1670 for a number of difficulties, including getting the original data.

4.3.1 The first liquid thermometer: the Little Florentine

The story. The development of the Thermoscope does not bring to the spirit-in-glass thermometer that was a totally revolutionary instrument with a different origin. The thermoscope was based on the discovery that gases expand when heated; the liquid-in-glass thermometer on the discovery that also liquids are subject to thermal expansion although their expansion coefficient is much smaller than for gases. Vincenzo Viviani, disciple and biographer of Galileo, wrote that Galileo invented in Padua “the thermometer with air and water” (i.e. the Thermoscope) and that the Grand Duke of Tuscany Ferdinand II invented in Florence the spirit-in-glass thermometer (Viviani, 1717 posthumous). In reality, the invention was due to a synergism between the Grand Duke and Torricelli, who will also discover two years later (i.e. 1643) the atmospheric

pressure and the barometer as well. We don't know exactly when the Florentine Thermometer was invented; however, we know that one of them was built in 1641, as described in the Diario Grande (i.e. Main Diary) of the Accademia del Cimento written by Alessandro Segni (1633 - 1697), secretary of the Academy till 19 May 1660 (Targioni Tozzetti, 1780; Antinori, 1841). This was the last year of life of Galileo, and we will see that this discovery too benefitted from some findings by Galileo.

We will follow, step by step, the principal findings that led to this second type of thermometer that was the prototype of all modern liquid-in-glass thermometers.

Galileo, his pupils, the Grand Duke, studied also the density of fluids and invented a "Densitometer". The instrument was based on the buoyancy of a graduated glass cylinder that remained floating, but more or less dipped into the fluid, depending on the density of the liquid. A particular application was to recognize the percentage of spirit in alcoholic beverages. They also recognised that the density varied with temperature, and this suggested the idea to Galileo to build a Thermometer based on this principle, the "Termometro Infingardo" i.e. "Sluggish Thermometer" (literally: who takes time before to react) for its long response time.

The choice of the thermometric liquid. The Densitometer and the Sluggish Thermometer were based on the same principle that fluids too have a variable density, but this should be much greater of that of the glass of which the instrument is made. The first reason to use spirit as thermometric liquid was motivated for it does not freeze in winter and does not break thermometers, differently from water (Antinori, 1841). After numerous tests to characterise the density of various spring waters, beverages and various types of liquids, including mercury, it was recognized that the coefficient of thermal expansion of pure spirit i.e. $1.1\ 10^{-3}\ °C^{-1}$ although much smaller than air, i.e. $3.4\ 10^{-3}\ °C^{-1}$ is relatively large compared with glass, i.e. $8\ 10^{-6}\ °C^{-1}$, and other liquids and may be a good candidate for thermometric liquid. Another strong point was that spirit does not adhere too much to the tube, making possible readings.

The first step was to obtain a popular alcoholic drink distilled from wine grapes or distilled from wine, e.g. eau-de-vie, cognac. The typical percentage of Ethyl alcohol by volume (ABV) of this drink is 42% ABV. After successive distillations it is possible to increase the percentage of alcohol reaching 80% ABV or more. This highly

concentrated solution of alcohol after refinement was used as spirit for the thermometers (Magalotti, 1666; Targioni Tozzetti, 1780). This concentrated solution is called "acquarzente". Pure water has a small expansion coefficient (2.1 10^{-4} $°C^{-1}$) and is not convenient as thermometric fluid; as opposed spirit (Ethyl Alcohol, or Ethanol) is 11.2 10^{-4} $°C^{-1}$ and its sensitivity is more than 5 times larger. For this reason thermometers were made with a well-refined "acquarzente" as resolution and sensitivity of the instrument were proportional to the percentage in Ethyl alcohol and it was crucial to use the same "acquarzente", with exactly the same % ABV, to build instruments identical each other. However, the expansion of spirit was in any case small and needed magnification. The solution was inspired to the Thermoscope, i.e. a large volume with the expanding fluid (in that case air) and a thin tube where to observe the air changing of volume after the expansion. It was simple to invert up-down a smaller Thermoscope with the ampulla filled of spirit on the bottom, like a standing bottle. The upper top was open. It worked, but spirit evaporated at fast rate. Like a bottle with spirit, it was necessary to close, better to seal, the upper top. The upper top was sealed with a flame at melting glass temperature. This solved the problem of the evaporation of spirit and made the instrument easily portable and independent from its position. Some air at atmospheric pressure was left inside the tube because they had no other chance, but the atmospheric pressure was necessary to avoid spirit boiling.

Building a Florentine Thermometer. All Florentine Thermometers were built by Giuseppe Mariani nicknamed "il Gonfia", i.e. "the Blower". These thermometers were a masterpiece of science and technology. Several types of spirit-in-glass thermometers were built, most of them with scientific purposes and some as amazing artworks, e.g. frog shaped. The scientific thermometers had a very large bulb in the bottom and a more or less long tube that was graduated to read temperature. The tube was either rectilinear or spiralling to reduce the occupied space, with the scale divided into 50, 100, 300 and 400 levels, some of these models are still preserved in perfect conditions at the Institute and museum of the History of Science (IMSS) in Florence as visible in Figure 4.6.

The Grand Duke had in mind the problem that all the thermometers should have the same scale to interpret the readings. For this reason he ordered a number of thermometers identical each others, the famous Little Florentine Thermometer (LFT). From Magalotti (1666), Crivelli (1744), Targioni Tozzetti (1780) and Antinori (1841)

we have reasonably good information about the LFT: all instruments were made identical, with the same scale based on the range of temperature in Florence. We find also specified the thermometric liquid and how the ampulla was filled and the capillary sealed. However, some important details are missing and we will search to provide a general image of the manufacture.

Figure 4.6: From the left to the right: a) Tall-stem thermometer: The stem carries enamel buttons indicating the degrees of one of the thermometric scales used by the Accademia del Cimento (1657-1667). The black buttons indicate single degrees, the white buttons 10 degrees, and the blue buttons 100 degrees. b) Spiral thermometer: thermometer with spiral or "snail" stems used by the Accademia del Cimento. 420 enamel buttons indicate the degrees: the black buttons indicate single degrees, the white buttons 10 degrees, and the blue buttons 100 degrees. c) Cluster thermometer called “infingardo” (slothful): this thermometer used by the Accademia del Cimento consisted of six phials, numbered from 1 to 6, clustered on a column. The phials contain alcohol, in which small glass spheres of different density are immersed.

Mariani filled the thermometer with repeated operations. First he heated very much the sphere, i.e. the ampulla, to expand the air inside, reversed up-down the glasswork and immersed the open top of the capillary into the refined spirit. When the sphere returned to room temperature, the contraction of the air pocket caused the suction of a certain amount of spirit inside the ampulla, passing through the narrow capillary. Mariani drawn up the thermometer, overheated the partially filled ampulla and repeated the operation until the capillary was filled at the same bead as in the LFT reference instrument.

Mariani had then the possibility to built identical glassworks, marking a same scale, and then regulated the calibration filling all instruments with spirit reaching the same bead. Moreover he verified if the instruments responded in the same way immersing them in

some baths at arbitrary temperatures and checking their correspondence. The instruments that passed the cross-comparison tests could be hermetically sealed by melting the top of the capillary with a well-addressed flame. A test made by Vittori and Mestitz (1981) recognized that the standard deviation (SD) between 15 LFT survived at the Institute and Museum of History of Science, Florence, is SD = 0.5 °C. In conclusion, all LFT were built identical each other, i.e. they had the same glass envelope, the same refined liquid with the same expansion coefficient, i.e. the same percentage of Ethyl alcohol, the same scale.

Scale of the LFT. The calibration as we can imagine today, was not reported in the original documents of the Grand Duke and his Academy simply because the existence of fixed points was unknown. Fixed points have been discovered after experiments made with the newly invented thermometers, e.g. the study of water freezing and melting ice. From Magalotti (1667) and Antinori (1841) we know that all LFT measured that ice melted at 13.5°G (for °G see later), but this should be considered an important finding, not a calibration. The members of the Cimento's Academy in fact used the results obtained from melting ice experiments to set this lower point of the scale in the thermometers. We should consider that the LFT was the first thermometer in the world, and necessarily it had a fully arbitrary scale. It was dimensioned to include the full range of temperature in Florence, from extreme winter cold to the hot experienced after noon in summer, exposed to sunshine. The scale of the LFT was divided into 50 not numbered levels, marked with vitreous enamel beads, being one white every 9 black (see Figure 4.7).

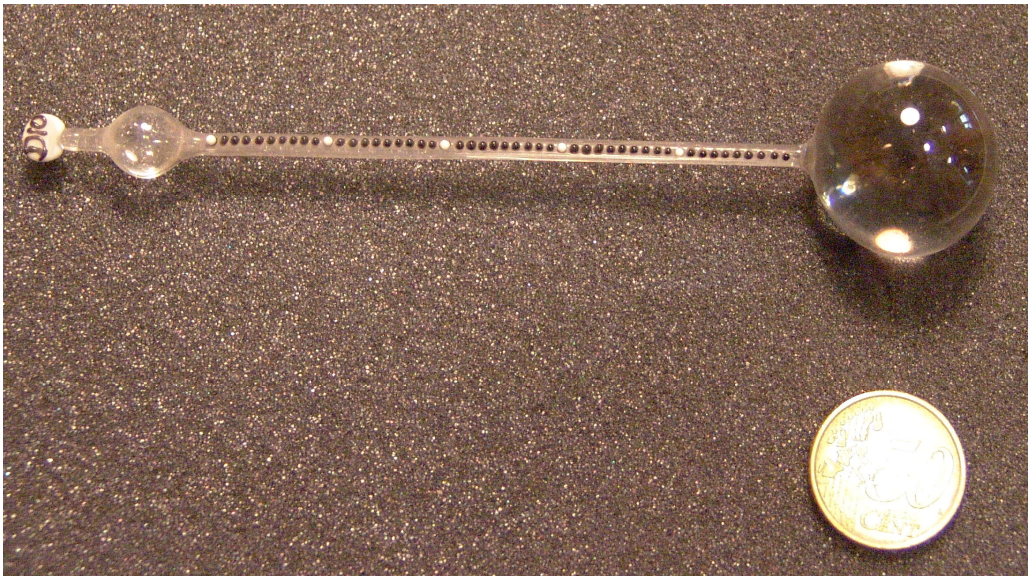

Figure 4.7: The spirit-in-glass little Florentine thermometer (LFT) used to take temperature instrumental readings for the first meteorological Network at world (i.e. the Rete Medicea Network) during the years 1654-1667 (1670) in 11 stations in Europe. The instrument was standardized to permit a comparison among the measuring performed in the different station, created to stand outdoor and with portable dimension (in the picture a comparison with a 50 cent coin is visible). Picture courtesy of Institute and Museum of History of Science, Florence.

Each bead corresponded to one degree of this scale, the degree being named "G" in honour of Galileo. The scale marked on the tube of the LFT is 9 cm long and once divided by 50, the space resolution of each °G is 1.8 mm. We will see that after calibration 1 °G = 1.44 °C approximately so that the resolution is 0.5 °G = 0.7 °C. The comparability of the readings was necessary because the Grand Duke wanted to distribute the instruments to observers in different sites and from the comparison of the readings determine the differences of the local climates per each site. The regularity of replicas and the instrumental precision show an incredibly advanced technological level and rejection of imperfect copies.

Modern calibration of LFT. We have five late calibrations of the LFT with similar results (summarized in Table 4.1).

Table 4.1: The five late calibration of the LFT, with indication on Authors, date and Methodology

Author	Date	Methodology
L. Cotte	1748	Unknown
G. Libri	1830	17 LFT in Florence
J.F. Schouw	1839	Based on literature
C. Maze	1895	1 LFT in Paris
O. Vittori & A. Mestiz	1981	15 LFT in Florence

- The first is due to Father Louis Cotte and his famous Traité de Météorologie (i.e. Treatise of Meteorology, 1748). He published a drawing that compared side-by-side fifteen different scales in use at his time. Details about calibration are totally missing.
- G. Libri (1830) made a calibration in 1829-1830 by cross comparing with a Réaumur thermometer seventeen LFT found in 1829 in the Museum of Science, Florence.
- J.F. Schouw (1839) made a scale based on Libri and some other literature existing in the Museum of Science, Florence.
- G. Maze (1895) made a calibration based on only one LFT used in Paris by cross comparing it with another known thermometer.
- Vittori and Mestitz (1981) re-calibrated in controlled calibration bath fifteen Little Florentine Thermometers still preserved in good conditions at the Museum of History of Science, Florence. These were the same tested by Libri, except two that were damaged during the flood of the river Arno in 1966. The 1981 calibration was very accurate, although glass and spirit had more than 3 centuries.

In practice, all the calibrations are very similar between each other (Figure 4.8).

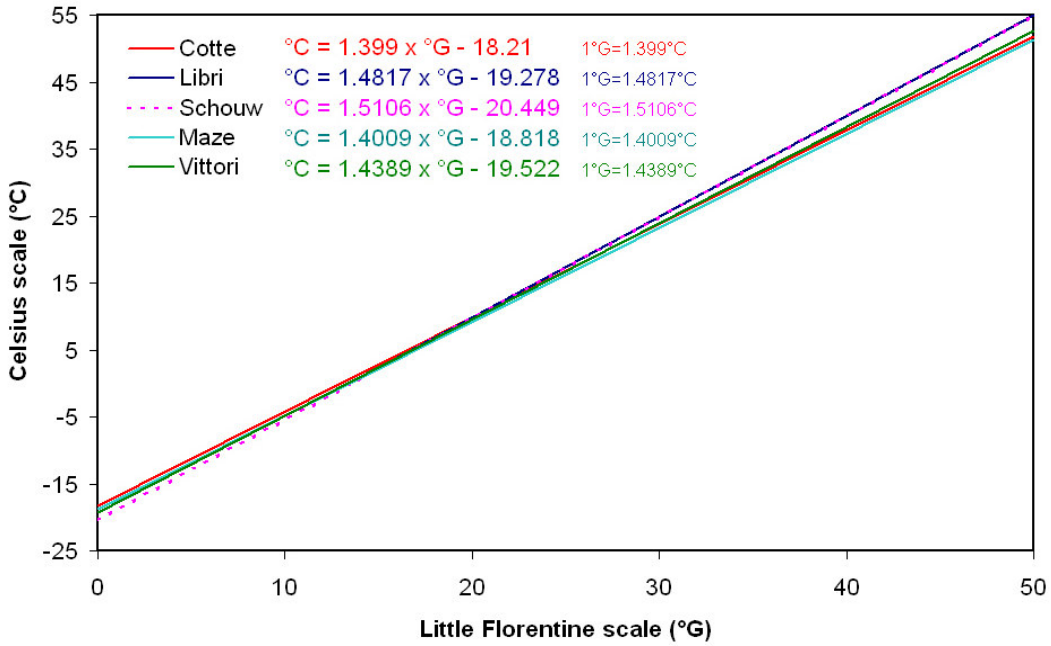

Figure 4.8: Five late calibration of the Little Florentine Thermometer (LFT). Father Louis Cotte (1748), G. Libri (1830), J.F. Schouw (1839), G. Maze (1895) and Vittori and Mestitz (1981). In data analysis and elaboration we followed the Vittori and Mestitz calibration.

We could suppose the older the calibration, the better, as glass and spirit might have transformations with aging. In such a case we should prefer the scale by Cotte (1748), but the lack of information and the reference to a drawing are a weak point. However, we preferred the calibration by Vittori and Mestitz because it is well documented and very accurate, based on 15 originals; it is the closest to the earliest calibration by Cotte (potentially the most attractive) and the closest to the average of all calibrations. The fact that the earliest and the latest calibrations are very close each other means that the drift for glass and spirit ageing was very modest.

Linearity of the LFT. All calibrations show a linear response of the LFT. In particular Vittori and Mestitz (1981) calibrated at 0°, 10°, 14°, 20° and 34 °C and the correspondence was linear. This is apparently surprising because ethyl alcohol strongly departs from linearity and its expansion coefficient is variable with T. However, the non-linearity of spirit is a problem when fixed points are 0° and 100 °C, not when the calibration is made at temperatures between 0° and 40 °C because the reduced range makes the calibration fitting with the real behaviour of glass. As a consequence, temperatures in the range 0° to 40 °C are well represented by a straight line, while some departure is expected for the lowest temperatures, obtained as an extrapolation of the

scale. Vittori and Mestitz deliberately avoided to continue the calibration below °C to avoid any risk for the preservation of these precious instruments. For the climate of Florence, the LFT was as good as a mercury-in-glass thermometer.

4.3.2 The first European meteorological network the Rete Medicea (1654-1670)

Galileo, his pupils, the Grand Duke Ferdinand II and his bother Leopold were aimed to discover some key meteorological parameters, to invent instruments to measure them, to look at their distribution in time and space, to discover the fundamental laws of physics, biology and other sciences. The interest for Meteorology was not limited to the thermometer. In 1639 Castelli invented the raingauge and the evaporimeter (Castelli 1639), in 1643 Torricelli invented the barometer (Marsenne, 1647) and in 1655 Ferdinand II the condensation hygrometer. In order to make extend the observational activity outside the geographical limits of Florence, Leopold and the Grand Duke decided to organise the observations and founded the first meteorological network, called Rete Medicea, i.e. Medici Network from the Family name of the Grand Duke and his brother Leopold. The Medici Network was composed of 11 stations in Europe and flourished in the period 1654-1667 (1670).

The Network was created to know the main climatic features of some localities, and especially to give an answer to the following questions: What is the range of temperature in various countries on the plain and the mountains, in the middle and higher latitudes? Does ice melt always at the same temperature, disregarding geographical or height differences? How much density of liquids changes with temperature? What is the temperature difference between sunshine and shadow exposure? The Medici Network was the first international meteorological network, with the same instruments and exposure, and with regular readings sampled following a precise schedule.

The Network, formally active from 1654 to 1667, but really till 1670 for the main stations in Florence and Vallombrosa, was organised and leaded by a Secretary, Father Luigi Antinori, Jesuit, was chancellor of Jesuit Fathers (Antinori, 1858) and chaplain of the Grand Duke. Task of Antinori was to provide the instruments, identical each other to get comparable results, to provide instructions how to operate, i.e. a thermometer

hung on a wall facing North and another in a wall facing South, to see the air temperature and the effect of sunshine, how to make other observations, the time schedule for readings. Observers were monks of the Camaldolense Benedectine Order in Florence and Vallombrosa, Jesuit Fathers in other stations. This choice was dictated because monks and fathers were with elevated cultural level, always on the site, free from civil business, able to perform regular readings by day and by night, at monastic hours in which prayers and observations were scheduled.

Sampling was based on the so-called Italian Time, and observations at monastic hours. Following the Italian Time, the day began at twilight with the monastic celebration of "Compieta", i.e. "The Angelus" about half an hour after sunset. All the subsequent hours were counted starting from this moment that varied day-by-day during the calendar year. Most observers were monks, because with elevated cultural level, free from civil business and able to perform regular readings by day and by night, at monastic hours. Observations continued at midnight, at "Matutinum", i.e. the celebration before sunrise and then at regular intervals during the day. The station of Vallombrosa had eight readings a day. Other stations less, but generally from five to eight. All readings were daily collected in a sheet with all the observations of the same day (Figure 4.9), and sent daily, or weekly, depending from the distance, to the Grand Duke.

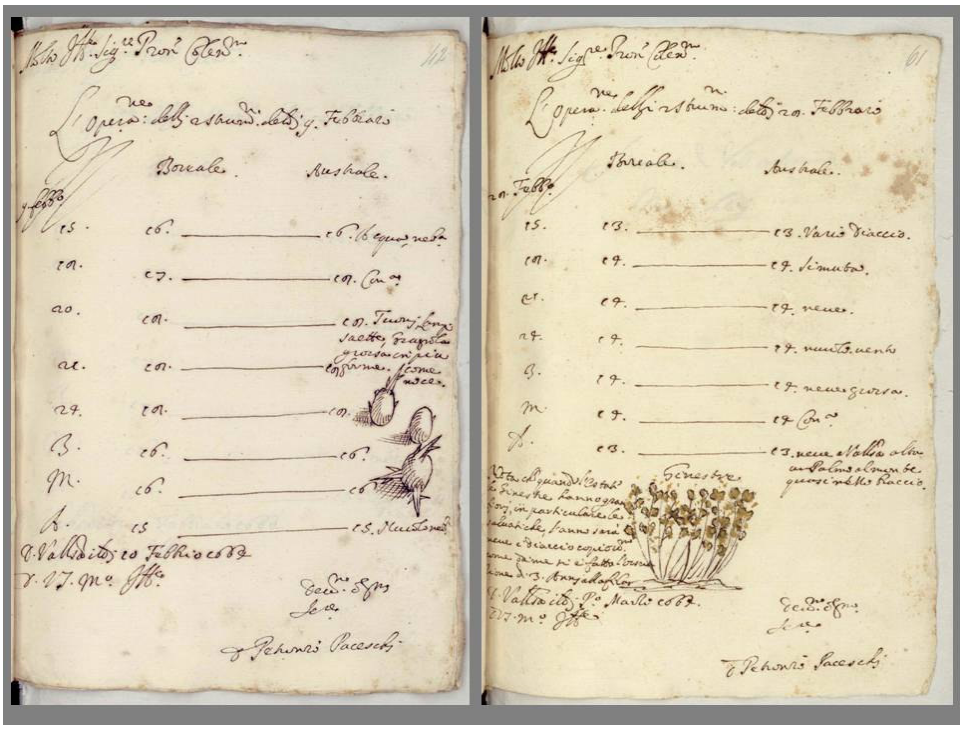

Figure 4.9: Two letters with meteorological observations from Vallombrosa: (a) with Hailstones, (b) with blooming flowers. Readings were generally taken five to eight times a day, depending on sites, but at hours that varied with the seasons, because the new day started at twilight.

These daily sheets with temperature and visual observations were produced some ten years before than Robert Hooke (1635-1703) drawn the first standardized sheet to be used in UK as weather log (1663) and later as a model at international level. A copy of the readings was kept at the stations. The practice of sending a duplicate saved several of the readings arrived up to us.

Stations and activity of 'Medici' Network (1654-1667 (1670)). The activity was concentrated in two primary stations, i.e. Florence and Vallombrosa, which operated continuously with several observations by day and by night for the whole duration of the Network. Other stations were secondary stations and had a shorter activity, often fragments of some months to record the seasonal extremes, i.e. hot in summer and cold in winter. Paris was a special case. The geographical extension of the Medici Network is displayed in Figure 4.10.

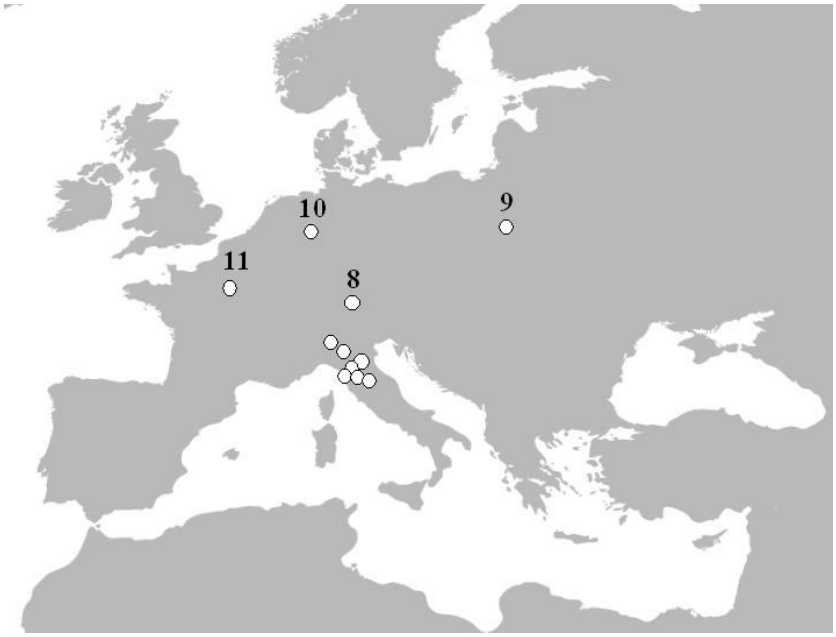

Figure 4.10 (a): Map of the eleven European stations of the Medici Network, formally active for the period 1654-1667 and in practice from 1654 to 1670. Stations outside Italy were: 8-Innsbruck, 9- Warsaw, 10-Osnabruck and 11-Paris.

Figure 4.10 (b): Map of the seven Italian stations of the Medici Network, i.e. 1-Florence, 2-Vallombrosa, 3-Pisa, 4-Cutigliano, 5-Bologna, 6-Parma and 7-Milan.

The interest of the Grand Duke for summer and winter was not only to know extremes, but also to deduce what was called "The Temperate", i.e. the temperature in the mid

between the warmest and the coldest weather, that was supposed to be the basic temperature of the region. Stations and correlated information on location, observational period and observers are reported as follows in Table 4.2.

Table 4.2:Stations active in the Medici Network.

	Location	**Lat E**	**Long N**	**Altitude**	**Period**	**Observer**
1	Florence	43°47’	11°15’	50 m	15-12-1654 31-03-1670	Unknown
2	Vallombrosa	43°44’	11°34’	980 m	01-01-1656 31-05-1670	Petronio Paceschi, Filiberto Casini and Nicola Signorini
3	Pisa	43°43’	10°24’	4 m	26-11-1657 08-05-1658	Alfonso Borelli and Vincenzo Viviani
4	Cutigliano	44°6’	10°45’	678 m	06-03-1658 31-03-1659	Unknown
5	Bologna	44°29’	11°20’	54 m	01-12-1654 31-03-1656	Giovan Battista Riccioli
6	Parma	44°48’	10°20’	57 m	23-12-1654 31-12-1660	Antonio Terrillo
7	Milan	45°27’	9°11’	137 m	17-02-1655 30-04-1656	Giulio del Re
8	Innsbruck	47°16’	11°23’	574 m	06-03-1655 30-04-1655	Unknown
9	Warsaw	52°13’	21°00’	97 m	10-05-1655 16-05-1655	Unknown
10	Osnabrück	52°17’	8°03’	63 m	All readings lost	Unknown
11	Paris	48°51’	2°20’	33 m	05-1658 09-1660	Ismaël Boulliau

Florence was the main station, under the strict control of the Grand Duke. The location was in the Convent of Angels, in the city centre (Figure 4.11). Observers are unknown. Libri (1830) stated that the observer was Father Vincenzo Renieri, but this was an error because Renieri died several years before the institution of the Network.

Figure 4.11: :Northern corner of the cloister of the monastery of St. Mary of Angels, Florence where observations were taken in the shadow. Additional measurements exposed to sunshine in the opposite corner.

Pisa was the only station to measure atmospheric pressure, observed by Vincenzo Viviani and Alfonso Borelli for the period November 1657 – May 1658. These were the very first regular pressure readings in Europe. Readings were generally taken three or four times a day. Winter 1657 was characterised by higher pressure and cold; Spring 1658 had pressure lower than normal. The Azores High had difficulty to Enter Mediterranean and the season was chilly and rainy. For more details see Camuffo et al. (2009).

Milan had as observer Giulio del Re (Borchi, 2009). Libri (1830) stated that observer were Father Bonaventura Cavalieri and Ticcioli. Cavalieri should be excluded because it was died years before the institution of the Network. No other information about Ticcioli.

Paris needs a further comment. The queen of Poland, the Italian Maria Luisa Gonzaga, was in good contact with the Gran Duke of Florence and joined the Network with the station in Warsaw that was operative since 1655. In 1657, she sent to the Grand Duke the physicist Tito Livio Burattini, who returned back with some LFT as a gift. One of these LFT was given to the astronomer Father Ismaël Boulliau (1605 - 1691) to observe in Paris. Although late, Paris was formally part of the Network and Boulliau made observations from 1658 to 1660 in rue de Poitevins dans l'hòtel de Thou, later transformed in headquarter of the Sociétés Savantes (Society of Savants). These observations were reported in some tables with the comment: "readings made in Paris, year 1658, with a Florentine Thermometer" and in another column readings with an a mercury thermometer with the same shape and dimension as the LFT.

Another LFT was brought to England by Robert Southwell, president of the Royal Society, in 1661. Robert Boyle was impressed by the studies of Galileo and his pupils and started to analyse them carefully. He made a duplicate of the thermometer brought by Southwell (Hellmann, 1908), used it two years later for his study and described the perfect gases in an appendix (Boyle, 1662) to his work New Experiments Physico-Mechanical.

The Network was officially closed in 1667 for religious and political reasons. Only the Convent of Angles, particularly close to the Grand Duke residence in Florence, continued operating after the official closure of the Network. It continued regular observations till 1670, when the Grand Duke died. Then every activity was stopped. Fortunately, we have today observations covering the whole period 1654-1670, except a few short gaps. After the Academy was closed, the instruments were preserved in the Pitti palace, headquarter of the Academy, and part were sent by Leopold to Pope Alexander VII. In 1737, the instruments survived in Florence were given to Philippe Vayringe, Professor of Physics at the court of Francis I of Lorraine, Grand Duke of Tuscany. At Vayringe's death, in 1746 a part of the old instruments returned back to Pitti palace, a part were sent to Vienna, Theresianum College. Finally, the instruments that remained in Pitti palace were moved to the Museum of History of Science of Florence, forgotten and discovered by Antinori in 1829 (Libri, 1830, Antinori, 1841).

Methodology for data analysis. A seek for all original data and metadata has been performed in three directions: history and climate research institutions and museums of science potentially interested to preserve documents concerning Galileo and the scientific activity in Tuscany in the 16th and 17th centuries; public archives and libraries that had, or might have had original documents, including the remote possibility that the documents were improperly catalogued and not easily identifiable; religious orders that cared the observations, either locally or headquarters of monastic orders where original documents, or duplicate of them, could be either officially or unconsciously preserved. Thanks to a very kind cooperation, we had access to most originals either in paper support or digital reproduction. Some unknown sheets with further data for some months were found. In the Institute and Museum of History of Science, Florence, where a number of Florentine thermometers are preserved, 17 of them being LFT, we had the possibility of observing and measuring them.

After the efforts in data recovery and the solutions, already described, to the problems met with the understanding of the LFT building, scale and calibration procedures, another problem to solve remained the sampling time. During the 17th century, until the French Revolution, sampling time was based on the so-called Italian Time, i.e. the day began at twilight and the subsequent hours were counted starting from this moment that varied day-by-day and place by place during the calendar year. For this reason a necessary step was to recalculate all reading hours from astronomical formulae of the apparent position of the Sun (Camuffo, 2002c) for each station of the Medici network. The formulae involved concern the height H_Θ of the Sun above the horizon and considering that at sunset $H_\Theta = 0$, i.e:

$$\sin H_\Theta = \sin \delta_j \sin \varphi + \cos \delta_j \cos \varphi \cos Z_\Theta \tag{4.1}$$

$$A_\Theta = \arcsin \frac{\cos \delta_j \sin Z_\Theta}{\sqrt{1 - \left(\sin \delta_j \sin \varphi + \cos \delta_j \cos \varphi \cos Z_\Theta\right)^2}} \tag{4.2}$$

where δ_j is the solar declination computed as

$$\sin \delta_j = -\sin \delta_0 \cos \left(\frac{2\pi j}{365.24} \right) \tag{4.3}$$

and δ_0 is the declination for December 21th, j is the number of the day starting from the winter solstice. Other symbols in equations (4.1) and (4.2) are φ for latitude and Z_Θ for the hourly angle of the sun from the culmination meridian.

A day by day correction is due because the Solar motion is perturbed by planets as described by the so-called equation of time (ET) that is the difference between apparent solar time and mean solar time, both taken at a given place (or at another place with the same geographical longitude) at the same real instant of time. ET ranges between –14min (advance) and +16 min (delay) and time difference Δt can be calculated with an astronomical formula, or found reported in ephemeredes, as follows

$$\Delta t \approx 229.18\left[-0.0334\sin\left(\frac{2\pi}{365.24}\,j\right)+0.04184\sin\left(\frac{4\pi}{365.24}\,j+3.5884\right)\right] \tag{4.4}$$

After the astronomical sunset is known, the twilight length, i.e. the duration of illumination due to the atmospheric refraction, is calculated per each day of the calendar year with the formula

$$\frac{(b+2e)-b}{2}=\frac{\dfrac{ar\cos(1-n)}{\pi}-\dfrac{ar\cos(1-m)}{\pi}}{2} \tag{4.5}$$

where the left hand in the formula represents the duration of twilight in hour being half the difference between the day length b and the arc comprising the day length and the two twilights. Symbols in equation (4.5) are derived from the following formulas:

$$b=\frac{ar\cos\,(1-m)}{\pi} \tag{4.6}$$

$$1-m=\tan\varphi\cdot\tan\left(\varepsilon\cdot\cos\left(\frac{2\pi\ j}{365.24}\right)\right) \tag{4.7}$$

$$1-n=\tan\,\varphi\cdot\tan\left(\varepsilon\cdot\cos\left(\frac{2\pi\ j}{365.24}\right)\right)+\frac{h}{\cos\,\varphi} \tag{4.8}$$

where ε is the obliquity of the ecliptic (i.e. the angle 23.439° almost constant that changes slowly only within thousands of years) and h being the tangent of the twilight angle, i.e. the Sun below the horizon.

In this way we calculated per each observing day the Civil Twilight, i.e. when the Sun is 6° below the horizon and the visual perception is strongly reduced. It was considered the end of the day and the start of the new one. It is possible to transform the Italian Style Time to West European Time adding for each day of the calendar year the difference between the midnight and the twilight. Per each station and each day, the reading time is converted into West European time.

Another feature of the Medici series was the particular Calendar Style. During the 17th century in fact, Italy was divided into a number of small states and dukedoms, each of which had their own calendar. Florence used the 'Incarnation style'(Camuffo and Enzi 1992) with the 25th March starting day, i.e. postponed by 84 days in comparison to the modern dating style (see Figure 4.12 for an example).

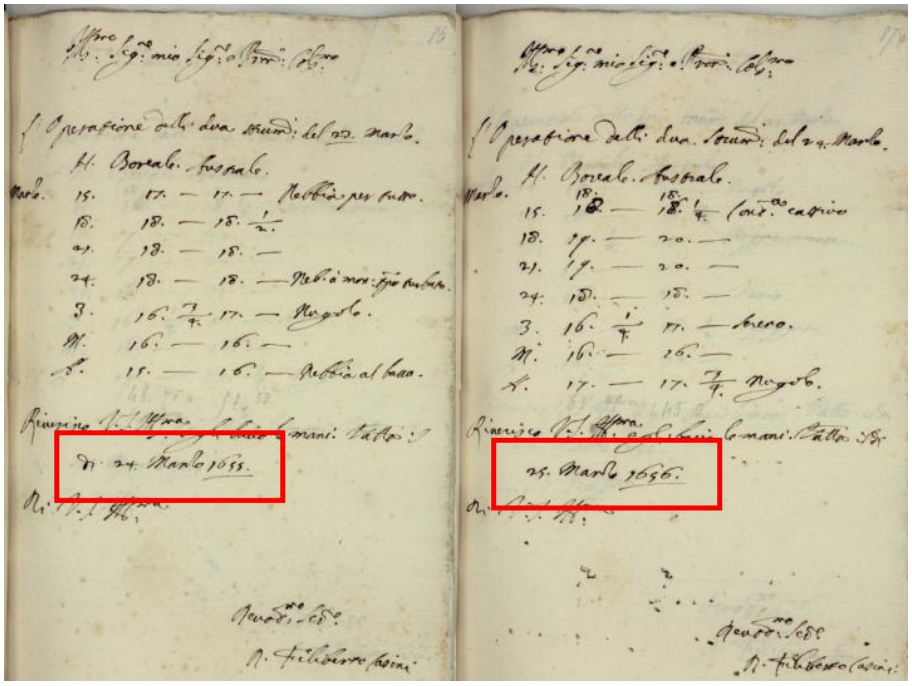

Figure 4.12: Example of a different dating stile in the Italian dukedoms during the 17th century. Here, are reported two letters coming from the Vallombrosa station of the Medici Network where the 'Incarnation' calendar style was adopted with the 25th March new year's day.

Each stations had two thermometers one hung to a wall facing North (second column in the log) and one to a wall facing South exposed to direct sunshine (third column), obviously with a higher temperature. However, in a few cases in the Vallombrosa Abbey, the thermometer in the second column registered a higher temperature. This could be attributed either to a misleading transcription in the columns or to some

uncontrolled transmission of heat to the thermometer. The thermometers were almost certainly kept inside the cloister to allow daily and nocturnal readings not only repaired from rainfall, but especially without needs of affording the risk of leaving the monastery. An inspection on the site demonstrated that cardinal points were aligned with the corners of the cloister and that no fireplaces, ovens or other heat sources were located near the walls where the thermometer was probably located. This confirmed the hypothesis of a misleading column transcription, and in such a case the lower between two simultaneous readings has been selected.

The Florence and Vallombrosa series were affected by some minor gaps as reported in Table 4.3a and b.

Table 4.3a Gaps in the Florence series filled from other series and station used to fill.

1-1-1657 to 31-1-1657, VA	2-4-1657 to 30-4-1657 VA	15-6-1657 to 19-6-1657 VA
25 and 26-6-1658 CU	2-9-1658 to 31-10-1658 CU	25 and 26-11-1658 CU
2-8-1660 to 30-9-1660 VA	2-5-1661 to 31-5-1661 VA	2-8-1661 to 31-8-1661 VA
1-3-1662 to 31-3-1662 VA	1-1-1664 to 10-5-1664 VA	1-1-1670 to 31-5-1670 VA

Legend: VA= Vallombrosa, CU = Cutigliano reference station

Table 4.3b Gaps in the Vallombrosa series filled from other series and station used to fill.

15-12-1654 to 31-1-1655, FL	25 and 26-8-1657 FL	11-9-1657 to 19-9-1657 FL
27-11-1657 to 29-11-1657 FL	1-1-1658 to1-9-1658 FL	1-11-1658 to 31-12-1659 FL
2-10-1662 to 31-10-1662 FL	1-1-1663 to 30-6-1663 FL	9-9-1663 to 1-10-1663 FL
1-1-1668 to 31-3-1670 FL		

Legend: FL=Florence reference station

The minor gaps have been filled by plotting in abscissa the reference series (e.g. Florence) and in ordinate the series with gaps to be filled (e.g. Vallombrosa). From the scatter of dots we obtained the best-fit transfer function with $R^2 = 0.89$ for Florence to Vallombrosa and vice-versa, similarly for Cutigliano to Florence we obtained $R^2 = 0.91$ with actual observations transformed in °C and $R^2 = 0.45$ with data transformed in terms of anomaly.

The transfer equations (TE) for the mean temperature reconstruction are respectively:

$$\langle T_{VA} \rangle = \mathbf{0.8159} \cdot \langle T_{FL} \rangle - \mathbf{4.161}$$ to fill Vallombrosa gaps with Florence data

$$\langle T_{FL} \rangle = 1.0898 \cdot \langle T_{VA} \rangle + 6.2163$$ to fill Florence gaps with Vallombrosa data

$$\langle T_{FL} \rangle = 1.1761 \cdot \langle T_{CU} \rangle + 3.4268$$ to fill Florence gaps with Cutigliano data

Discussion on the results. An illustrative comparison between the continuous activity of the two main stations in Florence and Vallombrosa and the fragmentary activity of the secondary stations is shown in Figure 4.13 in term of mean daily temperature for a limited period, i.e. December 1654-1658.

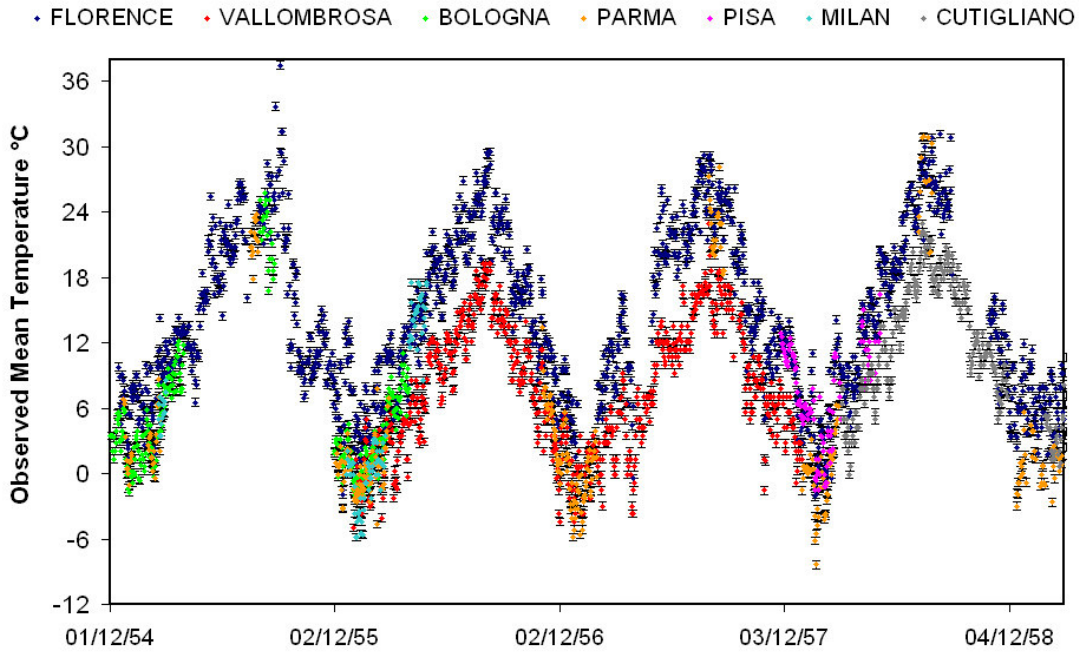

Figure 4.13: An illustrative comparison among the seven original temperature series of Medici stations for the 1654 to 1658 period. Florence station, blue full dots; Vallombrosa, red full dots, Bologna, light green full dots, Parma, orange full dots, Pisa violet full dots, Milan, cyan full dots and Cutigliano, grey full dots. Error bars: ±0.35 °C.

The mountain stations, i.e. Vallombrosa and Cutigliano, show a lower temperature compared with those on the plain. Fragments in secondary stations were taken to know the seasonal extremes, mainly winter and summer. The error bars reported in the plot are the same for each stations (i.e. ±0.35 °C). This was the maximum reading error that one observer could make rounding up or down the reading in this particular scale, with resolution 0.7°C.

The mean daily temperature in Florence and Vallombrosa for the 1654-1670 period are reported in Figure 4.14 and Figure 4.15 respectively.

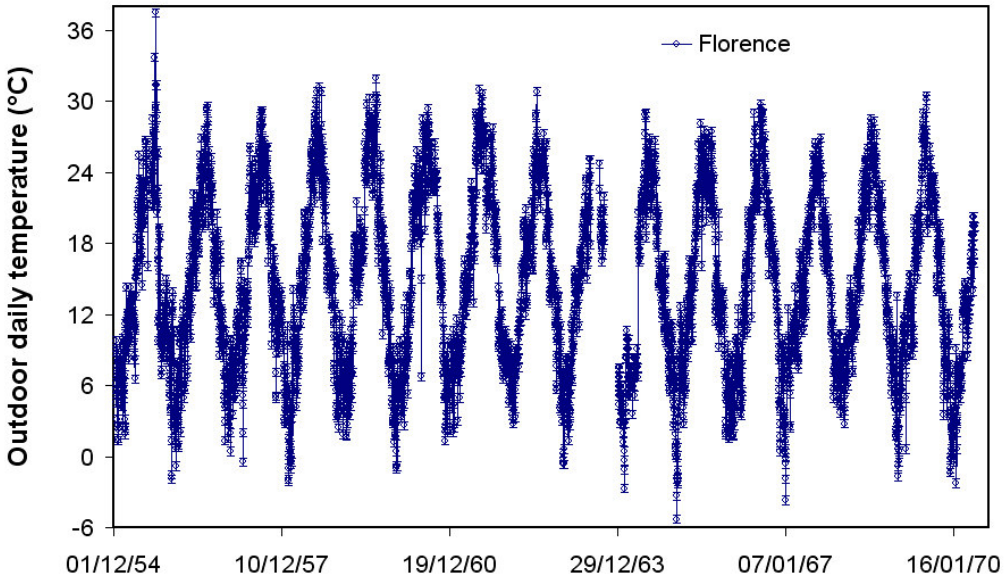

Figure 4.14: The daily temperature series of Florence expressed in Celsius degree, thin and open blue dots. The reconstructed period are reported in detail in Table1. The series spans in a time range from December 1654 to May 1670. Error bars: ±0.35°C.

The average temperature in Florence was 14.73 °C and 7.89 °C in Vallombrosa and the difference between the two stations 6.84 °C. The hottest summer was in 1655. The most severe cold happened in January 1665 in Florence and in December 1662 in Vallombrosa. The lowest of the highest summer temperature was in June 1663. The two mildest winters were in 1662 and 1668 in Florence and 1668 and 1659 in Vallombrosa. No trends are visible.

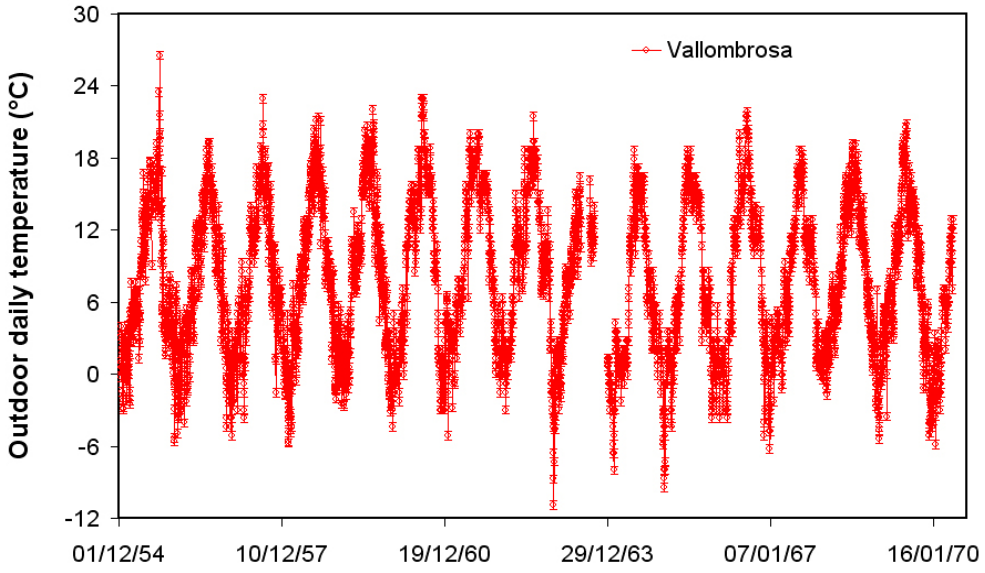

Figure 4.15: The daily temperature series of Vallombrosa expressed in Celsius degree, thin and open red dots. The series spans in a time range from December 1654 to May 1670. Error bars: ±0.35°C.

A cross comparison between the individual series has been made, by calculating the determination coefficients R_{ij}^2 between all pairs of stations, label i and j. Figure 4.16 shows how R_{ij}^2 decreases by increasing the distance from Florence, selected as reference station. The result is that R_{ij}^2 exponentially decreases with the increasing distance (d_{ij}) between stations following the equation:

$$R_{ij}^{\ 2} = e^{-0.0016\, d_{ij}} \tag{4.9}$$

The exponential interpolation is characterized by an elevated value of R^2, i.e. $R^2 = 0.90$ considering that some scatter is justified due to the different altitude of stations, some of them being located on the mountains and others on the plain.

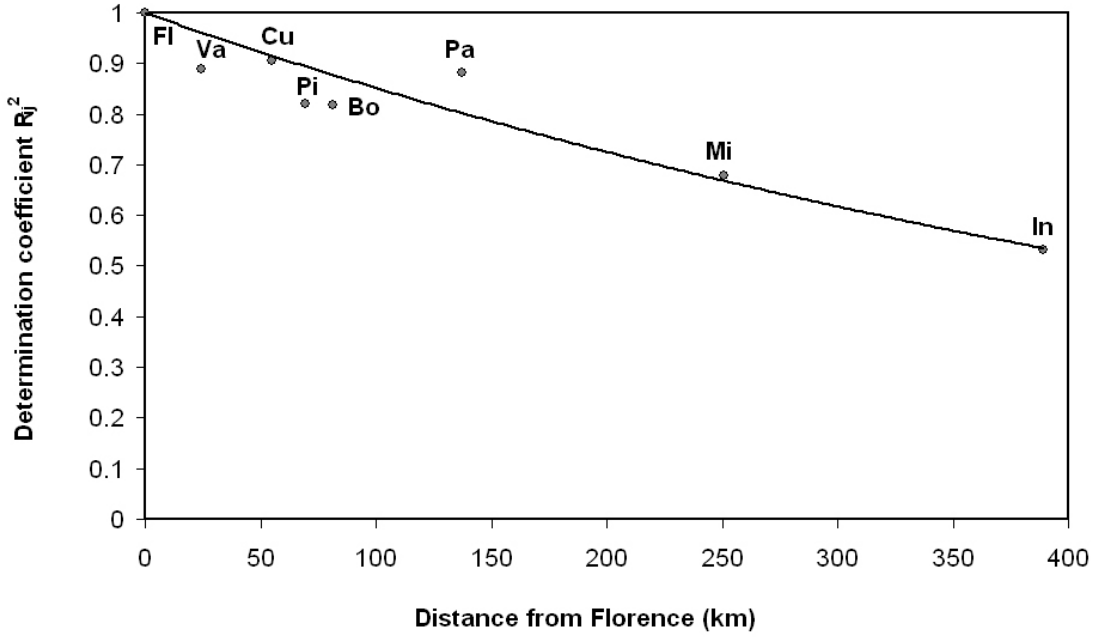

Figure 4.16: Cross comparison between the individual series of the Medici Network. Determination coefficient R_{ij}^2 is plotted versus distance between stations referred to Florence, headquarter of the Network. The correlation between stations exponentially decreases as the distance increases.

The mean daily temperature anomaly in Florence and Vallombrosa for the 1654-1670 period are reported in Figure 4.17 and in Figure 4.18. The anomaly has been expressed in expanded scale to be more easily readable. In addition to the daily data, a low-pass bell shaped filter has been applied, i.e. Hamming filter (Wei, 1990):

$$D(\tau) = \begin{cases} 0.54 + 0.46 \cdot \cos\dfrac{\pi\tau}{\tau_m}, |\tau| \le \tau_m \\ 0, |\tau| > \tau_m \end{cases} \tag{4.10}$$

where τ_m = 11 day is the window and τ the time variable advanced with 1 day steps. The persistence of values scattered around the same level is a further demonstration that the series are homogeneous, without drift and the temporary departures are really due to extreme weather conditions. The 1961-1990 reference period exceeds the average of all the 1654-1670 observations by +0.09 °C for Florence city centre (Ximenian Observatory) and +1.18 °C for Vallombrosa.

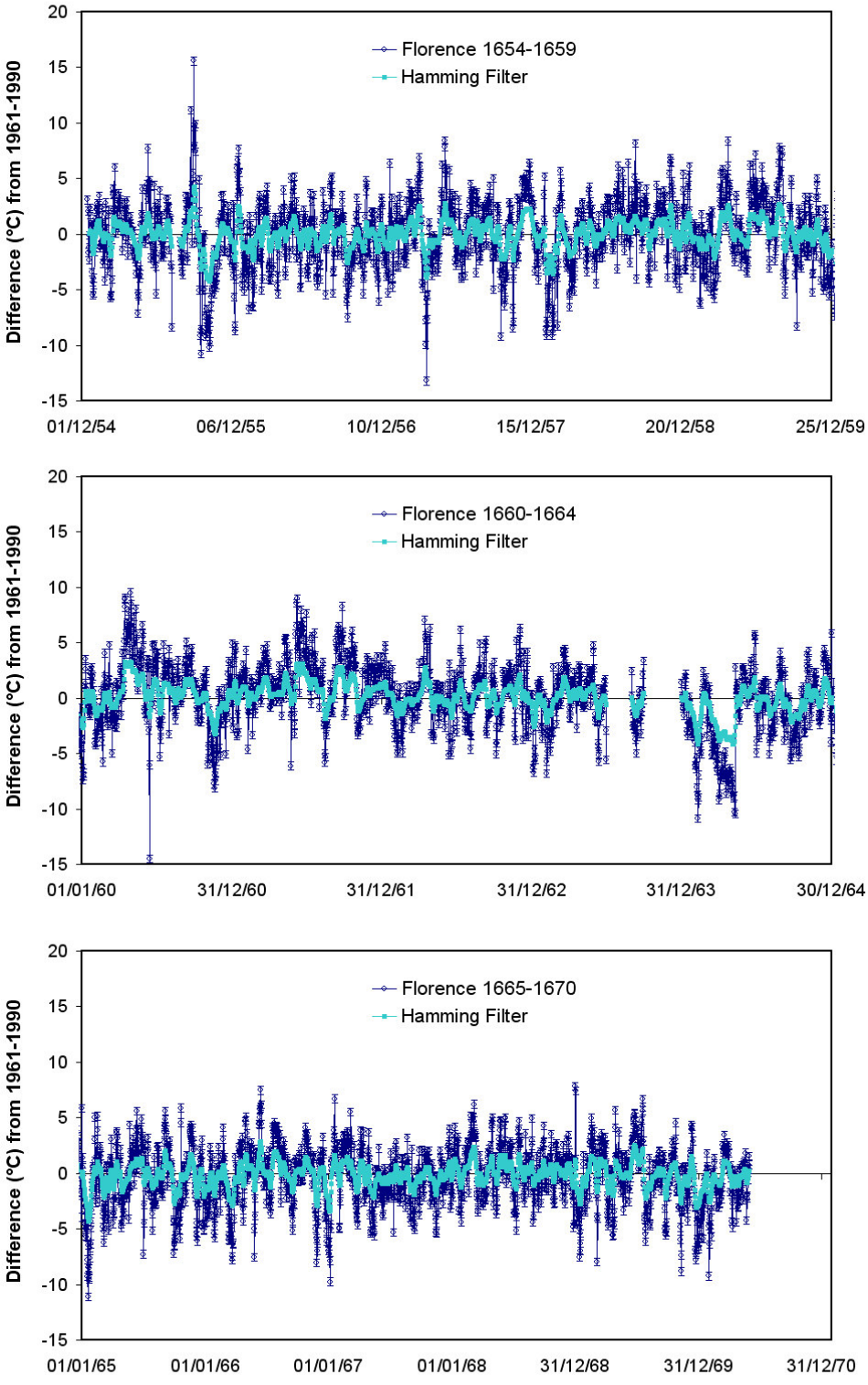

Figure 4.17: The daily series of temperature anomaly (reference period 1961-1990) for Florence expressed in Celsius degree, thin and open blue dots. The Hamming filter with 11 days windows is reported (thick cyan line) in order to follow the anomaly trend during tome. Error bars: ±0.35°C.

.

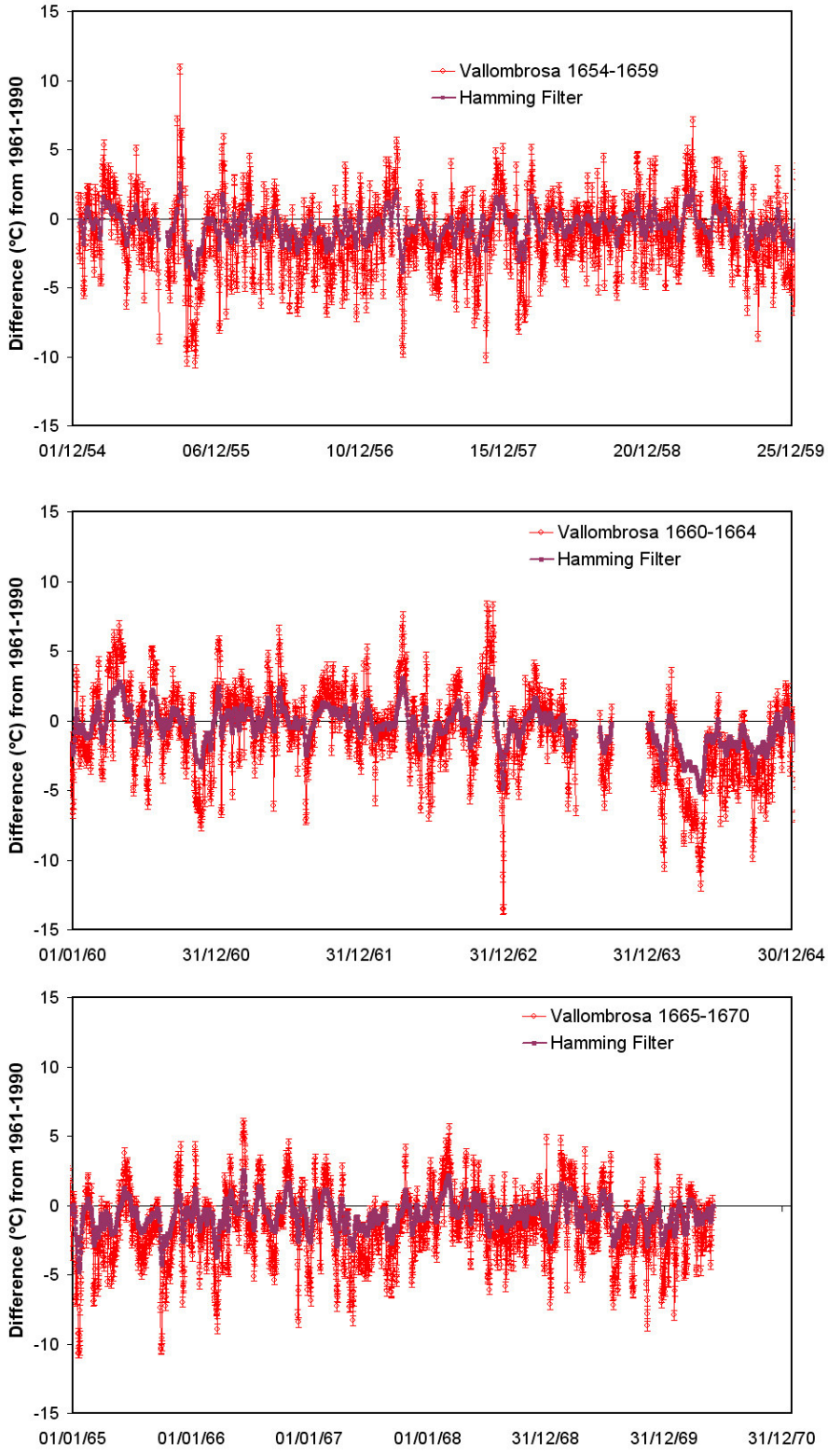

Figure 4.18: The daily series of temperature anomaly (reference period 1961-1990) for Vallombrosa expressed in Celsius degree, thin and open red dots. The Hamming filter with 11 days windows is reported (thick violet line) in order to follow the anomaly trend during tome. Error bars: ±0.35 °C.

It is surprising to find so a small difference for Florence despite the growth of the urban heat island and the global warming. However, the historical centre was practically unchanged from the times of the Grand Duke except for an expansion of the town outskirts and the traffic. The landscape and urban heat island evolution are problems common to all series and in the actual case of an historical city centre, controlled by a specific agency for the preservation of cultural property, changes have been relatively modest. Another difference can be found because the early observations at the Angels cloister were made at ground floor level, and today in the Ximenian Observatory on the meteorological brickwork tower located 25 m above the soil and 15 m above roof level. This elevated location attenuates the effect of the urban heat island. A comparison between the 1961-1990 averages measured at the Ximenian Observatory and the rural site Firenze Peretola (local airport) shows that Ximenian Observatory is only 0.36 °C warmer than the rural site. If we crudely sum the two above values, i.e. 0.09° and 0.36 °C, we obtain 0.45 °C local warming.

Vallombrosa had a minor local deforestation, new asphalted roads, some new buildings built for mass tourism and related business and a small village not far from the monastery that suggest the influence of a recent minor heat island in addition to global warming.

A comparison of the Florence and Vallombrosa series with the Central England (CE) series (Manley, 1974) for 1659-1670, is useful to assess the quality of the early part of the CE series, defined as follows by its Author: “it must be considered less reliable, being based on extrapolation from the results of readings of highly imperfect instruments in uncertain exposures at a considerable distance, generally in South-East England, or on estimates based on interpretation of daily observations of wind and weather”. Figure 4.19a shows the temperature scale of Florence (left side) shifted and compressed in comparison with the CE in order to overlap the two plots from March 1666 - April 1667 which corresponds to the sequence of thermometer readings made by John Locke when he was interested in Medicine in Oxford. From Figure 4.19a we see that in the 1666 – 1667 overlapping period of instrumental observations, both stations have the same yearly range. From 1664 to 1670, except 1666 – 1667, the comparison shows the same summer temperature but the overestimated CE winter minima. From 1659 to 1663, the CE yearly range is reduced with underestimated summer maxima and

overestimated winter minima, assuming the typical appearance of measurements taken indoors although the data have been derived from descriptive notes. Figure 4.19b for Vallombrosa and CE has the same scale for both stations and the yearly temperature range appears to be the same from 1665 onwards. The reduced range of CE for 1659 – 1663 is confirmed.

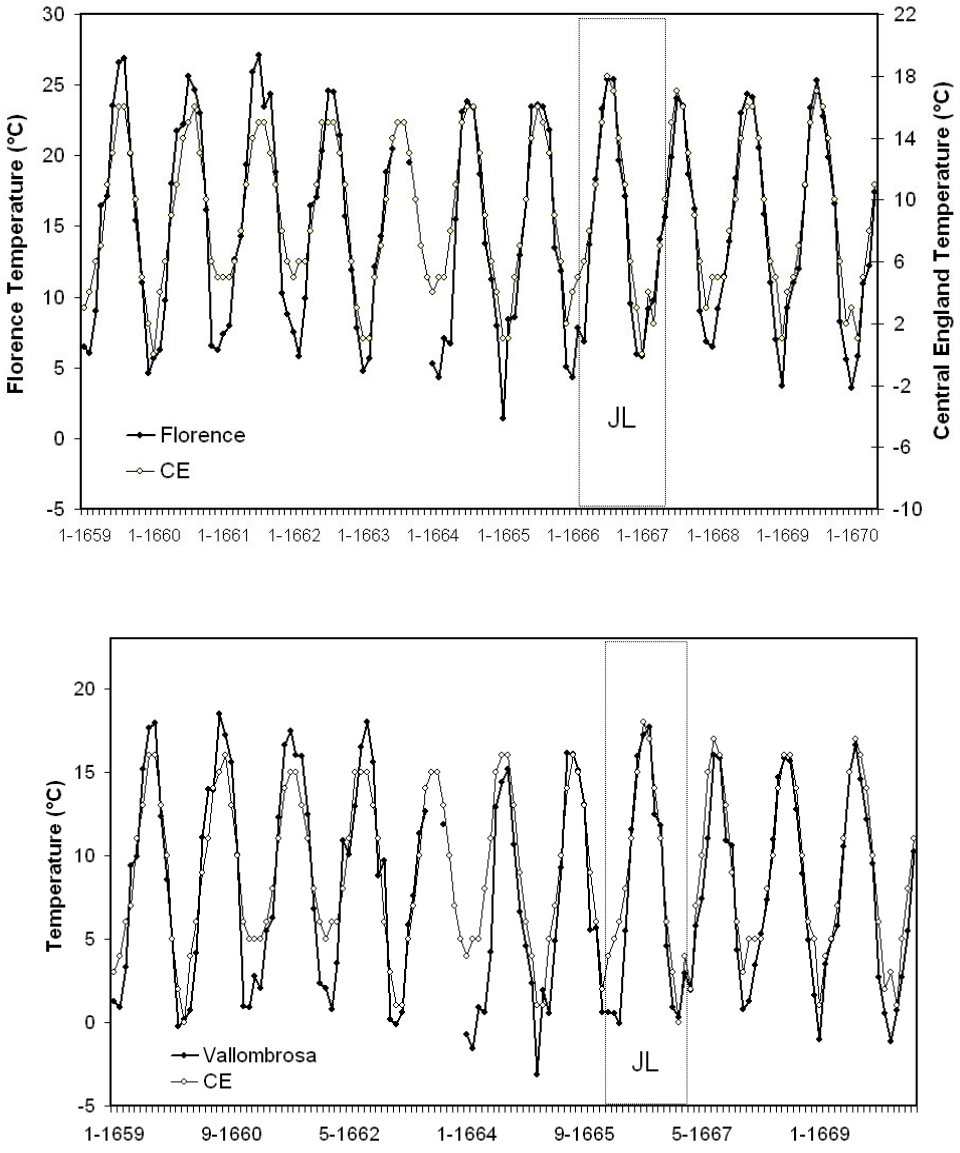

Fig.4.19: (a) Comparison between the Florence and the Central England (CE) series (Manley, 1974). The temperature scale of Florence (left side) is shifted and compressed in comparison with the CE in order to overlap the two plots from March 1666 - April 1667 which corresponds to the sequence of thermometer readings made by John Locke (JL). (b) Comparison between the Vallombrosa and CE series. The scale is the same for both stations.

We have elected this work at case study for the importance that it holds both from an historical and scientific point of view. The earliest temperature observations made after the discovery of the thermometer, i.e. 1654-1670, have been recovered, transformed into modern units of temperature (°C) and time (hours starting from midnight) and analysed. In order to appreciate such data and their quality, a preliminary thorough analysis of the scientific context in which the instruments have been created and the observations have been made. This has been useful to clarify some obscure points that have characterised the dawn of the meteorology and the scientific research in Italy. We have seen that in the antiquity the thermoscope was known and then forgotten. The transformation from a mere curiosity to a scientific instrument was made by Galileo in Padua, in 1593, after having read the books by Heron or Della Porta, maybe with some contributions of Della Porta, Father Paolo Sarpi and Sagredo. We know that another teacher of the Padua University, Santorio, was the first to apply a graduated scale for quantitative measurements around 1515. However, the main merit of Galileo was of having clearly understood the operational principle, based on the law of thermal expansion of gases, later expressed by Gay-Lussac. This makes Galileo the father, or the grandfather, of the air thermometer. However, to transform the thermoscope into a real air thermometer two possible solutions exist: to add the contribution of atmospheric pressure, and this will be made by Amontons (1702), or to seal the tube to avoid the communication with the atmospheric pressure, and this will be made by Stancari (1707). In conclusion, no temperature measurements were possible with the air thermometer until 1700s, when the Amontons or the Stancari thermometers have been invented to remove the influence of atmospheric pressure.

The evolution of the thermoscope brings to the air thermometer, and required about one century to be perfectioned, but it does not arrive to the spirit-in-glass thermometer. The spirit-in-glass thermometer was the first thermometer able to do temperature measurements. The spirit-in-glass thermometer was invented slightly before 1641, in Florence, by the Grand Duke Ferdinand II and Torricelli as a conclusion of the studies on the density of liquids and their expansion conduced by Galileo and his pupils in the previous years. Among the spirit-in-glass thermometers invented in Florence (see Figure 4.6), the best was the LFT with scale divided into 50 °G (Figure 4.7), as all thermometers had the same scale calibration. This made possible to realize the first

international network of 11 stations (Figure 4.10) making temperature and weather observations made at regular intervals from five to eight times a day. These observations correctly made with a thermometer hung on a wall facing North, as well as with another on a wall facing South to know the effect of sunshine, cover the period 1654-1670 in Florence and in Vallombrosa. In other stations we found mainly fragments to know the seasonal extremes, i.e. hot in summer and cold in winter. The thermometers were of high quality and linear and the operational methodology known, accurate and correct. This makes extremely important these unique data that are the first in the world after the invention of the thermometer and regularly cover 16 years in the hearth of the Little Ice Age.

The main advantage of the LFT was that the spirit is sealed within the glass, and the exterior is fully made of glass. The scale is made with labels directly welded on the tube. For this reason it is very resistant outdoors, either in the case of rain or sunshine. Outside Florence, thermometers were built with a poor technology, i.e. tube directly fixed to the tablet with an iron wire. Wooden shrinkage and swelling made impossible to keep them outdoors, and indoor observations were preferred. This choice that dominated most of the 18th century was suggested for a technological limit and by a theoretical reason. In 1660, John Locke, an English medicine doctor and empiric philosopher, made indoor observations related to health popular. This was another additional reason for the directives of the Network of the Royal Society, London, lead by James Jurin (1723) that recommended indoor observations. The next generation of thermometers resistant outdoors was with the "Societas Meteorologica Palatina", Mannheim (1780-1795) that (partially) abandoned the wooden tablet and used metal or glass or ceramic support for tube and scale.

The observations of the Medici Network have remained unexploited and this case study based on our paper 'The dawn of Meteorology in Italy and the earliest Meteorological Observations (1654-1670)', presents for the first time their analysis which extends back to 1654 our knowledge of past climate. All the series of the Network, either unbroken or fragments, have been recovered, controlled and transformed into modern unit of time and temperature. The series are well related each other, with determination coefficient exponentially decreasing with increasing distance. The small scatter shows a good quality of instruments and observational modalities. The two main series, i.e. Florence

and Vallombrosa, expressed in terms of anomaly with reference to the 1961-1990 period, show that today the climate in Florence has warmed by +0.09 °C with reference with the Ximenian Observatory in the city centre and 0.45°C with reference with the rural station Firenze Peretola. The warming in Vallombrosa was +1.18 °C partially due to landscape transformation and local business activity. Although the limited knowledge of the local heat island suggests some prudence in drawing conclusions, in Italy this period in the mid of the Little Ice Age appears less cold as generally believed on the ground of proxies. The comparison between Florence and Vallombrosa with the early part of the CE series obtained by Manley (1974) from a combination of thermometer readings and non-instrumental daily entries shows a very good agreement in the period of instrumental readings by John Locke (1666-1667); a bit less but still good for 1667-1670; a fair agreement for the early part from 1659 to 1663, which is not uniform to the rest of the series, because its seasonal extremes are reduced. This suggests that the early part of this important series would benefit from some revision.

Chapter 5:

Methodology of Climatic Analysis based on Early Instrumental Data: a Case Study

Contents

5.1 The Amontons air thermometer
5.2 Recovery of the Early Period of Long Instrumental Time Series of Air Temperature in Padua: a case study
5.2.1 Data recovery, discussion and analysis

The Florentine thermometer was an instrument more evolved than the air thermometer because it was not dependent by the atmospheric pressure and it had a scale based on two temperature considered unchangeable for the Florentine climate. In 18th century, there was the development of different meteorological instruments, scales and calibrations. The key problem in this large panorama remained the standardization of the calibration performed on the thermometers. The Florentine thermometer, in 18th century, was the starting point of this process of research of temperature values really constant and easily reproducible, i.e. the so named "fixed points".

However, not all scientists were satisfied of the Florentine thermometer validity. In particular the French scientist Guillaume Amonton (1663 – 1705), in order to solve some drawbacks existing in the Florentine thermometers, invented an air thermometer (Amontons, 1695; 1699; 1702). This air thermometer was the natural evolution of the thermoscope which was more or less simultaneously and independently invented and developed by some scientists in the turn between the 16th and 17th century, i.e. Galileo in 1593, Santorio in 1612-15, Fludd or Drebbel (Middleton 1966, Frisinger, 1983). Amonton discovered that the air elasticity inside a pot was dependent both by pressure and temperature and that keeping constant the temperature, increased with pressure and moreover he discovered the water boiling fixed point. From a general point of view,

these operating principles, were simple and reliable to apply with a building of a thermometer, but complex in details as we present in the following section.

5.1 The Amontons air thermometer

The thermometer and the operating principle. The Amontons thermometer was described in a memory of the Académie des Sciences of Paris in 1702. It was composed of two independent instruments, a thermoscope and a barometer in order to compensate the effect of atmospheric pressure on the thermoscope with the pressure readings (see Figure 5.1).

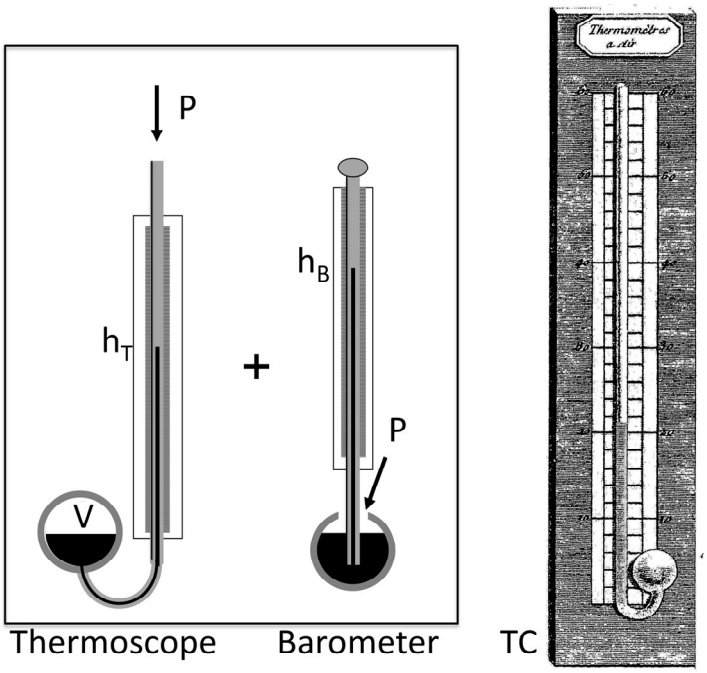

Figure 5.1: The Amontons thermometer, composed of a thermoscope and a barometer. Both the air pocket V in the ampulla of the thermoscope and barometer respond to atmospheric pressure P. The actual temperature is the sum of the two mercury columns: h_T and h_B. P is the atmospheric pressure acting on the mercury. On the right, T_C is the image of an Amontons thermoscope illustrated by L. Cotte (1774, Table III, Fig.4).

Both the thermoscope and the barometer were about 1 m long. Both instruments being filled with mercury the Amontons thermometer was heavy and hardly portable on short distances. For these reasons, after an initial popularity at the end of 17th and in the first half of the 18th century, it was abandoned. The thermoscope devised by Amontons was composed of an ampulla connected to a J-shaped tube open in the upper top. Inside the ampulla was a pocket of air which was compressed by the column of mercury in the

glass tube and the atmospheric pressure active on the open top. The latter is known after the associated reading of a barometer, and the actual temperature is obtained as the sum of the two mercury columns in the thermoscope and the barometer. From this point of view, the name 'thermometer' for this instrument is inappropriate, as it gives only one of the two readings necessary to determine the temperature, and only the sum of the two readings, i.e. Amontons' thermometer and the barometer, gives the real temperature. As these pressures were given by the heights of the mercury columns in the thermometer and the barometer, a measure of length represented either the pressure in the ampulla or the air temperature (e.g. the boiling water had an height of 73 French inches, the freezing water of 51 French inches, both making reference to an height of 28 inches in the barometric column). The disadvantage was the need of two instruments to determine the temperature.

The operating principle of this instrument was based on the expansion of atmospheric air by heat that was well known already at time of Galileo and his followers, but that was determined and quantified for a given rise of temperature only by Amonton himself. He made various experiments upon different volumes of air and he concluded that the pressure of different quantities of air increased by the corresponding rise in temperature and that the relationship between pressure and temperature was independent of initial pressure. He thus postulated a linear relationship between pressure and temperature (Taton, 1961; Middleton, 1966).

If we take in exam an Amontons thermometer as depicted in figure 5.2 is possible to verify this assumption through simple equations (extracted by Camuffo 2002b).

In the ampulla, a change in ambient temperature dT determines a change in the pressure dP and volume dV of the air pocket, which is obtained by differentiating the equation of state for perfect gases, i.e.,

$$dT = \frac{P_0\, dV + V_0\, dP}{n\, R} \tag{5.1}$$

where n is the number of air moles entrapped in the pocket, and R the gas constant for air. From the instrument features, it is easily seen that

$$dV = S_a\, dh_a = S_c\, dh_c \tag{5.2}$$

$$dP = \rho\, g\, dh_c \tag{5.3}$$

where S is the section, h the height of the mercury; the labels a and c refer respectively to the ampulla and the capillary; ρ is the density of the mercury and g the acceleration of gravity

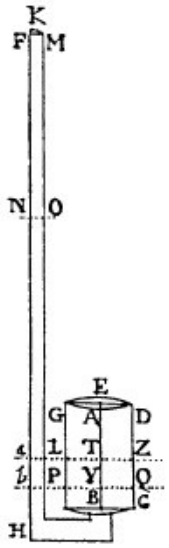

Figure 5.2: Scheme of the Amontons' thermometer: a J-shaped glass tube with an ampulla. The air pocket entrapped in the cylindrical ampulla expands displacing the level of mercury from the initial level LTZ to the final level PYQ, in the ampulla, and from NO to FM in the tube. The height of the column was from LTZ to NO before warming; and from PYQ to FM after warming (After Poleni; 1709).

After substitution of the formulae for dV and dP in (5.1), we obtain

$$dT = \frac{P_0\, S_c + V_0\, \rho\, g}{n\, R}\, dh_c \tag{5.4}$$

i.e., a change dT results in a change dhc observable in the capillary, and the sensitivity of the instrument dh_c/dT is directly proportional to the number of moles entrapped in the air pocket, and inversely proportional to the sum $(P_0\, S_c + V_0\, \rho g)$ where the second term is the dominant one. In the capillary, the change dh_c in the height of mercury, determines in the ampulla a change in volume $dV_c = -dV_a = S_c dh_c$ and a change in pressure $dP = \rho\, g\, dh_c$. The ratio

$$\frac{dV_a}{dP} = \frac{S_c}{\rho\, g} \tag{5.5}$$

is of the order of 2.5×10^{-3} cm^3/hPa for a capillary radius r = 1 mm, and 6.1×10^{-2} cm^3/hPa for r = 5 mm (1 mm-Hg = 1.333 hPa). Smaller the capillary section S_c, smaller dV compared to dP and the better the 'constant-volume'approximation. When the capillary is very thin and S_c approaches zero, and at the same time the air pocket volume V_a is large enough, then in equation (5.4) the term P_0 S_c can be neglected when compared to V_0 ρg. In this case,

$$dT = \frac{V_0 \rho g}{n R} dh_c = \frac{V_0}{n R} dP \tag{5.6}$$

which is the equation for constant-volume gas thermometers. Under these conditions, P is proportional to T, the coefficient of proportionality being V_0/nR. In Amontons' real themometer, V remains (nearly) constant and P is (nearly) linearly proportional to T. Finally, the change in level of mercury in the ampulla $\Delta h_a = \Delta h_c \times \Delta S_c/S_a$ depends on the ratio of the sections of the capillary S_c and the ampulla S_a. Smaller this ratio, more stable the level of mercury in the ampulla, to which the 'zero' of the scale refers, and the more reliable the readings. A good Amontons' thermometer has, therefore, a thin capillary and a wide ampulla.

The error due to different density of mercury. Error due to different density of mercury in Amontons' thermometer is instead explained looking at Figure 5.1.

The sum $h_T + h_B$ represents the actual value of temperature (i.e. T) only when both h_T and h_B are determined at the same ambient temperature T. This can be demonstrated as follows (extracted by Camuffo 2002b). The pressure P inside the ampulla is given by the sum of the two pressures that can be written according to Stevin's law:

$$P = \rho g h_T + \rho g h_B \tag{5.7}$$

where ρ is the density of mercury, g the acceleration of gravity. By substituting P from equation of state for perfect gases, one obtains:

$$T = \frac{(h_T + h_B) \rho g V}{n R} \tag{5.8}$$

where the sum $h_T + h_B$ is proportional to T . This sum was independent of atmospheric pressure, in the case of changes of atmospheric pressure Amontons' thermometer was

similar to an inverse barometer and its decreasing mercury column compensated exactly for the increase of the barometer, and vice versa, so that $\Delta h_T = - \Delta h_B$.

The height h_T was not affected by large errors resulting from the variation in the density of mercury induced by temperature changes, in that case the calibration included this effect at two fixed points, and each intermediate temperature was correctly evaluated. On the other hand, the barometric reading h_B caused an error, which was particularly large in the summer, which is evaluated as follows. If, in the first approximation, ρ is independent of T, Equation (5.8) is always true. However, with reference to the explicit expression of ρ(T):

$$\rho\,(T) = \frac{\rho\,(0)}{(1 + \beta\,T)} \tag{5.9}$$

where ρ(0) is the density at T = 0 °C and $\beta = 0.1818 \times 10^{-3}$ °C^{-1} is the cubic expansion coefficient of mercury, the problem arises when the mercury in the two columns has different temperatures T_T and T_B. Therefore, in Equation (5.8) each height, h_T and h_B, should be multiplied by the respective density $\rho(T_T)$ and $\rho(T_B)$, while $h_T + h_B$ is no longer proportional to T_T. The error may arise in the case of the barometer at room temperature T_B and the thermometer exposed outdoors at a very different temperature T_T.

In the realistic case that the calibration was made in winter (in order to have snow or ice), the thermometer was immersed in snow or melting ice, and the barometer was at ambient temperature close to 0 °C. At the zero point T(0), T is proportional to $h_T + h_B$ in the resulting calibration, as seen above. At the upper point, the actual problem consists in the method of calibration, because the thermometer was at boiling point, while the barometer remained at ambient temperature, near 0 °C. With regards to the point T (100) corresponding to boiling water, the thermometer was situated at a temperature of 100 °C while the barometer remained at 0 °C so that the situation at the two fixed points was, respectively:

$$T\,(0) = \frac{[h_T\,(0) + h_B\,(0)]\,\rho\,(0)\,g\,V}{n\,R} \tag{5.10}$$

$$T\,(100) = \frac{[h_T\,(100)\,\rho\,(100) + h_B\,(0)\,\rho\,(0)]\,g\,V}{n\,R} \tag{5.11}$$

However, a large error derives from the fact that only the heights h_T and h_B were read, without multiplying them by the due density value or correcting the barometer reading for expansion. In winter, temperatures were close to calibration conditions (cold thermometer and barometer) and therefore reliable, while summer measurements were less accurate. It is possible to evaluate the order of magnitude of the error which derives from an incorrect reading of the barometer with the help of Equation (5.9). If the average height of the mercury column in the barometer is $h_B = 760$ mm, then for T = 30 °C, the expansion $\Delta h_B = 4.12$ mm which corresponds to an overvaluation $\Delta T = 1.03$ °C. A more exact evaluation of the error could be made by also taking into consideration the real behaviour of a fixed well barometer, that is, the dilatation of the reading scale, the glass capillary and the metal ampulla of the well containing the mercury. A detailed analysis of the problem, found in all writings on meteorology, leads to an evaluation that is only slightly inferior to the above, that is $\Delta h_B = 3.8$ mm, equivalent to $\Delta T = 0.94$ °C. If Amontons' thermometer and the barometer are both displaced to a level which is different from that of calibration, the variations in the two mercury columns compensate each other exactly. A problem could arise instead, when only one of the instruments had been moved to a different level, for example the barometer. The variation in pressure can be calculated from the hypsometric formula which gives, for each rise of 10 m, a drop in the column of about $\Delta h_B = -0.9$ mm, which corresponds to a temperature error of $\Delta T = -0.2$ °C.

The Problem of Establishing Comparable Scales. A fundamental step in order to compare temperature observations performed by different observers in different places, it was the need to standardize the instruments and the calibrations themselves. The first attempts in this direction were performed by the meteorological networks that were born since 17th century, i.e., the Rete Medicea established 1654 by Ferdinand II de' Medici (Targioni Tozzetti, 1780), the Royal Society, London (established in 1723 by James Jurin (1723) and the Academia Meteorologica Palatina, Mannheim (established in 1781 by Karl Theodor von Pfalz (Hemmer, 1783). Inside each Network, identical instruments were sent to the various stations and the observers followed precise recommendations to take meteorological readings.

However, today, only few early thermometers are survived intact to verify their calibration, as the case, previously described, of the Little Florentine thermometer; in

the other cases the few information on the thermometer building and calibration we obtain are extrapolated from scientific literature.

In 18th century, the main problems to solve were: the response of thermometric fluid that could be either linear (e.g., gas) or non-linear (e.g., spirit); the scale that could be forward or reverse (e.g., Delisle, early Celsius) and many types of units that were used. To establish a standardised temperature scale, which could be easily reproduced everywhere by anybody, it was necessary to define the type of instrument, to define the thermometric liquid (i.e. spirit, mercury or other), choose one or more repeatable fixed points (i.e. of the temperature of the human body, of freezing water, of melting ice, of the cellars of the Paris Observatory or of the boiling water) and find a way of graduating the scale. If only one fixed point was used, e.g., the gas thermoscope by Santorio, one degree should correspond to a stated proportion of the increase in the volume, or the pressure, or the length of the thermometric substance, above or below the fixed point. If two or more fixed points were used, the interval between them was linearly subdivided into a number of equal parts, called degrees. Both methods assumed that the change of the thermometric substance, taken as an index, was linearly related to changes in the actual air temperature, so that equal increases in the index would indicate equal increases in temperature (Camuffo 2002b). Louis Cotte (1774) published a table that compared the 15 most popular scales of his times, including the scales used in Padua by Poleni. The early thermometric scales most in use in Europe as well as in Padua were:

- *The Fahrenheit's scale*: invented by Daniel Gabriel Fahrenheit (1686–1736) that used both spirit and mercury thermometers and described their calibration (Fahrenheit, 1724). He used three fixed points for graduating his thermometer: the first, at the beginning of the scale, was obtained from a mixture of ice, water and 'ammonia salt' or sea salt. This corresponded to 0 °F. The second was obtained by mixing ice and water without any addition of salt and corresponded to 32 °F. The third point was found at 96 °F and represented the temperature of a healthy human body. The scale was practically dimensioned to cover the yearly temperature range of the air in Europe. The boiling point of water was not originally used as a fixed point, in that it was considered too far away from the usual range of meteorological temperatures, but Fahrenheit did actually measure it by extrapolating the scale upwards, whereby he calculated it at 212 °F. Poleni

used Fahrenheit's thermometer for his meteorological observations, but he did not specify the calibration, i.e. whether it was the original Fahrenheit's thermometer with three fixed points, or as described by PeterMusschenbroek (1731–1732), with two fixed points only. The calibration was in any case not the standard one, as the observations departed too far from the other parallel series. Fahrenheit's thermometer built and used by Poleni departed by some 5 °C to 7 °C with reference to the other thermometers exposed in different parts of his house. This departure can be interpreted in terms of bad calibration of the lower point (Camuffo 2002b).

- *The Réaumur's scale* The scale proposed by René-Antoine Ferchault de Réaumur (1683–1757) became particularly popular in France, Italy and central Europe. In Padova it was used by, among others, Morgagni and Toaldo and it was abandoned in the second half of the 19th century. This French scale was commonly used in mercury thermometers, which were uniformly graduated between two fixed points: the melting point of ice (0 °R) and the boiling point of water (80 °R). The calibration was based on only one fixed point, 'zero' on the scale, i.e., the degree of cold at which water began to freeze. The subdivision in degrees corresponded to a constant increase in the volume occupied by spirit at zero, after having established a standard dilution. Réaumur knew, in fact, that the expansion of spirit varied according to the proportion of water. This method has two weak points, i.e., the imprecise definition of the temperature in which the water 'begins' to freeze, and the non-linear expansion of spirit. In Padova it was used by, among others, Morgagni and Toaldo and was abandoned in the second half of the 19th century.

- *The Delisle's scale*: Another scale invented by Joseph Nicolas Delisle (1688–1768) and utilised by Poleni, was based on only one fixed point. The original scale, established in 1732, took the temperature of boiling water as the fixed point, considered 'zero' on the scale, and the degrees were marked on the basis of the contraction of mercury with respect to the volume occupied at 'zero' (Delisle, 1734). This was an 'inverted' scale, Celsius too, presented the original centigrade scale in its inverted form. A scale with two fixed points was therefore established: the boiling point being represented by 0° and the freezing point at

150°. Delisle sent thermometers which had been calibrated by himself to various scholars, among whom Celsius in Uppsala and Poleni in Padova, who then carried out meteorological observations with them. Fortunately, the thermometer sent to Uppsala survived, and it is still preserved at the University (Bergström and Moberg, 2002).

Calibration Points and Scale Linearity. The common use of the two calibration fixed points of freezing and boiling water was not easily reproducible in early time and its standard use was not so immediate. The reason was that, at the beginning, each observer built himself his own instrument carrying out his own calibration. The problem therefore was to reproduce correctly the two fixed points. The lower point (i.e. freezing water, melting ice), being difficult to define, had a corresponding temperature not always exactly the same and invariable and the upper point (i.e. boiling temperature) being too high compared with the meteorological span or the body temperature, was hardly reproducible. This fact, obviously, led to a great deal of confusion and made the comparison of measurements taken with different thermometers difficult. In Italy, the immersion of a thermometer in snow was a fairly reliable method (followed in Padua too), according to a tradition that began with Sebastiano Bartolo in 1679, Carlo Renaldini in 1681. This practice became widespread with Newton's (1701) authoritative suggestion. Outside of Italy, the lower fixed point was obtained with the freezing of water (e.g., Réaumur and Jean Antoine Nollet before the year 1732), or the melting of ice (e.g., Fahrenheit, Réaumur and Nollet after the year 1732) (Middleton, 1966). In theory, the point of equilibrium between the liquid and solid state is well defined, and in very slow dynamic conditions the point of change of state from liquid to solid coincides with the inverse one which, for water, corresponds to 0 °C under normal pressure. In reality, the two used processed lead to departures when there were sufficient differences between ambient temperature, water and ice. In the case of freezing, the water temperature proceeded from an initial higher value to zero towards a final lower one (e.g., the environment or the container). In this case the departure was due to the bulb that was in contact with the liquid phase which, for the greater part, was at a still higher temperature than zero, while the capillary was often exposed to air, where the temperature could well be below zero. In the case of melting ice, the departure was due to the inner part of the ice that remained below zero, while the liquefied part reached

temperatures above zero because of exchanges with the external environment, of necessity above zero, otherwise the ice would not be melt.

Another problem with the early period concerns the non-standard pressure in establishing the fixed points. First of all, the boiling point was not so well defined especially because it was observed that the temperature of boiling water was not constant. The fact that atmospheric pressure could influence the boiling point of water was noted at the beginning of the 18th century. Fahrenheit (1724), discovered that the boiling point varied according to pressure and that pressure had to be specified at each calibration. Although a standard pressure was not established, it was, however, possible to determine the differences in temperature between boiling points fixed under different conditions, once the pressure was known.

The boiling point of water T_{BP} depends on atmospheric pressure P according to the law (Camuffo 2002b):

$$\Delta T_{BP} = 100 + \frac{(P - 1013.25)}{35.8\ [°C]} \tag{5.12}$$

from which $\Delta T_{BP} = 1/35.8 = 2.8 \times 10^{-2}$ °C/hPa. With normal atmospheric ranges of ±30 hPa, $\Delta T_{BP} = \pm 0.84$ °C. The thermometer readings should therefore be corrected on the basis of the indication about the calibration procedure, when this is specified. In the case of missing indication, the error is proportional to the distance from zero, and is therefore negligible in the winter. In the summer, when T = 30 °C, this error may range from 0 °C (no calibration error) to (30/100) $\Delta T_{BP} = \pm 0.25$ °C (maximum calibration error).

Also the temperature of melting ice T_{MI} depends on atmospheric pressure, but such dependence is fortunately negligible, in that the variation is $\Delta T_{MI} = 8 \times 10^{-6}$ °C/hPa (Rivosecchi, 1975). Calibration methodology became correct after 1777, when a Commission charged by the Royal Society, London, formed by Cavendish, Heberden, Alex- Aubert, Deluc, Maskelyne, Horsley and Planta published in the Philosophical Transactions (Cavendish et al, 1777) recommendations for finding the reference points and how to operate.

Calibration point of Amontons' thermometer: For an ideal Amontons' thermometer, only one calibration point is sufficient (if unknown, this can be derived from knowledge

of its readings during snowy days) and the other can be calculated with this simple equation

$$Po(100\,°C) = Po(0\,°C)\frac{R_T}{R_V} = 1.366 \cdot Po(0\,°C) \tag{5.13}$$

where Po (0 °C) is the temperature in °Po (which equals the pressure in London inches) at 0 °C, RT = 1.366 and Rv = 1. In the case of a real thermometer, this approximation (equation 5.13) is good in winter, and the error may approach 1 °C in the summer. This equation allows us to interpret data taken with an unknown scale and calibration, e.g., the first period in Padova, 1716–1719. In addition, the formula derived for an ideal thermometer allows us to verify how a real thermometer departs from ideal conditions and a test on calibrations of famous thermometers (Amontons', Lambert's, Gay Lussac's, Poleni's at Venice and Padova) gives departures lying between 2.7%. The above instrument analysis has been useful to know how an Amontons' thermometer works.

However, in the analysis of early instrumental temperature series, the most important problem does not consist in random errors, but in systematic ones. For this reason, in order to make reliable correction of data, it is necessary an accurate knowledge of the series, with its own history and metadata. Then, further validation can be performed by comparing the actual series with other highly correlated, reliable series, or with the help of statistical tests. We started with the analysis of thermometers used at the dawn of meteorology, first of all to understand as they worked but above all to test the reliability of the original temperature observations. The excellent results obtained with the early instruments was due to incredibly careful and precise methodology carried out for building and calibrating the instrument itself.

The case study of the Padova series, which is one of the longest and best documented, has shown that careful corrections, validations and homogenisation are necessary before drawing any climatic analysis, in order to avoid unreliable conclusions. The complex problem of correcting calibration and instrumental errors must be faced individually for each series, first on the basis of metadata from an accurate historical and critical analysis concerning instruments, operative methodology and then on a statistical analysis of errors, comparing teleconnected series.

5.2 Recovery of the Early Period of Long Instrumental Time Series of Air Temperature in Padua: a case study

Under the EU funded project IMPROVE (Camuffo, 2002a, b, c; Cocheo and Camuffo, 2002; Camuffo et al., 2006), the daily meteorological observations made in Padua by Giovanni Poleni and his son Francesco in the 1725-1769 period have been recovered from the original registers preserved in the old library of the Astronomic Observatory of the University of Padua and published. However, some problems were left unresolved, i.e. (i) indoor observations, (ii) only one reading a day, (iii) the use of variable and/or different sampling times. In our paper 'Recovery of the Early Period of Long Instrumental Time Series of Air Temperature in Padua, Italy (1716-2007)' presented here as case study, the 1725-1761 indoor observations have been transformed into outdoor ones with the help of the simultaneous 1740-1768 indoor and outdoor observations made by Giovan Battista Morgagni in Padua, one mile nearby the Poleni house. In addition, newly recovered data have been analysed. First, the daily data by Giovanni Poleni for the 1716-1718 period were copied from the original log preserved at the Marciana Library in Venice (Poleni, 1716-1725). Secondary, the monthly averages of the readings made by Francesco Poleni for the 1765-1769 period, found in a publication by Giuseppe Toaldo (1770, 1781).

Simultaneously, in Bologna, 120 km far from Padua, Jacopo Bartolomeo Beccari was performing similar observations at the local Science Academy, first only with indoor readings, later with both indoor and outdoor ones (Baiada, 1986). This fortunate combination gave us the opportunity for cross controls to check the data quality and to fill a short gap in the Padua series.

As described in the previous section, the main thermometer used in Padua was an Amontons thermometer built by Poleni in Venice, in 1709 (Poleni, 1709) shortly before he moved to Padova, being appointed teacher of Astronomy and Atmospheric Phenomena at the University. He started regular daily observations in 1716, at his first home in an unknown address where he taught too. In 1718 he moved to another house, in Pellegrino Street, where he made observations till his death in 1761. His son Francesco continued readings till 1769. For the subsequent history we make reference to the above IMPROVE publications.

In the case of the instrument built by Poleni in 1709, the sum of the two heights (h_T + h_B) was expressed in Poleni degrees ($°Po_{1716-1718}$) expressed in Paris inches in the first period, i.e.1716-1718, and London inches for the second one, i.e. 1725-1769 ($°Po_{1725-1769}$). When Poleni moved in 1718, he removed the mercury for transport, so that the air pocket and the scale changed. Therefore, the degrees $°Po_{1716-1718}$ are different from $°Po_{1725-1769}$.

The complete Padua series once again will improve our knowledge especially for the 18th century, a scarcely known but relevant period of the Little Ice Age, subsequent to the Maunder Minimum of Solar Activity (1645-1715). In fact, only a few long instrumental series that reach three centuries exist.

5.2.1 Data recovery, discussion and analysis

Daily outdoor temperature readings 1716-1718. Giovanni Poleni made outdoor temperature readings with his thermometer hung on a northern facing wall, following the Italian traditional style established by Luigi Antinori in 1653 for the Medici Meteorological Network (1654-1667) (Antinori, 1841). The observations were reported in a log, with monthly tables and daily rows from 1716 to 1725, but regularly filled for the period 1716-1718 and limitedly to the warm and cold seasons, the observer being particularly interested in knowing the seasonal extremes. The log had columns for date (i.e. day of the month), hour, wind vane direction, barometer height, thermometer height, state of the sky and precipitation amount, either rainfall or snowmelt. The hour was calculated from twilight, following the Italian style, and the observations were made at scattered times in the morning. Sometimes two readings were made in the same day. From the consistency of data it was possible to establish that the figures reported in the log temperature column was the actual sum of the thermoscope and the barometer readings, i.e. the true Amontons temperature (h_T + h_B), as later used in the register for the period 1725 onwards.

Observations were practically stopped, or rarely made, after Poleni moved to his next house in Contrada San Giacomo, now Beato Pellegrino street, number 5, one mile away. In 1725 he began a new regular series of indoor observations (1725-1769) to follow the invitation by James Jurin (1723) to join the network of the Royal Society, London. Poleni used the same instruments, i.e. thermometer and barometer built in Venice, for

both 1716-1718 and 1725-1769 periods. However, at each move he removed the mercury from the ampulla of the Amontons thermometer and when the ampulla was filled again, the air pocket was different, thus changing the instrument response and needing a new calibration. We know the first Amontons calibration made in Venice (Poleni, 1709) and the third calibration for the 1725-1769 period; no information was found about the 1716 calibration. For 1716-1718 readings and the later loose readings, the units were in Paris inches; in 1725-1769 in London inches to publish data in the Philosophical Transactions. In 1725 Poleni changed the instrument scales that were probably strips of paper glued to the walnut tablet supporting the glass tube and the ampulla.

In the Venice period (1709) we know two calibration points of the Amontons thermometer. Although, for the gas thermometers only one calibration point was necessary, the equation being determined by the perfect gas law. This equation (i.e. equation 13) was determined on the ground of the sizes obtained from Poleni's drawings and the other calibrations. A previous study on this instrument and its calibration (Camuffo, 2002b) confirmed that the instrument used in Venice and in Padua was the same, except for the air pocket which determined the instrument response, i.e. its transfer equation. We needed therefore at least one key calibration point for the first Padua period (1716-1718). In this case study we established this point by looking at the days with snowfall alone or mixed to rain, i.e. 15 days in total. A problem arose when the temperature was read in the morning and the precipitation was during the night. For this reason we considered only the seven cases in January, when the daily temperature range is smallest. 0 °C corresponded to 44.47 Paris inches and the boiling point was calculated to be 60.75 inches. Briefly, $1°Po_{1716\text{-}1718} = 6.15$ °C. The readings were expressed in mercury inches, lines (a Paris inch divided by 12, and a London inch divided by 10 when he will change unit in 1725) and fractions of line (e.g. ½). In the 1716-1718 period Poleni made his outdoor readings at different times, mainly between 7:00 and 16:00 with a frequency peak between 8:00 and 10:00 (Figure 5.3).

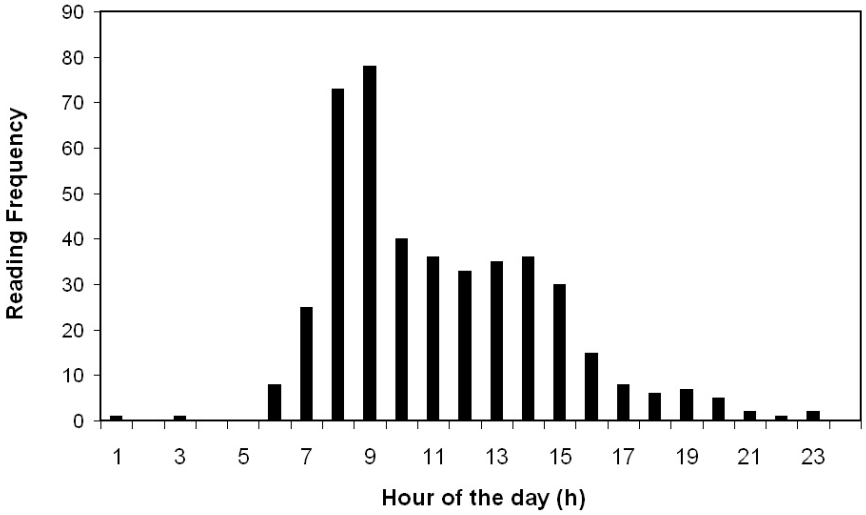

Figure 5.3: Sampling time performed by Giovanni Poleni for his outdoor readings in 1716-1718. The most frequent reading time was around 8-9 in the morning.

The problem of such scattered data can be easily solved in terms of anomaly, making the difference between the observed value and the corresponding one at the same hour and the same day of the calendar year averaged over the 1961-1990 reference period. This is equivalent to transforming such an irregular sampling into a regular one representative of the daily average, i.e. supposedly made at the time in which, for each individual month, the instantaneous value of the temperature cycle equals the daily average. To this aim, for each month, the daily cycle was computed on the ground of high frequency sampling (10 min) performed from 1985 to 2008. From these data the temperature difference between each sampling time and the daily average was calculated. A distinction was made for the cloud cover, i.e. (i) clear or partially overcast sky and (ii) thick cloud cover, with or without precipitation. The appropriate correction was possible because the state of the sky and the precipitation were reported in Poleni's original log. Each individual original reading was transformed into a modern daily average with a correction based on the ground of the original specific sampling time and cloud cover of the day.

The early Poleni observations have gaps in some months, i.e. August and September 1716, from July to November 1717, May and June 1718 and after August 1718. From the simultaneous indoor and outdoor observations made by Beccari in Bologna (the Bologna series will be not discussed in this thesis) it was possible to establish the transfer function, i.e. the key to transform indoor into outdoor readings. Beccari made

three meteorological readings a day, sampled at 8:00, 14:00 and 21:00, from which it was possible to calculate a daily average taking into account the thermal inertia of the building.. A cross comparison between the Poleni and Beccari readings lead to the equation T_P=0.9942 T_B -11.017 where T_P is for Poleni's and T_B is for Beccari's readings; R^2 = 0.82 with good agreement. With this equation it was possible to fill the gaps in the Padua series. However, in the Beccari indoor observations the variance is reduced compared to the outdoor observations in Padua because of the damping due to the inertia of the building envelope. The damping should not be evaluated from the simple standard deviation (SD) of the actual readings because the seasonality influences it. The seasonality can be eliminated by considering the temperature difference between consecutive days, i.e. the inter-diurnal SD. The outdoor observations by Poleni have SD 2.1, the indoor ones by Beccari 1.5, the calculated data to fill the gaps, which suffer in lower variability from the damping on the mother series, have 1.5. The smoothing for the building inertia may be a problem with high frequency resolution, not with monthly averages. The series obtained for the 1716-1718 period is reported in Figure 5.4 and Figure 5.5. From the data we see that the 1716-1718 period had substantially the same temperature level as the 1961-1990 reference period, and the daily temperature was scattered in the range ±9°C.

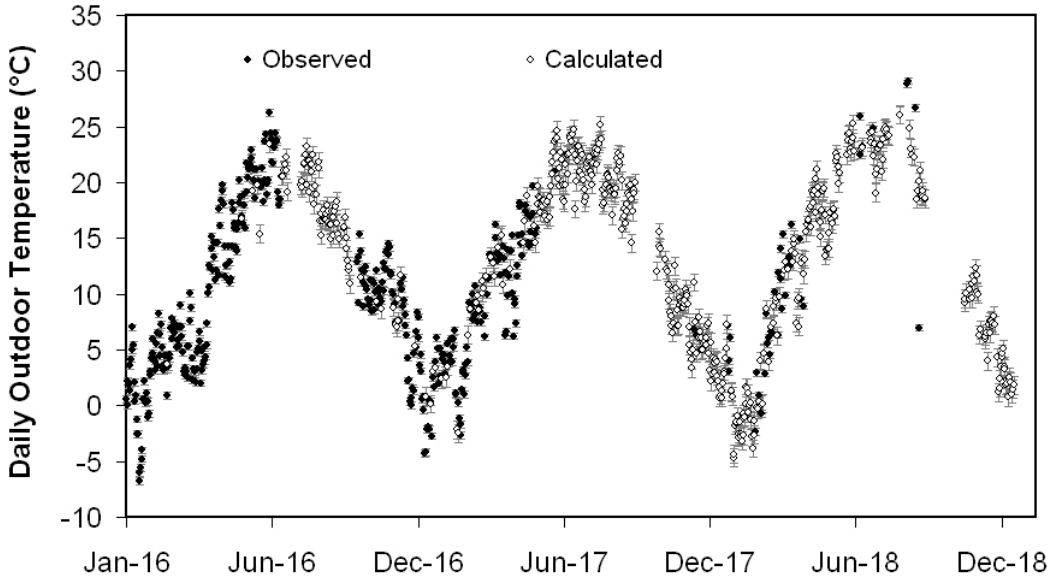

Figure 5.4: Mean daily outdoor temperature observed by Poleni in Padua in the years 1716-1718 (black) and gaps filled by means of a transfer function (white). Estimated error bar as in Table 5.1.

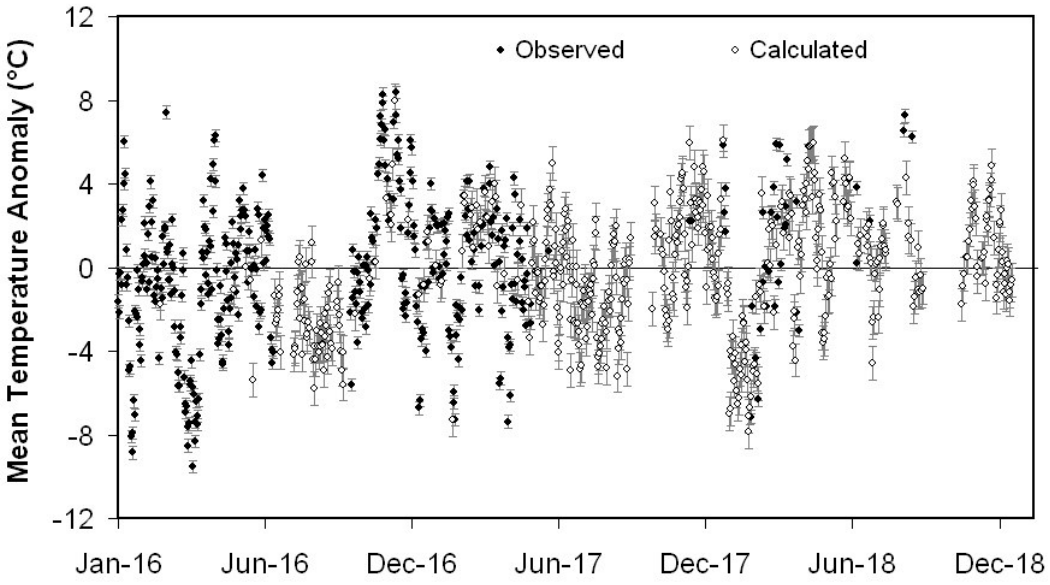

Figure 5.5: Daily temperature anomaly for the period 1716-1718 in Padua. Observed temperature: black, calculated: white. Estimated error bar as in Table 5.1.

An estimate of the errors in this period is reported in Table 5.1 taking into account the specific instrumental errors of the two series and the error introduced by the transfer function from Bologna to Padua in the case of gaps.

Table 5.1: Sub-periods in which the early part of the Padua series can be subdivided, corrections and transformations applied and estimated error for each sub-period.

Sub-Period	Comments	Estimated Error
1716-1718 fragments	Outdoor readings on a north facing wall. Sampling at scattered times in the morning. Corrected day by day. Statistically good correction at monthly level.	0.2°C
1716-1718 fragments filled gaps	Gaps filled with two conversions, i.e. indoor to outdoor and Bologna to Padua conversion.	0.55°C
1719-1724	Indoor readings. Two conversions applied, i.e. indoor to outdoor and Bologna to Padua conversion.	0.55°C
1725-1740	Indoor readings corrected within the EU Improve Project. Indoor to outdoor conversion based on the simultaneous indoor-outdoor readings in the 1740-1764 period.	0.29°C
1740-1764	Precise operational methodology. Simultaneous indoor (G. Poleni) and outdoor (Morgagni) readings in Padua used for calibration of the 1725-1740 indoor to outdoor conversion.	0.2°C
1765-1769	Relocation of indoor readings (F. Poleni). Unchanged outdoor readings (Morgagni). Simultaneous indoor (F. Poleni) and outdoor (Morgagni) readings in the 1765-1768 period. 1768-1769 transformed indoor to outdoor.	0.35°C

Poleni measured on a north-facing wall with an Amontons thermometer with estimated error 0.3 °C. Beccari used a Stancari thermometer with estimated instrumental error 0.25. The error for Bologna indoors to Padua outdoors transformation is 0.55 °C as deduced from the scatter of the corresponding data in the period the two series overlap. The total error in filling gaps is 0.8 °C. In the reconstructed periods in which we have only fragments in Padua (black dots in Figure 5.4 and Figure 5.5), observed data fit well with calculated one (white dots). Passing from daily data to monthly averages, the uncertainty is reduced in correspondence with the number of samplings per month (Parker and Horton, 2005).

Transformation from indoor to outdoor readings for the 1725-1764 period. In 1725, Poleni started a long series of regular daily observations accepting the invitation by J. Jurin (1723) to join the Royal Society, London. The instructions were to follow the style suggested by John Locke, with the instrument located indoor in a room without fire. Poleni made readings after having well ventilated the room for some time (half an hour or more) compensating in some way the low-pass filter operated by the building envelope.

Poleni used the same instrument as for the previous period but with a new calibration for the air pocket after the move in 1718. Fortunately, the two calibration points were reported in the log and the new scale corresponded to $1°Po_{1725\text{-}1764} = 6.33$ °C.

Some years later, in 1740, G.B. Morgagni started another parallel series with two Réaumur thermometers, one exposed indoors and one outdoors. Morgagni's readings were scheduled at 8 am and 2 pm. An example of how the scheduled sampling time fits with the diurnal cycle is reported in Figure 5.6a and Figure 5.6b for two selected months. From the Morgagni readings, and the shape of the daily temperature cycle, it has been possible, month by month, to calculate the expected reading at 12 am, i.e. Poleni's sampling time.

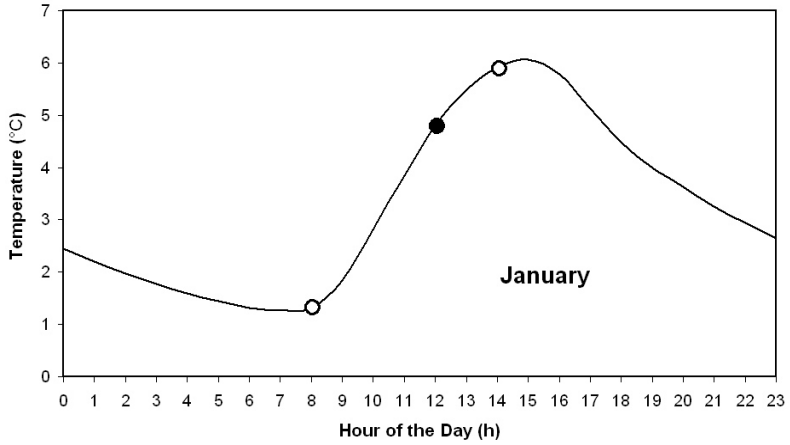

Figure 5.6a: Daily temperature cycle in January, Padua, period 1980-2007. White dots: the two Morgagni reading times (8 a.m and 2 p.m.); black dot: temperature at 12 a.m.

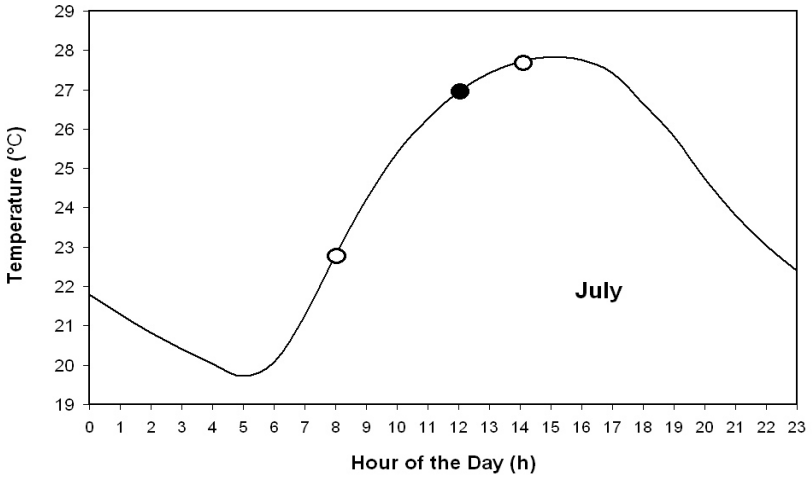

Figure 5.6b: Daily temperature cycle in July, Padua, period 1980-2007. White dots: the two Morgagni reading times (8 a.m and 2 p.m.); black dot: temperature at 12 a.m.

From the observations in the common period 1740-1764 it has been possible to cross-compare Poleni's indoor observations with Morgagni's outdoor ones calculated for the same sampling time. The transfer function is $T_{OUT} = 1.116\ T_{IN} - 5.737$ where T_{OUT} is for the Poleni's outdoor reading and T_{IN} the indoor one. The determination coefficient is $R^2 = 0.97$. The SD for the Poleni indoor readings, but in a well ventilated room, is SD = 1; for Morgagni outdoor readings SD = 1.2, and for Poleni's calculated outdoor readings SD = 1.1, with close values. In this way we got a corrected series of external data from 1725 to 1764, with daily readings as they were sampled at noon. However, the next step is to see of which time this sampling is representative, because it is affected by the inertia of the building envelope that acts as a low-pass filter.

In order to evaluate how this filter cuts high frequencies, we have calculated first the difference between each day and the previous one, and then the variance of this difference (Cocheo and Camuffo, 2002). Today in Padua the variance of outdoor interdiurnal temperature variability is around 10 and in the case of Poleni observations it is 1. This means that the building inertia filters most of the day-by-day variability which is reduced by 1/3. From the attenuation of the amplitude of the daily temperature cycle the averaging period is about two days. We obtained the same result by looking at the indoor-outdoor readings correlation and then repeating this exercise by shifting the outdoor readings by 1, 2, 3… days. The simultaneous indoor-outdoor observations are highly correlated, i.e. R = 0.98, but the highest correlation, i.e. R=0.987, was found with a 2-day delay, showing that the building structure introduces some delay, as expected. Lowering the variance of the high frequency signal introduces a smoothing to daily variability, but it becomes an advantage when passing from a specific sampling time to the daily average. The indoor-outdoor transformation can easily be made once the transfer function is known after the long, homogeneous 1740-1764 period in which the two Poleni and Morgagni series overlap. The limit is that it reduces the daily variance, but it has no relevant effect when we pass from the daily to the monthly scale. The main problem is for exceptional short periods of very cold or warm air invasions because the building envelope damps the high frequency variability. This was recognized during an invasion of very cold air in February 1740. Therefore, exceptional short periods of extreme temperature are badly represented by indoor readings at daily resolution. In theory, this becomes irrelevant at monthly resolution. In practice, Poleni was aware of this problem and, in the case of exceptional cold, he made additional external samplings. The building envelope acts as a low-pass filter that is representative of the last two days, but the open windows update the internal temperature. In conclusion, the readings are approximately representative of the last day and are slightly affected by the choice of the particular sampling time. In this case study they have been expressed in terms of daily averages (Figure 5.7). We see that the most severe winter was that of 1740, followed by 1745, and that a consistent number of mild winters was found, even in the mid of the Little Ice Age. The anomaly (Figure 5.8) shows that this period was in average very similar to the reference period 1961-1990, but with frequent, marked departures, especially due to the cold.

An estimate of the errors in this period is reported in Table 5.1. The above table includes the evaluation of the actual errors and does not include all problems of the raw data and the instrument that have already been adequately corrected and homogenised as extensively discussed in specific papers (Camuffo 2002a,b,c; Cocheo and Camuffo, 2002). These included: transformation from the Italian time to Western European Time, sampling made at different times, conversion from original temperature units to °C, calibration of the Amontons thermometer at the two fixed points, barometric corrections for temperature and height above sea level, drift of the instrument, building influence, potential (minor) error due to shrinkage and swelling of the wooden board with the scale, homogenisation control after cross comparison with other daily series.

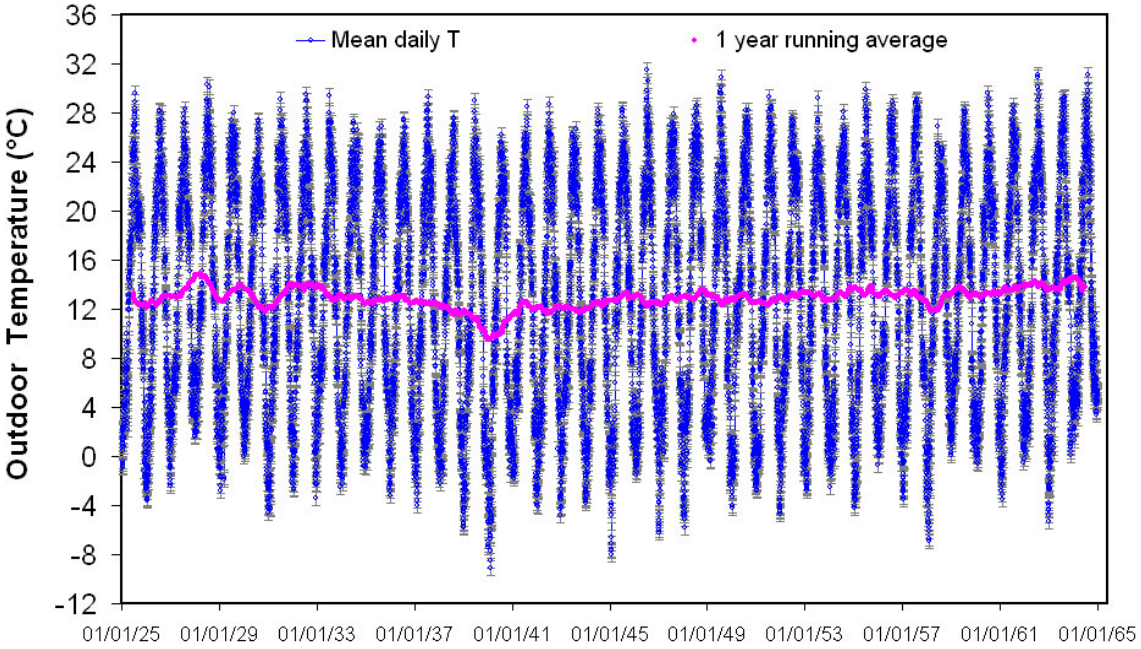

Figure 5.7: Outdoor temperature for the 1725-1764 period. Daily readings: open dots and blue line, with estimated error bars as in table 1. 12-month moving average : thick pink line.

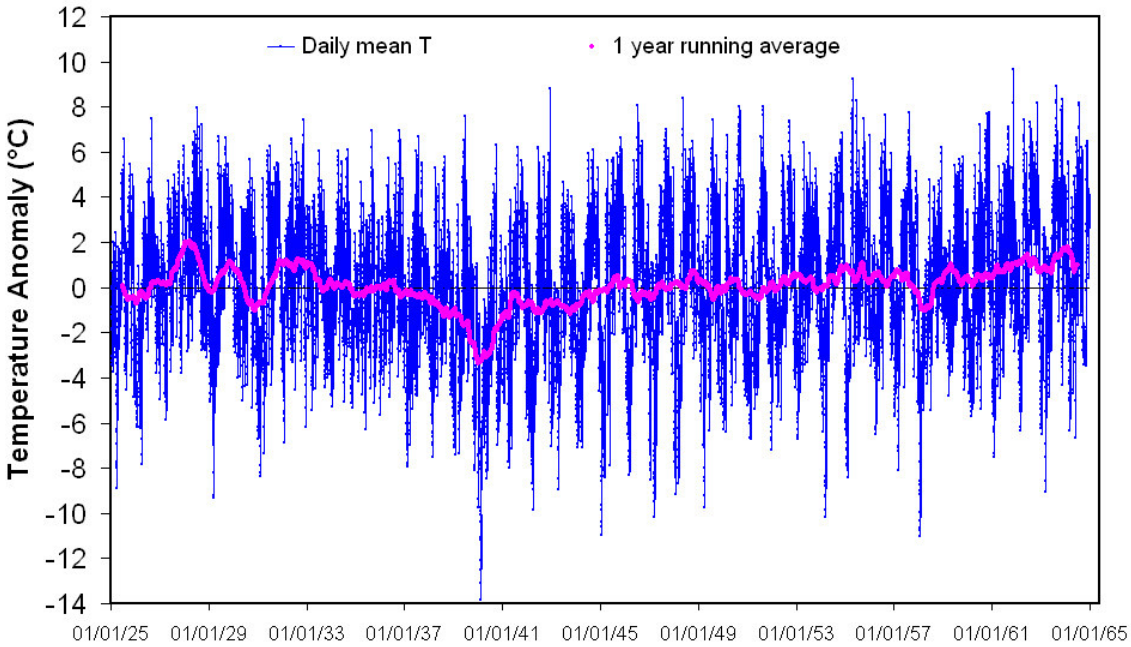

Figure 5.8: Outdoor temperature anomaly for the 1725-1764 period. Daily readings: full dots and blue line. 12-month moving average: thick pink line. Severe cold is evident in 1740 and 1758.

Daily minimum values of outdoor temperature in February 1740: In a letter to A. De Pompeiis (Poleni, 1740), Poleni wrote some observations in the occasion of an Aurora Borealis on 29th March 1739, a Solar Eclipses on 30th December 1739, a Lunar Eclipses on 13th January 1740 and, in addition, meteorological observations made outdoors for the whole month of February 1740 that was anomalous for the severe cold. After the first week with rain and snow, the air arrived from the north bringing cold air and clear sky. Poleni wanted to record the exceptional cold of this period and for this reason he installed a mercury-in-glass Fahrenheit thermometer outside, outdoors, hung on a northern facing wall, following the early Antinori recommendations. The readings were taken before sunrise to record the absolute minima. It is interesting to compare all the indoor and outdoor readings made in Padua during this cold air invasion (Figure 5.9).

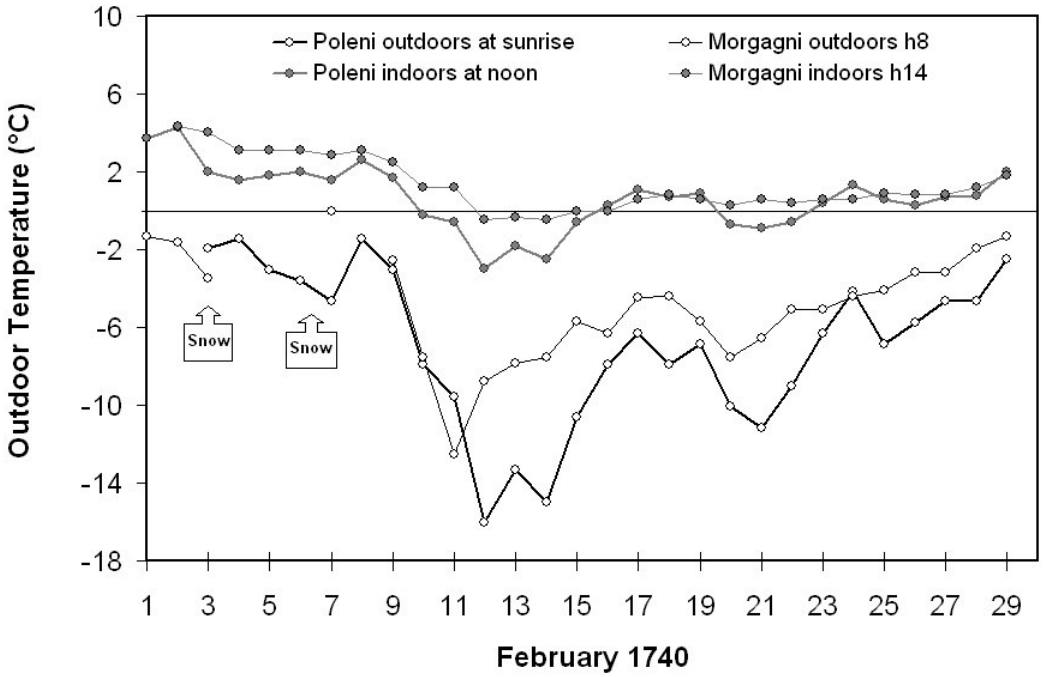

Figure 5.9: Outdoor and indoor readings by Poleni and Morgagni in February 1740. White dots: outdoor readings; Full dots: indoor readings; Thick line: Poleni readings; thin line: Morgagni readings. Arrows: snowy days.

A minor difference is found between the indoor readings taken by Poleni (Amontons thermometer, noon readings) and Morgagni (Réaumur thermometer, slightly affected by home life). In the first week of observations, characterized by rainfall and snowfall, all measurements show a certain coherence. A major difference is found between indoor and outdoor observations, as well as between outdoor ones during the cold air invasion. Outdoor observations by Poleni were made externally, with a thermometer which was well exposed to ventilation, before sunrise and this explains why they generally constitute the absolute minimum. The outdoor thermometer used by Morgagni was hung to the window-jamb, partially affected from the milder building envelope. In addition, the Morgagni readings were made at 8:00, i.e. 60 min after sunrise at the beginning of the month and 90 min after, at the end. This justifies why Poleni readings depart so much from the others during the extreme cold. The departure was particularly relevant during the most severe spell, i.e. 12, 13 and 14 February, when the difference between the two Poleni readings reached 13 °C, which largely exceeds the diurnal range. Therefore, the short periods of extreme temperature are badly represented by indoor readings.

Monthly temperature values collected by Francesco Poleni (1765-1769). After Giovanni Poleni died (14th November 1761), his son Francesco continued the observations with the same modalities till 26th April 1764 when he moved to the convent of the Philipine Fathers in San Tomaso Street, this site being 1260 m south of the previous house in Beato Pellegrino Street. He continued to observe indoors till 31th December 1769. In this period, the 1765-1769 average was different from the 1725-1764 average, and we evaluated that it was 1 °C higher. For this reason, Francesco Poleni, under the influence of Giuseppe Toaldo, who was Professor of Astronomy and Meteorology at the University of Padua, was convinced that there was something wrong and the reason was attributed to the escape of some air bubbles from the air pocket in the ampulla during the move. The readings were considered to be affected by error and thrown away, although a simple recalibration of the instrument would have been sufficient. However, we should reject the Toaldo hypothesis for three reasons: (i) air can escape from the ampulla only in the case the Amontons thermometer is rotated more than 90°, and this is unrealistic; (ii) in the case of loss of air, the thermometer would have provided lower temperature readings (not higher). In such a case we should hypothesize the entrance of external air; however, it is quite impossible that external air can cross the whole tube filled with mercury and then enter the ampulla. (iii) Francesco Poleni was extremely accurate and made regular observations even on the day of his father's death; for this reason it is unbelievable that he damaged the instrument during the move. We should conclude that the thermometer did not suffer losses of air for the move and that the calibration was unchanged and that the difference was either due to relocation or natural climate variability, as we will discuss later.

Francesco Poleni's readings were later published by Toaldo (1770; 1781) as monthly total of Poleni degrees accumulated day by day above or below the whole 1725-1764 average. For each month Toaldo separately summed the positive and the negative deviations from the 1725-1764 average and divided the total by the number of days. These values were called "Sums of Hot" in the case they were positive and "Sums of Cold" if negative and represent something like a positive or negative anomaly expressed in terms of degrees-day above or below the average (Camuffo, 2002a). Here, the "Sums of Hot" and the "Sums of Cold" originated from $°Po_{1725\text{-}1764}$ have been transformed into modern units, i.e. monthly averages in °C. The transformation was made month by

month, by calculating the degrees making reference to the whole 1725-1764 period average. The obtained data were then referred to the monthly averages of the simultaneous outdoor readings by Morgagni, to transform them as if they had been observed outdoors, as described in the previous sections.

The 1719-1724 gap has been filled thanks to the simultaneous and unbroken measurements by Beccari in Bologna, once the transfer function for the common period T_P=1.0434 T_B - 1.6606 with R^2=0.97 was established where T_B is the monthly mean temperature measured by Beccari and T_P by Poleni.

The whole series of monthly temperature and anomaly averages for the 1716-1769 period are reported respectively in Figure 5.10 and Figure 5.11, together with the yearly and the 11-year running average. This period had a number of oscillations around the 1961-1990 average but substantially it had the same mean temperature. Cold reached an extreme value in 1740, but it was compensated by a number of mild winters. Summer temperature departed much less from the modern values.

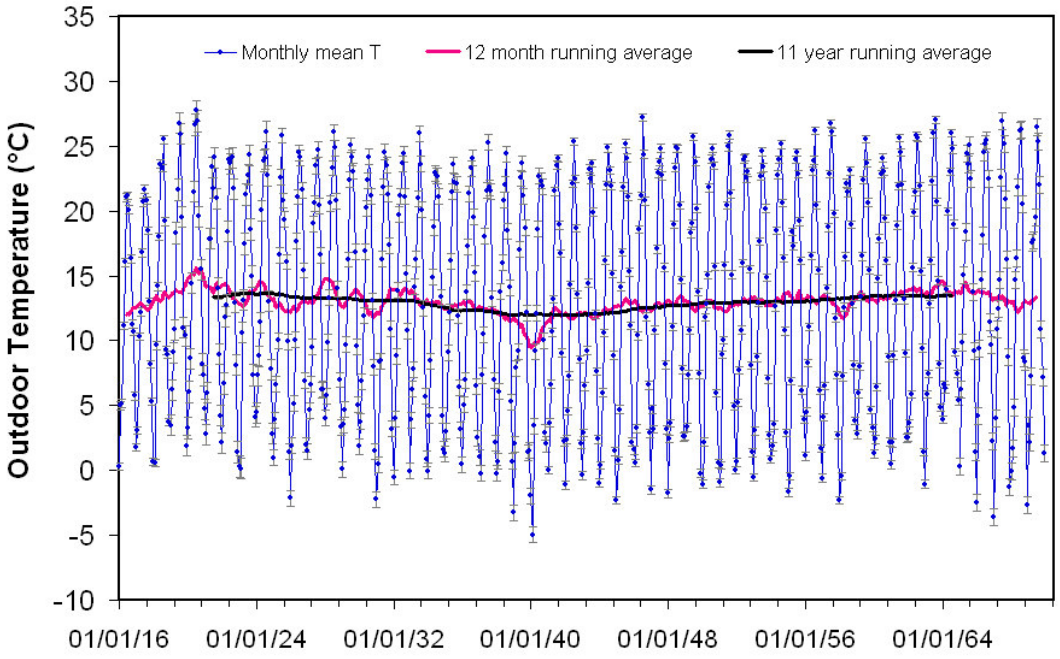

Figure 5.10: Outdoor monthly temperature for the period 1716-1769 in Padua. Thin blue line with filled blue dot: observations by Giovanni and Francesco Poleni; thick pink line: 12-month moving average; thick black line: 11-year moving average.

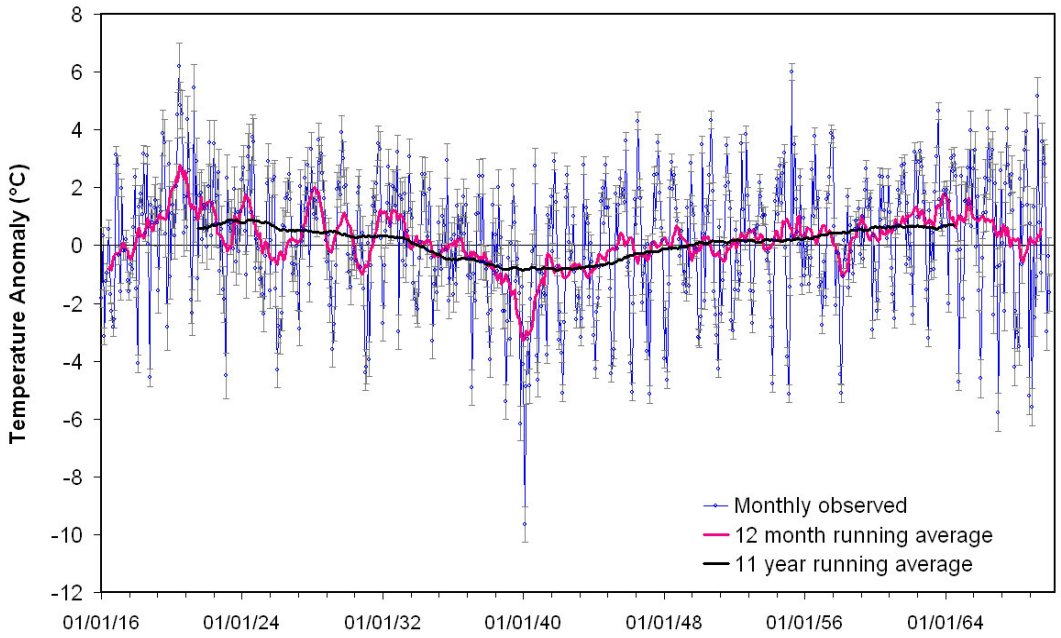

Figure 5.11: Outdoor monthly temperature anomaly for the 1716-1769 period in Padua. Thin blue line with open dots: observations by Giovanni and Francesco Poleni; thick pink line: 12-month moving average; thick black line: 11-year moving average.

An estimate of the error bars in Figure 5.10 and Figure 5.11 is reported in Table 5.1. The Standard Normal Homogeneity Test for Single Shift (SNHTss) (Alexanderson and Moberg, 1997) is of little help in showing discontinuities because the interval to test is too short and close to the end of the series. This forced us to use another approach, i.e. the Cumulative Values Test of the actual series, e.g. Padua, versus a reference series, e.g. Bologna. In the case there are no discontinuities we obtain a bent straight-line, otherwise the line continues with a change in slope after the discontinuity. We applied it to the series of monthly averages in Padua and Bologna. No changes were observed and the data should be considered homogeneous.

The seasonal temperature anomaly computed for winter (months DJF), spring (MAM), summer (JJA) and autumn (SON) and referred as usual to the 1961-1990 period, is reported in Figure 5.12. Severe cold characterized most of the winters in the 18th century with a peak in 1740. In the same figure, spring in the 18th century was characterized by a similar, but less severe trend as the one described for winter. In the most recent 50 years, some warming is visible: in winter no or rare severe cold is found; in spring an exceptional warm season occurred in the last decades.

The 18th century was anomalous for the warm season too, indeed several hot summers were repeated up to 1760. Similarly, autumn was generally warmer in the same period but with a cold peak in 1740. Summer shows a marked warming, similar to spring in the last decades. Autumn had no specific trend. The main anomalies were in the period before 1760 with cold winters and springs opposed to hot summers and autumns; a general warming is evident in the last decades.

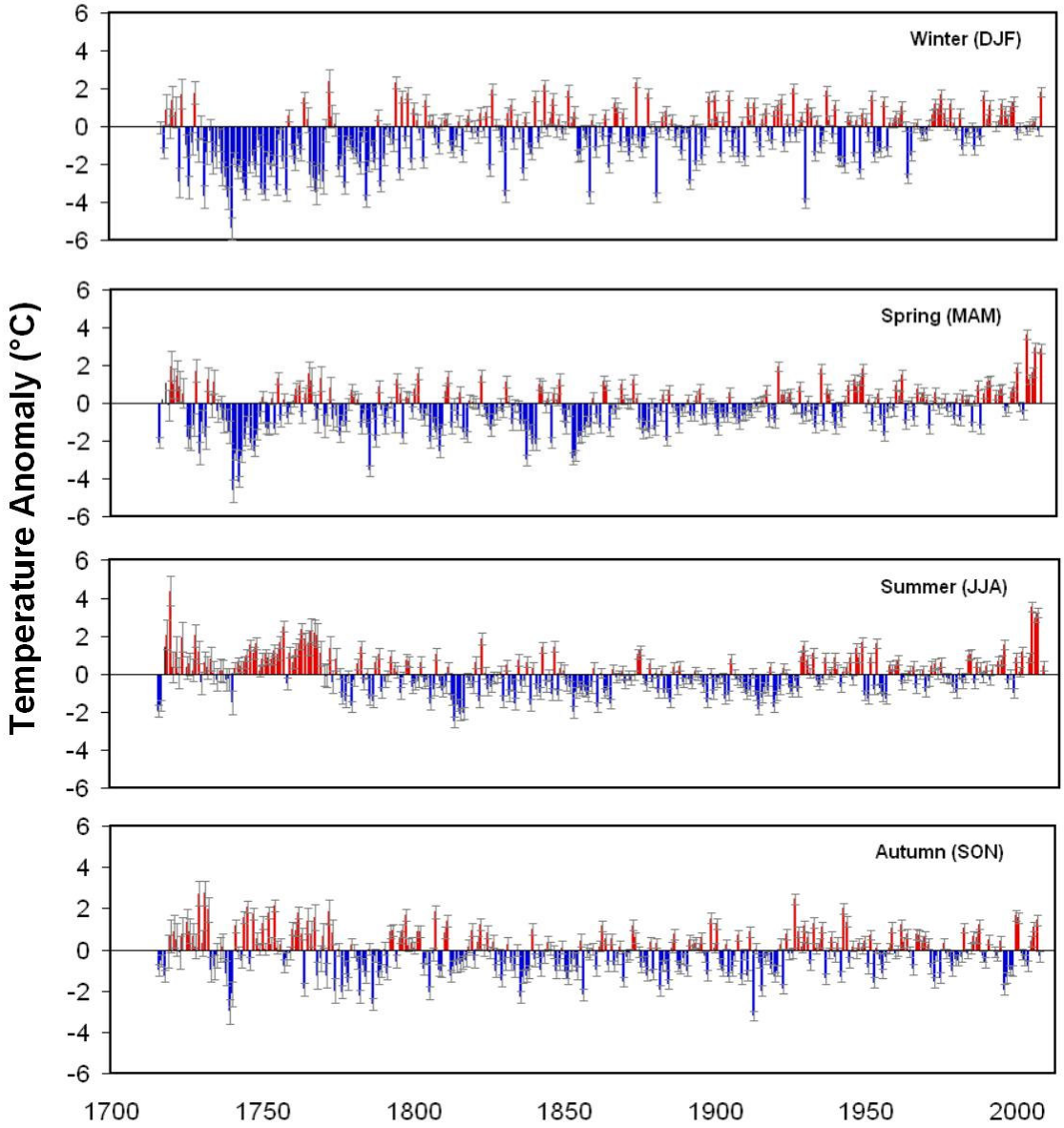

Figure 5.12: Outdoor seasonal temperature anomaly for the Padua series (1716-2007). Blue/red: colder/warmer years compared with the reference period 1961-1990.

If we consider the yearly averages (Figure 5. 13), the situation changes.

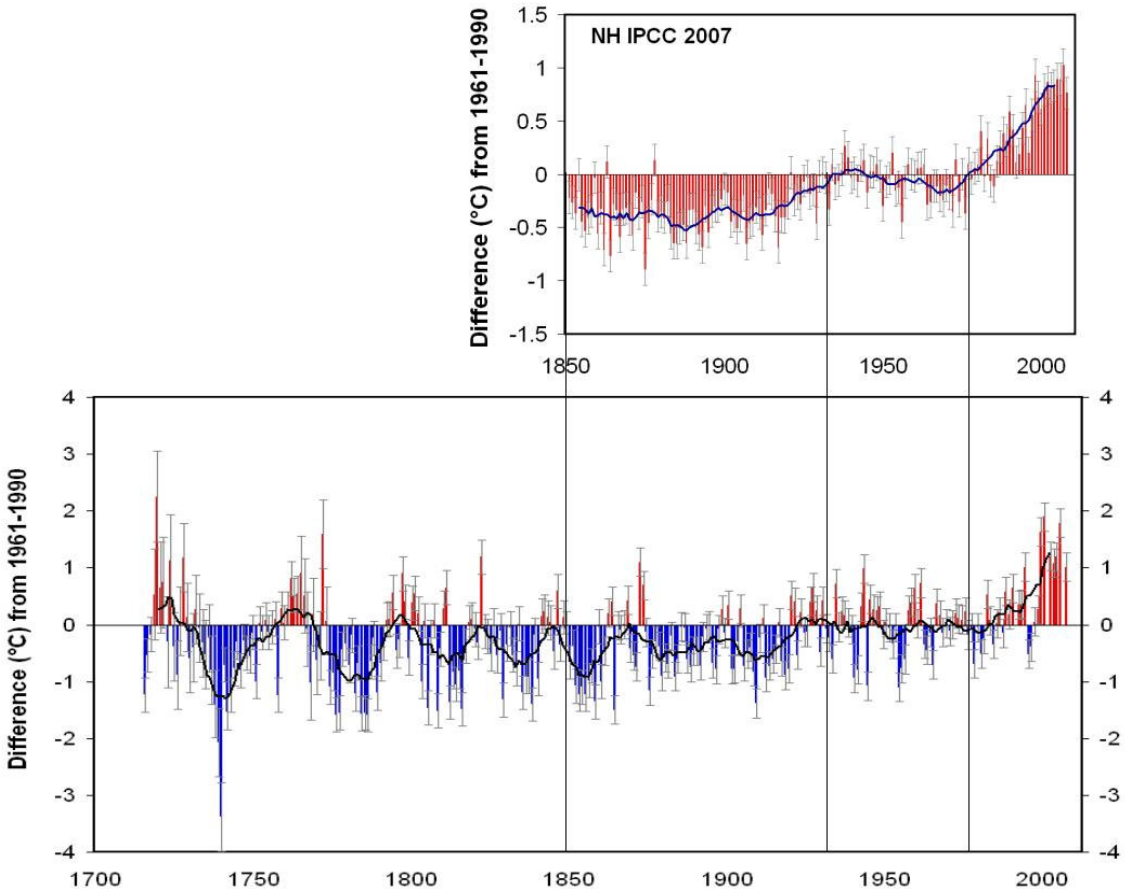

Figure 5.13: Top: Yearly temperature anomaly for the Northern Hemisphere after IPCC 2007 (Le Treut et al., 2007, WP1, data HadCRUT3). Thick line: binomial filter giving near-decadal average. Bottom: Yearly temperature anomaly for the Padua series (1716-2007), Blue/red: colder/warmer years compared with the reference period 1961-1990. Thick line: 11-year moving average.

Seven oscillations were repeated from the origin to 1930, although there was an amplitude attenuation going on in time. The average period of this smoothed oscillation studied with Fourier analysis in Figure 5.14 gives 35.8 yr and 23.9 yr. The 35.8 yr oscillation is the Bruckner cycle, interpreted as the results of the non-linear effect of solar activity on climatic processes (Raspopov et al., 2000). The 35.8 yr cycle exceeds the red noise level in the yearly average of the Padua temperature, but not in each individual season.

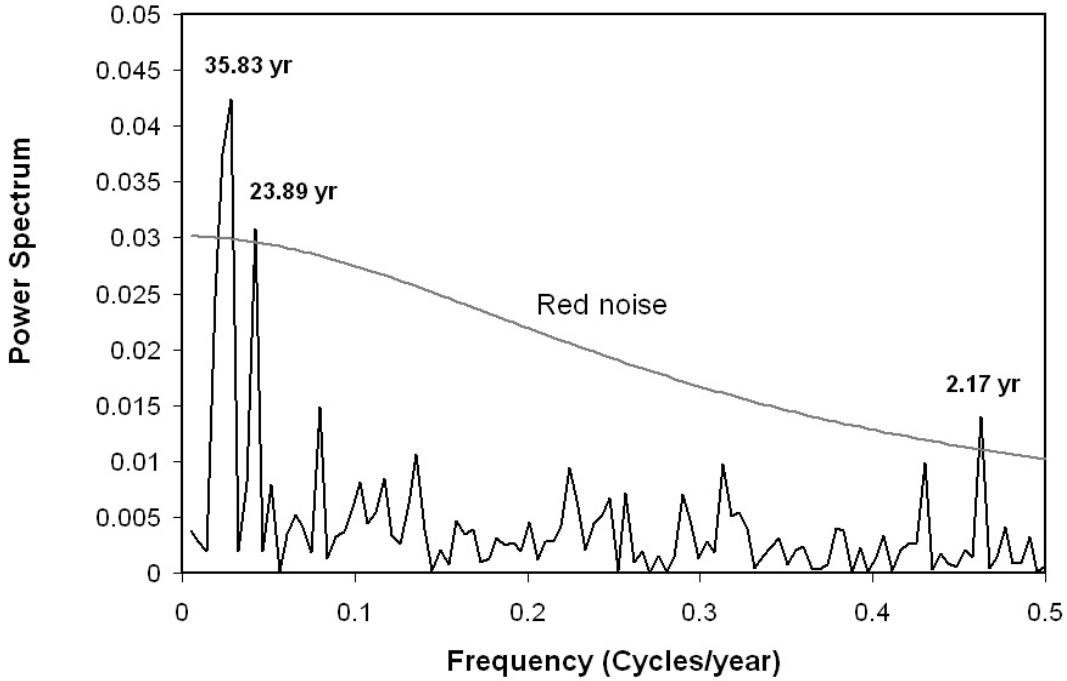

Figure 5.14: Power Spectrum to investigate periodicity in the Padua series for the 1716-1930 period. 35.8 yr (Brückner), 23.9 yr (Hale) and 2.2 yr cycles exceed the red noise level.

In winter this oscillation is absent, whilst in spring, summer and autumn it is visible but below the red noise level. Once the partial contributions are combined to form the yearly averages, the peak exceeds the red noise level. The 23.9 yr oscillation lightly exceeds the red noise and is the well-known Hale cycle of magnetic solar activity.

From 1930 to 1980 all oscillations are almost completely damped and a raise in temperature is visible since 1980. The above situation reflects, for the common period 1850-2007, the general trend of the famous temperature difference from 1961-1990 reported in IPCC 2007 (Le Treut, 2007) for the instrumental readings in the Northern Hemisphere (Figure 5.13). In the IPCC 2007 graph, the general impression is of continual warming with some intervals of temporary stagnation, the whole period being concluded with a sharp final warming.

This study extends back to 1716 the long daily temperature series in Padua with the addition of newly recovered data and the transformation of initially obscure indoor readings into outdoor observations in terms of modern units and observational methodology. This long work was justified by the scarcity of information about the early instrumental period and the exceptional contribution they can provide to our knowledge. In this study we fortunately found a number of parallel, simultaneous

observations, both indoors and outdoors, performed by independent observers in locations which were close to each other. These gave us the possibility to check the high quality of the data, to find the indoor-outdoor transfer function and to fill short gaps.

In the 18th century, in Padua, winters and springs were characterized by prevailing cold, with their absolute minima in 1709 and 1740; as opposed to the summers and autumns were warm except for 1740. In the 1716-1930 period the climate oscillated following a marked Bruckner cycle (35.8 yr) and a weak Hale cycle (23.9 yr). The climate oscillations were attenuated with progressing time and their amplitude was almost completely damped for the 1930-1980 period, after which the present-day warming started. It is clear that Padua is only one station and cannot be compared with multi-station graphs representative of a wide scale. Nevertheless, it is interesting to see how this station is responding to climate changes and global warming and compare it with the well-know trend of the Northern Hemisphere produced by IPCC 2007 (Le Treut, 2007). The comparison shows that, after 1860, Padua follows in general what is happening in the Northern Hemisphere, with marked warming after 1980 in spring and summer, but less in winter and autumn. The Padua series, adding some 150 years before the IPCC 2007 report, gives the opportunity to observe the almost regular oscillation that has preceded the 1850-2007 period. A wider time scale and the repetition of warmer and colder periods over two-thirds of the series seems to suggest that such cycles might be repeated in the future too. The same has been observed for the Mediterranean Basin (Camuffo et al., 2010) presented in Chapter 3 (see Figure 3.11). We agree that the problem is very complex, with many open questions (Jones and Moberg, 2003; Parker and Horton, 2005; Frank et al., 2007) and that no general hypotheses can be drawn on the ground of what has happened on a local scale for its limited representativeness. However, this may be a further, interesting newly open question.

II Part

Methodology of Climatic investigation:

Sky quality from satellite data

Chapter 6:

Climatology applied to the astronomical site testing

Contents

6.1 General description of Atmosphere
6.1.1 Classification of the atmospheric regions based on temperature distribution
6.2 Seeing and atmospheric turbulence in Astronomy
6.3 Parameters to test site quality
6.3.1 Overview on concepts and instruments for site testing

Over the next decade, the world will invest several billion dollars in new ground-based astronomical telescopes. Astronomical telescopes must be placed at the best possible sites to achieve their full scientific potential. The earth's atmosphere places limitations, sometimes extremely severe ones, on the sensitivity, spatial resolution and wavelength coverage of all telescopes, particularly in the optical, infrared and submillimetre parts of the spectrum. This is why some observations can only be carried out from space, despite the enormous cost. Site conditions that are crucial to the design of large telescopes, including those using adaptive optics or interferometry are concerning with cloud cover, sky brightness and transparency (including water vapour content), and in particular the nature and distribution of atmospheric turbulence.

The results from a site-testing programs determine where such a new telescope should be built. These detailed design studies often represent major international programs in their own right, taking many years to complete. Astronomical site testing has become vastly more sophisticated in recent years, stimulated by the construction of the billion-dollar Atacama Large Millimeter Array array in Chile (for sub-mm astronomy) and plans to build billion-dollar Extremely Large Telescopes (ELTs) in Chile and elsewhere (for optical and infrared astronomy). Astronomical site testing is a highly

multidisciplinary activity, bringing together atmospheric physicists, climate modelers and instrumentation experts.

6.1 General description of Atmosphere

The atmosphere is a gaseous envelope surrounding the Earth, held by gravity, having its maximum density just above the solid surface and becoming gradually thinner with distance from ground, until it finally becomes indistinguishable from the interplanetary gas. There is, therefore, no defined upper limit or 'top' of the atmosphere. As we go away from the surface of the Earth, different regions can be defined, with widely different properties, being the seats of a great variety of physical and chemical phenomena. If we want to understand the atmosphere, our first step will be to introduce some sort of classification that will help to consider separately all these phenomena.

If we look at atmosphere representation in Figure 6.1 we can see, by comparing the pressure scale at the right side with the height scale at left that: 90% of the mass is contained within the first ~ 20 km (top at 100 mb level) and that 99.9% is contained within the first ~ 50 km (top at 1 mb level).

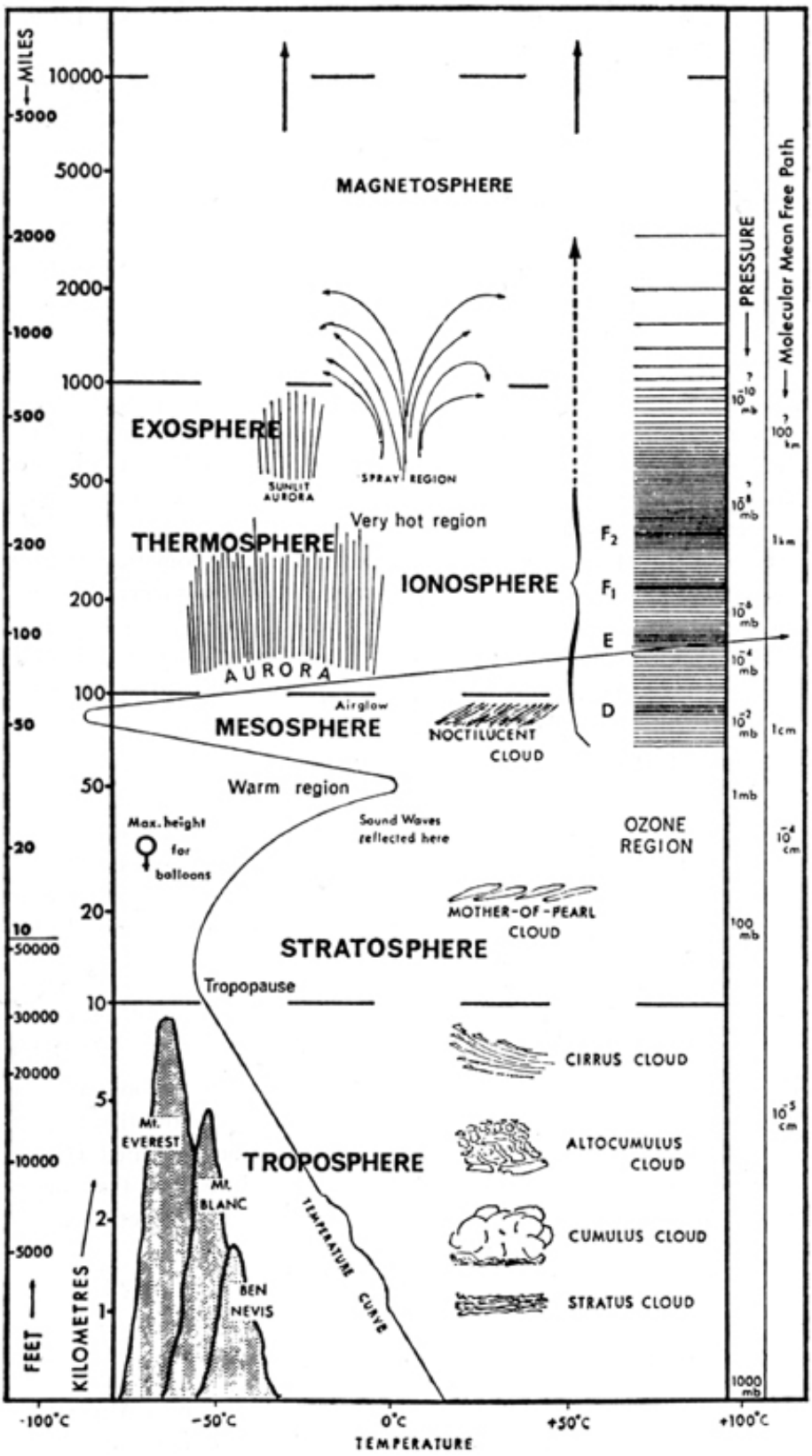

Figure 6.1 The atmosphere representation showing the main features of the terrestrial atmosphere.

This fact is explained if we consider that pressure, at each level, is given by the weight of all the air above it, per unit area of surface, and this weight is given by

$$\int_z^\infty g\ \rho\, dz \tag{6.1}$$

Where ρ is density, g acceleration gravity and z the height. The value of g varies only slowly with height, therefore, the pressure can be taken as roughly proportional to $\int_z^\infty \rho\, dz$, i.e. to the total mass above the level z. It is clear that from the point of view of its mass, the atmospheric envelope, although of diffuse limits, is a very thin sheath around the planet.

The 'thickness' of the atmosphere is characterized by the scale height parameter. We can consider the atmosphere as a fluid in hydrostatic equilibrium. This means that for every infinitesimal layer of unit cross section we have a situation of hydrostatic equilibrium (Figure 6.2):

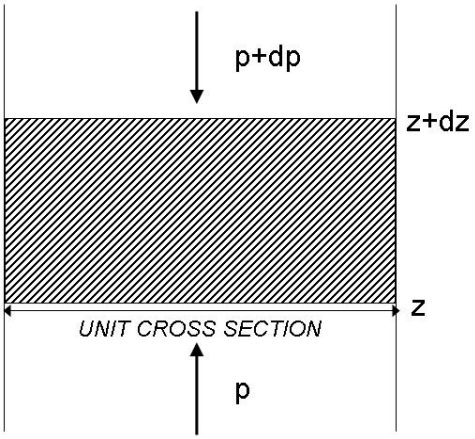

Figure 6.2: Layer of air column of unit cross section and thickness dz.

Upward force due to pressure gradient is equal to the weight

$$-dp = g\ \rho\, dz \tag{6.2}$$

Moreover, the air, at the temperatures and pressures of the atmosphere, behaves like a mixture of ideal gases, within at most a few percent of error. For the mixture

$$p = \sum p_i \tag{6.3}$$

$$p\,V = n\,R\,T \tag{6.4}$$

Where p is total pressure, V the volume, n the total number of moles, R the universal gas constant and T the absolute temperature. If we express the hydrostatic equation (6.2) as

$$d \ln p = -\frac{g\,M}{R\,T}\,dz \tag{6.5}$$

Where M=m/n is the average molecular weight and m the mass. Equation (6.5) can be integrated to

$$p = p_0 \exp\left(-\int_0^z \frac{g\,M}{R\,T}\,dz\right) = p_0 \exp\left(-\int_0^z \frac{dz}{H}\right) \tag{6.6}$$

Where have defined the parameter H=RT/gM, which is the (local) scale height of the atmosphere. H varies roughly proportionally to T up to 100 km because in this range M can be considered as a constant and g varies with z only about 3%. So if the temperature was uniform, the equation 6.6 could be written as

$$p = p_0\, e^{\frac{-z}{H}} \tag{6.7}$$

But T varies with height, so does H (i.e. H(T,g)), but up to 100 km, only within the range of 5 to 9 km.

If we consider the problem more closely and we make an example only with a mixture of two gases in the gravitational field, assuming g and T constant so that H varies only through the value of M, we obtain:

Gas 1, $$H_1 = \frac{R\,T}{g M_1}; \qquad p_1 = p_{01}\, e^{\frac{-z}{H_1}} \tag{6.8}$$

Gas 2, $$H_2 = \frac{R\,T}{g M_2}; \qquad p_2 = p_{02}\, e^{\frac{-z}{H_2}} \tag{6.9}$$

With $M_1 > M_2$ and $H_1 < H_2$. If we make the initial assumption that gas 1 is predominant at the surface, gases having two different distribution and height scales, they will intersect themselves at a certain level, above which the lighter gas 2 will become predominant (Figure 6.3). However this diffusive equilibrium takes very long to be reached.

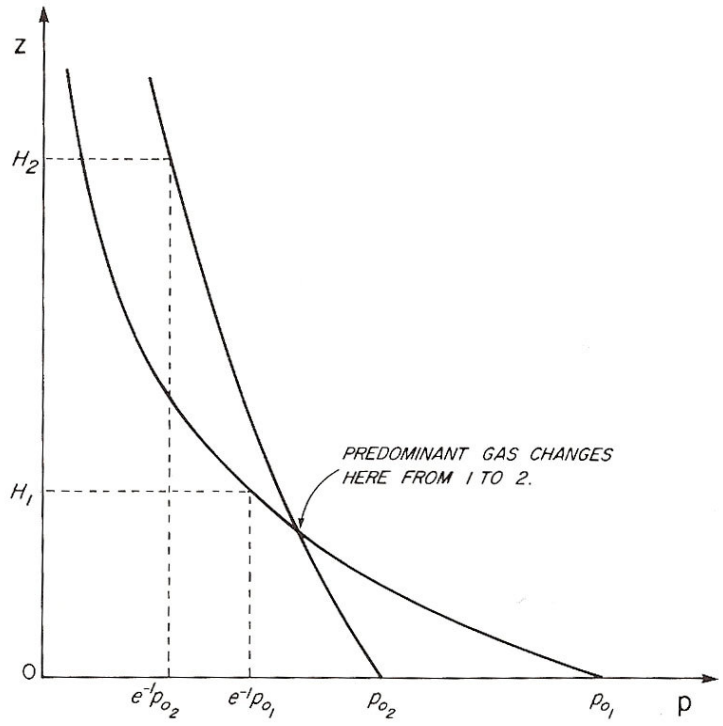

Figure 6.3: Height distribution of gases in diffusive equilibrium. P=partial pressure; z= height over reference level; p_{01}, p_{02} =partial pressure of gas 1 and 2 at z=0; H_1, H_2 = scale height of gas 1 and 2. H_1 and H_2 have been assumed constant so that the two curves are exponential.

Under 100 km mixing mechanism (turbulence and convective overturning) are active enough to keep the atmospheric air well mixed. The hydrostatic distribution, on the other hand, becomes established very quickly and at every instant we can assume that it exists and that air composition, except for trace gases, is constant and equation 6.6 is applicable and is therefore called homosphere. Above 100 km the situation changes because there is no mixing and the mechanism should better be described by the set of equations as in 6.8 and 6.9 for its varying composition and for this reason is called heterosphere. Thus we have come to a first classification of regions of the atmosphere, based on chemical composition. In this respect we should also mention a trace gas of particular importance, ozone, which forms photochemically in the stratosphere, where it has a maximum concentration in the region of 20 to 30 km. This ozone layer which absorbs the short wave range of solar radiaton and is responsible for a maximum of temperature at about 50 km, is known as ozonosphere. There is also another important gas which is variable in the lower layers of the atmosphere: water vapour. Here we only

mention that from its condensation we obtain in the troposphere the different kinds of clouds, whose typical altitudes are represented for reference in Figure 6.1.

6.1.1 Classification of the atmospheric regions based on temperature distribution

Other classification of the atmospheric regions are also possible as that one based on temperature distribution. Starting from the ground and up to a certain height, the temperature normally decreases at a rate of 6 degrees per km equals to the theoretical value of the vertical wet adiabatic lapse rate. This is variable with time and space, and even occasionally there occur shallow layers within which the temperature increases with height: the so-called inversions. The region that we consider in this work is called the troposphere and it is the seat of the weather phenomena that affect us at the ground. It contains about the 80% of the total atmospheric mass, almost the whole amount of water vapour and it is rich of aerosol and dust. Moreover this region is the most important atmospheric layer concerning the astronomical observations because it is responsible of the great part of the optical absorption, it is unsteady and it has an high refractive index. If we look at Figure 6.1, its upper limit is define by a sudden change in the temperature trend, often appearing as a discontinuity in the curve. This limit is called tropopause and its height, being larger at the equator than at the Poles, can vary between 7 and 17 km. the temperature at the tropopause in middle latitudes is -50 to -55 °C. The next region shows a gradual increase of temperature, reaching a maximum of around 0°C at 50 km. The region is called the stratosphere and its upper limit (at the temperature maximum), the stratopause. Then the temperature drops again through the region called mesosphere, to a minimum of the order of -100 °C defining the mesopause, at about 85 km. From there, the temperature increases steadily and the region is called the thermosphere. The temperature reaches high values and then remains constant; at 500 km it may reach values between 400 and 2000 °C, depending on the time of the day, degree of solar activity and latitude; the diurnal variation is of 500-800 °C, with minimum near sunrise and maximum at about 2 p.m.. In Figure 6.4 is indicated the type of nightly and daily temperature distribution. It is important to note that these high temperatures in the thermosphere do not imply that an object crossing this region, such as a satellite, may be much affected, because the pressure is too low (10^{-8} mb at 500 km) to permit any appreciable heat transfer. The meaning of the

temperature at these pressures is best understood by considering that it gives a measure of the average kinetic energy of the molecules.

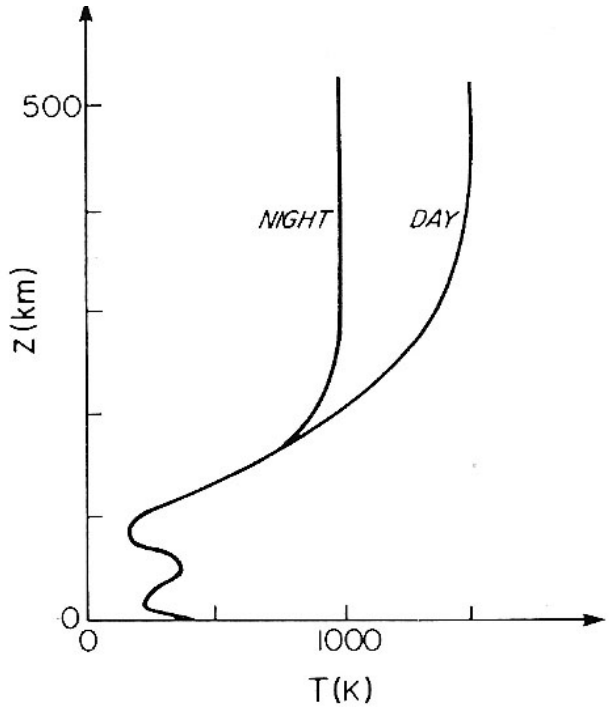

Figure 6.4: Vertical distribution of temperature in Earth's atmosphere.

Ionosphere. At high levels, the shorter wavelengths of solar radiation produce a considerable amount of ionized atoms and molecules and the corresponding free electrons. Thus in the ionosphere, a vertical distribution of electron density exists associated with photochemical processes, the typical distributions are therefore different for night and day conditions. The ionosphere can be studied from the ground by radiowaves. When this electromagnetis radiation passes through the ionosphere, the free electrons oscillate in response to the electromagnetic field of the wave and for high concentration of electrons, reflection takes place. The height at which the beam is reflected depends both on the frequency and on the electron number concentration N under the condition:

$$N = \frac{4\pi^2 \varepsilon_0 m\, v^2}{e^2} = const\; v^2 \qquad (6.10)$$

Where ε_0 is the free-space permittivity, m the mass of electron and e its charge. For each frequency the concentration N can be derived by this equation, while the corresponding height is found by the time lag of both the emitted pulse and the echo. The ions would

also reflect the waves, but only at higher concentrations, due to their larger mass. It is important mention also the periodical variations of the ionosphere, that are associated with sun spots and solar flares, referred to a or an 'Active Sun' period.

Exosphere: At the right side of Figure 6.1, a scale indicates the values of the mean free paths, λ, of molecules. This parameter is defined as the average distance travelled by a molecule between two collisions. It can be derived from the kinetic theory of gases that

$$\lambda = \frac{1}{\sqrt{2}\,\sigma n} = \frac{kT}{\sqrt{2}\,\sigma p} \tag{6.11}$$

Where σ is the collision cross section of the molecules, n is the concentration number, k the Boltzmann constant, T the absolute temperature and p the pressure. Mainly because p becomes small rapidly and also because the increase in T, λ increases from 10^{-5} cm at the surface to tens of kilometres at 500 km. This value is so large that collisions between molecules cease almost completely at these heights, and the molecules or atoms perform parabolic trajectories in the gravitational field. This region, above 500 km, that marks the gradual transition from terrestrial atmosphere to the interplanetary gas, is called the exosphere. Its base is actually defined as the level for that λ becomes equal to the scale height H.

In the next sections we will deal with the concept of seeing and atmospheric turbolence in astronomy.

6.2 Seeing and atmospheric turbulence in Astronomy

Despite the Earth's atmosphere limitations from one hand and the huge advances in the use of spacecraft as observatory platforms from the other hand, astronomy remains in large part still ground-based and for observations conducted from the surface the seeing as well as the atmospheric turbulence remain some of the biggest problems.

The seeing. When an electromagnetic wave of uniform amplitude pass into a refractive no uniform medium, some of the energy of the wave is scattered by the refractive inhomogeneities and as the wave propagates it exhibits amplitude and phase fluctuations. Therefore, an optical image formed by focusing such a wave exhibits fluctuation in intensity, sharpness and position. All these effects, referred respectively

as scintillation, image blurring and image movement are called seeing phenomenon and largely affect the astronomical image quality.

There are different way to define the astronomical seeing conditions:

a) The FWHM of the seeing disc

b) The Fried parameter r_0 and the coherence time τ_0

c) The C_N^2 profile of the atmospheric turbulence

FWHM. To evaluate the signature of atmospheric turbulence, a first method to highlight the long exposure parameter is that one to measure the seeing. The seeing value is obtained through the measurement of the diameter (i.e. the Full width at half maximum FWHM) of seeing disc represented by the point spread function PSF for imaging through the atmosphere. In a typical astronomical image of a star, the different atmospheric distortions average out as a filled disc just called PSF or seeing disc. The PSF diameter represents the best possible angular resolution which can be reached by an optical telescope in long time exposure and it is equal to the diameter of the fuzzy spot seen observing a point-like star through the atmosphere. In order to estimate the intrinsic seeing, its contribution must be isolated from all other sources of image degradation including telescope tracking errors, defocus and dome seeing. The differential image motion image monitor (DIMM) was developed specifically for this task. The DIMM measures the strength of the aberrations due to the atmosphric turbulence, and then predicts the seeing FWHM for a large telescope assuming the standard seeing model. The aberration strength is parametrised by Fried's parameter. Small values of r_0 indicate strong turbulence, and hence poor seeing.

From the DIMM seeing monitor we can use the follow equation

$$FWHM(\lambda) = 0.98\frac{\lambda}{r_0} \tag{6.12}$$

where the scaling length r_0 is the Fried parameter and it is a measure of the strength of the seeing distorsions and is defined as

$$r_0(\lambda) = \left[0.423\left(\frac{2\pi}{\lambda}\right)^2 \sec(\varsigma)\int_0^{\infty} C_n^2(h)\,dh\right]^{\frac{-3}{5}} \tag{6.13}$$

The *Fried parameter* is a measure of atmospheric seeing quality, which scales as the 6/5 wavelength power, the image FWHM has only a weak ($\lambda^{-1/5}$) dependence on wavelength. Hence for a given telescope diameter r_L, thus as λ increases, the ratio r_L/r_0 decreases and slowly approaches diffraction-limited imagery as wavelength is increased by improving the match between telescope size and atmospheric limitations.

The standard model for astronomical seeing, based on the work of Kolmogorov, (1941) on atmospheric turbolence stresses the attention on the follow theoretical points. In the case of starlight incident on the Earth, the light from a point source, propagates as spherical waves. After long distances of propagation a small section of these spherical waves can be assumed to be planar waves. The atmosphere induced effects on starlight, can be considered as two separate items: attenuation effects and index of refraction effects. We illustrate the distortions in response to the changes of refractive index in the atmosphere in Figure 6.5. Atmosphere is a non-homogeneous system sensitive to changes in pressure, temperature, humidity and wind speed/direction. All these properties, due to the atmospheric layers, also vary as a function of the altitude with respect to the Earth surface. The turbulent fluctuations in the refractive index, that produce phase fluctuations in the travelling wavefront, are just due to this atmospheric specific nature. Turbulence on the optical field, leads to scintillation, absorption and scattering. The absorption and scattering effects by the atmosphere are wavelength dependent and give rise primarily to attenuation of the optical wave.

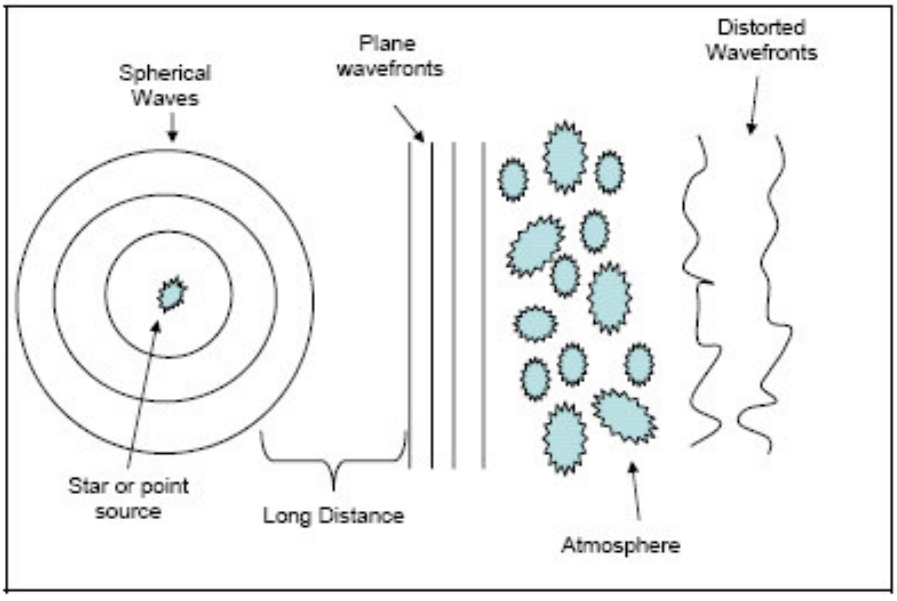

Figure 6.5: Representation of light from a point source travelling through the atmosphere.

The scintillation effect is defined instead to be wavelength independent and it is related to the physical parameter used to describe the magnitude of the atmospheric turbulence for the optical range, i.e. *C_n^2 structure parameter of refractive index.*

Turbulence is an effect of turbulent air motion and fluctuations and its source of energy, caused mostly by sunlight and diurnal cycle, is the vertical temperature gradient from Earth's surface. The C_n^2 physical meaning is that one to give a measurement of the strength of atmospheric refractive index. This parameter can be classified in two different regimes: weak turbulence and strong turbulence. So, the scintillation, causing changes in intensity in the optical beam, can be described as the destructive and constructive interference of optical waves caused by the fluctuations in the refraction index along the optical path. The scintillation index is perhaps the most immediate and easy variable to measure in function of space and time that allows a direct relation with the C_n^2 parameter. For optical beam waves, the scintillation index is proportional to the Rytov variance, σ^2_R defined by

$$\sigma_R^2 = 1.23\, C_N^2\, k^{\frac{7}{6}} L^{\frac{11}{6}} \tag{6.14}$$

Equation 6.14 claims a direct relation between the C_n^2 and the scintillation index, where k is the optical wave number, and L is the propagation path length. This relation is true for the weak turbulence regime which is defined as $\sigma_R^2<1$. Therefore the scintillation is a product of the small fluctuations on the atmospheric refractive index in function of time. The refractive index for optical and IR wavelengths can be written as

$$n(R) = 1 + 77.6 \cdot 10^{-6}\left(1 + 7.52 \cdot 10^{-3}\, \lambda^{-2}\right)\frac{P(R)}{T(R)} \tag{6.15}$$

This statistical approach is similar to the description related to random field of turbulent velocities, where inertial sub-range are bounded by the outer scale L_0 and the inner scale l_0. The concepts of outer scale and inner scale comes from Kolmogorov cascade theory of a turbulent flow, which assumes that size of turbulent eddies go from a macroscale to a microscale, as seen in Figure 6.6.

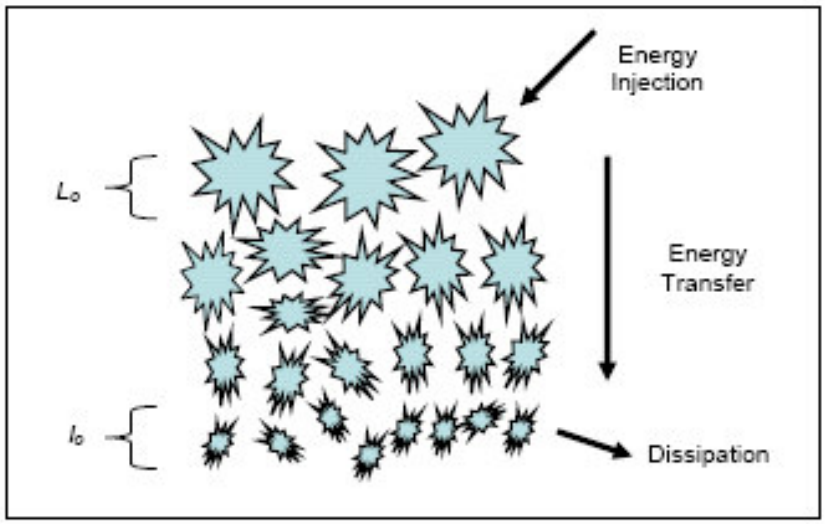

Figure 6.6: Representation of Kolmogorov cascade theory. The area between the outer scale and inner scale form the inertial sub-range. L_0 is the outer scale and l_0 the inner scale

For the theoretical Kolmogorov structure function, seeing distortions of the wavefront extend to infinitely large spatial scales. In reality an upper limit is imposed by the finite thickness of the contributing turbulent layers. Hence the crucial result is that for propagation through turbulence in the Kolmogorov model the structure function $D_p(r)$ of the wavefront perturbations p(r) at ground level scales as separation r to the 5/3 power

$$D_p(r) = 6.88\ (r/r_0)^{5/3} \qquad (6.16)$$

Where the scaling length r_0 is the Fried's parameter and is a measure of the strength of the seeing distorsions. Hence the 5/3 scaling will apply only to spatial scales smaller than the upper limit known as the outer scale of turbolence L_0. If the outer scale is not much larger than the telescope aperture diameter, then the image FWHM will be smaller than $0.98\ \lambda/r_0$, particularly at long wavelengths.

In conclusion, it easy to understand that the seeing is a variable value space and time depending i.e. it changes from place to place and from night to night. Good seeing nights are generally clear, cold with no wind gusts. Warm air rises degrading the seeing as well as wind and clouds presence.

Coherence time. The signature of atmospheric turbulence at an observatory can be described also by the short exposure parameters τ_0 and the mean wind speed. The shorter exposures allow to freeze some atmospheric effects and reveal the spatial structure of the wavefront corrugation (i.e. speckle structure appears when the exposure

is shorter than the atmosphere coherence time τ_0). These values become crucial to measure how turbulence is distributed throughout the atmosphere above all nowadays when the development of adaptive optics and interferometric techniques in the new telescopes, partially can compensate for the atmospheric turbulence effects. In the atmosphere above an astronomical observatory we will find an intense surface layer, a few narrow layers at altitudes 5–10 km, and a high altitude (20 km) layer associated with the jet stream. It is the highest layers that have the greatest influence, largely determining the correctable field-of-view of an adaptive optics system (the "isoplanatic angle") and the ultimate photometric precision ("scintillation index"). In addition to the intensity of the turbulence, it is equally important to know how quickly the turbulence becomes uncorrelated with itself, a quantity called the "coherence time", or τ_0. In most atmospheric models, the turbulent structure at a particular height is considered to evolve fairly slowly. This "frozen screen" of refractive index variations is then blown across the field of view by the wind speed at that height. In principle, τ_0 can therefore be calculated from a knowledge of the wind speed and turbulence at each height and corresponds to the time scale over which the changes in the turbulence becomes significant.

$$\tau_0 = 0.31 \frac{r_0}{\overline{V}} \tag{6.17}$$

Where r_0 is the Fried parameter and V is the mean wind speed as

$$\overline{V} = \left[\frac{\int_0^\infty C_N^2(h) |V(h)|^{5/3} dh}{\int_0^\infty C_N^2(h) dh} \right]^{\frac{3}{5}} \tag{6.18}$$

For a telescope equipped with adaptive optics, τ_0 has a direct effect on almost all of the important performance characteristics. For an interferometer, it directly affects the achievable signal-to-noise ratio on a given star.

Optical turbulence. The optimization of scientific observational programs for new class of ground-based telescopes pass necessarily by the forecast of the optical turbulence; this topic is therefore strictly correlated to the success and the survival of the ground-based astronomy of next decades.

The knowledge of the outer scale becomes very important for constructing large baseline telescope. When the diameter of the telescope is larger than the outer scale, in order to estimate the relative importance of possible wavefront distortion, it is necessary to know the statistical spatial coherence of the turbulence. A number of techniques exist to measure turbulence profiles, each with its own advantages and disadvantages. A direct in-situ measurement is to launch a series of meteorological balloons carrying in addition to the normal pressure, temperature and humidity sensors. A second way is to make use of the observed scintillation (intensity fluctuations imposed on the starlight by the intervening atmosphere) from a single or double star. Both the SSS (Single-Star SCIDAR) and MASS (Multi-Aperture Scintillation Sensor) are able to operate with relative modest telescopes. Intensive campaigns, although expensive and complicated to carry out, are the only way to obtain as long as possible database to have a comprehensive knowledge of the atmosphere above the observatory. In the top sites, it is very important to achieve an accurate statistical database with the relative contribution to the turbulence from the different atmospheric layers (i.e. strength of the optical turbulence C_n^2 as well as the velocity of the turbulent layers as a function of the height and time) using the SCIntillation Detection and Ranging observations SCIDAR technique and/or the MASS /DIMM, because the crucial importance of these data for the Adaptive Optics (AO) designs. We report some examples of instruments currently available to measure the atmospheric coherence length in top astronomical sites. At la Silla, Paranal and ORM, the seeing is continuously monitored using the Differential Image Motion Monitor (DIMM) that provides full atmospheric seeing with an accuracy better than 0.1". Moreover, intensive campaigns of SCIntillation Detection and Ranging (SCIDAR) observations have taken place in San Pedro Mártir (Mexico), La Silla (Chile) and Mauna Kea (Hawaii, USA) and monitoring campaigns are currently working at ORM and Observatorio del Teide (OT) in the Canaries.

To perform long term follow-up of observing conditions at an astronomical site parallel to the larger telescopes activity, is an important tool for understanding the effects of climatic cycles. An interesting example is given in Figure 6.7. In this plot monthly seeing values are presented for the 1987 – 2009 period in La Silla and Paranal observatories. Looking at the data, we see that the seeing quality get worse at Paranal after 1998. The ESO astroclimate staff looked for a possible explanation for these

unusual conditions of bad seeing which after 1998 became dominant and still occurred at Paranal with a frequency higher than in the past. This seeing new feature, was identified to be strongly correlated with a given wind pattern. Climate change, proposed as the weakening of the traditional Paranal westerly wind pattern (WNW to NNW wind), was identified as the main responsible for the degradation of observing conditions at Paranal as a new wind pattern allowed more frequently turbulent air from inland to blow over the coastal cordillera NNE to ENE (The ESO Messenger 97, September 1999).

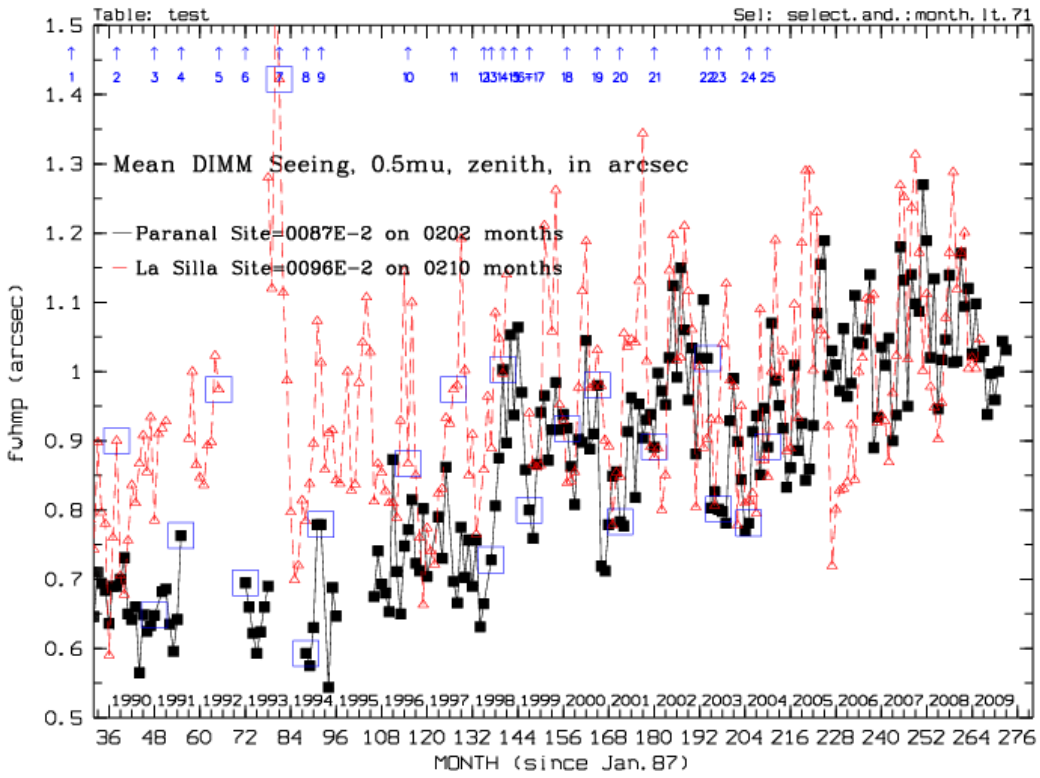

Figure 6.7: The monthly mean seeing at Paranal measured at 6 meter above ground and corrected for zenith and a wavelength of 0.5 micron in comparison with La Silla seeing values.

However in the plot is evident as from 1998 to 2009, the site quality has only marginally improved remaining below the standards of very good seeing (smaller than 0.5 arcsec) established during the extensive site survey (Figure 6.7). During that same period, La Silla, which is not undergoing any visible climate change had a minor degradation in seeing conditions. It was reported (The ESO Messenger 90, December 1997) that cloudiness at Paranal was obviously increasing with warmer see water, i.e. El

Niño events and this too could be the cause of the seeing worsening. In Figure 6.8, the running average of the past 12-months seeing values is given for both Paranal and La silla in 1988-2004 period in comparison with the El Niño Southern Oscillation Index SOI. Looking at the data, a long term degradation in coupling with the SOI index, is visible.

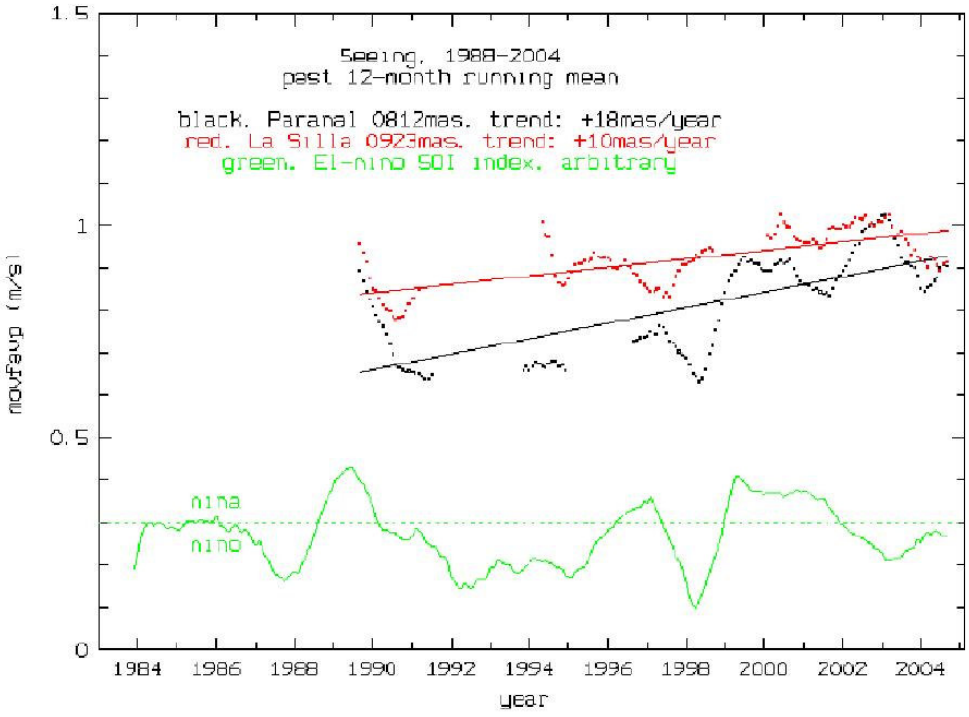

Fig 6.8: past 12-month running mean seeing value for 1988-2004 period at Paranal (black) and La Silla (red) in comparison with the El Nino Southern Oscillation Index SOI (green).

El Niño is the name given to the occasional development of warm ocean surface waters along the coast of Ecuador and Peru. When this warming occurs the usual upwelling of cold, deep ocean water is significantly reduced. El Nino normally occurs around Christmas and usually lasts for a few weeks to a few months. Sometimes an extremely warm event can develop that lasts for much longer time periods. The formation of an El Nino is linked with the cycling of a Pacific Ocean circulation pattern known as the Southern Oscillation. In a normal year, a surface low pressure develops in the region of northern Australia and Indonesia and a high pressure system over the coast of Peru (see Figure 6.9).

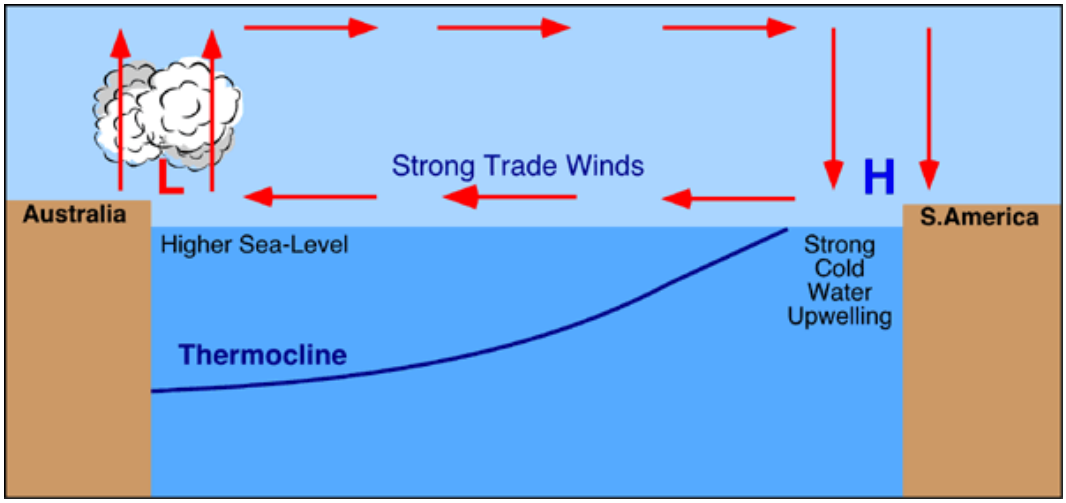

Figure 6.9: Cross-section of the Pacific Ocean, along the equator. The plot illustrates the pattern of atmospheric circulation typically found at the equatorial Pacific when does not occur El Niño events. Note the position of the thermocline, i.e. the water boundary where the greatest vertical change in temperature occurs, being usually the transition zone between the layer of warm water near the surface and the cold deep water layer.

As a result, the trade winds over the Pacific Ocean move strongly from east to west. The easterly flow of the trade winds carries warm surface waters westward, bringing convective storms to Indonesia and coastal Australia. Along the coast of Peru, cold bottom water wells up to the surface to replace the warm water that is pulled to the west. In an El Nino year, air pressure drops over large areas of the central Pacific and along the coast of South America (see Figure 6.10).

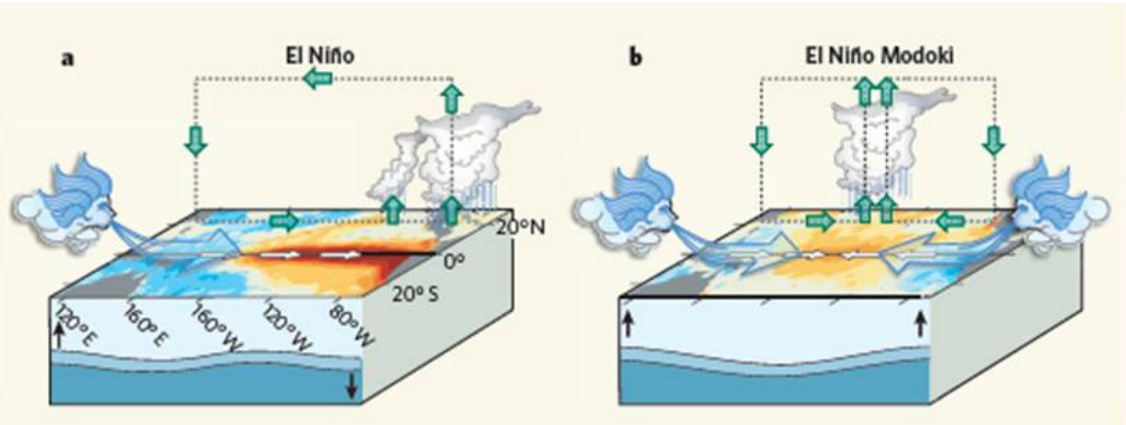

Figure 6.10: Cross-section of the Pacific Ocean, along the equator, illustrates the pattern of atmospheric circulation that causes the formation of the El Nino.

The normal low pressure system is replaced by a weak high in the western Pacific (the Southern Oscillation). This change in pressure pattern causes the trade winds to be reduced. This reduction allows the equatorial counter corrent (which flows west to east)

to accumulate warm ocean water along the coastlines of Peru and Ecuador. This accumulation of warm water causes the thermocline drop in the eastern part of Pacific Ocean which cuts off the upwelling of cold deep ocean water along the coast of Peru. Climatically, the development of an El Nino brings drought to the western Pacific, rains to the equatorial coast of South America, and convective storms and hurricanes to the coast of the Pacific. After an El Nino event weather conditions usually return back to normal. However, in some years the trade winds can become extremely strong and an abnormal accumulation of cold water can occur in the central and eastern Pacific. This event is called a La Niña. The dependency of Paranal seeing to El Niño cycles had been indeed similarly tested by ESO astroclimate team. Looking at this analysis, in 1988-1997 period, the comparison between seeing and SOI does not show any correlation (yellow squares in Figure 6.11). It was thus concluded that the basic Paranal observing conditions were weather independent. The seeing increase since 1998 (green squares in Figure 6.11), mainly due to a particular North-East wind pattern which lasts part of the night, a few times per month, shows some correlation with the standardized Southern Oscillation Index. In this last case, the most part of values belong to the current La Niña, in fact the SO negative index corresponds to warmer water (El Niño) and positive index to cooler water (La Niña).

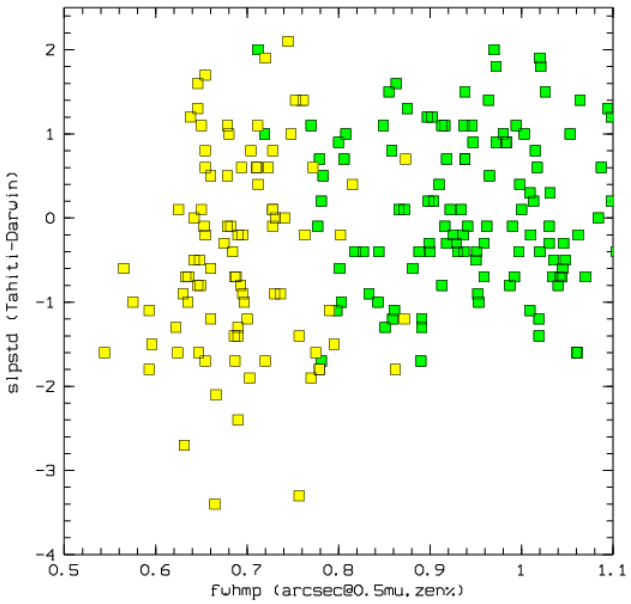

Figure 6.11: Correlation of the standardized monthly Southern Oscillation Index (SOI) with monthly average seeing at Paranal during 1988-1997 (yellow) and since April 1998 (green). A negative index corresponds to warmer waters (El Niño), a positive index to cooler ones (La Niña).

A last interesting comparison related to these coupled ocean-atmosphere interactions, is the cloud cover at Paranal and la Silla (Figure 6.12). In this plot, for 1984-2004 period, from one hand, it is evident a long term degradation in photometric night fraction at Paranal due to Bolivian High moving South and from the other hand a long term improvement in photometric night fraction at La Silla due to the Polar Low moving South. In both the sites, the coupling with El Niño is visible.

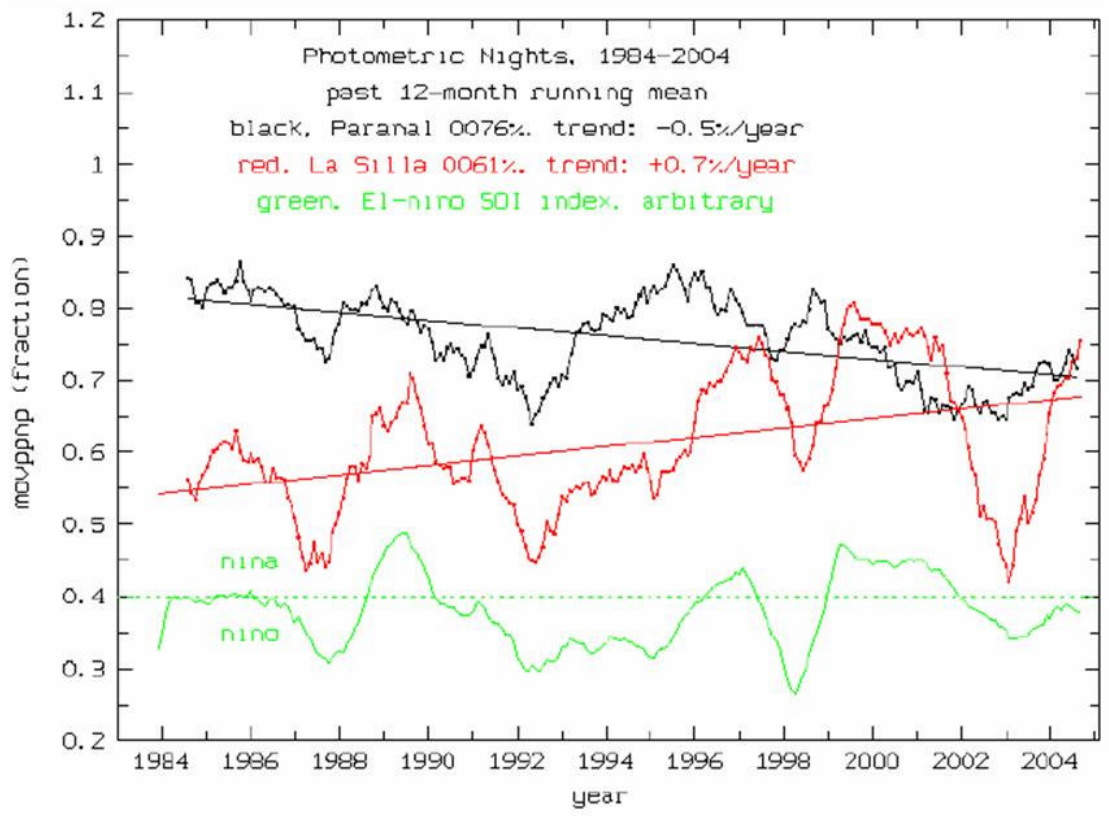

Fig 6.12: past 12-month running mean photometric nights fraction for 1984-2004 period at Paranal (black) and La Silla (red) in comparison with the El Nino Southern Oscillation Index SOI (green).

6.3 Parameters to test site quality

However to characterize an astronomical site adequately beside the seeing already presented in detail and the atmospheric extinction that will be dealt in depth in the next chapter, it is necessary to compare some other important parameters that define the astronomical and climatic site quality. They are:

a) Vertical structure of the atmospheric turbulence (i.e. optical turbulence, outer scale, isoplanatic angle and coherence time)

b) Number of nights / hours available for astronomy in visible range

c) Inversion layer

d) Airborne aerosols

e) Cloudiness, fog and dust

f) humidity and precipitable water vapour

g) Temperature

h) wind speed and direction; vertical profile in the boundary layer (BL)

i) light pollution and other contaminations (e.g. sky emission and sky darkness)

j) seismicity

k) site accessibility

Our research work, in this field, is based on the analysis of some specific parameters as the visible extinction, the airborne aerosol and atmospheric dust content for some among worldwide top selected astronomical sites (i.e. Roque de Los Muchachos Observatory, Teide Observatory in Canary Islands, Paranal, La Silla and Tolonchar as candidate site for ELT in Chile). Our aim is not to deal with each single site testing parameter but rather to study in detail a new technique to retrieve and analyse high quality aerosols content values in atmosphere and to search for possible relationship with climatic data.

This study is however only a starting point to develop a new approaching methodology at the wider range of site testing parameters. The increasing interest in international site testing campaigns find a strong motivation if we consider the following two points:

- The past recent astronomical projects and the present and future billion-dollars projects have required and will require in future, always more years to be completed (e.g. ESO-VLT at Paranal in the near past, ALMA array in Chile at present or the Extremely Large Telescopes (ELTs) in the near future). For this reason, the site choice for these big international projects became essential. The 'best' possible astronomical site, in fact, must assure optimal conditions for a wide range of parameters (e.g seeing, cloudiness, humidity, temperature and extinction) at the moment of the telescopes building, but it also must assure the

persistence of these best conditions for decades during telescopes life. It is therefore necessary to work on two fronts: first, carrying on excellent preliminary site testing campaigns to make the best possible choice at the moment of the project accomplishment and, secondly, continuing site-testing monitoring in parallel with the main telescopes activity in order to guarantee the maintenance of the best sky quality conditions and create, year by year, a complete database with the more relevant parameters for evaluating the site conditions. Such database will be a sort of milestones by taking into account in performing campaigns for future projects. Moreover, in the comparison with climatic values (e.g. temperature for monitoring Global warming, changes in local or large scale weather conditions as cloud formation, humidity, wind force or direction, pressure conditions…), such database could be useful for understanding the causes of changes that affect the atmosphere of an astronomical site.

- Nowadays, the target of astronomical international project is increased in term of scientific communities, policymakers involved, scientific objectives and economic investments. As consequence, the significance of the investments is weighted not only on the base of the present and future scientific and technological innovation but also on merely economic base. Of course the scientific motivation are the background of each project but the economic point of view becomes more and more relevant with time. If we consider, for example, that one observational night at the ESO-VLT at Paranal, Chile costs about 100,000 $ we understand the importance of optimizing also the number of hour available for astronomy. In the choice of an optimal site it enters therefore the number of observational hours or dark time available for a specific latitude (as we see later) during a calendar year, as well as the choice of the best possible values of seeing and all the parameters related to the atmospheric turbulence useful to project the Adaptive Optic design of a telescope. It appears clear as more and more, in these last years, the instruments are optimized and designed taking into account the conditions of the atmospheric layers above the astronomical site taken in exam. A such high correspondence between the place where the instrument is going to work and the instrument itself not could be

possible if good site testing studies were not available in past as well as are available in present time.

6.3.1 Overview on concepts and instruments for site testing

As told in the list presented above, since astrophysical observations require minimum interference from the Earth's atmosphere, in searching for the best site with astronomical qualities, the main parameters to take into account are:

Dark Time. Besides to the greater number of clear nights it is necessary that a site must have the maximum duration of astronomical night, i.e. a maximum in number of hours available for observations during the calendar year. To this end, it is interesting to see in Figure 6.13 as the total yearly amount of hours of astronomical nights (i.e. dark time) changes with the latitude of the astronomical site (Sarazin and Sadibekova, 2005). This plot shows that astronomical polar sites as Dome C provides only half the observing time of what is available at mid-latitude (i.e. Paranal site). This fact derives from the definition of astronomical twilight. In Chapter 4 we already saw the formulas to calculate the duration of sunset and we mentioned the difference between the astronomical and civil twilight. We explain better these concepts. For a time before sunrise and after sunset, light from the sun illuminates the atmosphere to produce some skylight, known as twilight. Twilight is arbitrarily divided into three increments. The period when the sun is six degrees or less below the horizon is called civil twilight . When the sun is between six and twelve degrees below the horizon, the period is called nautical twilight. During this period it is dark enough to see the brighter stars, used for navigation, and still light enough to see the horizon. When the sun is between twelve and eighteen degrees below the horizon, the period is called astronomical twilight. When the sun is below 18 degrees, the faintest stars which can be seen by the naked eye are visible. Using the traditional definition, the total number of dark hours available per year is shown on Figure 6.13 as a function of the geographic latitude.

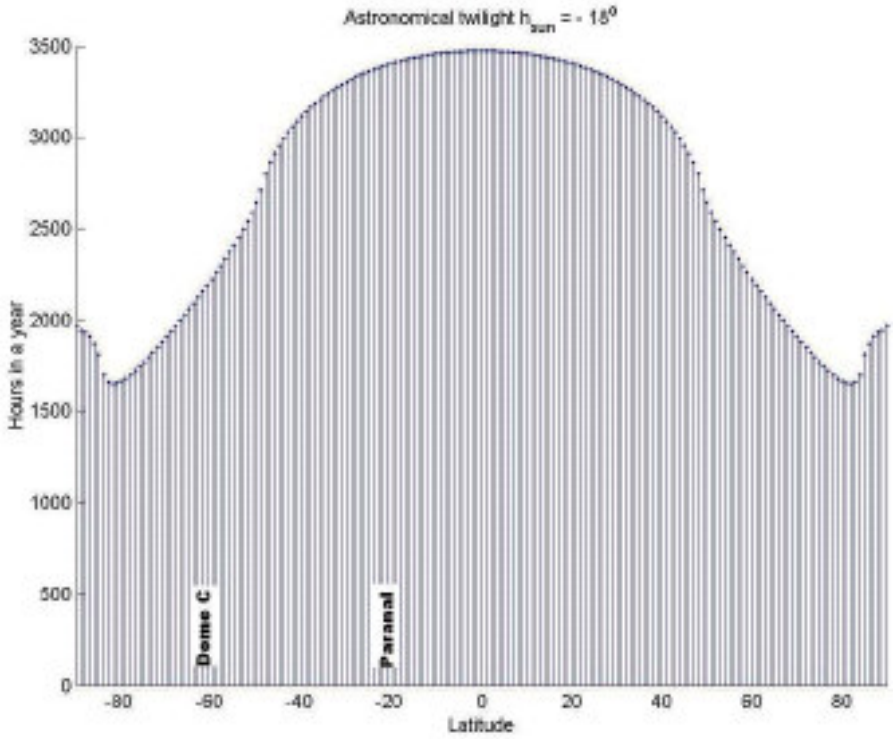

Figure 6.13: Total available number of dark hours per year as a function of latitude. Astronomical dark time is by convention defined when the sun is more than 18 degrees below horizon.(Sarazin and Sadibekova, 2005)

The minimum occurs at a distance from the pole equal to the difference between the earth axial tilt (23.45°) and the required minimum solar elevation.

The inversion layer. Most international observatories are located at mid-latitude, in islands or on coastal mountains because a site candidate for an astronomical observatory must guarantee the persistence of climatic best conditions for great part of the year with permanent anticyclones and stable air masses. In particular the inversion layer, that pulls apart the subsidence of dry air coming from higher altitudes from the thermal convection of the lower altitudes, must to be under the observatory quote. This fact in principle should assure a great number of clear nights and reduced atmospheric turbulence. If we consider the example of the Roque de los Muchachos Observatory (ORM) in Canary islands, we see that air circulation caused by the anticyclone gives rise to a predominantly north-easterly pattern of winds at sea level, which are cool and humid from passing over the maritime current of the Canaries, whilst the winds at mid-level are north-westerly, dry and warm. As a result of these factors, at the latitude of the Canaries' archipelago the frequent presence of a near subtropical anticyclone, the predominance of the Trade Winds and the existence of a cold ocean current, there is a

stratified air with largely stable layers. This usually prevents air from rising and producing the convective phenomena that would cause precipitation. The inversion layer is normally between 1200 (in summertime) and 1600 m (in wintertime) as described in Figure 6.14, thereby producing a clear dividing line between the lower and upper layers of air circulation.

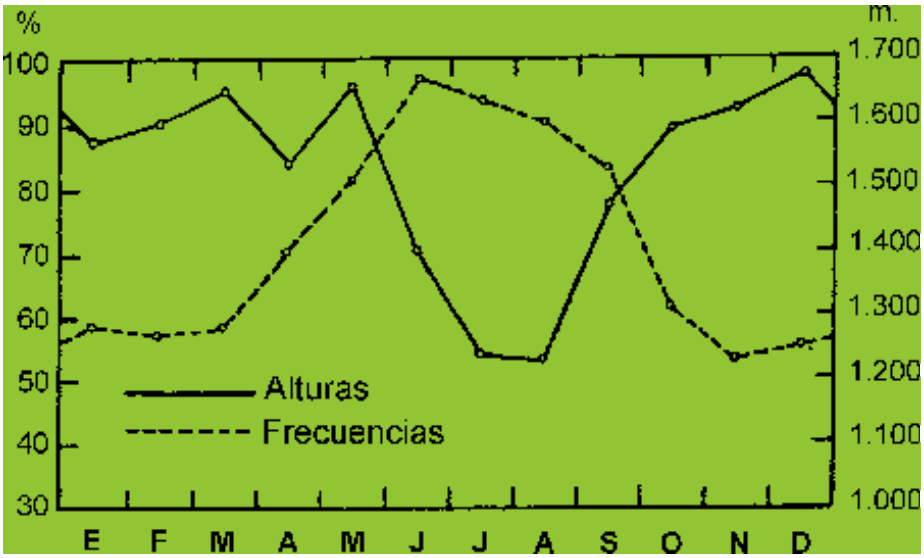

Figure 6.14: Annual variation of the scale height and frequency of the sea of clouds in Tenerife from Font-Tullot, 1956.

This is marked by a stationary sea of cloud at the inversion layer, with a generally cloud-free, dry sky above it.

Airborne aerosols. This site-testing parameter will be study in detail both from a theoretical point of view in Chapter 7 and from a practical point of view in Chapters 8 and 9 making a comparison of the optical aerosol depth values in top sites during the last six years. The instruments used to measure size and density of local airborne aerosol usually are Portable Counter Particle used for example at Paranal and ORM. The vertical structure of aerosol, i.e. the aerosol optical depth and the height of aerosol layer, is obtained instead by remote sensing measurements for example from the Ozone Monitoring Instruments onboard of AURA platform. UV aerosol index from Total Ozone Mapping Spectrometer on board of Nimbus7:1978-1993; Meteor-3: 1991-1994; ADEOS: 1996-1997 and Earth Probe: 1996-2004. All these satellite platforms has been studied in this second part of the thesis and the results will be presented in Chapters 8 and 9.

Cloudiness, fog and dust. Sites are judged for their low probability of cloud cover, fog, smoke and haze, based on the annual percentage of sunshine, orographic effects and height of the inversion layer. Fog and smog tend to stay below the inversion layer, so the site, at higher elevation, should not be affected. All these parameters affect the observational quality. The presence of clouds avoid the possibility to have clear photometric nights and fog and dust at the observatory level, considerably increase the atmospheric extinction. The dust is considered for example one of the main decay element for the observational quality at ORM. The dust reaches the Canary islands during the summer, coming from the Central Sahara. It is transported horizontally by the dominant wind (i.e. Trade wind) and during the travel it undergoes a separation process, with the larger particles (> 10 μm) that sediment at ground in little time and the smaller that are moved through the Atlantic ocean, for thousands of kilometres from the original site. A relevant amount of about $200 \cdot 10^6$ tons of dust is removed each year from the Sahara desert (Murdin, 1986). The dust creates a Western big plume visible from the satellite images too with a 20° latitude typical wide. In wintertime the prevalent wind carries dust over the Cape Verde islands as in Figure 6.15. During this period the plume does not reach La Palma island, in summertime instead, wind over four kilometres of altitude can bring dust particles at Northern latitude, investing the ORM sky. Instruments used to retrieve these parameters are remote sensing detectors (TOMS, OMI and MODIS) on board of different satellite platforms. The Moderate Resolution Imaging Spectrometer, on board of TERRA (since 1999) and AQUA (since 2002) operates in bands of astronomical interest (visible and NIR) and with higher spatial resolution (1km x 1km).

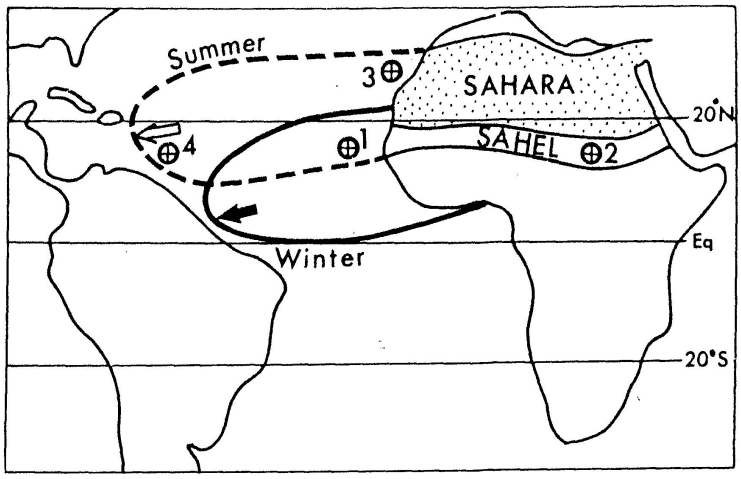

Figure 6.15: Seasonal dust transport over the Atlantic. 1: cape Verde Islands; 2: Jabel Marra Mountains, Sudan; 3: Tenerife, Spain; 4: Barbados.

Humidity and precipitable water vapour. High values of relative humidity prevent astronomical observations because they impair the instrumental functionality. Precipitable water vapour (PWV) is defined as the total water vapour content contained in a column of unit cross section extending from the earth's surface to the "top" of the atmosphere. It affects on the water vapour absorption lines in IR range and at 0.9 μm. The resources most used to measure these parameters are satellites that provide daily measurements of humidity and PWV as the IR Operational Satellite (TIROS) and the Operational Vertical Sounders (TOVS) with a spatial resolution of 0.5 degrees.

Temperature. This parameter is very important to perform good astronomical observations. Temperature difference affect the seeing. When light enters the Earth's atmosphere in fact, the different temperature layers distort the waves leading to distortions in the image of a star.

Wind speed and direction; vertical profile in the boundary layer (BL). Wind presence gives vibrations to the telescope and in some cases can generate local turbulence into the dome that make worse the mirror-seeing conditions. The wind speed and direction measurements of turbulence layers can be obtained from SCIntillation Detection and Ranging SCIDAR and SLOpe Detection and Ranging (SLODAR) or from climate archives (Garcia-Lorenzo et al. 2005) as in Figure 6.16.

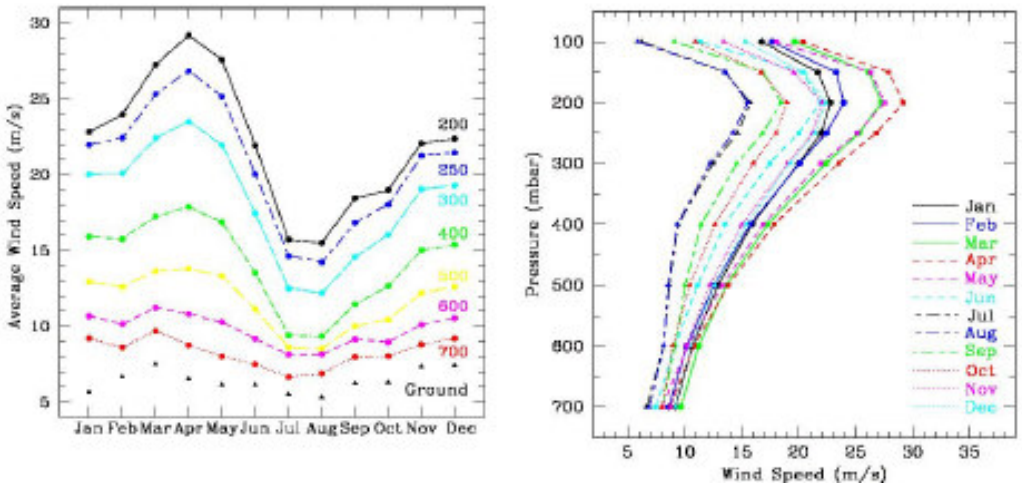

Fig.6.16: The monthly averaged wind velocity for the period 1980-2002 at the pressure levels indicated in the figure at ORM (from Garcia-Lorenzo et al. 2005).

Instead the vertical turbulence structure and the wind profile of the lower layer of the atmosphere (i.e. the boundary layer) can be obtained from SOnic Detection And Ranging (SODAR) measurements.

Light pollution, sky emission and sky darkness. The night sky is not completely dark because it exists a natural luminosity. The main sources of this natural luminous background are the zodiacal light and the auroral light. The first is of extraterrestrial origin and it is due to solar light diffused in the visible range by interplanetary dust and it is due to black body IR emission at 160-220 °K. This zodiacal light is concentrated on the ecliptic plane. The second, is generated in the high terrestrial atmospheric layer, at 100 km of altitude and it is due to the solar UV radiation, that during day has ionized the ionosphere atoms and molecules. The particles de-excite give rise at emission lines that hold over all night long. These lines depend on the solar activity because they are correlated to the solar cycle. The combination of these two sky emissions constitute the natural sky darkness for the ground based astronomical observations and they give a minimum value in the visible range of about 22 mag/arcsec^2.This value however does not take into account the luminous contribution given by light pollution. Nowadays almost in all the terrestrial sites, the night darkness has been reduced by the progressive increase of light pollution as consequence of the artificial lighting. This kind of pollution ranges up to large distance and it depends by some parameters as the number of luminous contributions or the soil albedo. Walker calculated the percentage of increase luminosity (I_{art}) in function of the population of a urban site (P) at a distance r

expressed in km if one observes at a zenithal distance of 45° toward the urban site. The formula is

$$I_{art} = 0.01\, P\, r^{-2.5} \qquad (6.19).$$

Seismicity. This parameter is relevant for the building and instrumental damages when earthquakes occur but above all for the micro-vibrations of the seismic swarm that can deteriorate the astronomical images in interferometry. Seismicity is induced by regional tectonics, oceanic effects, volcanic and anthropogenic activities. Several different types can be found:

- Regional seismicity > 1mb (very low)
- Microseismicity
- Low frequency seismicity (volcanic tremors, oceanic effects..)

The seismicity is measured with broadband seismometers and generally all countries monitor the regional seismicity. Another aspect to take into account is the ground deformation that are induced by (a) barometric pressure loading and hydrologic loading: rain and snow, (b) deformations induced by temperature changes and (c) in magma motion at great depths that can produce landslides.

Site accessibility. At present, the automated telescopes are designed to operate remotely, so there will be no operators present at the telescope to keep an eye on the equipment or to fix any problems that may arise. It is therefore important to locate the telescopes at a present observatory site, where someone in charge could periodically check up or repair damages on it.

Chapter 7:

Atmospheric Extinction and Aerosol Physics

Contents

7.1 The Tropospheric Aerosol
7.2 Atmospheric extinction
7.3 Optics of individual aerosol particles
  7.3.1 Rayleigh scattering
  7.3.2 Mie scattering
7.4 Optics of the atmospheric aerosol
  7.4.1 Reflection, transmission and absorption radiation change

7.1 The Tropospheric Aerosol

In this section we deal with the lower atmospheric layer in which atmosphere contains many solid and liquid particles in suspension, which constitute what we call atmospheric aerosol or particulate matter (PM) with different chemical and physical properties. The origin and chemical composition of these particles may be summarized in the following list of sources:

- Combustion: forest fires, industrial combustions. The particles may have various salts, carbon, soot (These are primary aerosol of natural and anthropogenic emissions respectively)
- Gas phase reactions, including photochemical with the formation of sulfates and nitrates (secondary aerosol)
- Dispersion of solids. Chemical reactions in the ground followed by water erosion and wind erosion can result in the introduction of particles from mineral rocks into the air: silicates, sodium, potassium and calcium salts.

- Dispersion of solutions. The bursting of tiny bubbles in the sea introduces particles in the air, essentially with the composition of sea water.
- Volcanoes.

An indication of the typical size distribution in continental air is given in figure 7.1.

The size is an important parameter to define the aerosol properties because it affects removal mechanisms in atmosphere, visual extinction and man health. A first rough distinction depending on aerosol size is to separate particles lower than 2.5 μm, called fine particles and greater than 2.5 μm, coarse particles. Particles different in size have different chemical composition, physical behaviour and moreover they are characterized by different emission and removal mechanisms. The fine particles are mainly products of molecular processes as sulphates, nitrates, carbon and metals, the coarse particles instead, derive by industrial activity or by mechanical processes of earth's crust erosion and present typical soil elements. The fine particulates have mean time residence in atmosphere of some days or weeks and they can move over distance of thousands kilometres. The coarse particulates have instead minutes or hours mean times residence and the typical distance they can do are minor than ten kilometres.

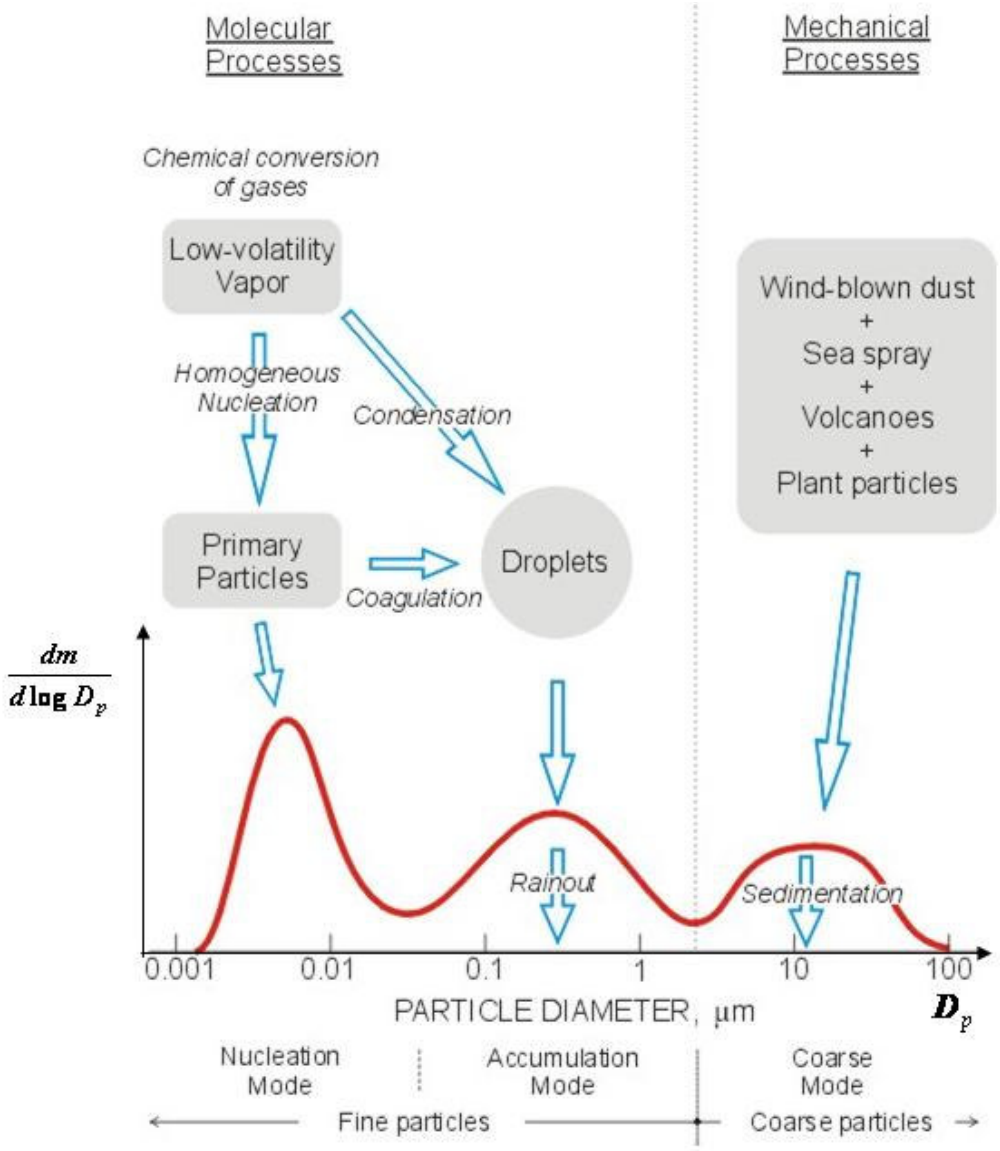

Figure 7.1: Schematic diagram of the size distribution (expressed as mass per increment in log particle diameter) and formation and removal mechanisms for atmospheric aerosols

Looking at Figure 7.1 is possible to distinguish the main features of aerosol particles using the size as discriminating factor as follows:

0.01 µm represents a more stable and permanent size, at which reasonable storage times are possible and coagulation at atmospheric concentration is not excessively fast. The size range lower than 0.01 µm is defined as Nucletion mode and includes aerosol from chemical conversion of gases or particles emitted in atmosphere by primary sources. Particles in 0.01 -0.1 µm range are defined as Aitken mode and can be the result of an increasing diameter of the nucleation mode particles or can be aerosol coming from a primary combustion at high temperature.

0.1 μm is considered to be 'predominant', in the context of atmospheric aerosol, as number of particles. It is also a size region which is little affected by both Brownian movement and by gravitational settling and particles of this size are likely to have the longest survival as individuals since both diffusive and inertial coagulative processes are inefficient. Particles in 0.1 – 1 μm range are defined in fact as accumulation mode and include aerosol coming from coagulation, particles that act as nuclei for cloud condensation droplets (CCN) or particles of nucleation and aitken modes that have increased their diameters.

1 μm the falling speed under gravity of this set of particles is only about 1 mm every 5 seconds, but even this slight sedimentation amounts to 20 m per day and the falling speed increases quadratically with radius in the size region.

10 μm this is the approximate size of cloud droplets, which of course are a special subgroup of the atmospheric aerosol. The falling speed of a 10 μm particle of density 2 g cm^{-3} under normal surface conditions is about 2 cm sec^{-1}.

100 μm this is the size of fine drizzle drops (falling speed about 1m sec^{-1}). These particles are quite rare n fine weather everyday experience but they are present in dust storms episodes, natural or caused by man. Drops of this size are produced by sea spray, but they fall out quickly and do not usually travel very far from their source.

The main processes of aerosol formation are: *nucleation*, *condensation* and *coagulation* that, for particles, act as the number size distribution discriminating factor.

Nucleation is a process where vapour in gaseous phase is transformed in liquid or solid phase.

Condensation is a mechanism responsible of the particle growing, in particular conditions in fact the vapour condensing on particulate surface causes an aerosol accretion.

Coagulation is another important process for aerosol accretion; thanks to Brownian motions or turbulences, this phenomenon particles are joined together through collisions.

Also the efficient processes of elimination from the atmosphere depend on the size range. The largest particles have an appreciable falling velocity and therefore

sedimentation is important for them (aerosol greater than 2.5 μm). Particles around 0.5 - 10 μm in size act as CCN when precipitation develops, these particles are carried down to the ground in the raindrops or ice particles (rainout mechanism). Larger particles can also be scavenged by raindrops (washout mechanism). On the other hand, the small particles (<0.1 μm) cannot be eliminated in this ways. But they can attach to drops by Brownian motion or other effects (diffusiophoresis, thermophoresis); they will also be included in the rainout. Coagulation eliminates smaller particles with production of bigger ones. Figure 7.2 summarizes these elimination processes. It may be seen that the sizes around 0.1 μm, too small for acting as CCN or to be scavenged by impact, and too big to be captured by Brownian motion, are removed with more difficulty.

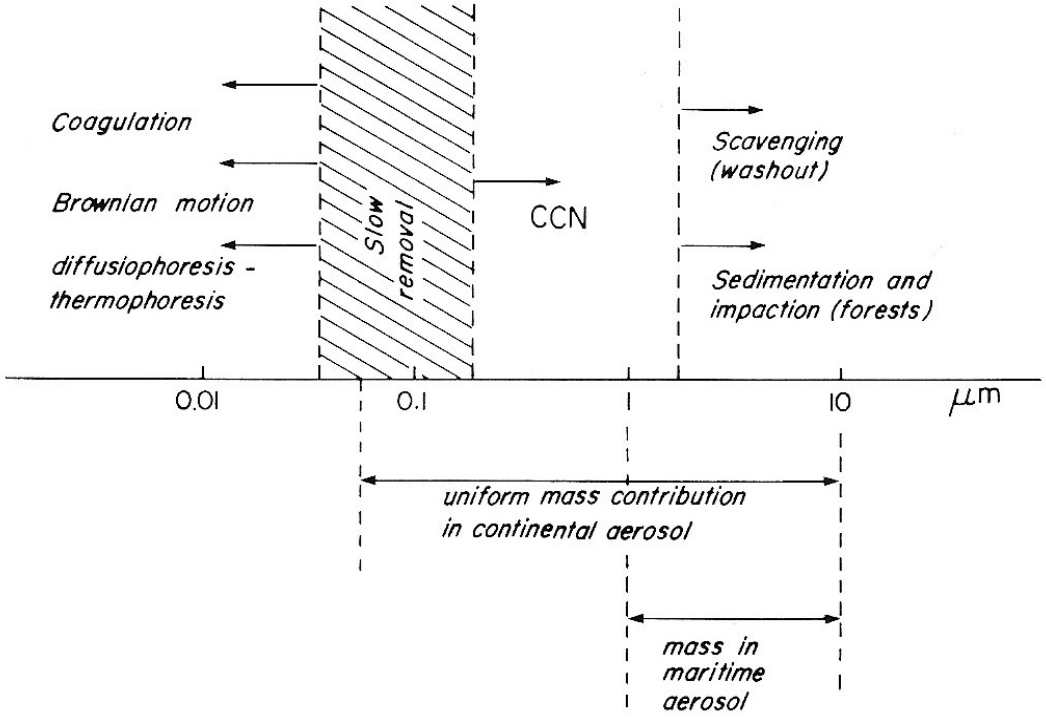

Figure 7.2: Aerosol elimination processes. The predominant processes of elimination according to the size range are indicated schematically. The horizontal logarithmic scale indicates the radius of the particles. CCN: activity as cloud condensation nuclei. The ranges of continental and maritime aerosol are also indicated.

7.2 Atmospheric extinction

Another important parameter strictly related to the aerosol presence and essential to define the sky quality above an observatory is the atmospheric extinction. Great part of our data research and analysis in this second part of the thesis will be based on it. Man's

subjective impression of the clear atmospheric surrounding is based almost entirely on visual estimates of the optical quality of the atmosphere. If the air seems transparent and distant horizon is seen with clarity the air is judged 'clean'. Most gaseous pollution is transparent at visible wavelengths, so this impression is based on the absence of particles and, as we will see later, one portion of the particulate size range dominates the optical behaviour of the aerosol. In the same way, in the next chapter we will see that astronomical extinction is a good indicator of clear and dusty night, as well as the aerosol optical thickness is an indication of the extinction determined by the aerosol content of the air when a solar beam traverses the atmosphere. In order to understand this variable, now we deal with the optics of individual aerosol particles.

Sky with lower dust content, limited cloudiness give better observational conditions. The different contributions to the total atmospheric extinction (see Figure 7.3), are summarized as:

$$A(\lambda) = A_{Ray}(\lambda, h) + A_{Oz}(\lambda) + A_{WV}(\lambda) + A_{Aer} \qquad (7.1).$$

For optical, NIR, and MIR, a dedicated telescope is required to determine the atmospheric extinction (e.g. Carlsberg Automatic Meridian Circle CAMC or Mercator at the ORM).

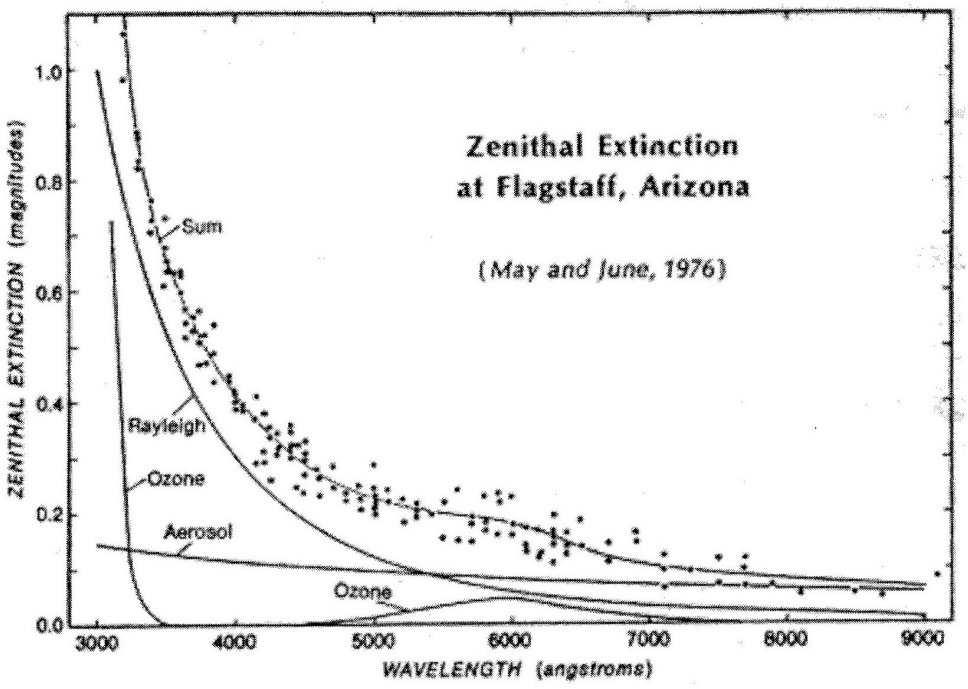

Figure 7.3: Different contribution to the total atmospheric extinction.

Low scattering is important to atmospheric visibility because as many photons as possible need to be detected. Aerosol content diminishes with elevation, improving visibility with higher elevation. A shorter path through the atmosphere will decrease scattering making it possible to receive weaker signals since the amount of atmospheric attenuation will be lower. Sites should therefore be located away from sources of aerosols and dust at high elevation.

To derive theoretically the atmospheric coefficient in the plane parallel atmosphere assumption, we use the Beer's law

$$\frac{I}{I_0} = \exp\left(-\tau\right) \tag{7.2}$$

Where I_0 is the light beam intensity at the 'top' of atmosphere, I the intensity for the observatory height reduced of scattering and absorbing changes underwent by radiation and τ is the optical depth observed at the zenith. When one observes at the zenith, he obtains the minimum extinction value through the atmosphere (1 airmass), at different observational angles the airmass value is

$$airmass = \sec\left(\theta_z\right) - \Delta airmass \tag{7.3}$$

Where Δairmass is a correction factor due to the real curve nature of atmosphere. The method to obtain the extinction coefficient is measuring the difference of extinction at different airmasses. Usually it is retrieved from the slope of the points in an instrumental magnitude versus airmass plot for a given star (equation 7.4).

$$K = 2.5\log\left(\frac{I_0}{I_{obs}\left(\theta = 0\right)}\right) = \frac{\Delta m_I}{AM_{t1} - AM_{t2}} \tag{7.4}.$$

K and τ are two ways slightly difference to quantify the atmospheric extinction. The relation between these two parameters is

$$K = 1.086\,\tau \tag{7.5}.$$

We know that the atmospheric extinction is linked to the dust presence. Our work develop a new remote sensing technique to deal with the study of aerosol extinction coefficients at different wavelengths under different atmospheric condition in a

comparison among top sites observatories around the world. In this analysis, K itself is used as mean to distinguish 'clear' days with low extinction from 'dusty' or absorbing days when dust is present, for sites most affected by this problem, e.g. Canary island observatories. Extinction values at Canary islands under different meteorological regimes versus the wavelength dependence are represented in Figure 7.4.

Moreover, the correlation between the extinction coefficients K_λ at different λ, one with each other, gives information on the wavelength extinction dependence. If we represent in a plot $K_{\lambda 1}$ versus $K_{\lambda 2}$, we observe grey behaviour with slope equals to one (Figure 7.5). The straight line slopes are near one with high extinction values, while points with lower extinction values show higher slopes that however becomes smaller with the wavelength increase (Table 7.1).

Table 7.1: straight line slope referred to wavelength change with two different meteorological conditions (clear and dusty days).

$\lambda(nm)$	Clear days	Dusty days
450	2,132 (+/-) 0,105	1,028 (+/-) 0,042
500	1,333 (+/-) 0,025	1,011 (+/-) 0,015
770	1,159 (+/-) 0,033	0,999 (+/-) 0,009
870	1,026 (+/-) 0,029	1,009 (+/-) 0,012

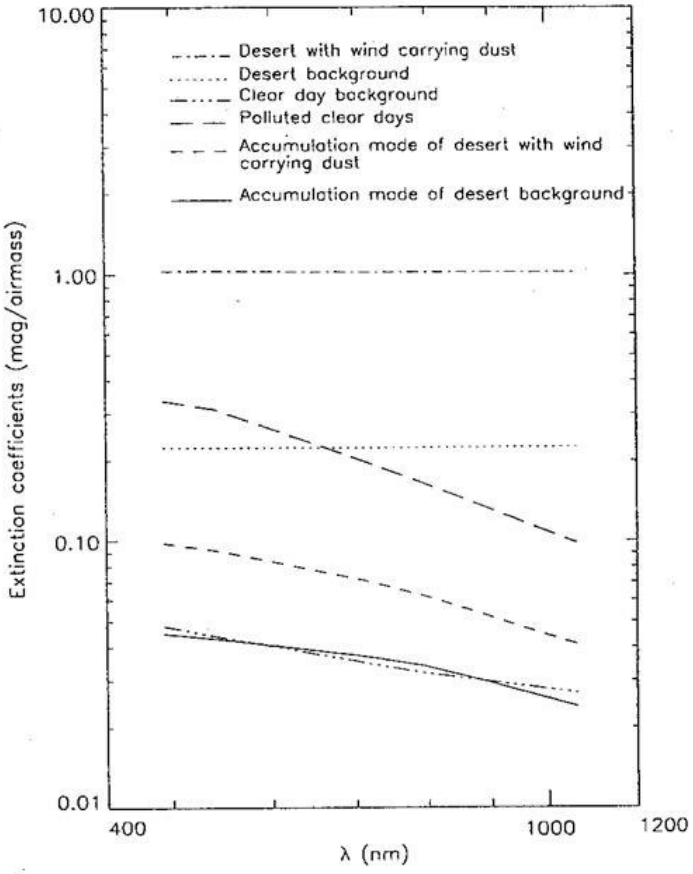

Figure 7.4: Extinction coefficients depending with wavelength, calculated with Mie's theory for different meteorological conditions as reported in figure itself.

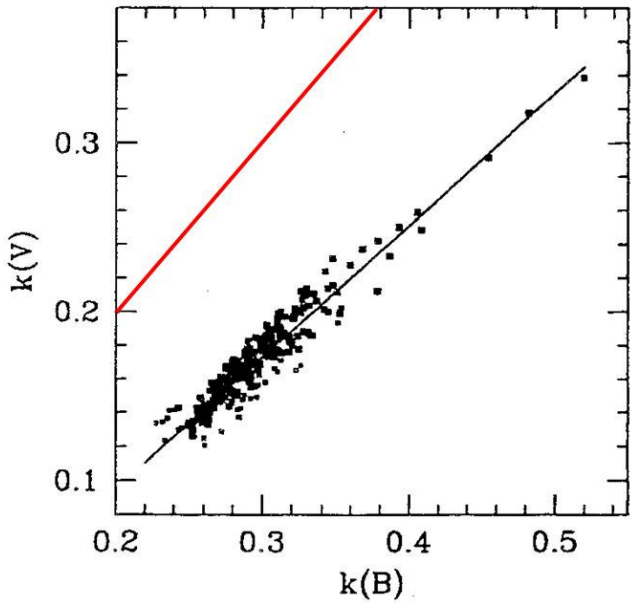

Figure 7.5: K(V) versus K(B) correlation coefficient (black). Grey behaviour of points with slope equal to one (red).

The λ dependence with the aerosol atmospheric extinction coefficient for the optical range is in good agreement with the Ångstrom formula

$$K_\lambda = \beta\, \lambda^{-\alpha} \qquad (7.6)$$

Where β represents the turbidity coefficient and α the Ångstrom coefficient.

The main causes to the extinction changes are:

a) Volcanic aerosol effects (e.g. the Pinatubo eruptions gave a maximum peak in extinction that was about 1000 days long before to vanish as visible in Figure 7.6) and episodes of atmospheric pollution due to big fires that have global scale influence.

b) Yearly variations due to local dust or transport of dust coming from deserts, as well as changes in humidity values and wind patterns.

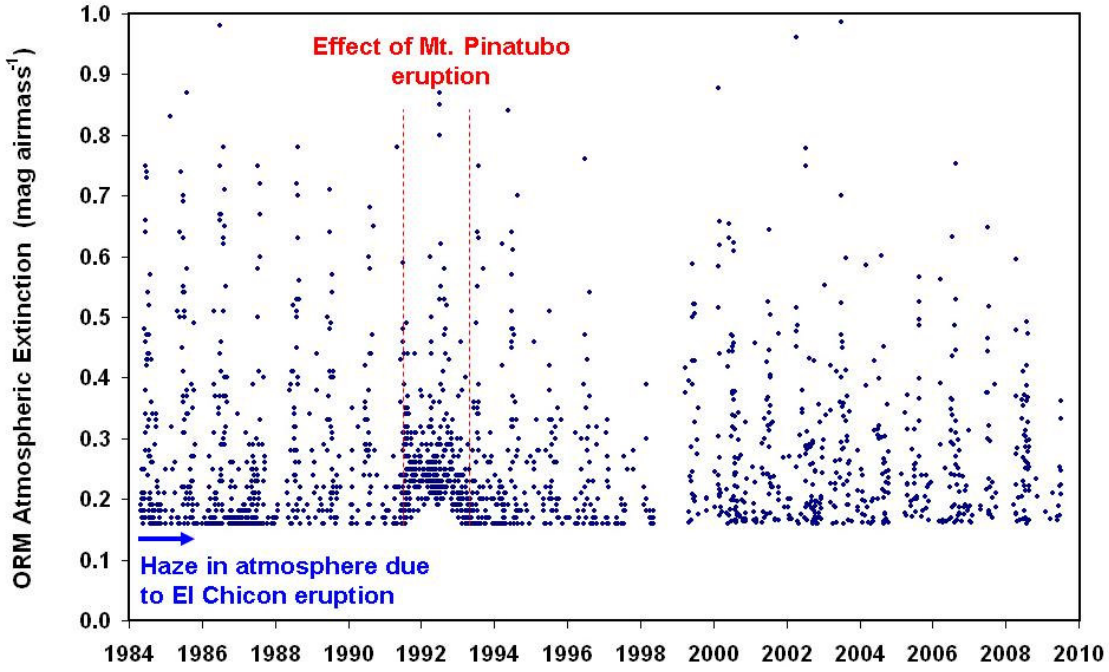

Figure 7.6 Atmospheric extinction measured at the Carlsberg Automatic Meridian telescope CAMC at Roque de Los Muchachos ORM, La Palma, Canary Islands. The original data have been homogenized at V band. In the plot the increase of Extinction in V band due to the Pinatubo eruption occurred in 1991 is cleraly visible.

Figure 7.6 has been derived from the Carlsberg Meridian Telescope CAMC nightly values of atmospheric extinction in V (λ=551 nm) (r' = 625 nm from April 1999) for La Palma. The original data for 1999 and after differ from those taken between 1984 and

1998 because for the first time a CCD camera has been used and a restricted range of zenith distances were observed each night. The extinction value is generated for each frame by using an instrumental zero-point derived from the long-term performance of the CCD i.e. an assumption is made that the dust-free extinction value is constant over the long term. Only those CCD frames considered photometric in quality have been used. Each frame has an average of 30 - 40 calibrating stars on it, that were about 50 photometric standards per night pre-1999. The effect of the eruption of Mount Pinatubo in June 1991 on the extinction is clearly visible. The number of high extinction values that occur every summer is normally caused by Saharan dust. Our work on data calibration is started with the research of these atmospheric extinction AE values from CAMC at Roque de Los Muchachos ORM at 2325 masl. This data bank is composed of yearly files where the explanation of data columns is as follows:

(1) Evening date ie. date before midnight.

(2) Version number of data. If 0 then unchecked.

(3) Extinction in r'. This is the median value of the extinction from all photometric frames. : indicates an uncertain value due to the night probably not being photometric.

(4) Standard error on (3) = Scatter/sqrt(N_frames)

(5) Scatter (robust estimate of the Gaussian sigma based on percentiles of the distribution). If this value is high (0.060), then the night was probably not photometric.

(6) Number of photometric frames

(7) Number of hours of photometric data taken.

(8) Number of hours of non-photometric data taken.

(9) Comment

In the next chapter we will present the correlation between these extinction values and the aerosol optical depth data retrieved by remote sensing satellites over the ORM astronomical site.

However to perform these comparison it was necessary to homogenize the extinction values in r' band with the original values taken in V band. This operation was possible thanks La Palma Technical Note No 31 (King, 1985) that could be used to convert

values of extinction at r' to other wavelengths, simply using the values in Table 1 to determine a differential extinction between r' (or V for the old data) and the passband of interest and applying this to the extinction data.

From the mathematical point of view, the conversion of extinction values from r' to V band is

$$K_{ext}(V) - K_{ext}(r') = \Delta K_{ext} \tag{7.7}$$

Substituting the values reported into the Technical note table we obtain ΔK_{ext}=0.0282, value that must be added to K_{ext}(r') in order to obtain a series of value homogeneous in time referred to K_{ext}(V) values (Figure 7.6).

7.3 Optics of individual aerosol particles

7.3.1 Rayleigh scattering

Particles in the atmosphere can scatter and absorb electromagnetic radiation. Molecules also scatter and absorb radiation and a particle which is small compared to the wavelength of the radiation scatters radiation very much; this type of scattering is known as 'Rayleigh scattering'. When the particle dimensions are not negligible compared to the wavelength, a more complicated scattering pattern is found and this type of scattering is known as 'Mie scattering'.

Electromagnetic theory shows that a single dipole radiates a polarized wave which contains one component the amplitude of which falls off as r^{-2} (r being distance from the dipole) and another which falls off more slowly, as r^{-1}. The latter dominates the situation everywhere except in the immediate vicinity of the dipole and is known as the 'far-field solution'. If we consider a small spherical particle in an electric field, the induced moment of dipole $\vec{p}_0$ of a polarizable molecule is proportional to the surrounding electric field,

$$\vec{p}_0 = \alpha \vec{E}_0 \tag{7.8}$$

α being the polarizability. The diffuse electric field at far distance r from the dipole is

$$\vec{E} = \frac{1}{c^2}\frac{1}{r}\frac{\partial \vec{p}}{\partial t}\sin(\gamma) \tag{7.9}$$

Where γ is the angle between the moment of diffuse dipole $\vec{p}$ and the direction of observation. The moment of dipole, in terms of induced dipole and the electric field are given by

$$\vec{p} = \vec{p}_0 \exp(-ik(r-ct)) \tag{7.10}$$

$$\vec{E} = -\vec{E}_0 \frac{\exp(-ik(r-ct))}{r} k^2 \alpha \sin(\gamma) \tag{7.11}$$

Resolving the electric vector into two perpendicular components, one lying in the 'scattering plane' (a plane containing the incident and diffuse radiation), we have:

$$\vec{E}_\perp = -\vec{E}_{0\perp} \frac{\exp(-ik(r-ct))}{r} k^2 \alpha \sin(\gamma_1) \tag{7.12 and 7.13}$$

$$\vec{E}_| = -\vec{E}_{0|} \frac{\exp(-ik(r-ct))}{r} k^2 \alpha \sin(\gamma_2)$$

Knowing that

$$I = \frac{1}{\Delta\Omega} \frac{c}{4\pi} |E|^2 \tag{7.14}$$

The perpendicular and parallel component of the intensity are respectively:

$$I_\perp = I_{0\perp} k^4 \frac{\alpha^2}{r^2} \tag{7.15 and 7.16}$$

$$I_| = I_{0|} k^4 \frac{\alpha^2 \cos^2(\theta)}{r^2}$$

In the assumption where the incident beam is composed by not polarized light, the two above components are the same and we obtain

$$I = I_\perp + I_| = \frac{I_0}{r^2} \alpha^2 \left(\frac{2\pi}{\lambda}\right)^4 \frac{1+\cos^2(\theta)}{2} \tag{7.17}$$

The equation (7.17) gives the intensity diffuse by molecules for an incident no polarized light-beam, being θ the scattering angle. In radiative transfer work it is often advisable to employ the 'normalized phase function' P(θ) which describes what fraction of the scattered radiation appears per unit solid angle in the direction θ. For Rayleigh

scattering this is evidently given by multiplying $(1+\cos^2\theta)$ by a normalizing factor which is obtained by integration over all solid angles.

$$P(\theta) = \frac{3}{4}(1+\cos^2(\theta)) \tag{7.18}$$

So, the equation (7.17) now becomes

$$I(\cos(\theta)) = \frac{I_0}{r^2}\sigma_{Rayleigh}\frac{P(\theta)}{4\pi} \tag{7.19}$$

The single molecule section (in area unit) is

$$\sigma_{Rayleigh} = \alpha^2\frac{128\pi^5}{3\lambda^4} \tag{7.20}$$

This cross section permits to calculate the optical depth of the whole atmosphere due to molecular scattering as

$$\tau_{Rayleigh}(\lambda) = \sigma_{Rayleigh}(\lambda)\int_0^{z_{top}} n_{Air}(z)dz \tag{7.21}$$

Where n_{air} is the air molecular density.

The main relevant things for a Rayleigh scattering by particles to highlight are the following:

- The angular distribution of the scattered intensity is given by $(1+\cos^2\theta)$; it is symmetric in the forward and backward directions.
- The scattered intensity and the energy removed from the incident beam by scattering are proportional to the square of the polarizability and hence for a spherical particle the sixth power of the radius.
- The scattered intensity and the energy removed by scattering is proportional to the -4th power of wavelength (see table 7.2)
- For a particle to be legitimately considered as a Ryleigh scatterer, means to have a small size parameter, i.e. $r<<\lambda$
- The phase function $P(\theta)$, which is proportional to $(1+\cos^2\theta)$, applies only to isotropic particles

- The intensity of the rayleigh scattering is proportional to the sixth power of the radius. The absorption on the other hand is proportional only to the cube of the radius (i.e. the volume). The consequence is that, with decreasing size, scattering falls off more rapidly and the absorption although decreasing tends to become dominant compared to the scattering (i.e. the single scattering albedo decreases with decreasing size).

Table 7.2 Optical depth values due to Rayleigh scattering at different wavelengths

$\lambda\,[nm]$	τ_{Ray}
250	2,74
300	1,25
350	0,650
400	0,373
450("blue")	0,229
500	0,149
550	0,101
600	0,0708
650	0,0512
700("red")	0,0379
750	0,0287
800	0,0221
850	0,0173

In the table is possible to see as the optical depth for blue wavelength is greater that red. An example of this evidence is the scattered light that constitutes the diffuse luminosity of the clear sky during the day. It is predominantly a blue color because the shorter wavelengths are scattered more than the longer ones being the Rayleigh optical depth inversely proportional to 4th power of λ.

7.3.2 Mie scattering

When the particle dimensions are appreciable compared to the wavelength λ, it is no longer sufficient to consider merely an induced dipole. The Mie's theory uses the Maxwell's equations for the electric field around a dielectric sphere, and it becomes necessary if the particle size parameter (i.e. $x=2\pi r/\lambda$) is equal or greater than 1. For the atmosphere applications, the observations of Mie scattering are calculated in the far-

field zone from the particles. The assumptions are that the incident light is linearly polarized and that out of the dielectric sphere the refractive index is equal to 1. At far distance from the sphere, the solution of the wave equation for the electric field is given by

$$\begin{bmatrix} E_{\parallel}^{k} \\ E_{\perp}^{k} \end{bmatrix} = \frac{\exp(-ikr + ikz)}{ikr} \begin{bmatrix} S_2 & 0 \\ 0 & S_1 \end{bmatrix} \begin{bmatrix} E_{\parallel}^{k} \\ E_{\perp}^{k} \end{bmatrix} \tag{7.22}$$

where parallel and perpendicular component of the incident and diffuse electric field are indicated together with the matrix of the scattering amplitudes. In the assumption of spherical particles the matrix elements $S_3(\theta) = S_4(\theta) = 0$. The equation 7.22 gives the radiation diffused by a sphere. For unpolarized incident radiation I_0, the intensity of diffuse light, depending from the scattering angle θ, is

$$I(\theta) = \frac{I_0(i_1(\theta) + i_2(\theta))}{2k^2d^2} \tag{7.23}$$

Where $k=2\pi/\lambda$ is the wave number, d is the distance from the particle center and i_1 and i_2 are the squared absolute values of the scattering amplitudes S_1 and S_2. Where S_1 is concerning the light with plane parallel polarization and S_2 the light perpendicular to the plane. From the Mie's theory follows that the cross-section for the particle extinction is

$$\sigma_0 = \frac{4\pi}{k^2}\mathrm{Re}[S(0^0)] \tag{7.24}$$

Where for a forward direction (i.e. $\theta=0°$), we have

$$S_1(0^0) = S_2(0^0) = \frac{1}{2}\sum_{n=1}^{\infty}(2n+1)(a_n + b_n) \tag{7.25}$$

Where a_n and b_n are the Mie's coefficients that characterized the diffuse wave. These complex-valued coefficients, are function of the complex refractive index m, of the size parameter x and of y=mx, and provide the full solution of the scattering Mie problem. The Mie coefficients themselves give directly some important integrated quantities: the extinction, scattering and absorption efficiencies and the single scattering albedo.

$$Q_e = \frac{\sigma_e}{\pi r^2} \qquad Q_s = \frac{\sigma_s}{\pi r^2} \qquad Q_a = \frac{\sigma_a}{\pi r^2} \tag{7.26}$$

The efficiency factors (eq. 7.26) are defined as follows: the energy removed from an incident wave with energy flux density I_0 is $\pi r^2 Q_e I_0$, Q_e being the extinction efficiency; the energy which reappears as scattered energy is $\pi r^2 Q_s I_0$, Q_s being the scattering efficiency; the energy absorbed is $\pi r^2 Q_a I_0$, Q_a being the absorption efficiency and the single scattered albedo w_0 is the fraction of the energy removed from the incident wave which reappears as scattered radiation. These all can be written in terms of the Mie coefficients:

$$Q_s = \frac{\sigma_s}{\pi r^2} = \frac{2}{x^2}\sum_{n=1}^{\infty}(2n+1)[|a_n|^2 + |b_n|^2] \qquad \text{(7.27) and (7.28)}$$

$$Q_e = \frac{\sigma_e}{\pi r^2} = \frac{2}{x^2}\sum_{n=1}^{\infty}(2n+1)\,\mathrm{Re}[a_n + b_n]$$

$$Q_a = Q_e - Q_s \qquad (7.29)$$

In Figure 7.7 the extinction efficiency is plotted against size for several values of refractive index m. It will be noted that as absorption (imaginary part of m) is increased the oscillations in Qe are damped out. In fact the imaginary part (i.e. k) of the refractive index (m=n-ik), gives the wave absorption, while the real part (i.e. n) gives the phase velocity of the wave propagation. An interesting aspect of the Mie scattering is that, as the particle size increases, the extinction efficiency Q_e for a conservative scatter, tends to two, so that very large particles remove from direct beam twice the energy that falls on their cross-sectional area (Figure 7.7).

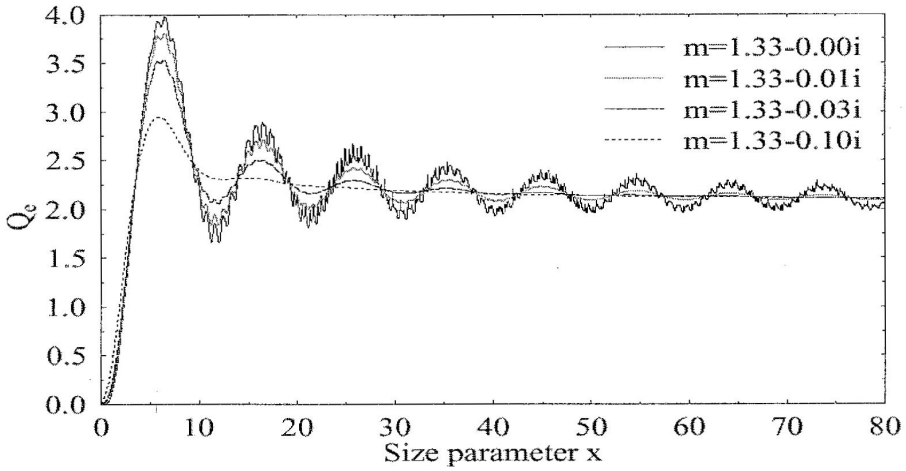

Figure 7.7: Values of extinction efficiency calculated with Mie's theory for different imaginary refractive index.

However, in reality, it is concerned not with the properties of single particles but with integrated properties relating to a volume element of the atmosphere, which contains many particles of varying size, shape and composition in addition to the molecules of air and trace gases contained therein. Therefore the macroscopic scattering and extinction coefficients are given by the integration on the size distribution N(r) for a given particles mode, as follows

$$K_s = \int_{r_1}^{r_2} \sigma_s(r) N(r) dr \qquad K_e = \int_{r_1}^{r_2} \sigma_e(r) N(r) dr \qquad \text{(7.30) and (7.31)}$$

The ratio of the scattering and extinction coefficients for an aerosol population, is its single scattering albedo

$$\omega_0 = \frac{K_s}{K_e} \qquad (7.32)$$

w_0 describe the percentage of light that is diffuse in each single scattering event, (for example, if $w_0 = 0.95$, we have 95% of solar light diffuse and only the 5% absorbed). Generally w_0 changes with the particle dimension and the wavelength and it is equal to 1 if there is no absorption; in this case the scatter is conservative and the refractive index is real as well as the Mie coefficients, this is the case of sulphate and marine aerosol in the visible range.

The last important parameter to define is the optical depth (i.e. τ) of an aerosol population with homogeneous density and vertical thickness Δz.

$$\tau_\lambda = \int_{r_1}^{r_2} \pi r^2 Q_e(m, x) N_e(r) dr \qquad (7.33)$$

The most notable feature of Mie scattering is the 'forward peak'. This is partly due to diffraction of photons that have not actually passed through any part of the sphere. If we start with a very small Rayleigh scatterer, the scattering diagram (i.e. the visual representation of the phase function $P(\theta)$) would be found to be symmetric, equal amounts of energy being scattered in backward and forward directions. If the particle size increased, the smooth $(1+\cos^2\theta)$ shape of the Rayleigh scattering diagram would first remain, but an asymmetry would begin to develop, the particle no longer being in the centre of the oval diagram, but rather moving to one side, implying more forward

directed than backward directed scattering. When the particle size parameter (i.e. x) exceeds units the scattering diagram begins to develop peaks and troughs, there being always a strongly peaked maximum in the forward direction $\theta = 0$. As the size parameter approaches 10, a finer structure develops in the scattering diagram. The forward peak is primarily made up of diffracted light which has not actually passed through the particle, instead it is the radiation in the 'backward' hemisphere that is most affected by absorption.

7.4 Optics of the atmospheric aerosol

There is a particular problem which emerges when optical parameters are involved, because these can vary greatly with particle size and most optical measurements tend to be weighted heavily in favour of a rather restricted size range within the much wider interval spanned by the natural atmospheric aerosol. Expressions such as those just given in equations for the single scattering albedo represent the ratio of the moments of the particle distribution function n(r) (i.e. the size distribution). In fact in atmosphere, most commonly measured optical quantities are heavily dominated by portion of the size range, smaller particles being without much influence because of their diminished efficiency and larger particles being without much influence because of their numbers fall off more rapidly than their cross-section increases. Unfortunately the 'optically dominant' region tends to coincide with a 'grey zone' being close to the probable lower limits of size for particles produced from the bulk, and the probable upper limit for particles produced directly from gas phase. The size spectrum of atmospheric aerosol being so wide and heterogeneous for formation, dispersion, conversion and decay mechanisms, in order to compare experimental results to the theoretical one usually a size distribution model in aerosol is assumed. In this way, with some assumption concerning the curve n(r) for aerosol, scattering and extinction properties can be evaluated with the Mie theory. The size distribution more widely used in literature are the following:

Power Law or Junge size distribution. Experimental observations suggest that at least over portion of the atmospheric particle size range power law tend to be found, especially when distributions are averaged (see figure 7.8). This tendency can be expressed mathematically as:

$$n(r) = A\left(\frac{r}{r_0}\right)^{-\nu} \tag{7.34}$$

Where r_0 is the unitary radius and the exponent ν was obtained by Junge and it is 3.5 ± 1. In Figure 7.8, it is possible to see, mostly in the range from 0.1 μm to 10 μm, a continuous decrease in concentration that obeys the Junge's law.

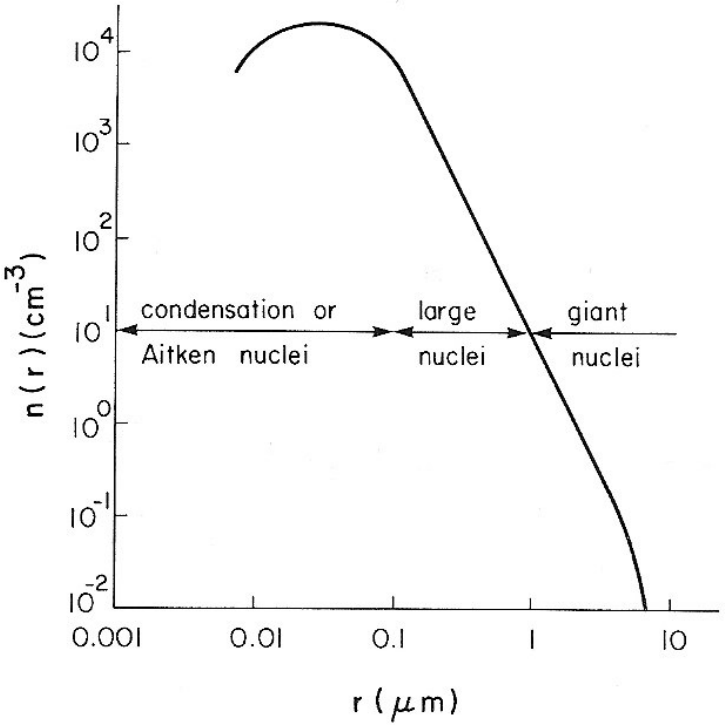

Figure 7.8: Size distribution in continental aerosol. The figure gives a typical plot of the distribution function over log r: n(r) =-dN/dlog r, where r is the spherically equivalent radius and N is the number concentration of particles with radius >r.

Exponential size distribution. in order to avoid the drawback of the Junge's distribution given by a cut-off at a certain minimum radius, sometimes an exponential size distribution is used

$$n(r) = A\exp\left(-\frac{r}{r_0}\right) \tag{7.35}$$

where A is an aerosol concentration value and r_0 is a changing parameter with the effective radius of the whole aerosol size distribution.

Modified Gamma size distribution. Both the previous size distributions are not at all characteristic of what is known concerning the dry aerosol or of what theoretical calculations of aerosol coagulation indicate for dry aerosol because both suggest a rapid

falling off of concentration at the low-size end. More realistic distribution is the modified Gamma distribution as follows

$$n(r) = \frac{A}{\Gamma(\alpha) r_n} \left(\frac{r}{r_n} \right)^{a-1} \exp\left(-\frac{r}{r_n} \right) \tag{7.36}$$

The distribution mode is given by r_n that is the radius characterizing distribution, α being the variance of distribution and Γ the gamma function.

Log-normal size distribution. A Gaussian (normal) distribution is symmetric about its mean (which is also therefore the mode and median) and takes non-zero values as its argument goes from - ∞ to + ∞. A normal curve in which radius is the argument is a poor approximation to the size distributions found in natural aerosol. There are instead logical grounds for using log-radius as a measure of size; furthermore if we are concerned with the production of particles about a mean it is quite unrealistic to presume that a particle of radius (r-a) is as likely to be produced as one of radius (r+a); with a mean of 1 μm this would equate a 0.1 and 1.9 μm particle, for example. It is more plausible to equate the probability of finding a radius of (a·r) and a radius of (a^{-1}·r), saying that a particle of twice the mean radius is as likely to be found as one of one-half the mean. This amounts of using log r as the measure of size and a log-normal distribution is simply a normal curve in which the argument is log r.

$$n(r) = \frac{A}{r \ln \sigma} \exp\left(-\frac{\ln^2(\frac{r}{r_m})}{2 \ln^2 \sigma} \right) \tag{7.37}$$

Where A is the aerosol concentration value for a precise size-mode with precise values of r_m (i.e. the mode radius) and σ (i.e. the standard deviation) that change with the size mode.

7.4.1 Reflection, transmission and absorption radiation change

Solar radiation is composed by two distinct components: the direct part and the diffuse one as $I = I_{dir} + I_{diff}$ as in Figure 7.9.

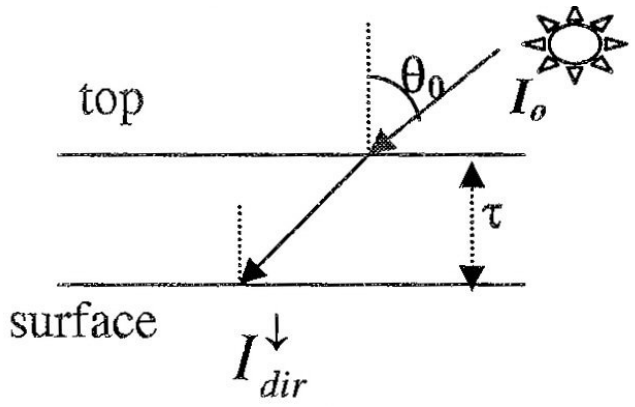

Figure 7.9: Solar radiation change after it passes through an atmospheric layer.

The direct radiation is the remaining intensity of the radiation stream after it is passed through a layer with τ as optical depth; it is expressed with the Beer-Bouguer-Lambert law

$$I_{dir}^{\downarrow} = I_0 \exp(-\frac{\tau}{\mu_0}) \tag{7.38}$$

where I_0 is the incident radiation on the layer and μ_0 is the cosine of the zenith angle measured from the vertical (i.e. θ_0). Diffuse radiation is when the solar beam has single or multiple scattering. In the last case the equation is

$$dI_\lambda(\vec{\Omega}) = k_{s,\lambda} ds \int_{4\pi} \frac{P_\lambda(\vec{\Omega},\vec{\Omega}')}{4\pi} I_\lambda(\vec{\Omega}') d\Omega' \tag{7.39}$$

Where the phase function changes the direction of the incident intensity from Ω' to Ω and the integral consider all the scattering events into the solid angle 4 π. According with the emission Beer-Bouguer-Lambert law, we have

$$dI(\lambda) = K_{ext}(\lambda) J(\lambda) ds \tag{7.40}$$

So we can define the source function for the scattering as follows

$$J_\lambda(\vec{\Omega}) = \frac{\omega_{0,\lambda}}{4\pi} \int_{\vec{\Omega}'} I_\lambda(\vec{\Omega}') P_\lambda(\vec{\Omega},\vec{\Omega}') d\vec{\Omega}' \tag{7.41}$$

This equation depends first on the intensity along the incident direction, second on the fraction of diffuse radiation and third on the fraction diffuse in the new direction.

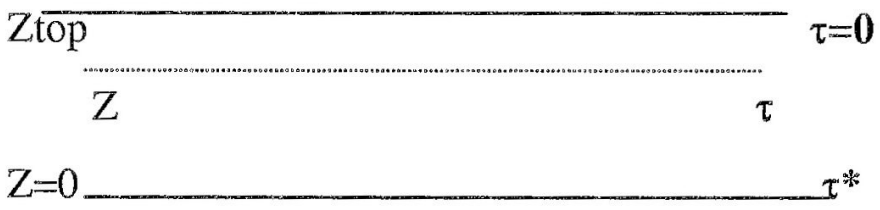

Figure 7.10: plane parallel atmosphere assumption

The transfer of radiation in the assumption of a plane parallel atmosphere (see Figure 7.10) is described by the equation of transfer:

$$\mu \frac{dI_\lambda(\tau,\mu,\varphi)}{d\tau} = I_\lambda(\tau,\mu,\varphi) - J_\lambda(\tau,\mu,\varphi) \tag{7.42}$$

which describes the balance between removal by extinction (scattering + absorption) and gain of energy in the direction (μ,φ) by scattering from other directions, τ being the optical depth from the atmosphere upper limit to the lower one, as

$$\tau_\lambda(z,0) = \int_0^z k_{e,\lambda}(z)dz \tag{7.43}.$$

The aerosol mean effects can be estimated using the two streams approximation for the radiative transfer. In this assumption, the downward stream includes direct beam and downward diffuse radiation while the upwelling stream combines all upward diffuse radiation. The solutions of the transfer equation (7.42) written both for the downward and the upward streams in the single scattering approximation give

$$F^{\downarrow}(z) = F_0^{\downarrow} \exp(\frac{-\tau}{\mu_0}) \tag{7.44}$$

this represents the solar radiation at altitude z being F_0 the annual solar constant in the upper limit of the atmosphere (F_0=1367.5 Wm^{-2}) and the source of diffuse radiation is the scattering of the direct beam as follows

$$J(\tau,\mu,\varphi) = \frac{\omega_0}{4\pi} F_0^{\downarrow} \exp(\frac{-\tau}{\mu_0}) P(\mu,\varphi,\mu_0,\varphi_0) \tag{7.45}.$$

For the upstream flux we have instead

$$F^{\uparrow} = \omega_0 b \tau F_0^{\downarrow} \tag{7.46}.$$

In two-stream approximation, b is the backscattering ratio and it is the fraction of upward scattered energy. In each interaction between solar beam and aerosol, the fraction of absorption is given by ($1-w_0$), best known as coalbedo.

The change in the planetary albedo ΔR is the ratio of the radiation reflected upward by the aerosol layer in the atmosphere and the incident radiation on the upper limit

$$\Delta R = \frac{F^{\uparrow}}{F_0^{\downarrow}} = \omega_0 b \tau \tag{7.47}$$

The change in albedo due to the aerosol is given by $\Delta R_a = f_a \Delta R$ where the empirical value f_a is equal to 0.2 and includes the effects of atmospheric gases, water vapour and clouds. If we make an example using equation 7.47 for no-absorbing aerosol with $w_0 = 1$, b= 0.3 and $\tau = 0.1$, we obtain that $\Delta R_a = 0.006$. Planetary albedo being about 0.3, this value (ΔR_a) means that aerosol increases the albedo of about 2%.

The aerosol have roughly two effects on the downward solar radiation that can be expressed in the equation

$$F^{\downarrow} = (1-\tau)F_0^{\downarrow} + (1-b)\omega_0 \tau F_0^{\downarrow} \tag{7.48}$$

Where, on the right side, the first effect, given by the equation (7.44), is the direct beam attenuation due to scattering and absorption, and the second effect is the sum of diffuse radiation (i.e. the solar light scattered toward the surface by the direct beam). These two addends have opposite signs. Moreover, being

$$0 \le (1-b)\omega_0 \le 1 \tag{7.49}$$

the increasing of diffuse flux will be always lower than the reduction of direct flux, so the aerosol net effect is to reduce the solar light total amount reaching the earth surface.

The change in transmission is given by the ratio of the downward flux variation and the incident solar flux at the top of the atmosphere as in

$$\Delta T = \frac{F^{\downarrow} - F_0^{\downarrow}}{F_0^{\downarrow}} = (1-b)\omega_0 \tau - \tau \tag{7.50}$$

Finally, the energy conservation principle gives the solar light amount absorbed by aerosol. In the assumption of the atmosphere as a closed system, the albedo represents

the upward radiation, the transmission is the flux toward the surface and the absorption represent the light conversion in atmosphere internal energy. Also if aerosol are present in atmosphere, the incident solar energy does not change, so the sum of the albedo (reflection), transmission and absorption is equal to zero and therefore it is possible to solve this equation for the absorption term as follows

$$\Delta A = -(\Delta R + \Delta T) = (1 - \omega_0)\tau \qquad (7.51).$$

Chapter 8:

OMI aerosol remote sensing and in-situ atmospheric extinction retrieval: the Roque de Los Muchachos astronomical site case study

Contents

8.1 The Ozone Monitoring Instrument
8.1.1 OMI measuring principles
8.1.2 OMI aerosol algorithm
8.2 High spatial resolution OMI aerosol data: comparison with in situ atmospheric extinction records over the ORM site
8.3 Lower spatial resolution OMI aerosol data: height of aerosol layer comparison in world's top astronomical sites
8.4 Evidences and conclusions

The use of satellite platforms, at present is the more effective mean to perform a worldwide survey of different climate parameters related to astronomy site testing for three main reasons:

a) using sun-syncronous satellite it is possible remote sensing monitoring climate parameters adopting the same method, algorithm, spatial and vertical resolution. These data give an homogeneous worldwide coverage that make us able to daily compare ground sites with different climatic and orographic characteristics. This task would be hard to reach and time-consuming if instead of satellite data we would use ground-based stations measurements.

b) At present time satellite data bank extends back to more than thirty years. A climate analysis over this whole temporal range is possible thanks a chain of platforms that partly have maintained, in recent time, an heritage with similar

algorithm used for the pioneer instruments This is the case for example of the Aerosol Index or of the cloud cover percentage measured since the 1978 by different satellites disused with the end of the scheduled missions.

c) Today, from satellite data we can obtain a wide spectrum of climatic values over both oceans and lands. In the case of the Ozone Monitoring Instrument for example, the products make available are the ozone layer monitoring, air quality monitoring, monitoring of constituents that affect Earth's climate as the percentage of cloud coverage and the aerosol content.

The main problems, in handling all these data, are their interpretation, their quantitative calibration to pass from one probe to another and the search for satellites with best possible vertical and spatial resolution. This last point become of great importance when we compare satellite data with a large 2-D field of view to in-situ measurements with a dot-shaped resolution. In order to make reliable, such kind of analysis, in principle, it is necessary to work with satellite data of spatial resolution as high as possible, however, in this chapter, we will prove that this is not the main condition to assure good results. In this thesis, in order to test and quantitatively evaluate the weight that the spatial resolution hold in site testing analysis, we handle two different levels of data. Taking into account the Roque de Los Muchachos Observatory case study we deal both with satellite high spatial resolution level 2 data and with lower resolution level 3 data. This is a good test to show that the correlation between aerosol content and atmospheric extinction is led rather than the satellite field of view by other spurious effects that enter in the algorithm theoretical basis of the satellite.

Finally, using the level 3 data sets of the Ozone Monitoring Instrument on board the NASA Aura satellite, we perform a comparison among selected world's top astronomical observatories. This comparison is performed to search for appropriate techniques able to reveal astronomical sites climatic properties exploitable to look at new sites hosting future extremely large telescopes. Several interesting results are obtained already with low resolution satellite data.

8.1 The Ozone Monitoring Instrument

In this work, the selected data set, is the nadir-viewing near-UV/Visible spectrometer Ozone Monitoring Instrument aboard NASA's Earth Observing System's (EOS) Aura satellite. This satellite is one of the three platforms in the NASA's atmospheric chemistry mission Earth Observing System (EOS) with the objective of studying the chemistry and dynamics of Earth's atmosphere from the ground through the mesosphere. The goal of the mission is to monitor the complex interactions of atmospheric constituents (e.g. natural sources as biological activity and volcanoes or biomass burning from man-made sources) that are contributing to global change and to the creation and depletion of ozone. In the same way, OMI's scientific mission objectives seek answers on the recovery of the ozone layer, on the understand of sources and transportation of aerosols and trace gases.

The Aura satellite, launched on 15th July 2004, orbits at an altitude of 705 km in a sun-synchronous polar orbit with an almost complete daily global coverage. The orbital inclination is 98.1 degrees, providing a latitudinal coverage from 82° N to 82° S. Apart from OMI, the Aura satellite also carries onboard three other instruments: the High Resolution Dynamics Limb Sounder (HIRDLS), the Microwave Limb Sounder (MLS) and the Tropospheric Emission Spectrometer (TES). OMI has collected data since 9th August 2004.

OMI measurements cover a spectral region of 264–504 nm (nanometers) with a ground footprint of 13 km x 24 km at nadir. The significantly improved spatial resolution of OMI measurements as well as the vastly increased number of wavelengths observed, as compared to TOMS, GOME and SCIAMACHY, sets a new standard for trace gas and air quality monitoring from space. The OMI observations provide the following capabilities :

- A mapping of ozone columns at 13 km × 24 km and profiles at 13 km × 48 km (a continuation of TOMS and GOME ozone column data)
- A measurement of key air quality components: NO_2, SO_2, BrO, HCHO, and aerosol

- The possibility to distinguish between aerosol types, such as smoke, dust and sulfates
- The possibility to measure aerosol absorption capacity in terms of aerosol absorption optical depth or single scattering albedo
- A measurement of cloud coverage
- A combination of processing algorithms including TOMS Version 8, BUV retrievals and forward modeling to extract the various OMI data products

8.1.1 OMI measuring principles

OMI is a wide-angle, non-scanning and nadir-viewing instrument measuring the solar backscattered irradiance in a swath of 2600 km. The telescope Field of View (FOV) is 115º wide in across-track dimension. The instrument is designed as a compact UV/VIS imaging spectrograph, using a two-dimensional CCD array for simultaneous spatial and spectral registration.

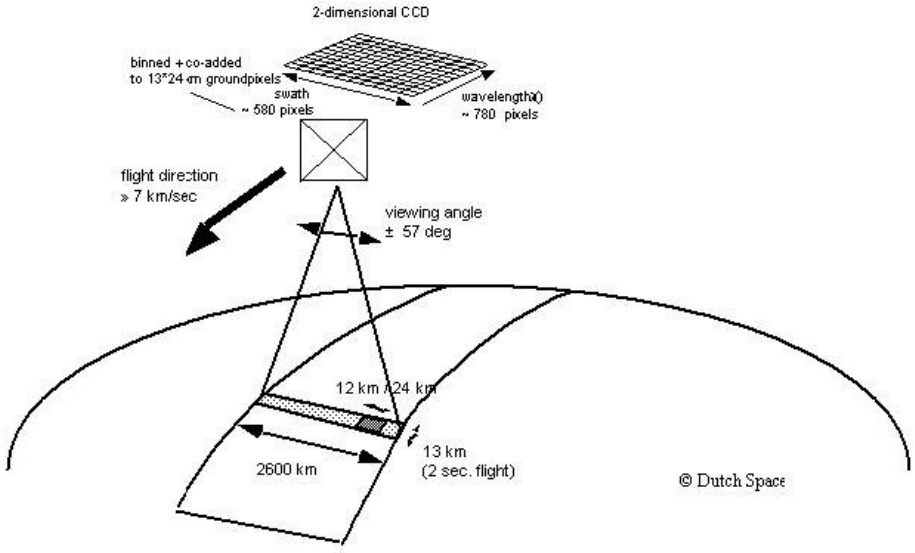

Figure 8.1 OMI measurement scheme

The high resolution OMI Level 2 products contain the geophysical parameters at ground-pixel resolution as shown in Figure 8.1. Each Level 2 file contains data from a single orbit i.e. observations made only in the daytime portion of an orbit (~ 53-minute duration). In addition to standard derived parameters, these files also contain some auxiliary derived parameters, temporal, spatial, solar and viewing geometry and ground-

pixel quality flags. Level 2 products contain data at 13 km × 24 km (nadir pixel size) resolution. OMI Level 3 daily global products are produced by using best pixel data over 1 degree × 1 degree covering the whole globe. They have a minor spatial resolution and are available only for certain OMI standard products as the case of clouds and aerosol products that we will use in this data elaboration.

Because of the relatively large footprint of the OMI observations (13 km x 24 km at nadir) with respect to an in-situ measurement, the major factor affecting the quality of aerosol products is the sub-pixel cloud contamination. In order to restrict this kind of error the alghoritm used to retrieve aerosol data adopts a cloud mask to recognize cloud free scenes from partly or cloudy ones. This mask is based on simple reflectivity and UVAerosol Index. However, old experience with Total Ozone Monitoring Spectrometer suggests that monthly mean AODs is well representative of the extinction due to aerosol content. In general the OMI algorithm used to retrieve aerosol products (OMAERUV) works better over land than over water surfaces. The near-UV retrieval method in fact is particularly sensitive to carbonaceous and mineral aerosols. The sources of these aerosol types are located over the continents, and the atmospheric aerosol load associated with these events is generally large. In addition, dust and smoke aerosol events tend to take place under meteorological conditions which do not favor the formation of clouds in the vicinity of the sources, such as arid and semi-arid areas in the case of dust, and the dry season in the case of biomass burning. The OMAERUV retrieved AOD of sulfate-based aerosols is less accurate due to its low values, higher spatial variability and increased levels of sub-pixel cloud contamination.

Ocean OMAERUV retrievals are affected by other factors. In addition to sub-pixel clouds, the ocean surface reflectance has both angular and spectral variations, the latter due to spectrally varying scattering from the water.

8.1.2 OMI aerosol algorithm

Aerosols are an important but complicated factor in climate and atmospheric chemistry. On climate system, aerosols have both a direct cooling effect by shortwave scattering of a fraction of the incoming solar radiation back to space, and an heating effect due to shortwave absorption. As seen in the previous chapter, these combined effects can produce change in the net heating rate. In addition they play direct effects also in air

pollution, in tropospheric chemical reactions and in reduction of surface UV irradiance as well as in direct climate effects, through their action as Cloud Condensation Nuclei.

Problems in detecting aerosols are their varied physical properties due to different sources and origins. For example aerosol refractive indices vary strongly, resulting in transparent to opaque particles; sizes vary from nanometers to microns; and shapes vary from spherical to irregular. The standard OMI pixel size of 13 km x 24 km is an important improvement for cloud and aerosol retrieval as compared to TOMS (35 km x 35 km) and GOME (40 km x 320 km). In fact smaller pixels lead to more cloud free scenes, which is essential for improving aerosol retrieval. Monitoring and process studies of clouds and aerosols are also planned with other satellite instruments that fly in formation with Aura (within about 15 minutes), in the so-called A-Train, namely: the global imager MODIS on EOS-Aqua, the cloud radar on CLOUDSAT, the aerosol/cloud lidar on CALIPSO, and the polarisation and bidirectionality imager POLDER on PARASOL. Important intercomparisons and synergisms will be possible between these co-located measurements and the OMI cloud and aerosol products. The OMI aerosol algorithm has been designed to produce the optical thickness and single scattering albedo of the tropospheric aerosol over ocean and land on a daily basis. The OMI aerosol algorithm derives aerosol optical properties by comparing the measured reflectance to results from radiative transfer calculations. These radiative transfer calculations are performed for cloud-free and horizontally homogeneous atmospheres, overlying a Lambertian surface. In this case, the reflectance emerging at the top of the atmosphere can be written as:

$$R(\lambda) = R_a(\lambda) + \frac{A_s(\lambda)}{1 - A_s(\lambda) \cdot s(\lambda)} T(\lambda) \qquad (8.1)$$

where R_a is the contribution of atmospheric scattering, A_s is the surface reflectivity, T the total direct and diffuse transmittance of the atmosphere for light that travels to the surface and then back to the sensor, and s is the spherical albedo of the atmosphere when it is illuminated from below. Radiative transfer models are used to determine the path reflectance, the transmission, and the spherical albedo for all wavebands used in the algorithm.

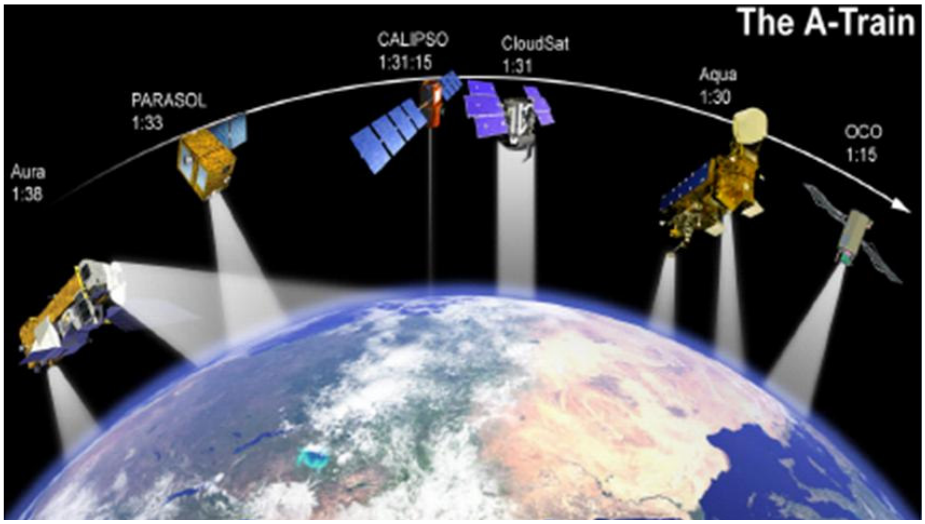

Figure 8.2: The NASA A-Train to monitor and process atmospheric aerosol and clouds

For cloud-free pixels the reflectance at Top Of Atmosphere (TOA) is influenced by surface reflection, which must be included in aerosol retrieval. To minimize the surface contribution, the algorithm uses the fact that in the UV most land surfaces (vegetation, dry soils) as well as the ocean are dark, whereas in the visible only the ocean is dark. However in the OMI aerosol algorithm there are more unknowns than equations. Retrieval of the optical thickness and single scattering albedo requires the use of a-priori aerosol models. In order to obtain a solution, the algorithm uses look-up-tables using several aerosol types with different optical properties (e.g. size distributions and refractive indices) which follow from Mie calculations. In OMI aerosol algorithm, models are grouped in five major aerosol types according to their origin. On a global scale, four main tropospheric aerosol types can be distinguished according to their production processes: urban-industrial aerosols originated from fossil fuel combustion; carbonaceous aerosols generated from natural and anthropogenic biomass burning; desert dust aerosols, injected in the atmosphere by the wind lifting capability; and the naturally produced oceanic aerosols. At last also a volcanic aerosol type is included being its aerosol size distribution represented by log-normal functions. Beside this initial selection based on geographical location and season, taking advantage of the known global distribution of sources of mineral aerosols and transport patterns, as well as the global distribution and seasonality of biomass burning activity and boreal forest fires, aerosol types are selected using spectral differentiation named aerosol indices. The Aerosol Index concept (Torres et al., 1998), which was developed based on the TOMS

observations in the near UV is applied to the OMI measurements, and is extended to the visible spectral region. As used in the OMI aerosol algorithm the Aerosol Index is defined as

$$a_{\lambda_2} = -100 \log\left[\left(\frac{I_{\lambda_1}}{I_{\lambda_2}}\right)_{MEAS}\right] + 100 \log\left[\left(\frac{I_{\lambda_1} A_{LER_{\lambda 1}}}{I_{\lambda_2} A_{LER_{\lambda 2}}}\right)_{CALC}\right] \quad (8.2)$$

These are colour indices, which are obtained by comparing the measured reflectance ratio at two wavelengths to the calculated reflectance ratio using a Rayleigh atmosphere only with an assumed surface albedo. When using λ_1= 342.5 nm and λ_2= 388 nm in equation 8.4, a UV aerosol index, a_{388} , is obtained. By the same token when λ_1= 388 nm and λ_2= 494.5 nm a visible aerosol index, a_{494}, is calculated. These aerosol indices are a measure of the change in spectral contrast (with respect to a pure Rayleigh atmosphere) due to the wavelength-dependent effects of clouds and aerosols. Clouds or any other type of non-absorbing large aerosol particle yield near zero UV aerosol index values (Hsu et al., 1996). In addition at the "traditional" UV aerosol index, OMI provides an alternate approach based on the use of the visible aerosol index over those areas of the world where the presence of either dust or smoke is likely to occur. Based on radiative transfer calculations, the visible aerosol index (a_{494}), allows the separation of gray absorbing particles (wavelength independent imaginary refractive index), such as carbonaceous aerosols, that in most cases yield negative a_{494} values, from colored absorbing aerosols (wavelength dependent imaginary refractive index) like mineral dust, that produce positive values of a_{494}. As shown in Figure 8.3, aerosol types can be identified with the combined use of the UV and visible aerosol indices.

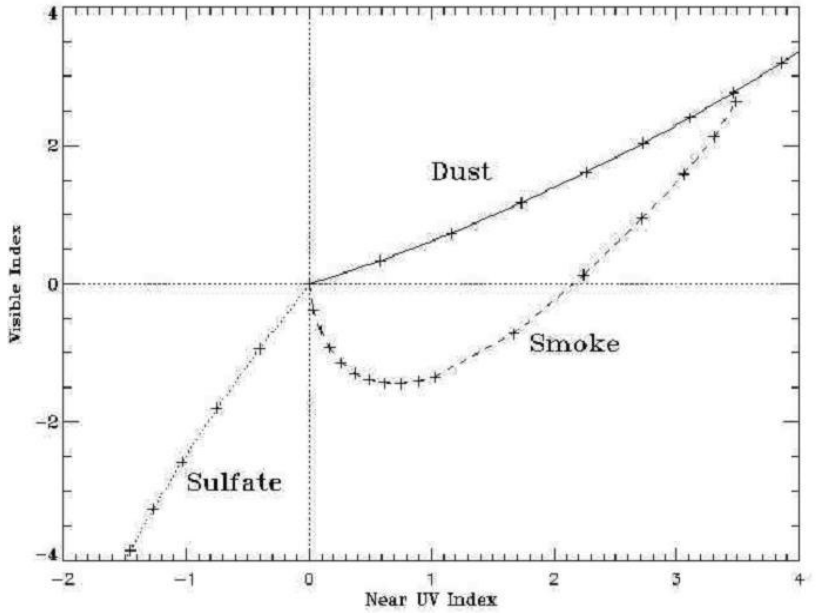

Figure 8.3: An example of the separation of aerosol types using the aerosol indices. Lines represent increasing aerosol optical thickness (550 nm) from 0 to 1.0 (in 0.1 steps) and from 1.0 to 4.0 (in 0.5 increments). (Torres et al. 2002)

To isolate the net aerosol effect, the spectral dependence of the surface reflectance must be taken into account. Since molecular scattering and gas absorption effects are well known, from satellite, it is possible to measure processes of scattering and absorption due to the presence of aerosol particles and surface reflection effects for cloud-free conditions. This measure is performed on the base of the radiation field departure from the pure Rayleigh scattering case. We see, in Figure 8.4, that in the simpler case with absence of aerosol particles and clouds, the radiance field emerging at the top of the Earth's atmosphere in the 330-500 nm region of the electromagnetic spectrum is mainly driven by the scattering of incoming solar radiation by air molecules, and the radiation reflected by the surface and transmitted through the atmosphere. The surface contribution depends on the surface type. In the 330-400 nm region the surface albedo is generally very small (less than 0.1) for all scene types including deserts (excluded snow and ice). At wavelengths longer than 400 nm, the surface contribution increases rapidly with wavelength over the arid and semi-arid regions of the Earth.

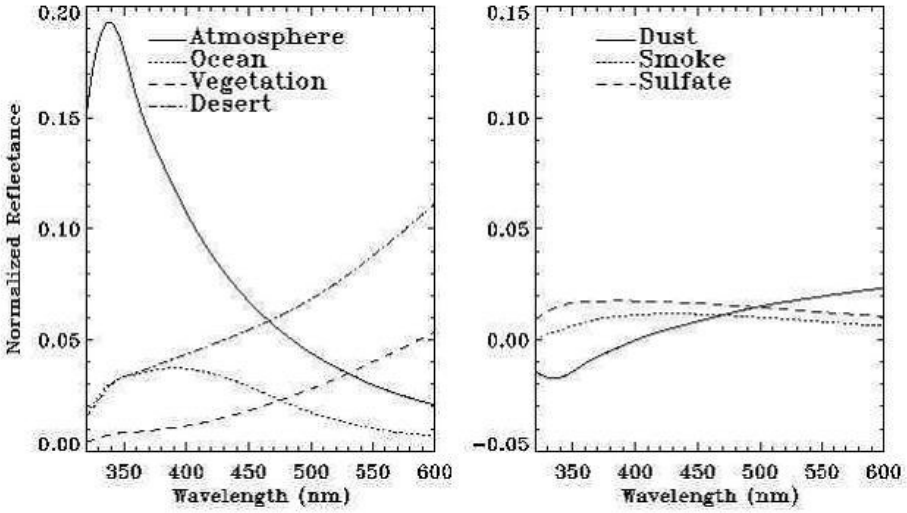

Figure 8.4. Left panel: Rayleigh atmosphere and several surface components of the reflectance at TOA as a function of wavelength. Right panel: Contribution by three aerosol types of optical thickness 0.2 (550 nm), to TOA reflectance as a function of wavelength. (Torres et al. 2002)

The detection capability for absorbing aerosols is therefore enhanced in the near UV where the large Rayleigh-scattering component enhances the aerosol 'color'. The capability of aerosol detection over the continents comes from the low value of the near UV albedo of most terrestrial surfaces. The manner in which particle scattering and absorption modify the up-welling radiation at the top of the atmosphere depends on the aerosol microphysical properties and loading. Aerosol absorption, therefore, can be inferred from satellite measurements in the near UV where multiple Rayleigh scattering is significant.

In the OMI algorithm, the last step of the aerosol retrievals is carried out using two approaches: an inversion method that uses two wavelengths in the near UV (TOMS heritage) and a multi-wavelength inversion approach that is an extension of the near UV method to a wider wavelength range (17 wavelengths in 331-500 nm range), (Torres et al., 2002). The multi-wavelength approach is the primary retrieval method over the oceans, and the near UV method is the primary retrieval technique over land. The method to retrieve aerosol properties over land and water surfaces has been developed in the last few years using measurements in the near UV region of the spectrum (330-380 nm) thanks the observations from the TOMS series of instruments (Herman et al., 1997, Torres et al., 1998). Before this date, it was thought that satellite retrieval of aerosols was only feasible in the visible and near infrared over dark surfaces such as

oceans, where the reflected radiance is dominated by aerosols. In this spectral range, over land areas, this retrieval becames difficult due to the surface contribution that can be significantly larger than the aerosol one. With TOMS near UV technique instead, is possible to retrieve aerosol properties over all terrestrial surfaces (free of ice and snow) including arid areas which are highly reflective in the visible and near infrared, but have very low reflectivity in the UV.

The OMI aerosol algorithm enhancing the advantages of the TOMS aerosol retrieval method and improving the spectral resolution and wavelength range from the UV to the visible (270-500 nm) is a sort of "bridge" that searches to fill the gap between aerosol satellite observations in the visible and near-infrared (e.g. MODIS, AVHRR) and those in the UV (TOMS). The near UV method will produce the aerosol optical thickness and single scattering albedo at 388 nm and the multi wavelength method will produce at selected wavelength between 330 and 500 nm, including 388 nm. The OMI aerosol optical thickness, τ, is defined in 8.3 equation, as the vertically integrated (from the surface to the top of the atmosphere, TOA) aerosol extinction coefficient, k_{ext}

$$\tau(\lambda) = \int_0^{TOA} k_{ext}(\lambda, z)dz \tag{8.3}$$

The spectral variation of the aerosol optical thickness contains information on the aerosol size distribution and wavelength dependent refractive index. The single scattering albedo is instead a measure of the fraction of aerosol extinction which is due solely to aerosol scattering effects. It is defined as the ratio of scattering to extinction coefficients (equation 8.4),

$$\omega_0(\lambda) = \frac{\int_0^{TOA} k_{sca}(\lambda, z)dz}{\int_0^{TOA} k_{ext}(\lambda, z)dz} \tag{8.4}$$

the single scattering albedo of non-absorbing aerosols being the unity.

In case of cloud contamination, the aerosol indices are the only aerosol parameters that are available in the output product. the retrieval of the aerosol optical thickness and single scattering albedo critically rely on the cloud screening. Therefore, strict cloud

screening is an essential step in the algorithm. Clouds give an increased radiance that may be detected using a simple threshold. However one has to distinguish between clouds and aerosols, to avoid marking pixels with high aerosol concentration as cloud-contaminated. For this reason, pixels that exceed the radiance threshold and have a near UV aerosol index near zero are rejected.

Finally the last important product is the height of an absorbing aerosol layer. In addition to aerosol micro-physical properties, satellite-measured radiances also depend on the height of the aerosol layer. This dependence is largest for absorbing aerosols and negligible when the aerosols are non-absorbing because scattering by aerosols does not appreciable reduces the amount of multiple Rayleigh scattering.. If the aerosol layer occurs high in the atmosphere, nearly all light that reaches the detector has to pass twice through the absorbing layer. If, on the other hand, the aerosol layer is located near the surface, only a fraction of the light that reaches the detector has to pass through this layer. Depending on the aerosol type, in OMI three vertical distributions are used. An exponentially shaped profile with a 2 km scale height is used for the industrial models. A similar profile but with a smaller scale height (1.5 km) is used for the oceanic models. For biomass burning aerosols, a single-layer Gaussian distribution of maximum concentration at 3 km and a half-width of 1 km is used. Two single-layer Gaussian distributions with peak concentrations at 3 and 5 km are used for the dust models to account for the seasonal variability of the altitude of a Saharan dust layer which is minimum in winter and maximum during summer.

8.2 High spatial resolution OMI aerosol data: comparison with in situ atmospheric extinction records over the ORM site

Site testing campaigns are at present performed within the classical scheme of optical-seeing properties, meteorological parameters, air transparency, sky darkness, cloudiness, etc. New concepts related to geophysical properties (seismicity and microseismicity), local climate variability, atmospheric conditions related to the optical turbulence (tropospheric and ground wind regimes) and aerosol presence have recently been introduced in the era of selecting the best sites for hosting a new generation of extremely large telescopes. In this point of view, the purpose of this study is the analysis of new approaches to the study of the aerosol content above astronomical sites. Our

objective is to calibrate the extinction values in the V band (550 nm) with remote-sensing data retrieved from satellite platforms.

As described in Chapter 7 atmospheric extinction is the astronomical parameter that determines transparency of the sky. Extinction is associated with the absorption/ scattering of incoming photons by the Earth's atmosphere and is characterized by the extinction coefficient, K. Sources of sky transparency degradation are clouds (water vapour) and aerosols (dust particles included). This coefficient is wavelength-dependent and can be determined by making observations of a star at different airmasses (King, 1985). Long baseline extinction values for the ORM have been measured continuously, since 1984, at the CAMC in the V band (550 nm) and more recently in the Sloan r' band (625 nm). To our knowledge, this is the largest available homogeneous data base for an observing site and is for this reason that we chose the ORM site at 2396 m above mean sea level as high resolution case study. Extinction values and their stability throughout the night are essential for determining the accuracy of astronomical measurements. As nights with low and constant extinction are classified as photometric, this parameter is considered among those relevant for characterizing an observing site.

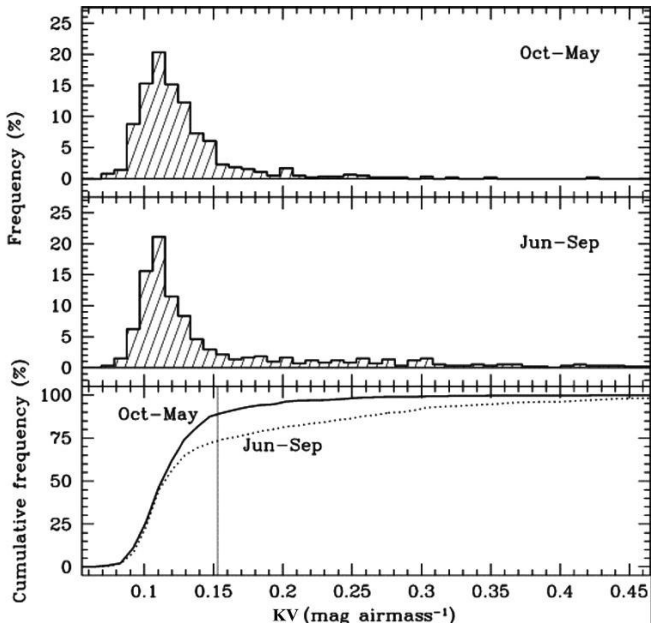

Figure 8.5 Frequency of extinction over the ORM during winter (top panel) and summer (centre panel). In both cases, the modal value is 0.11 mag airmass−1. Their corresponding cumulative frequencies are also shown (bottom panel). The vertical line indicates the extinction coefficient limit for dusty nights, KV ≥ 0.153 mag airmass−1 (Guerrero et al. 1998).

On photometric dust-free nights, the median of the extinction is 0.19 mag airmass^{-1} at 480 nm, 0.09 mag airmass^{-1} at 625 nm and 0.05 mag airmass^{-1} at 767 nm. The extinction coefficients reveal that on clear days, the extinction values at 680 nm are below 0.07– 0.09 mag airmass^{-1}, while on dusty days (diffuse-absorbing) they are always higher (Jimenez & Gonzalez Jorge 1998). The threshold that identifies the presence of dust is at 0.153 mag airmass^{-1} (Guerrero et al. 1998). At the ORM, the extinction in V is less than 0.2 mag airmass^{-1} on 88% of the nights, and extinction in excess of 0.5 mag airmass^{-1} occurs on less than 1% of nights. A statistical seasonal difference is also detected. Figure 8.5 shows the cumulative frequency of extinction over the ORM during winter (October–May) and summer (June–September). In summer, 75% of the nights are free of dust, while at other times of the year over 90% of the nights are dust-free (Guerrero et al. 1998). These results are consistent with those provided by Torres et al. (2003).

However in order to calibrate the extinction values measured in situ with aerosol content retrieved with remote-sensing techniques from Aura/Ozone Monitoring Instrument (OMI), Terra/Moderate-Resolution Imaging Spectroradiometer (MODIS) and Aqua/MODIS over the ORM observatory it is necessary to have clear the aerosol sources background together with the meteorological and geophysical scenarios over the Canary islands.

Concerning the aerosol sources background, most aerosols reaching the Canary Islands are marine, ClNa or of African (Sahara and Sahel) origin. In particular the latter (clays, quartzes, feldspars and calcites), because of their size, can reduce visibility in the optical wavelength range and can therefore affect astronomical observations. Aerosols also play an important role in astronomical site conditions, producing more stable condensation nuclei, delaying precipitation and causing the extinction, absorption, diffusion and reflection of extraterrestrial radiation. From a meteorological point of view, most of the airmass flux components reaching the Canarian archipelago come from the North Atlantic Ocean and consist of sea aerosols, which absorb chloride in the ultraviolet (UV). European (anthropogenic emissions from sulphates and carbon) and African dust intrusions affect the western and eastern Canary Islands differently. The most frequent are chlorides, i.e. clean salts of oceanic origin that do not affect astronomical observations and that reach or exceed half of the total contribution of mass

flux over the summits. European airmasses are almost always of anthropogenic origin (sulphates and carbon) and are of scant importance. A study of the origins and distribution of air flows performed by Torres et al. (2003) distinguished the origins of airmasses that affect the lower (MML) and upper (TL) layers, the latter being at the height of the astronomical observatories. The airmass provenance in the lower (mixing) layer close to the sea (MML) is Northern Atlantic (the mean is 59.6%), European (the mean is 19%) and African (0 per cent in summer and 23% in winter), whereas the TL is mainly Northern Atlantic (44.2%) and African (17.4%), with a minimum in April (5.3%) and a maximum in August (34.5%) (Torres et al. 2003). African summer intrusions are therefore almost absent in the MML and more intense in the TL because of the daily thermal convection reaching the higher atmospheric layers. In winter, intrusions into the TL are less frequent. The airmass is carried horizontally by the prevailing wind and is affected by a process of separation; the larger particles (>10 μm) leaving sediments at ground level over a short period of time and the smaller ones being carried across the Atlantic Ocean to distances of hundreds or thousands of kilometres from their place of origin. This sand creates a large feature (plume) that is visible in satellite images and extends from the African coast across a band about 20° in latitude. During winter, the prevailing wind carries the dust from the south of Canary Islands through an average of 10° in latitude to the Cape Verde islands and rarely reaches La Palma. Instead, in summer, winds above 4 km in altitude can take these particles as far north as 30° in latitude. In these conditions, the dust plume over the ORM is composed mainly of small quartz particles in the range 0.5–10 μm and the biggest particles precipitate (dry deposition). Typical dust storms take three to eight days to disperse and deposit 1–2.4 million tonnes per year. Finally, the clouds of aerosols dissipate through advective processes or through rain (sumid deposition).

At last, from the point of view of the geophysical scenarios, the presence of a stable inversion layer and the pronounced orography of the western islands (La Palma and Tenerife) produce different mass flux patterns in the lower (mixing) layers closer to the sea (up to 800 m) and in the median-upper (or free) troposphere layer (TL; above the thermal inversion layer, i.e. above 1500 m), causing a seasonally dependent vertical drainage of airborne particles. In fact during the summer, airborne particles intrusions, can rise to the peaks of the mountains (high-level gloom), at 2400 m, while in winter,

more frequently they remain in the lower troposphere (anticyclonic gloom). This anticyclonic gloom is associated with strong, stationary anticyclonic conditions and it can favour the decrease in height of the inversion layer and the formation of clouds that do not easily precipitate as rain, hence persisting for a longer time and providing a more stable sea of clouds. In this way the dust is trapped by the sea of clouds (sea of dust) and is prevented from reaching the topmost level in the islands (above 1500 m).

Taking into account that the trade-wind scenario and the cold oceanic stream, in combination with the local orography, play an important role in the retention of low cloud layers well below the summits to the windward (north) side of the islands, above which the air is dry and stable and considering all the aerosol features that characterize the geographical area of the ORM, the main step that remained to perform was to fit high spatial resolution satellite data with in stu measurements. In order to benefit from satellite data for local site characterization, we have centred our analysis on the aerosol content. To ensure that the retrieved remote-sensing data fields from different satellites (such as aerosol values or geolocation parameters) are precisely over the ORM site coordinates to compare with the atmospheric extinction by CAMC, we decided to work with Level 2 data, which have a projected effective pixel size given by the IFOV. Through a software procedure, we created files containing information on geophysical variables (data describing the solid earth, marine, atmosphere, etc., properties over a particular geographical area) and field values such as seconds, latitude, longitude, reflectivity in different channels, the AI, aerosol optical depth (AOD), cloud land and ocean fraction. Running this software we explored the use of some new detectors on board different satellites that operate in bands of astronomical interest (the visible and NIR) with higher spatial resolution than TOMS (Bertolin, 2005). Despite the much better spatial and spectral resolution of the recent satellite aerosol measurements (AI and AOD), we demonstrate in this paragraph that although this kind of information at the moment is quite accurate to monitor the aerosol content of an astronomical observatory, however the help of in situ data, in particular at those astronomical sites with abrupt orography, remains of huge importance to have stong feedback to check the reliability of satellite data analysis. The satellites/instruments and parameters used in this work published in the Monthly Notices of Royal Astronomical Society with the

title: "Astronomical site selection: on the use of satellite data for aerosol content monitoring" (Varela et al., 2008) are summarized in Table 8.1.

Table 8.1: Overview of instruments on board satellites that provide parameters useful for our work.

Satellite/instruments	Horizontal Resolution	Parameter	Period
Terra/MODIS	10 x 10 Km^2	AOD	From 2000
Aqua/MODIS	10 x 10 Km^2	AOD	From 2002
Aura/OMI	From 10 x 10 Km^2 to 24 x 48 Km^2	AI	From 2004

The parameters selected and retrieved are the AI provided by OMI on board oAura with visible and UV channels and with a spatial resolution from 13 km × 24 km to 24 km × 48 km and the AOD provided by MODIS on board Terra (from 2000) and Aqua (from 2002), with a spatial resolution of 10 km ×10 km.

Aura/OMI data:

Here, we show the results of comparing AI provided by TOMS and OMI. OMI on the Earth Observing Systems Aura platform continues the TOMS heritage, Figure 8.6 shows the AI values provided by EP/TOMS and OMI/Aura over the ORM on La Palma. Looking at the plot is possible to note an improvement in the OMI data in term of dispersion. In fact, comparing the OMI data deriving from better horizontal and vertical spatial resolution with its predecessor, TOMS in EP we note a large reduction in the data dispersion.

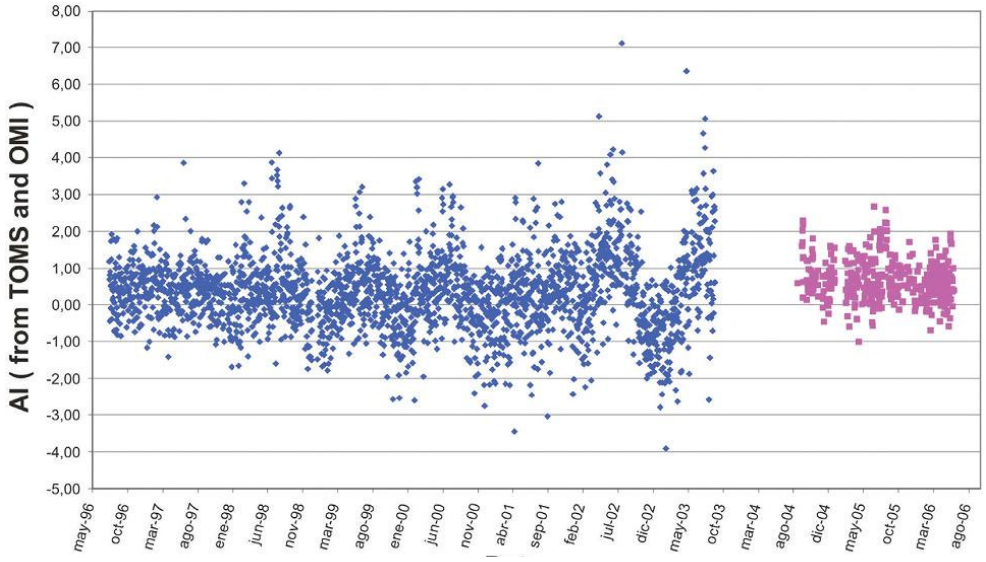

Figure 8.6. AI provided by EP/TOMS (blue points on the left) and Aura/OMI (pink points on the right) in time over the ORM on La Palma. The improvement shown in the OMI data (much less dispersion than TOMS data) derives from better horizontal and vertical spatial resolution compared with its predecessor, TOMS in EP.

Terra/MODIS and Aqua/MODIS data:

MODIS on board the NASA Terra and Aqua satellites provides not the AI values but an equivalent parameter, the AOD. In Figure 8.7, we show AOD for Terra and Aqua; we see that there exists a good relation between the maximum and minimum AOD values.

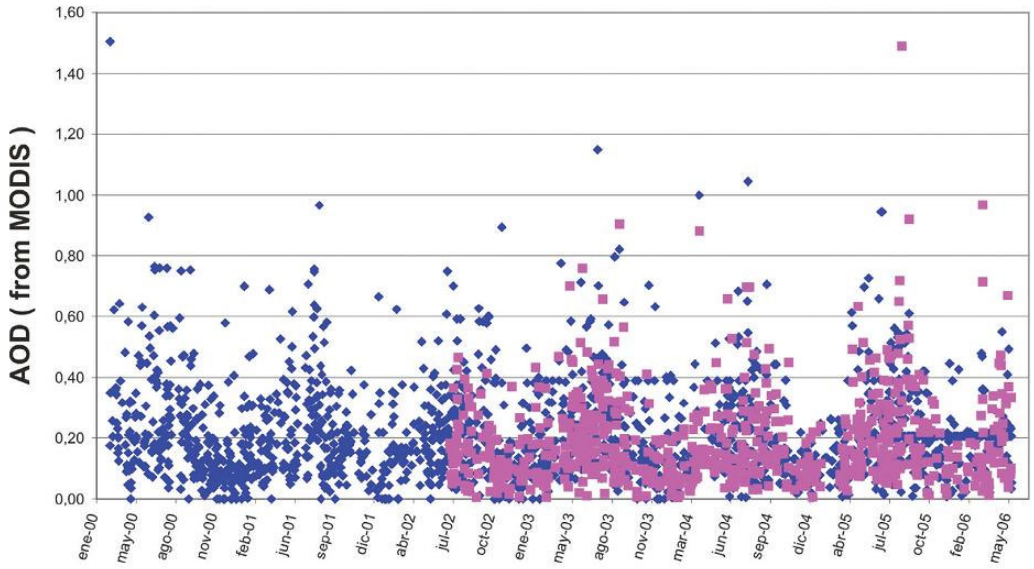

Figure 8.7. Aerosol optical thickness provided by Terra/MODIS (blue points) and Aqua/MODIS (pink points) in time over the ORM on La Palma.

The consistency of both data sets is excellent. At this step, we use our knowledge from previous study with TOMS data (Bertolin, 2005) that fixed the AI threshold for dusty

nights at 0.6, to reveal an analogous AOD threshold for dusty events. AI and AOD are not in a 1:1 ratio because they depend on several variables as refractive index, particle size distribution and height of the atmospheric layer. Therefore, to determine the AI and AOD threshold, we use information provided in a collaboration between the Spanish Environment Ministry, the Upper Council of Scientific Researches (CSIC) and the National Institute of Meteorology (INM) for the study and analysis of the atmospheric pollution produced by airborne aerosols in Spain. They provide us with the days when calima (dust intrusion) occurred in the Canary Islands. As we later demonstrate in the plots, in our opinion, these events happened at altitudes lower than those of the observatories so they do not influence the measurements of atmospheric extinction. In Figure 8.8, we show AOD for Terra and Aqua and AI for OMI. AI values are larger than 0.6, and most of AOD data points for Terra and Aqua fall above a limit greater than 0.10. This limit is consistent with that provided by Romero & Cuevas (2002). Therefore, AI>0.6 and AOD > 0.1 are considered the thresholds for dusty episodes.

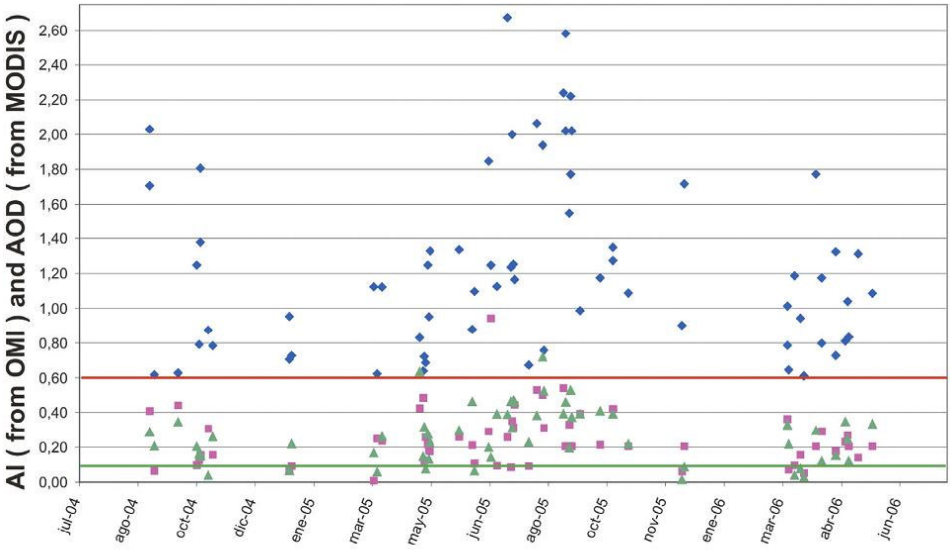

Figure 8.8. AI from OMI (blue rhombus) and AOD from MODIS (pink squares correspond to Terra values and green triangles to Aqua data) under dusty conditions detected by the INM from 2004 to 2006.

AI from OMI versus K_V:

In this section, we argue about the correlation between atmospheric extinction in V (551 nm) and the AI measured for OMI in the same channels of TOMS (331 and 360 nm) presented in Figure 8.9.

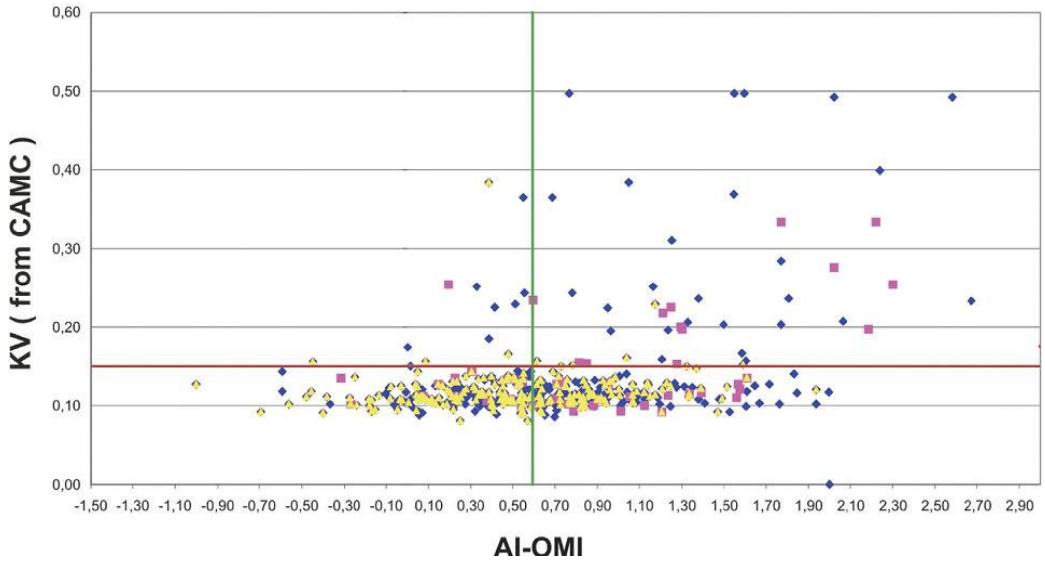

Figure 8.9. Correlation between AI provided by Aura/OMI and K_V from the CAMC. Pink points indicate dust episodes of calima retrieved by the INM, and yellow points correspond to cloud presence. Red and green lines indicate the K_V and AI limits for dusty nights, respectively. We can see that most of the points indicating the presence of absorbing aerosols (AI larger than 0.6) but non-atmospheric extinction (K_V smaller than 0.15 mag airmass^{-1}) correspond to the presence of clouds and calima below the level of the Observatory.

In order to determine if it exists a correlation between both parameters, we distinguish also between the cloud presence and the situation of days with calima intrusions. In Figure 8.9, we observe an interesting situation not revealed in the same graph for the aerosol EP/TOMS index (Bertolin, 2005; Varela et al. 2008). Once we put the atmospheric extinction (K_V) threshold (red line) and the limit for absorbing aerosols (green line), the situation reveals four quadrants. In the first quadrant (the upper right-hand side), we have a situation with absorbing aerosol and values of atmospheric extinction over the limit of photometric dusty nights. In the second quadrant (upper left-hand side), there are no points that fall inside. This result is very important because it means that non-absorbing aerosols do not influence the extinction above this threshold. In the third quadrant (bottom left-hand side), there are still non-absorbing aerosols but for clear nights, and it means that this type of sulphate and/or marine aerosols do not influence the extinction as we expect. In the last quadrant (bottom right-hand side), absorbing aerosols are again seen in the presence of low-extinction values. An explanation could be the presence of weakly absorbent particles, such as carbonaceous grains or clouds, or a more complex situation with a mixture of cloudy and aerosol scenarios, or the presence of absorbing aerosols below the level of the observatory. The

lack of correlation indicates that AI from OMI should not be used alone for atmospheric extinction characterization at the ORM. We added pink points as dust episodes of calima retrieved at the ground level, and yellow being those that correspond to cloud presence (reflectivity at 331 nm greater than 15%). This plot is very informative because from the pink points we can see that these calima episodes are mainly below the threshold of dusty nights; this means that they do not affect the measurements of extinction because the calima is at a lower level with respect to the altitude of the observing site, such dusty events reaching the Roque de losMuchachos Observatory and being detected only on some occasions. We also note that the clouds are almost all below this limit. This means that values above the threshold of dusty nights are dust-absorbing particles at the height of the observatory.We see that in this zone of the plot there are almost no clouds and some calima events that reach the astronomical site. Thanks to strong convective motions, in some occasions these dust particles may be driven along the orographic contours of the caldera that borders Roque de los Muchachos. In fact, the spatial resolution of OMI ranges from 13 km × 24 km to 24 km × 48 km and it can contain part of the caldera (Figure 8.10).

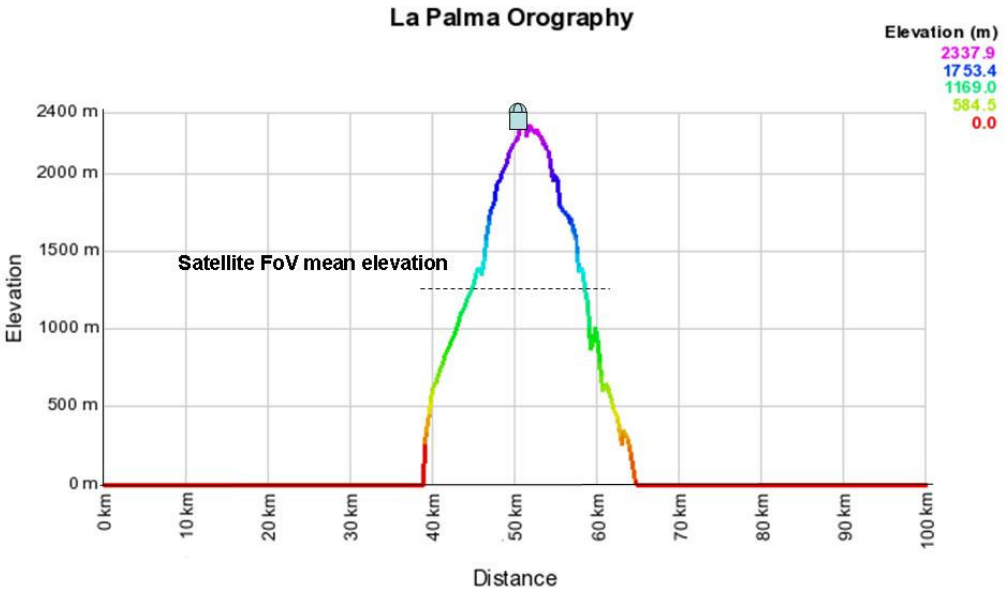

Figure 8.10. Plot of La Palma orography profile at a same latitude. In y-axis the elevation amsl in meter and along x-axis a spatial range of about 1° in km is displayed. Dotted line represents the mean OMI FOV at the satellite FOV mean elevation.

AOD from Terra/MODIS versus K_V:

The MODIS aerosol product monitors the ambient AOD over the oceans globally and over a portion of the continents. The aerosol size distribution is also derived over the oceans, and the aerosol type is derived over the continents. Therefore, MODIS data can help us to understand the physical parameters of aerosols affecting the Canarian Observatories. Daily Level 2 data are produced at 10 km × 10 km spatial resolution. The MODIS aerosol product is used to study aerosol climatology, sources and sinks of specific aerosol types (e.g. sulphates and biomass-burning aerosols), interaction of aerosols with clouds and atmospheric corrections regarding remotely sensed land surface reflectance. Above land, MODIS uses dynamic aerosol models deriving from ground-based sky measurements for the net retrieval process and in the same way, over the ocean, MODIS retrieves parameters that describe aerosol loading and size distribution. There are two necessary pre-assumptions in the inversion method of MODIS data: the first concerns the structure of the size distribution in its entirety and the second concerns a lognormal modes assumption that is needed to describe the volume–size distribution; a single mode to describe the accumulation mode particles (radius <0.5 μm) and a single coarse mode to describe dust and/or salt particles (radius >1.0 μm). The aerosol parameters that we expect to retrieve from the aerosol Level 2 product are the ratio between the two modes, the spectral optical thickness and the mean particle size. The quality control of these products as for OMI, is based on comparison with ground and climatology stations. In our work, the parameters that we have used from Level 2 MODIS data are: latitude and longitude as geolocation values and AOD (aerosol optical thickness at 0.55 μm for both ocean and land), aerosol-type land flag values that contain index 0 for mixed scenes, 1 for dust, 2 for sulphate, 3 for smoke, 4 for heavy absorbing smoke and cloud fraction land and ocean values in percentage. In Figure 8.11, we show AOD measured by MODIS on board of Terra platform against K_V.

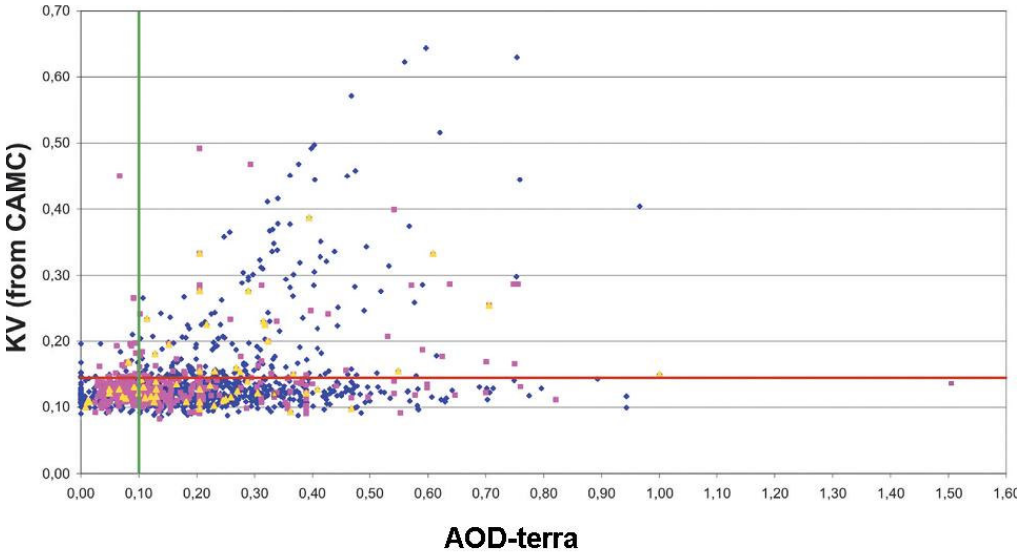

Figure 8.11. Correlation between AOD provided by Terra/MODIS and the K_V measured by the CAMC, distinguishing among the terrestrial (mixed dust, smoke, sulphate – blue points), marine (pink points) aerosols and the presence of dust events over the Canary Islands coming from Africa and collected at ground level (yellow points). The red and green lines indicate the K_V and AOD limits, respectively, for dusty nights.

In this plot, we find two tails of data within a certain dispersion of values and once more the majority of points that falls under the threshold of K_V smaller than 0.15: the flatter-tail groups together with most of the AOD values lower than 0.2, i.e. non-absorbing (<0.1) or weakly absorbing aerosols (marine particles, clouds above ocean and mixed scenarios with salt, sulphate particles and clouds). In Figure 8.11, we distinguish among terrestrial aerosols (composed of a mixture of dust and smoke sulphates) and marine particles marked, respectively, by blue and pink points, and we distinguish the presence of dust events coming from Africa (yellow points) using the data provided by INM at ground level. We see that pink values are situated in the tails of the plots and are present mainly at lower K_V and AOD values, where we expect sulphate sea-salt aerosols and CCN; only in some cases they are detected at higher AOD with small K_V values, probably these aerosols and clouds baing below the level of the observatory. The second tail covers two quadrants corresponding to small AOD but large K_V due to the presence of weakly absorbent aerosols at the level of the observatory or to a mixture of particles and clouds, and to large AOD and large K_V, mostly terrestrial aerosols at the level of the observatory. The calima (yellow points) is also below the K_V threshold, perhaps because of their closeness to ground level, except for some cases in which it can reach the level of the observatory.

AOD from AQUA versus K_V:

We perform the same analysis for the MODIS instrument on board the Aqua satellite that retrieves the same aerosol Level 2 data. In Figure 8.12, we show the AOD from Aqua data versus the K_V retrieved by CAMC data. We plot terrestrial (blue) and marine (pink) aerosols and the yellow points indicating days with calima. In this case too, there is evidence of the two tails as for the Terra data analysis. Here, most of the points being below the K_V threshold. Comments are very similar to those made previously, i.e. the marine aerosols are more clustered at small AOD values in a lower tail, whereas the terrestrial values are somewhat uniformly distributed with several points at large K_V indicating absorbing aerosols or clouds at the level of the observatory. Most of points falls below the threshold for dusty nights just as the majority of calima days. The interesting fact is that only the episodes of dust with large K_V follow a good linear relation with the AOD.

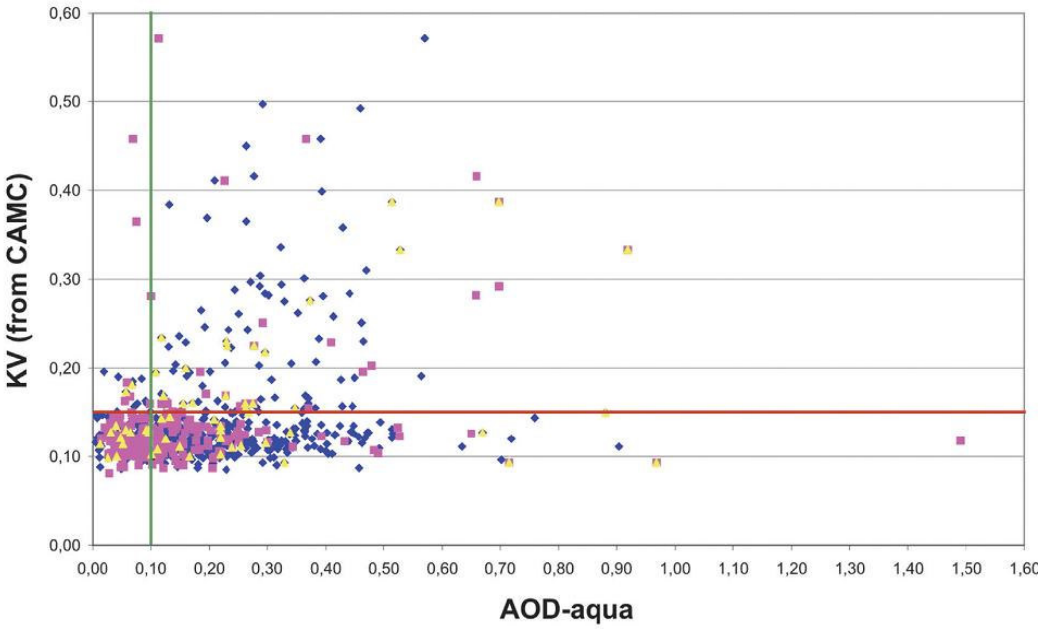

Figure 8.12. Correlation between AOD provided by Aqua/MODIS and the K_V measured by the CAMC, distinguishing among the terrestrial (mixed dust, smoke, sulphate – blue points), marine (pink points) aerosols and the presence of dust events over the Canary Islands coming from Africa and collected at ground level (yellow points). The red and green lines indicate the K_V and AOD limits, respectively, for dusty nights.

8.3 Lower spatial resolution OMI aerosol data: height of aerosol layer comparison in world's top astronomical sites

In this section we prove that high spatial resolution is not the main condition to assure good results using remote sensing satellite data. As announced in advance, for assessing the weight that the spatial resolution hold in site testing analysis, we handle two different levels of satellite data. The high resolution level 2 data has been discussed in detail in section 8.2 while the low resolution level 3 data is presented here using a six-year records from OMI instrument (2004-present). Using this data level, stored by NASA by resampling higher resolution data to provide an averaged value of 1°x1° resolution over space, we perform a comparison among selected world's top astronomical observatories. For each site we are able to obtain information on the height of aerosol layer, aerosol single scattering albedo and aerosol optical depth. The choice of analysing remote sensing data through the comparison of the world's top astronomical sites of La Silla, Paranal, La Palma and Tenerife was performed to look not only at the results in data elaboration but above all to search for an appropriate technique able to reveal astronomical sites climatic properties exploitable when we are in search of new sites hosting future extremely large telescopes. In this section we take immediately advantage of this approach applying the same method on the analysis of the Tolonchar site that is now weighed up by the site tesing group experts as a possible new ELT astronomical site.

In performing our data analysis, we first, downloaded from 'Giovanni' online data system, developed and maintained by the NASA GES DISC (http://disc.gsfc.nasa.gov/giovanni), the following level 3 OMI Aerosol Data Products (averaged on 1° x 1° grid): Aerosol index (AI), Aerosol Extinction Optical Depth (AOD at 388 and 500 nm) and Aersol Absorption Optical Depth (AOD at 388 and 500 nm). Then, we passed to elaborate the data following the theoretical basis given by Omar Torres in the description of the OMI aerosol UV alghoritm that he performed at the Goddard Space Flight Center and reported here (section 8.1.2) in its main guideline. Through the defined look up tables is possible clearly separate between absorbing (smoke, desert dust) and non-absorbing aerosols. We know, since our precedent results on TOMS data elaboration (Bertolin, 2005), that AI magnitude depends on aerosol

height, aerosol optical depth and optical properties (as Single Scattering Albedo). Since from downloaded data we have only information concerning the AI and the AOD, the other parameters (i.e. the SSA and the height of aerosol layer) had to be retrieved looking to the a-priori assumption made by Torres. For each astronomical site, distinguishing among three different aerosol sources (dust, carbonaceous/biomass burning and sulphate aerosols) we obtained the two unknown variables (SSA and h_{aer}) through these two look up tables (Figure 8.13).

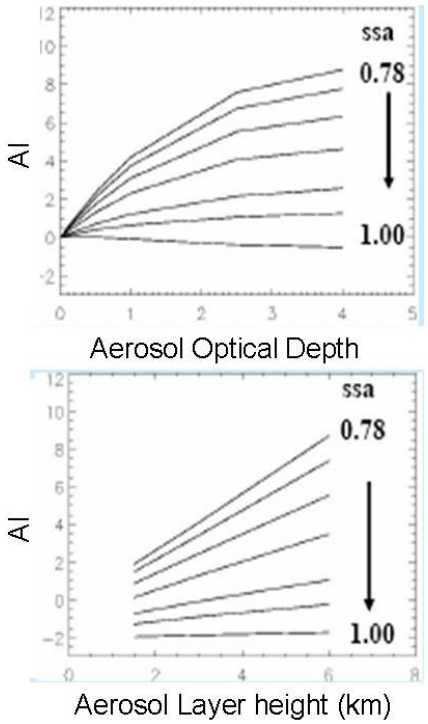

Figure 8.13. Look up tables on which the OMIAERUV alghoritm is based on. From the upper panel we can retrieve the aerosol type (D3, D2 and D1 for dust-type aerosols; C3, C2 and C1 for carbonaceous and biomass burning aerosol and the last model with SSA value equal to one, for sulphate aerosol. From the lower panel, entering with the AI and the SSA values, the aerosol layer height in km, is retrieved.

However, as told in the introduction at this chapter, in handling remote sensing data, to obtain reliable results more than the higher spatial resolution at the footprint of the satellite field of view, it is important to well known some spurious effects that enter in the algorithm theoretical basis of the satellite. In the case of OMI Near-UV algorithm we have best data retrieval filtering satellite data for cloud free scenes (less then 15% cloud coverage). As we will show in detail in the next chapter, the effect of clouds on the residue, used in TOMS and OMI products, is a delicate issue and it is comparable to the effect of a high surface albedo when the aerosols overlie the cloud. But when the

cloud overlies the aerosols the residue is completely determined by the cloud characteristics. In this case in fact, the cloud intercepts almost all incident radiation and acts as an opaque 'roof' over the aerosol layer; consequently the residue is almost entirely determined by the cloud characteristics. Cloud droplets are in fact scattering aerosols and produce zero or negative residues, depending on the solar zenith angle. This means that the residue method will not be affected very much by low clouds, but high clouds will certainly obsure absorbing aerosols layers. Tanking carefully into account all these theoretical indication, we start our analysis remembering that OMI data, also at lower resolution level, are able to detect absorbing aerosols over all terrestrial surfaces and above cloud decks.

La Silla site, Chile:

To analyse the data results in the way more correspondent at the satellite view, a careful analysis of the site orography, satellite ground footprint (1° x 1° grid) and mean height of satellite view was performed for each case study. This plot presented for la Silla (Figure 8.14) gives us the indication to read our results.

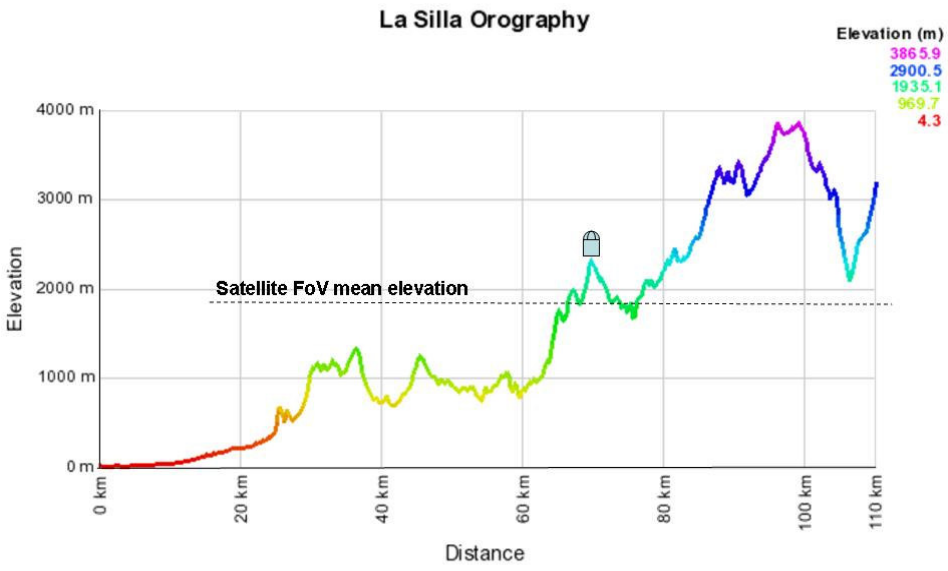

Figure 8.14. Plot of La Silla orography profile at a same latitude. In y-axis the elevation amsl in meter and along x-axis a spatial range of about 1° in km is displayed. Dotted line represents the mean OMI FOV centered on the astronomical site at the satellite FOV mean elevation.

After we retrieved the AOD values centered over La Silla and we calculated the values of SSA and height of aerosol layer, we presented the results in Figure 8.15. This plot

represents the vertical distribution of aerosol particles in function of their aerosol optical depth (blue color) and the distribution of different aerosol type using the single scattering albedo (pink color) as vertical discriminant. To remember that this analisys is concerning only with cloud free scenes the percentage of cloud cover (less than 2%) is displayed in green.

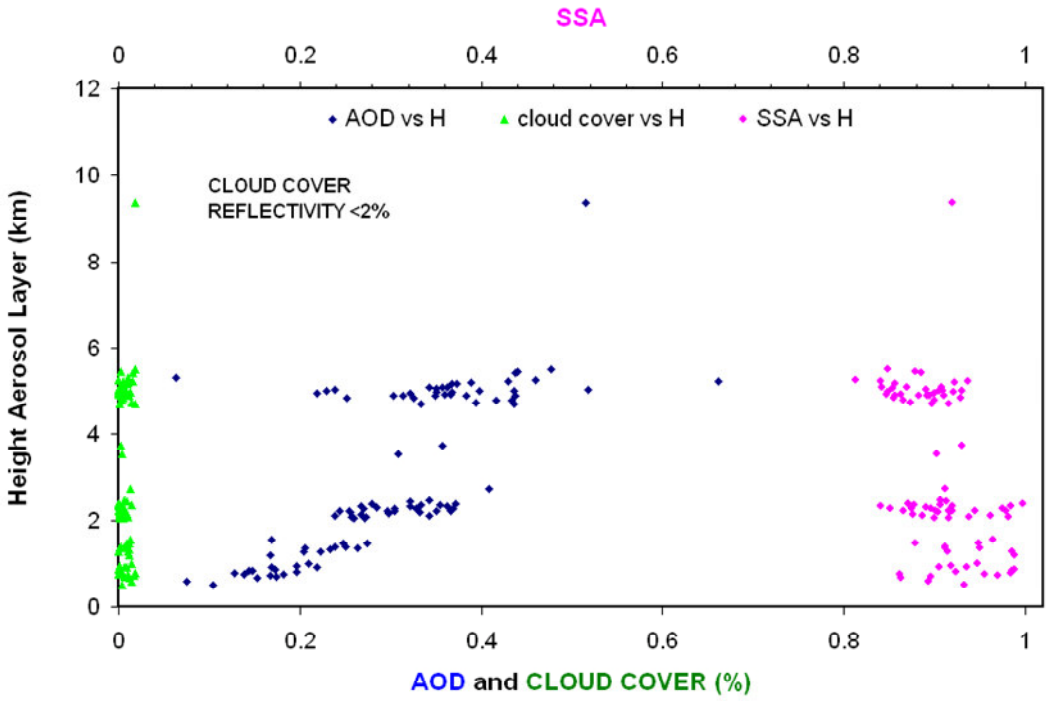

Figure 8.15. La Silla vertical distribution of aerosol particles in function of their aerosol optical depth (blue color-main x axis), vertical distribution of different aerosol type with different single scattering albedo (pink color sexondary x axis). Cloud free scenes percentage of cloud cover less than 2% (green color- main x axis).

The meaning of this plot is explained with the help of Figure 8.14. In fact the height (in km) of the aerosol layer in Figure 8.15 must to be added to the satellite FoV mean elevation showed with a dotted line in Figure 8.14. The AOD and AI level 3 satellite data are in fact averaged over a grid of 1° for side with a mean elevation represented by the dotted line marked in the plot 8.14. It means that when airborn particles intrusions from different sources occur over the La Silla local area, these aerosols range vertically from a bit less of 2000 m up to 8000 m. Being the particles from 2000 to 4000 m less absorbent (near to 1 as SSA) than, in mean, the higher one (smaller SSA values). Therefore, the particles with high AOD values that can affect the astronomical observations in La Silla lie at an height major than 6000 m asml. If we change a little bit

approach to this plot, studying the aerosol seasonal intrusion, in Figure 8.16 we observe that seasonal intrusions of airborn particles over La Silla. take part mostly during spring and summer (red and green points). Winter and Autumn aerosols instead do not reach the height of the observatory.

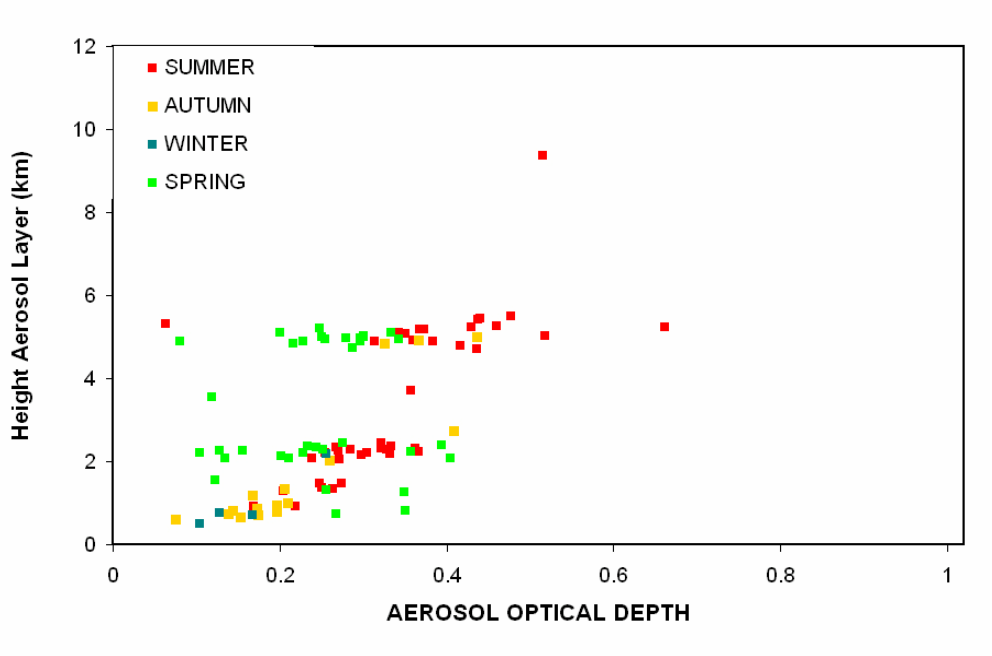

Figure 8.16. Height of the seasonal intrusion of airborn particles over La Silla. Most part of events take part during spring and summer (red and green points). Winter and Autumn aerosol do not reach the height of the observatory.

If we analyse the AOD, SSA and height of aerosol layer mean tendency during the calendar year taking the OMI six years records (2004-present) we confirm this result. In fact in Figure 8.17 we see that the maximum aerosol layer height occurs during the summer of the Southern Hemisphere while the minimum during the winter, the AOD following these trend too.

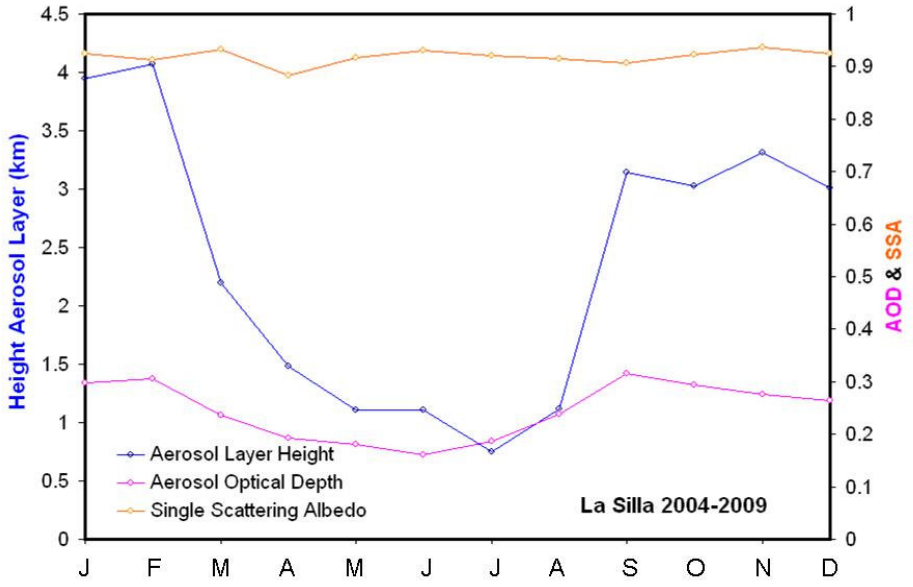

Figure 8.17. La Silla height of aerosol layer mean tendency (Blue) during the calendar year taking the OMI six years records (2004-present). AOD (Pink) and SSA (Orange) mean tendency(secondary y axis).

Paranal site, Chile:

The site orography, satellite ground footprint (1° x 1° grid) and mean height of satellite view for the Paranal site is presented in Figure 8.18.

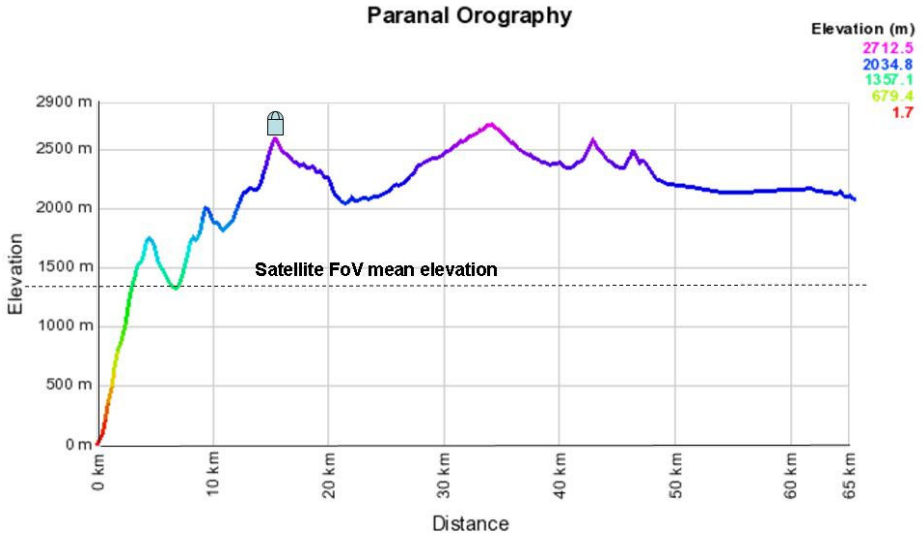

Figure 8.18. Plot of Paranal orography profile at a same latitude. In y-axis the elevation amsl in meter and along x-axis a spatial range of about 1° in km is displayed. Dotted line represents the mean OMI FOV centered on the astronomical site at the satellite FOV mean elevation.

In this plot is visible the abrupt coastal orography of Paranal and the site closeness to the ocean that enters for about 35 km in the satellite 1° side ground footprint. The same analysis of La Silla was performed locally over Paranal once retrieved for this site too, values of SSA and height of aerosol layer. In Figure 8.19, the vertical distribution of aerosol particles in function of their aerosol optical depth (blue color), and their SSA (pink color) are displayed. In this plot we see that aerosol particles reach higher height (up to 10 km referred to a satellite Fov mean elevation of about 1300 m) respect to La Silla local area, reaching in some cases the tropopause. Moreover from the plot we observe that the number of intrusion appears to be small also in comparison with La Silla but with higher aerosol optical depth values, probably meaning that when such events occur in this area, they can stongly affect the astronomical observations. However, in our opinion, a second hypothesis, probably more reliable, can be taken into account supported by the plot of photometric nights percentage that we present in the next chapter. The fact to see the aerosol layer at such high altitude could be a spurious effect due to the difficult of OMI retrieval method to mask the sea glint. In fact, seen the closeness of Paranal site to the sea, probably in the 1° satellite footprint the sea glint effect could be flagged in a wrong way as an high level aerosol scene.

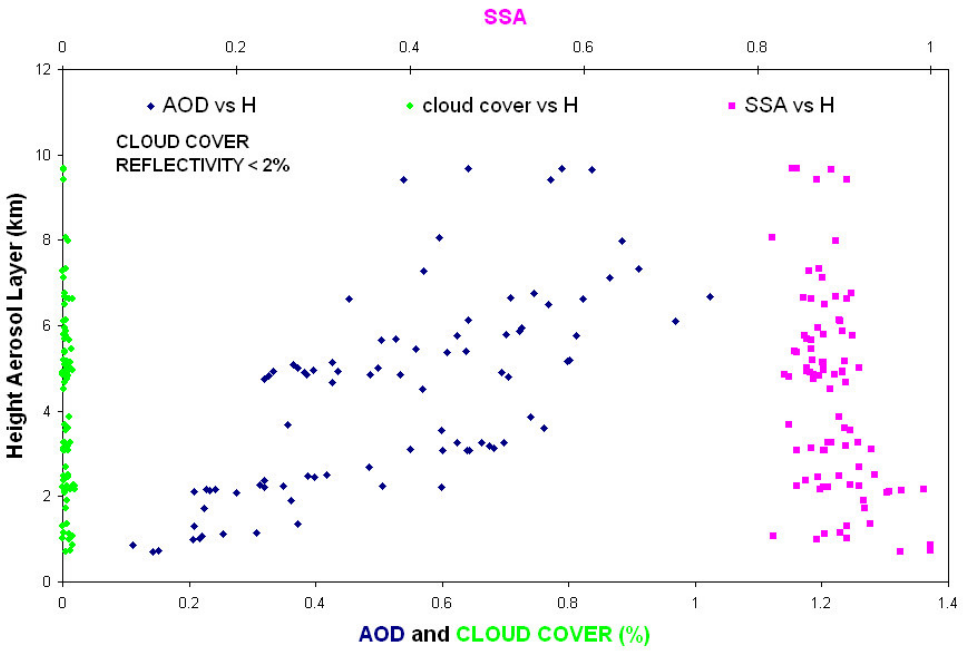

Figure 8.19. vertical distribution of aerosol particles over Paranal in function of their aerosol optical depth (blue color-main x axis), vertical distribution of different aerosol type with different single scattering albedo (pink color sexondary x axis). Cloud free scenes percentage of cloud cover less than 2% (green color- main x axis).

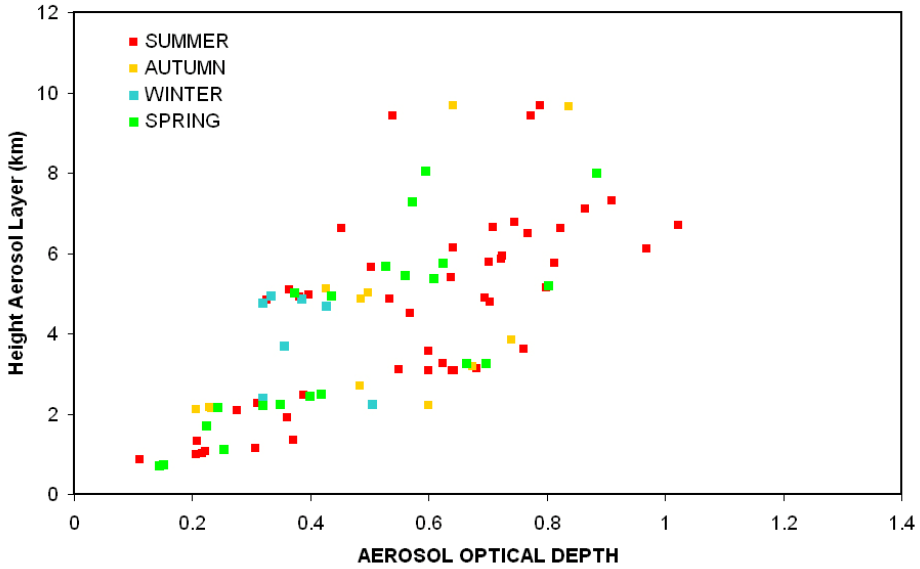

Figure 8.20. Height of the seasonal intrusion of airborn particles over Paranal. Most part of events take part during summer (red points). Seasonal events lower than 1600 m do not reach the height of the observatory.

The seasonal intrusion at Paranal (Figure 8.20) shows that summer airborn particles are blowed up at very high altitude thanks to the convective motion droven by such abrupt orography.

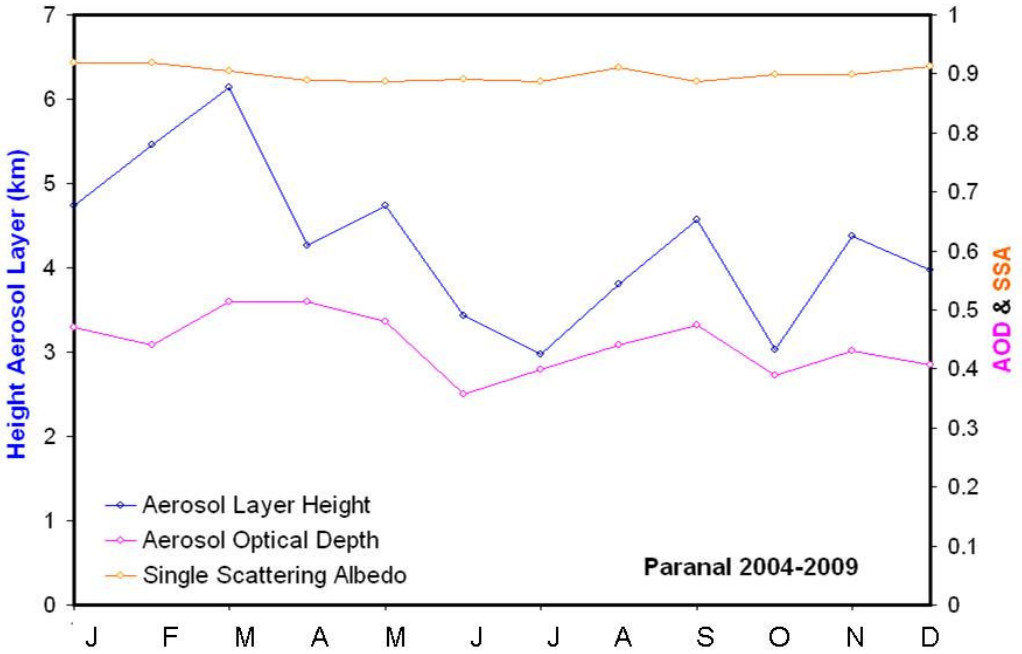

Figure 8.21. Paranal height of aerosol layer mean tendency (Blue) during the calendar year taking the OMI six years records (2004-present). AOD (Pink) and SSA (Orange) mean tendency(secondary y axis).

In Figure 8.21, the mean tendencies of AOD, SSA and height of aerosol layer at Paranal during the calendar year based on the analysis of the OMI six years records (2004-present), show a more oscillating trend in aerosol height with a peak in summer and a decreasing trend in winter but not so evident as in La Silla calendar year mean tendency.

Tolonchar as possible ELT site, Chile

In order to test our approach and reveal some useful climatic properties looking at new sites that could host future extremely large telescopes, in this subsection, we apply our thecnique more in detail over Tolonchar. This area is now under examination by the ELT site tesing staff. In Figure 8.22 we present the orography of this site with 1° satellite ground footprint at a mean elevation of about 3500 m asml.

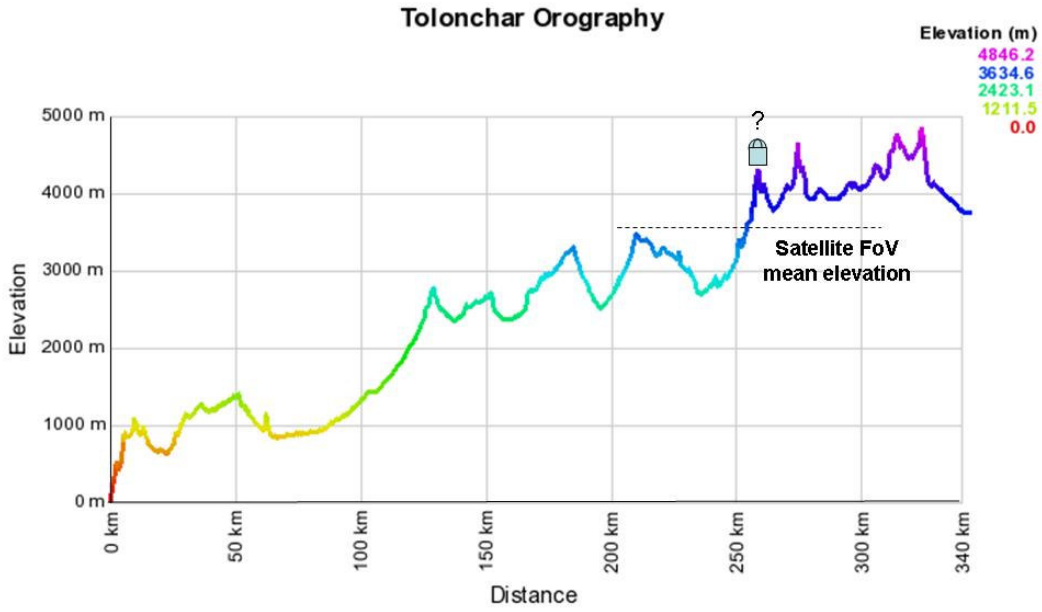

Figure 8.22. Plot of Tolonchar orography profile at a same latitude. In y-axis the elevation amsl in meter and along x-axis a spatial range since the ocean (in km) is displayed. Dotted line represents the mean OMI FOV centered on the astronomical site at the satellite FOV mean elevation.

For this site, the OMI values retrieved when both AI and AOD were different to zero in cloud-free scenes (cloud cover < 15%) were a lot in comparison with La Silla and Paranal area. This result was of great importance, first for the indication that Tolonchar area is practically free of cloud all year long (as we aspected) and secondly, because this more complete database of aerosol values gave us the opportunity to perform a more detailed analysis on the height of aerosol layer, AOD and SSA data. In order to study

the monthly signal variation since 2004 and detect in this way the aerosol monthly variability, we applied a 30-day running average for each dataset. In Figure 8.23, we observe in the result, a quite regular occurance of AOD peaks with higher aerosol height. The occurrence of these maxima from a "normal range" aerosol intrusion are evaluated to have an AOD value greater than 0.42.

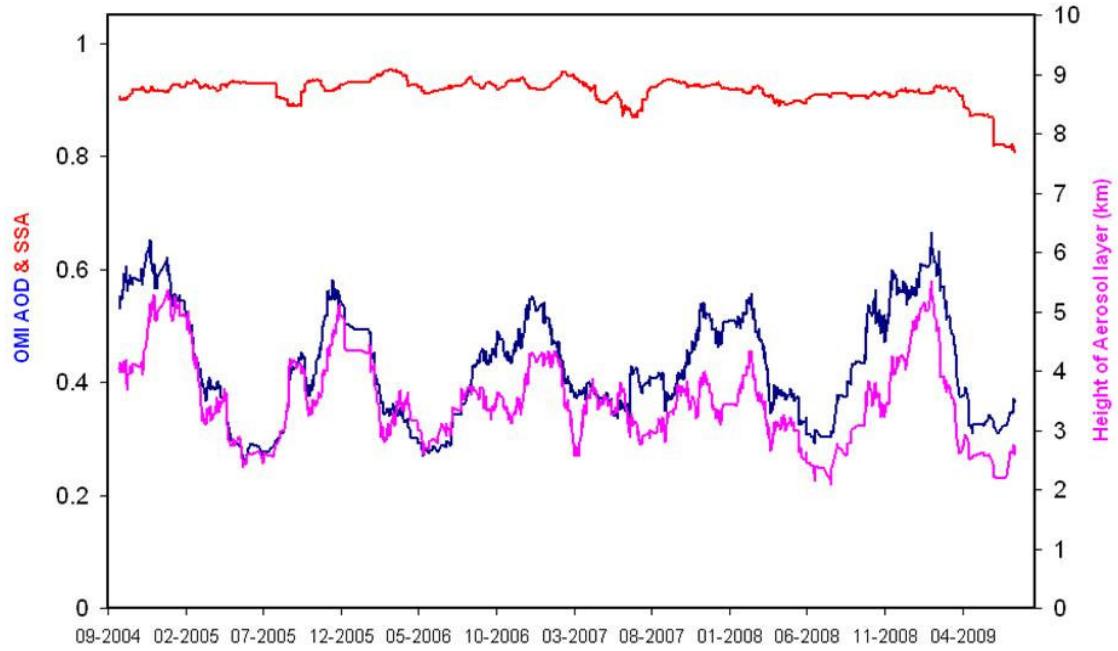

Figure 8.23. 30-days Running average of aerosol content in free cloud days (i.e. cloud cover <0.15) over the Tolonchar area. OMI AOD values are reported in y axis (Blue) together with the SSA (Red); Height of Aerosol Layer (in km) are reported in secondary y axis (Pink).

The vertical distribution of aerosol particles in function of the aerosol optical depth (blue color), and SSA (pink color) are displayed in Figure 8.24, taking into account of the threshold that distinguishes among a light optical extinction by airborn particles intrusion and a heavier one. Aerosols that exceed this threshold reach altitudes from 5500 m up to the stratosphere (at about 12000 m asml) making reference to the satellite Fov mean elevation. Moreover, in the plot we observe that the assumed 0.42 threshold in AOD is really the threshold that could affect the possible astronomical observations in Tolonchar. In fact aerosol with lower AOD values than 0.42 cannot affect the Tolonchar peak with higher values of atmospheric extinction as both they are represented by low-absorbing particles (SSA value near 1) and as they are at lower altitude respect the site elevation.

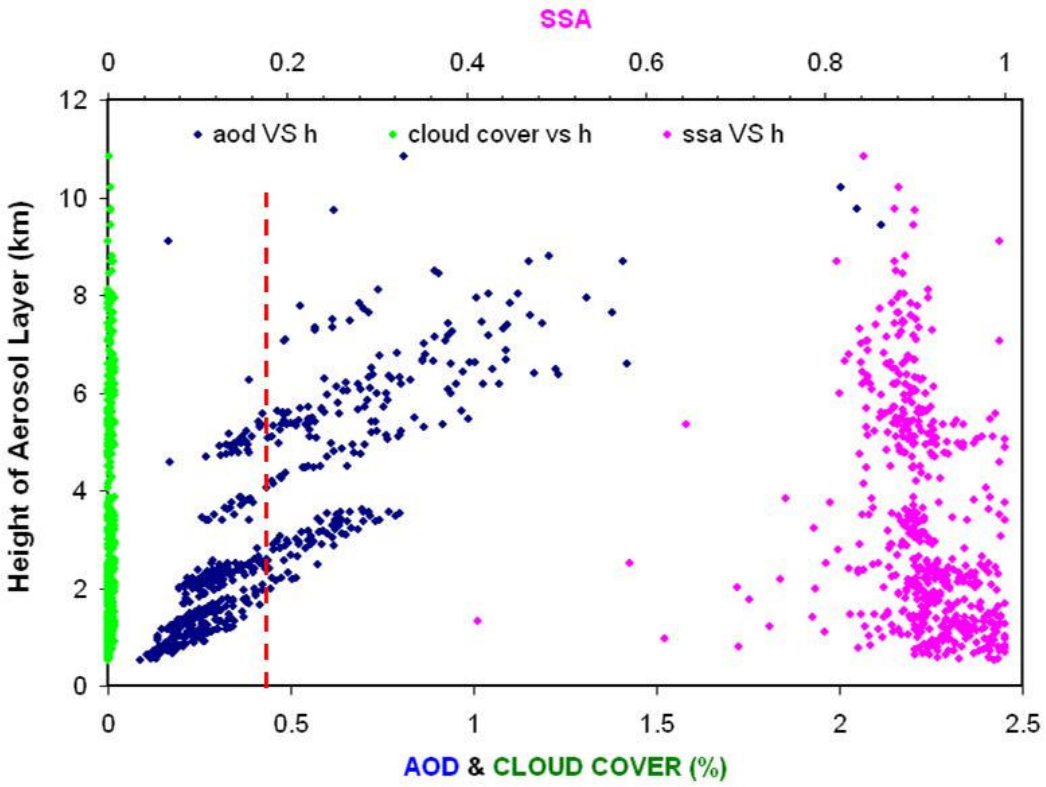

Figure 8.24. vertical distribution of aerosol particles over Tolonchar in function of their aerosol optical depth (blue color-main x axis), vertical distribution of different aerosol type with different single scattering albedo (pink color sexondary x axis). Cloud free scenes percentage of cloud cover less than 2% (green color- main x axis). Red dotted line is the AOD threshold for heavy extinction events.

Studying the possible aerosol sources (Figure 8.25) and the morphological conformation of this site, we make the hypothesis that this stratospheric aerosol load could be probably due to volcanic aerosols emitted by the near Lascar volcano from an altitude of about 5500 m up to the stratosphere, and then slowly gravitationally settled. However the majority of the aerosols load probably come from other nearby sources as the numerous nitrate mines of the zone.

Figure 8.25. Nitrate mines in the Northern Chile near Tolonchar site. Courtesy of Google Earth®.

The reason for this assumption is that particulates can have both primary or secondary sources. In the first case, particulate is emitted from fossil fuel and/or biomass burning (e.g. tipically carbonaceous aerosol and low volatile organic compound VOC) or can originate itself from crostal sources, due to soil erosion and to the wind action. In the second case instead, we have mainly sulphates, nitrate and secondary organic aerosol originated in atmosphere for VOC reaction. Moreover it is important to stress the attention that when we consider fine particulates we have a life mean time, in atmosphere, daily or weekly that makes possible a transport of these particles on regional scale. At the light of these notes, we believe that the most probably sources for the tropospheric aerosols in Tolonchar, are both primary crostal aerosols and secondary nitrate particles. To establish the possible particles provenience more precisely, we look at the dominant wind direction in Tolonchar. As told in the introduction to this chapter, Tolonchar is a site that is now under evaluation through a wide site testing campaign. Some preliminary information have been obtained concerning the predominant wind direction in Tolonchar, these results show exactly the same situation of Chajnantor (near San pedro de Atacama) where wind direction, taken for the ALMA site survey, have been already made available (see Figure 8.26).

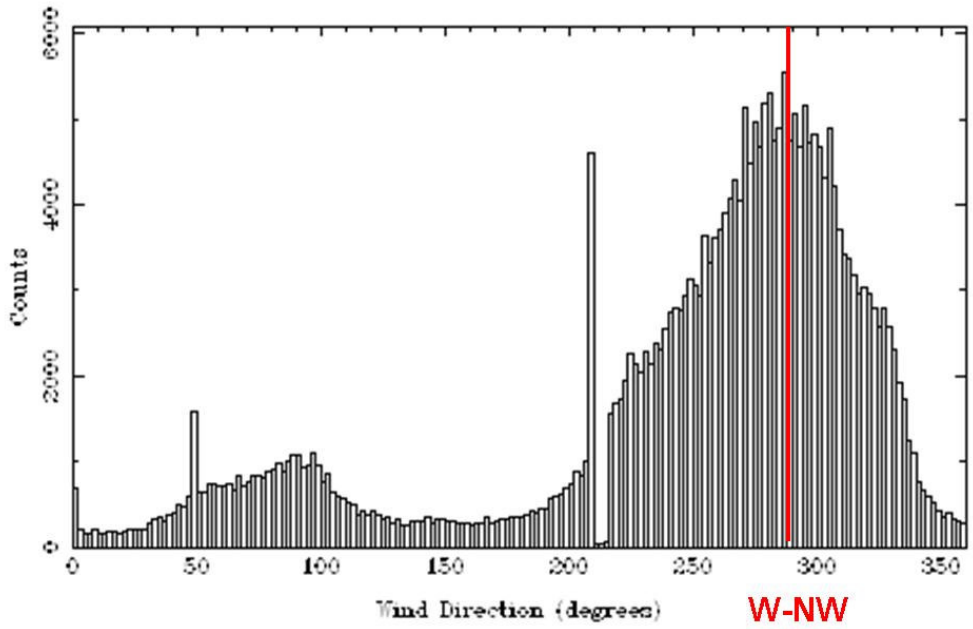

Figure 8.26.Cumulative counts of wind direction (degrees) for Chajnantar site calculated on the period from april 1995 to December 2004 from the ALMA staff. The mode being the West-NorthWest wind direction.

Looking at Figure 8.26, we see that more frequent wind directions blow exactly coming from the directions of all the nitrate mines pointed in the map (Figure 8.25) supporting our hypotesis.

Coming to the seasonal intrusion at Tolonchar, Figure 8.27 shows that the heights of stratospheric aerosols are quite homogeneously distributed over all the seasons. This evidence is concord both with our hypothesis of a volcanic source for stratospheric aerosols, both with the other one of the main particulate sources recognized in nitrate mines. However, we want stress the attention on the summertime major aerosol load at high altitude. In our opinion these events are crostal aerosols. These particles reach such elevations coming from soil erosion thank to the wind action and the increasing convective motions in the hottest season.

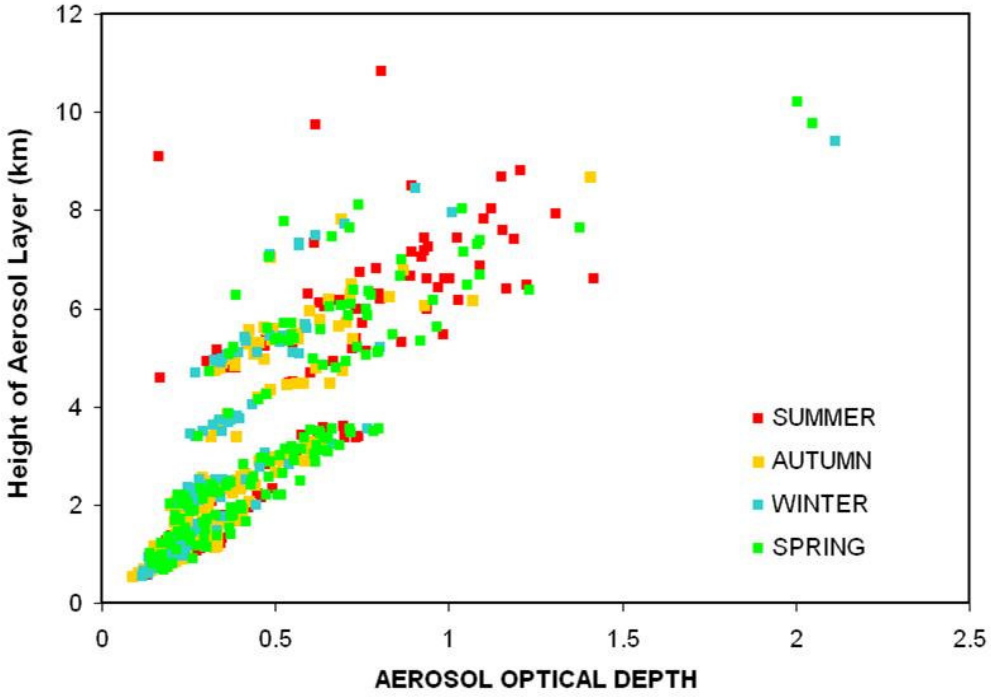

Figure 8.27. Height of the seasonal intrusion of airborn particles over Toloncharl. Stratospheric aerosol show a quite homogeneous distribution over all the season. A major aerosol load, coming from carbonaceous or soil sources, appens in summertime probably due to increasing convective motion in the hottest season.

It is thanks to the greater amount of data for the Tolonchar site that we can perform a more accurate plot also for the AOD, SSA and height of aerosol layer mean tendency during the calendar year (Figure 8.28). The 30-days running average over the OMI six years records (2004-present) gives some specific information concerning the peaks in extinction of aerosol optical depth. They occur mainly during the summer, confirming instead that Tolonchar site for great part of the year has good condition in term of low extinction. In order to quantitatively evaluate the percentage of days with AOD >0.42, we have added to the plot a black curve that it shows as the percentage of this strong airborn particle intrusions increases three times during one or two months in summer and one month in the late spring.

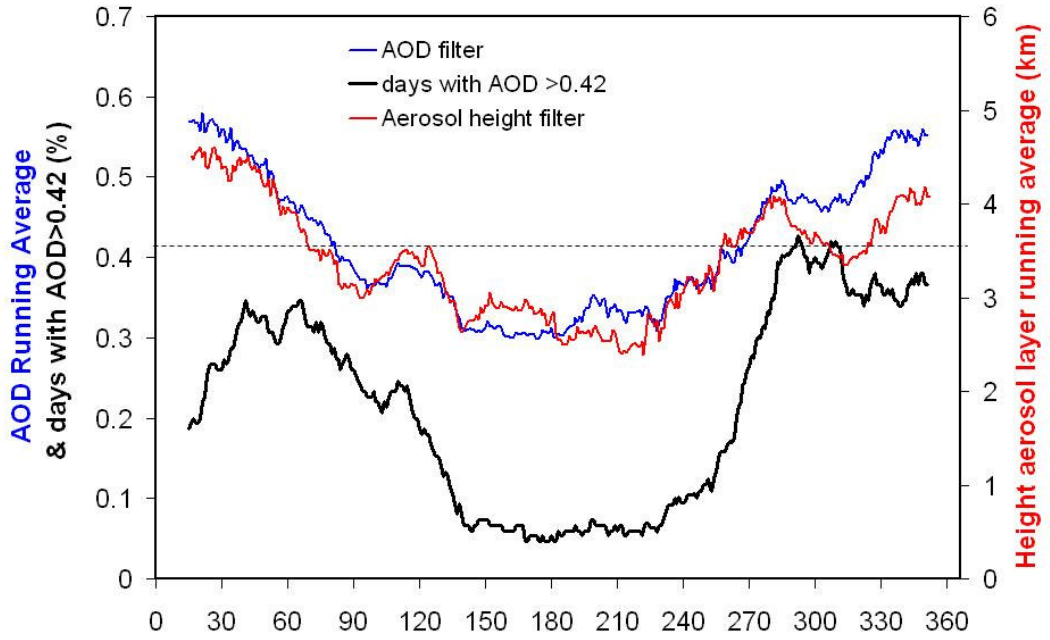

Figure 8.28. Tolonchar height of aerosol layer running average mean tendency (Red in secondary y axis) during the calendar year taking the OMI six years records (2004-present). AOD (Blue, y axis). Percentage of days with heavy extinction episodes (AOD>0.42) are also shown (black line).

La Palma site, Canary Island, Spain.

In Europe, La Palma is the top site for astronomical observations. Althought the Roque de Los Muchachos site has been already taken in exam as case study in the previous section, however, we perform here another analysis based on level 3 data to compare from one hand, the ORM with Chilean astronomical sites using a same methodological approach and from the other hand to test if lower satellite data level bring to different site information.

In Figure 8.10 we presented the site orography for La Palma using the high OMI spatial resolution equals to its IFOV (13 km x 24 km); now using level 3 data, the satellite ground footprint changes becoming large 1° (i.e. about 100 km) in side; for this reason also the mean height of satellite view changes as quoted in Figure 8.29.

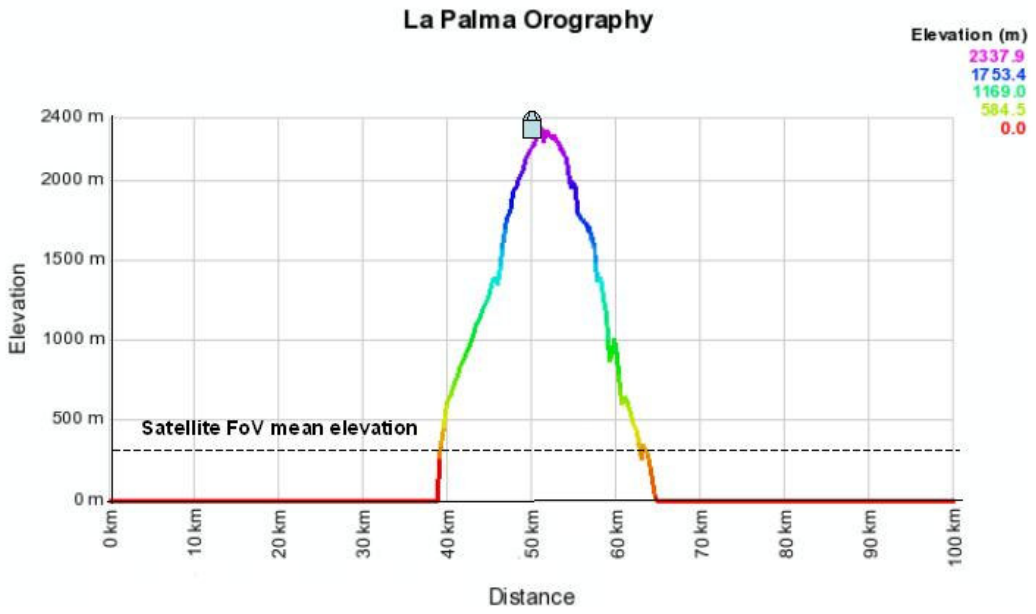

Figure 8.29. Plot of La Palma orography profile at a same latitude. In y-axis the elevation amsl in meter and along x-axis a spatial range since the ocean (in km) is displayed. Dotted line represents the mean OMI FOV centered on the astronomical site at the satellite FOV mean elevation for the averaged level 3 data.

With level 3 data, the satellite larger footprint makes enter in the scene also the ocean and the mean elevation averaged on a such large area becomes of about 350 m asml. The same analysis of that one performed over the Chilean observatories is carried on. Information have now a more local/regional meaning. In Figure 8.30 the vertical distribution of aerosol particles in function of their aerosol optical depth (blue color), their SSA (pink color) and in situ atmospheric extinction are displayed. In this plot we see that aerosol particles reach hights up to 11 km referred to the satellite Fov mean elevation (i.e.about 350 m) getting in some cases over the tropopause. However, if we analyse this result in detail, we see that in comparison with Chilean sites, at ORM we have a low number of airborn particles. This fact is mainly due to the efficient block performed by the 'sea of clouds' that remains below the astronomical site level. The satellite, in fact is not able to distinguish the aerosol below the sea of clouds because when they overlie the aerosols the method of residues used by OMI to retrieve the mean cloud coverage is completely determined by the cloud characteristics as they intercept almost all incident radiation and acts as an opaque 'roof' over the aerosol layer.

Naturally, being our graph limited only to that scenes free of clouds (cloud coverage less than 2%), it shows only days with aerosol intrusion and without cloud presence. In

such situations particles that affect atmospheric extinction (AE > 0.165 red points in major x axis) are in the vertical range between 0.5-6.5 km but only the aerosols above 1.5 km affect the astronomical observations being over the inversion layer. Looking at the single scattering albedo we can also define the aerosol type. First of all, we see that more absorbent particles (i.e. low SSA value) occur when atmospheric extinction values are above the threshold of dusty nights as we expect for, secondly we observe that aerosol into troposphere are mainly carbonaceous less absorbent, visible also from their values of extinction that rimain below the threshold of AE = 0.165.

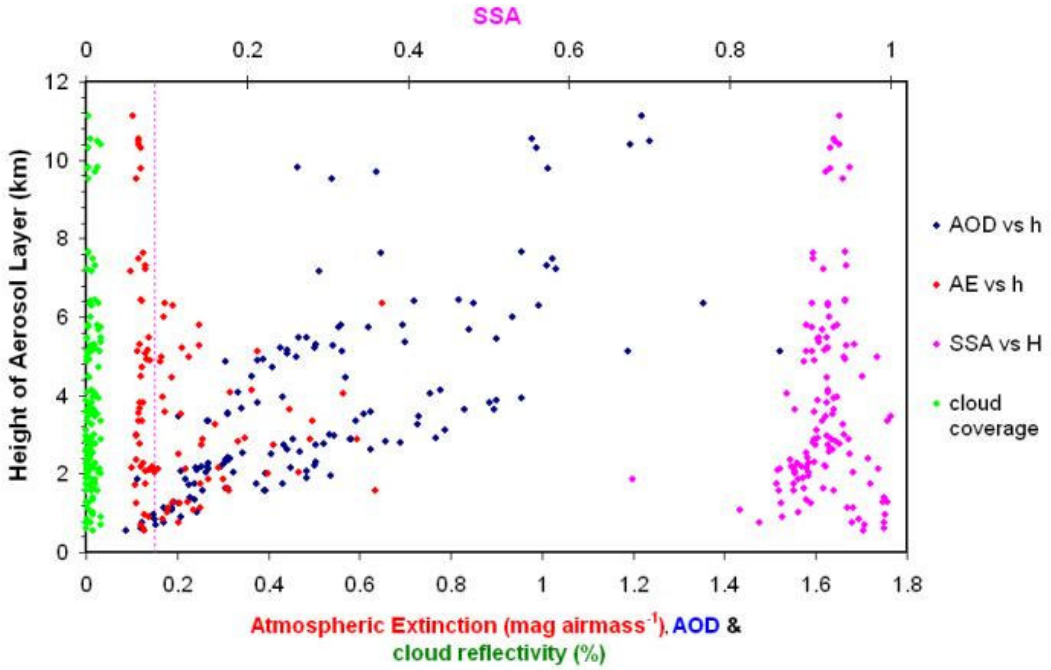

Figure 8.30. vertical distribution of aerosol particles over La Palma in function of their aerosol optical depth (blue color-main x axis), vertical distribution of different aerosol type with different single scattering albedo (pink color sexondary x axis). Cloud free scenes percentage of cloud cover less than 2% (green color- main x axis). In situ values of atmospheric extinction from CAMC (Red color- main x axis) are also added together with the threshold for dusty nights (red dotted line at AE>0.165).

From a seasonal point of view, aerosol intrusions at La Palma (Figure 8.31) show that summer airborn particles are blowed up at very high altitude thanks to the high trade wind that reaches Canary island bringing dust particles from Saharian sources. Much less events occur during winter. This fact is interesting because it is a good test to confirm the high stop potential of the 'sea of cloud' that in wintertime becomes a stronger and efficient sea of aerosol blocking intrusions at lower altitude respect to the astronomical site.

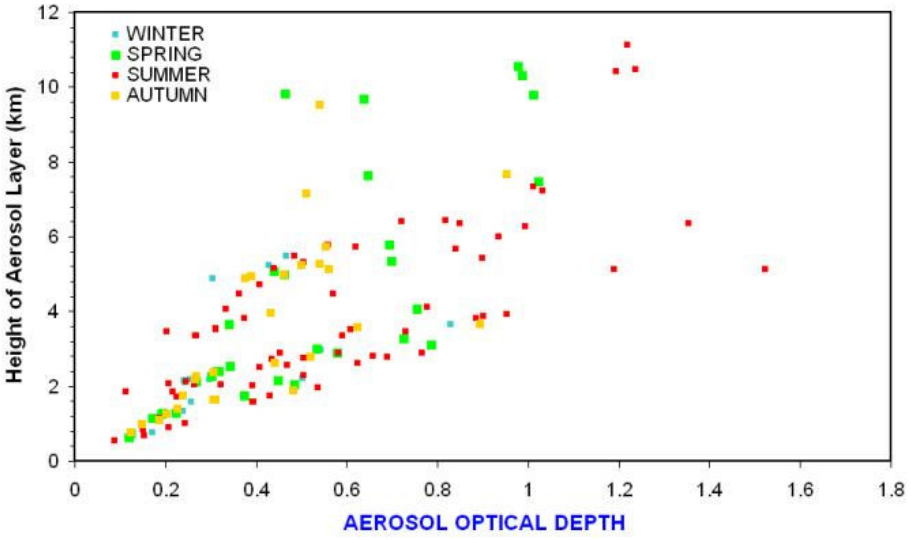

Figure 8.31. Height of the seasonal intrusion of airborn particles over La Palma. High altitude aerosol show a predominance during summertime or spring. Winter intrusion remaining at height lower than 6 km amsl. This plot is a good check for the already know wind circulation over La Palma island with trade wind that in summer reach very high altitude (TL) transporting dust and airmass that persists in the lower mixing layer (MML) during the winter.

This seasonal behaviour is also confirmed by the analysis of the calendar year trend of the atmospheric extinction (Figure 8.32). In this plot, the 1984-2009 monthly mean extinction values in V band (measured in-situ from the CAMC observatory) at Roque de Los Muchachos, show a peak in extinction during July and August and an homogeneous situation of low extinction dusty free night during the rest of the year, confirming that about a mean of 90% of nights in wintertime have good sky conditions for astronomical observations.

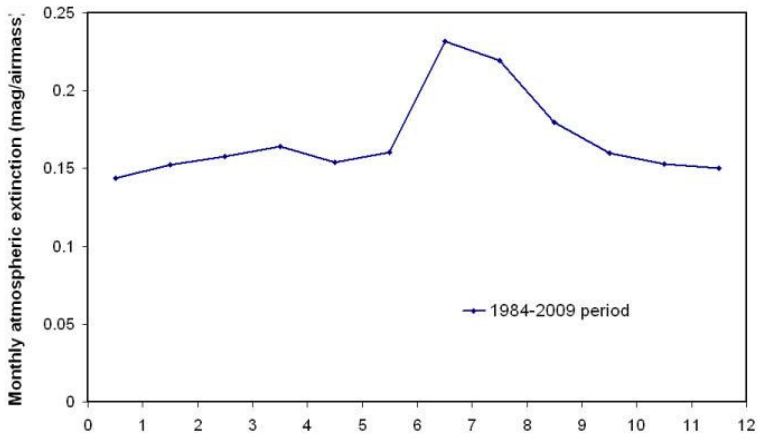

Figure 8.32. Monthly mean Atmospheric Extinction values over a 25-year period (1984-2009) as measured by the Carlsberg Automatic Meridian Telescope at Roque de Los Muchachos, Canary Island, Spain.

Tenerife site, Canary Island, Spain.

We perform here the same analysis on level 3 data for the Izana astronomical observatory in Tenerife, Canary Island. In Figure 8.33 we present the Tenerife site orography with 1° satellite ground footprint and the mean height of satellite view (about 700 m asml).

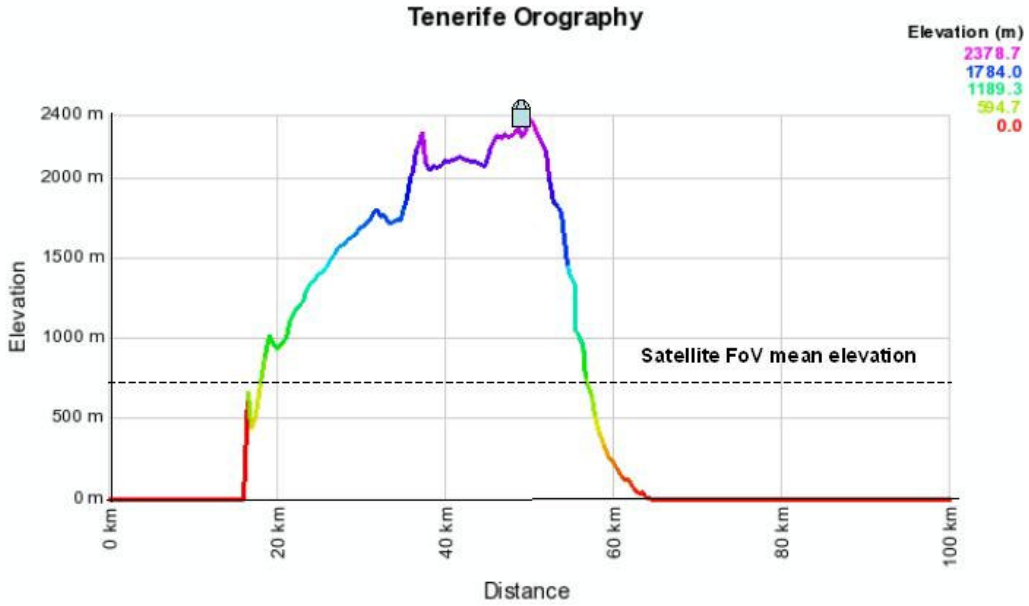

Figure 8.33. Tenerife orography profile at a same latitude. In y-axis the elevation amsl in meter and along x-axis a spatial range since the ocean (in km) is displayed. Dotted line represents the mean OMI FOV centered on the astronomical site at the satellite FOV mean elevation for the averaged level 3 data.

Likewise to La Palma, also in Tenerife, the ocean enters for about 50% in the satellite footprint at ground and this fact must be taken into account in data interpretation. The vertical distribution of aerosol particles (Figure 8.34) in function of AOD (blue color) and SSA (pink color) shows that aerosol particles remain in troposphere. Conditions of extinction for Izana appear very good too because aerosols below two kilometers do not reach the observatories altitude. Below this threshold different aerosol types are detected from the satellite, both aerosol very few absorbent (marine aerosols) and more absorbent particles as carbonaceous and dust. Increasing with the altitude we observe less intrusions, mainly due to carbonaceous particles.

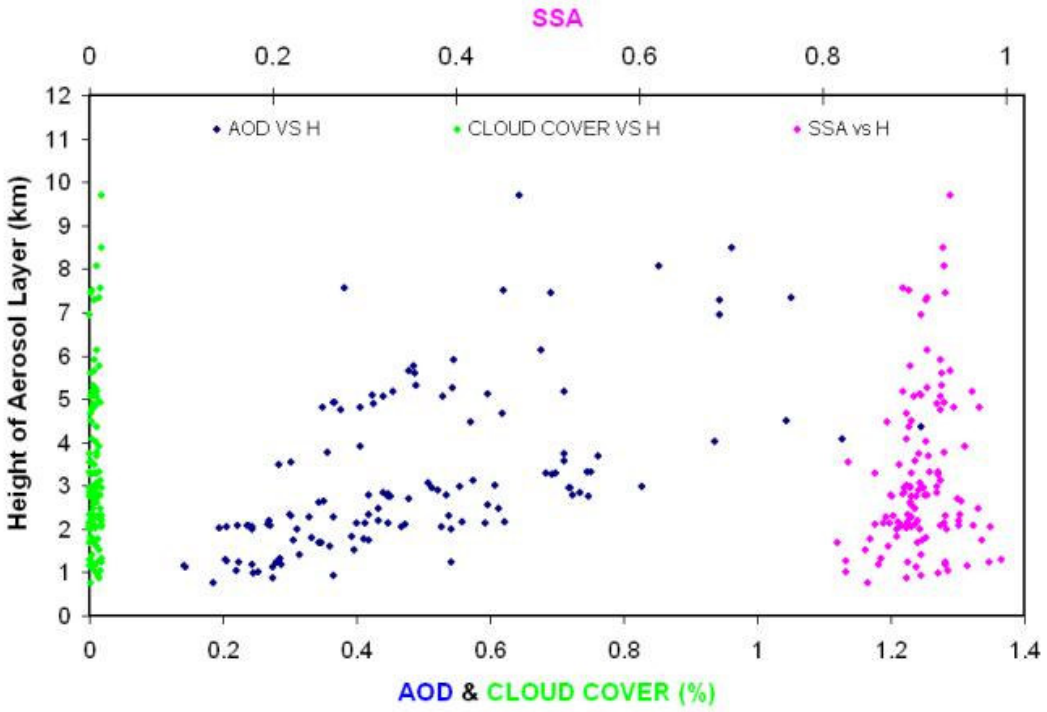

Figure 8.34. vertical distribution of aerosol particles over Tenerife in function of their aerosol optical depth (blue color-main x axis), vertical distribution of different aerosol type with different single scattering albedo (pink color sexondary x axis). Cloud free scenes percentage of cloud cover less than 2% (green color- main x axis).

Looking at the seasons in which aerosol intrusions occur, we observe in this case too a net predominance of summer events above the observatories quote. However, a few winter events still to a quite elevated altitude are observed (Figure 8.35). In our opinion, these intrusions are due to less absorbent marine particles that are blown up to the observatory peak driven and made easier from the steep slopes of the island as evident in La Palma too.

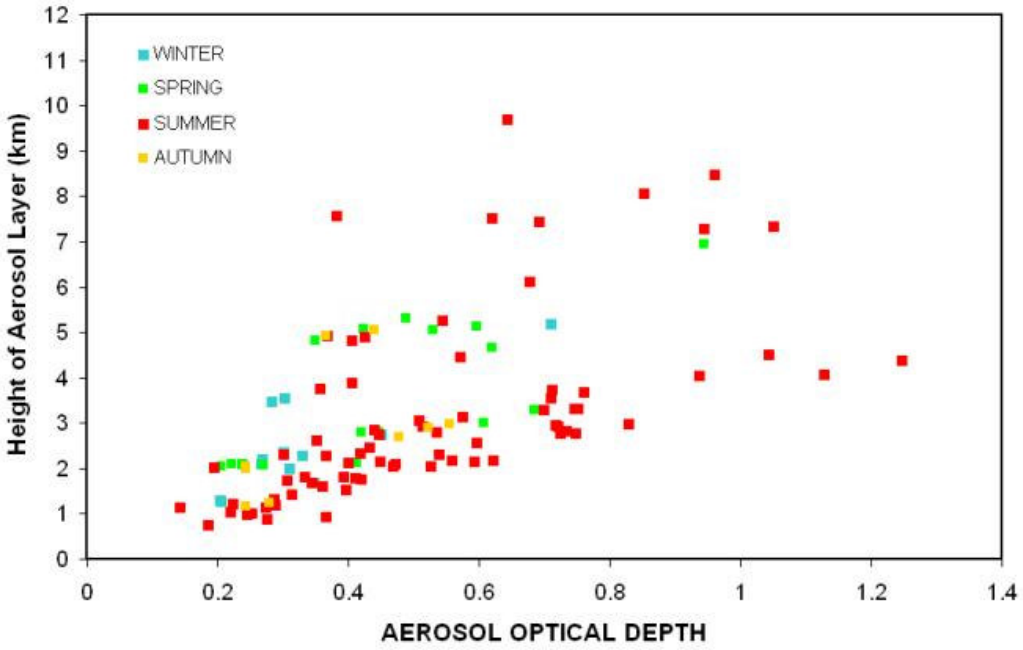

Figure 8.35. Height of the seasonal intrusion of airborn particles over Tenerife. High altitude aerosol show a predominance during summertime. Winter intrusion remaining at height lower than 6 km amsl and at low AOD.

8.4 Evidences and conclusions

From this study, we may draw the conclusions listed below. We have explored the use of other detectors on board different satellites that operate in bands of astronomical interest (the visible and NIR) and with improved spatial resolution than TOMS (Bertolin, 2005). The selected parameters for this study were the AI provided by Aura/OMI – with visible and UV channels and with a spatial resolution from 13 km × 24 km to 24 km × 48 km – and the AOD provided by Terra (from 2000) and Aqua (from 2002) in MODIS – with its 36 spectral bands, from 0.47 to 14.24 μm, with a spatial resolution of 10 km ×10 km. In order to obtain the best spatial, spectral, radiometric and temporal resolutions, we have decided to work with Level 2 data that have the same resolution as the IFOV satellite. From the obtained results we conclude that the OMI instrument detects aerosol presence with more precision than TOMS and does not detect nonabsorbing particles with high atmospheric extinction values (larger than 0.15 mag airmass^{-1}). This fact coincides with expectations because non-absorbing aerosols such as sulphates or marine aerosols do not give high extinction values (threshold greater than 0.15 mag airmass^{-1}). The result in Figure 8.9 shows at Roque de

los Muchacos (Spain) that most of the points fall at lower extinction values below the threshold for dusty nights, suggesting the presence of non-absorbing or weakly absorbing (e.g. carbonaceous) aerosols. In such situation, in order to obtain the limits for dusty episodes on the AOD scale, we have checked the calima days from the records of the Instituto Nacional deMeteorolog´ıa de Canarias Occidental, and we obtain a threshold near AOD > 0.1 units and AI > 0.6 for dusty episodes. We study where the calima events and cloud presence fall in the plot of correlation between atmospheric extinction and AI. Dust episodes measured at ground level, are mainly below the threshold for dusty nights on the atmospheric-extinction scale (K_V < 0.15 mag airmass^{-1}), meaning that the presence of calima affects low altitudes, and that only in a few cases do reach the Roque de los Muchachos Observatory.We also see that all clouds detected for their high reflectivity (greater than 15%) are below the threshold for dusty nights; they are above 0.15 unit in mag airmass^{-1} in only two cases, and in such cases they do not correspond to calima events. The study of Terra/MODIS data has shown that a great number of points fall in a range below 0.40 units for AOD and 0.15 mag airmass^{-1} for K_V, and that two tails are evident: the first one has high AOD values for low K_V and the second has high AOD and high K_V values, showing a large linear correlation between both parameters. It is important to underline that there are only a few points with low AOD values and high K_V (data being decontaminated of cloud presence). Chlorides and marine aerosols can be well identified and normally do not affect the K_V and correspond to AOD < 0.2, so this means that marine and sulphate aerosols are not absorbent as we expect. We can see that most of the points corresponding to dust (calima) events fall below the threshold of 0.15 mag airmass^{-1} because they are detected near the surface. Only in some cases they can reach the level of the observatory, carried by wind or convective motions, providing AOD larger than 0.1 units and K_V larger than 0.15. These measurements correspond mostly to terrestrial aerosols. The study of the Aqua data produces results almost identical to those of Terra. The most populated tail falls below the threshold of 0.15 unit in mag airmass^{-1}. Marine aerosols are more clustered at low AOD values (<0.20) and low K_V (<0.15), whereas terrestrial aerosols fall in the AOD > 0.2 zone. Dusty (calima) days correspond mostly to the presence of terrestrial aerosols and are present near ground level (inside the area of 10 km × 10 km). Only in some cases they reach higher altitudes and become

detectable from the astronomical observations (large K_V); this is the only case that presents a linear correlation between both AOD and K_V parameters.We therefore also need in situ data to distinguish between both situations. At present, the AI and AOD values provided by the NASA satellites alone are not useful for aerosol site characterization, and in situ data are required to study drainage behaviour, in particular at those astronomical sites with abrupt orography as the ORM case.

OMI Level 3 data analysis, although with a lower vertical and spatial resolution, give us several interesting results concerning both the possibility to compare different astronomical sites and searching for exploiting other of new. Thanks a detailed study of the aerosol alghoritm performed by Torres, based on aerosol types a-priori assumptions, we are able to define, for each couple of AI and AOD values retrieved from OMI level 3 data, both the SSA and the height of aerosol layer. In order to best evaluate these results however it is important to perform a study on the site orography to define the site vertical profile from the sea and on the satellite ground footprint and mean altitude in which the level 3 data are reasembled and averaged. After all these data and information are available, it is possible to compare the aerosol load among the different astronomical sites both in term of altitude and typology. We perform such analysis on four among the top world's sites (i.e. La Silla, Paranal, La Palma and Tenerife) and in particular we test this methodology to study a new exploitable ELT site: Tolonchar.

Concerning La Silla we observe that aerosol are found in cloud free days in 2000-8000 m amsl range. Among these intrusions only that one greater than six kilometers can affect the observations. These events taking part mainly during spring and summer.

In Paranal, airborn particles reach a little bit higher altitude than La Silla (i.e. up to 10 km), from data analysis we observe a few number of particles intrusions but with higher AOD values. In our opinion these high particles with elevated extinction values could be a result of a satellite bias. Paranal in fact is nearest to the ocean than La Silla; the sea glint could therefore affect in major part the retrieve OMI method. A more detailed analysis has been performed on Tolonchar in order to obtain as information as possible from OMI level 3 data for this area that is under evaluation as a possible ELT site. Our results are very important and show practically no cloud presence. The aerosol analysis performed here for the first time, shows regular peaks in AOD extinction due to airborn

particles at high elevations. Thanks the possibility to obtain a complete dataset (because the absence of clouds) we are able to estimate the threshold for high extinction events (AOD > 0.42) respect to 'normal' aerosol load. Above this threshold (from 5500 m amsl up to stratosphere), airborn particles intrusion could affect observations. Moreover, in order to search for possible aerosol sources we look at the surrounding area and at the local predominant wind direction. We find that the tropospheric aerosol sources are located in the several nitrate mines of the zone and on crostal erosion being the main wind direction coming from W-NW, instead the stratospheric source remaining the near active Lascar volcano. Finally the same analysis with level 3 data was performed also over the Canarian observatories of ORM and Izana, showing that in both sites it exists a very efficient inversion layer that, above all during winter, avoid airborn particles intrusion at the observatories quote, however ocasionally in summer, due to the higher Trade wind, some dust episodes reach the astronomical sites.

Chapter 9

A Thirty-year satellite records of cloud climatology from TOMS and OMI observations

Contents

9.1 The Impact of clouds on UV/visible measurements: measurement technique and cloud effects
9.2 A thirty-year satellite record of cloud climatology from TOMS and OMI observations
9.2.1 Cloud cover over the world's top astronomical site and its possible correlation with atmospheric and oceanic circulation
9.2.2 Photometric nights percentage on La Silla and Pranal: comparison between in situ and satellite measurements
9.3 Evidences and conclusions

In this chapter we analyse cloud climatology from satellite. We base our study on one of the longest dataset retrieved from satellite, using the Total Ozone Mapping Spectrometer onboard of Nimbus 7 and Earth Probe platforms and the Ozone Monitoring Instrument onboard of Aura. This chain of instruments is reliable for such data analysis because all instruments use the same method to measure cloud properties in the UV/visible range.

The first question we try answer to is concerning on what a satellite see from space. In the UV/visible spectral region, the satellite Earth's view is dominated by clouds, surface reflection, scattering on aerosols (visible from space as 'haze' on the Earth's surface) and molecules and atmospheric absorption. To have an idea of what it happens in the atmosphere without clouds and how much it increases the complexity of the phenomena with clouds presence we observe the radiative transfer phenomena in atmosphere (Figure 9.1).

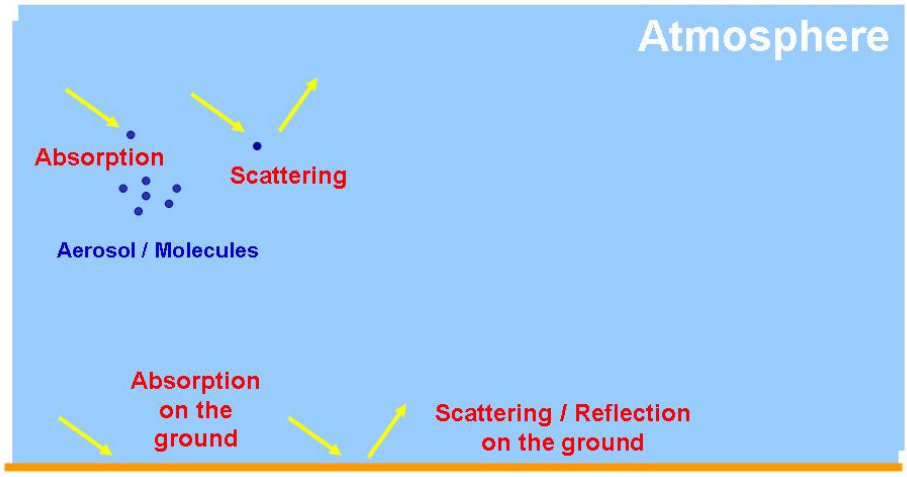

Figure 9.1 a) Radiative transfer in cloud-free atmosphere.

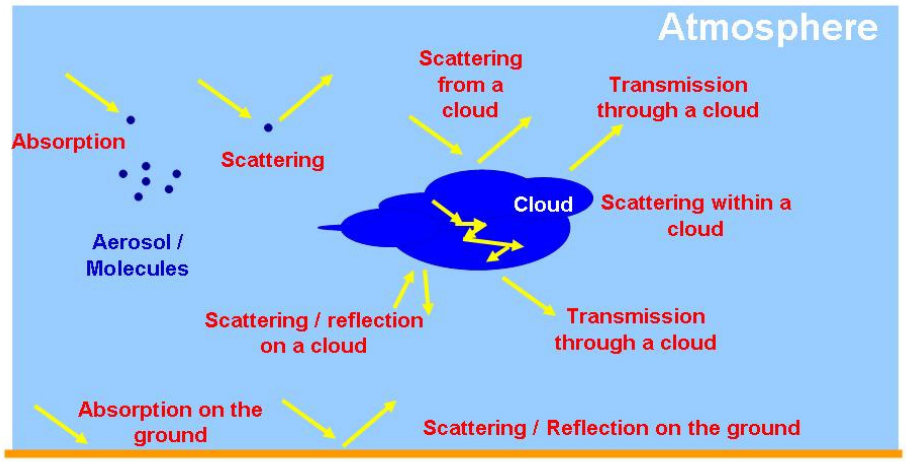

Figure 9.1 b) Radiative transfer changes when a cloud is present.

Naturally, as already mentioned, the reflectivity dependence with λ (i.e. the spectral albedo measured from satellite) changes if we consider different scenes on ground. For example the spectral albedo measured in 300-800 nm range follows well the Rayleigh scattering law ($\sim\lambda^4$) if measured over the ocean. When a satellite observes over vegetazion instead, the spectral albedo differs from a Rayleigh scattering at larger wavelength, increasing the reflectivity at 700-800 nm (colour of the surface) to the same UV values. When satellite looks at scenes over the desert the spectral albedo does not have only the same increased reflectivity of the vegetation (colour of the surface) but also an homogeneous higher threshold (both in UV than in visible) in reflectivity due to the surface brightness. Finally if satellite observes a 'roof' of clouds it has both brightness and whitness phenomena that bring reflectivity to a constant threshold for all

the spectral range taken in exam. Some important considerations can be therefore summarized concerning the albedo effect:

- In the UV/visible, the surface reflectivity is low with the exception of ice or snow
- In the presence of clouds, the instrument receives a much larger signal
- Cloud reflectivity depends on cloud droplet size and optical depth, but only weakly
- Even a small cloud can dominate the signal over dark surfaces (i.e. ocean)
- When clouds are present, the wavelength dependence changes completely (white).

From a theoretical point of view it is important also remember that over dark surfaces, the signal is dominated by a large Rayleigh scattering contribution, that is polarized (i.e. it depends on scattering angle). Cloud contributions are instead mainly from Mie scattering and therefore not polarized.

Another important consideration is concerning the light path effects when clouds are present. As visible in Figure 9.1b, within clouds, light paths can get very large. In this case two different observation are detected if taken ground or satellite-based. Observed from the ground, any photon coming from a cloud has experienced a very long path within the cloud, instead observed from space, most photons coming from a cloud have penetrated the cloud only weakly.

9.1 The Impact of clouds on UV/visible measurements: cloud effects and measurement technique

At the light of all these theoretical information we try to understand both how clouds impact the satellite instruments and how clouds impact the measurements. Besides the effects described above, clouds also can have 'technical' effects on satellite measurements. For example, three main cases are:

- broken cloud fields may illuminate the instrument slit inhomogeneously and distort the instrument function or wavelength alignment.

- clouds also change the spectral distribution of the incoming light, generally by enhancing visible /NIR radiation relative to UV radiation.
- broken cloud fields, finally, change intensity rapidly and as read-out of linear detectors is often sequential, changes in intensity can distort the spectral shape of the measurements.

More important is the direct impact of clouds on the retrieval, to make some instances, these impacts could be changes in the spectral composition of the signal, or changes in the sensitivity to different cloud altitudes in the atmosphere. Another cloud impact is for instance the shielding effect that consists on the fact that an absorber (for example an aerosol layer) situated below a cloud is basically 'hidden' from the satellite view. Usually this effect is larger than expected from the geometrical size of the cloud because of its brightness.

The main cloud properties be measured in the UV/visible, one would like to know for retrieval, usually are cloud fraction, cloud top height or cloud top reflectance. The methodology nowadays available from satellite remote sensing measurement are quite different:

- Intensity methods: the basic idea below this approach is that, clouds are bright, instead the surface remains dark and therefore after correction for Rayleigh scattering and surface reflectance, the intensity can be assumed to be proportional to the cloud cover. This method appears simple, however some problems remain unsolved as the snow and ice interference, the assumption that must be made on cloud albedo (e.g. all clouds have same reflectance) and the accuracy that must be used to retrieve surface reflectance in order to estimated correctly the low cloud fractions scenes.
- Colour methods: the theoretical approach here is that clouds are white instead surface is coloured, so after correction for surface reflectance and Rayleigh scattering, distance from 'white point' can be assumed to be proportional to cloud cover. Weak points being the same as before.
- Absorption methods: here the basic idea is that for some species with differential absorption in the UV/visible (O_2), the vertical distribution in the atmosphere is

known and it remains relatively stable. Thanks these features, the expected signal for different cloud fractions and cloud top heights can be modelled. From the models, a comparison with satellite measurements provides estimate for cloud fraction and cloud top height. However in these case too remain problems of snow/ice interference, of surface reflectance estimate and of the assumption that has to be made on cloud optical depth.

- Raman scattering method: the theroretical concept at the base of this technique is that most Raman scattering (i.e. inelastic scattering, source of the Ring effect, with intensity proportional to Rayleigh scattering) takes place in the lower troposphere and in presence of clouds, its relative contribution is decreased. It can be determined from Ring effect and compared to a model. The same problems already described are detected with this method too together with the assumption that has to be made on cloud albedo (e.g. all clouds with the same reflectance).

An other useful note to point out before passing at our data analysis is the search of a possible method for cloud screening because cloud contamination of a large part of UV/visible satellite measurements from space. The idea commonly used is to use only measurements without cloud contamination instead to apply some corrections. Naturally one problem is that there are only very few cloud free measurements (as shown in the Chapter 8 aerosol data analysis over completely cloud free scenes). Finally a more pragmatic approach to the cloud screening is the relax criterion to 5%, 10% or 20% cloud cover.

9.2 A thirty-year satellite record of cloud climatology from TOMS and OMI observations

In this chapter we use a dataset of more than 30-year of satellite data to analyse the cloud climatology over the top world's astronomical site of La Silla, Paranal, La Palma and Tenerife looking at Tolonchar to retrieve some useful information as case study too. A collection of a such large dataset has been made available for the first time in this thesis, thanks a sort of sattelite chain using the same theoretical methods to retrieve cloud fraction values. This dataset continues still today thanks the OMI products.

The presence of clouds is an important piece of information needed in the OMI trace gas and aerosol retrieval algorithms. Clouds strongly change the atmospheric radiation field as compared to the situation of a clear sky, and shield tropospheric species from observation (e.g. Koelemeijer et al. 2003). The effective cloud fraction retrieved by OMI, is a combination of the "true" cloud fraction and cloud optical thickness, In principle, this cloud information may also be obtained from meteorological satellites or MODIS on-board Aqua, with higher spatial resolution than OMI. However, by retrieving cloud information from the OMI reflectance data itself, optimal co-location, on-line availability, and independence from other data sources are achieved.

The standard techniques for cloud detection in satellite meteorology make use of visible and thermal infrared (IR) imaging (e.g. Rossow and Garder, 1993). The cloud fraction is determined from the contrast between clouds and the underlying surface. The cloud top pressure is usually derived from the thermal IR brightness temperature of the clouds: high clouds are colder than low clouds. Since OMI observes only UV-visible radiances up to 500 nm, IR methods cannot be used. Instead, a method build on the heritage of cloud detection developed for TOMS is used. The main cloud parameters retrieved from OMI are the (effective) cloud fraction. The cloud fraction is determined such that the average top of atmosphere reflectance over the fit window is reproduced with a Lambertian reflector. The retrieval of cloud fraction c is based on the contrast at TOA between a clear sky scene and the cloudy scene:

$$c = (R_{meas} - R_{clear}) / (R_{cloud} - R_{clear}) \qquad 9.1$$

Here R_{meas} is the measured reflectance, R_{clear} is the reflectance for clear sky, and R_{cloud} is the calculated reflectance of a completely cloudy pixel. Here a Lambertian reflecting cloud with albedo 0.8 is assumed. The clear sky reflectance of the pixel should be calculated or determined from a surface albedo database (for example based on a time series of minimum reflectance data).

For the effective cloud fraction of OMI, large differences may occur of snow and ice surfaces. The term "effective" in OMCLDRR cloud fraction are meaning that the cloud fraction does not represent true geometrical cloud fraction (especially in the case of multiple cloud layers). The effective cloud fraction is based on gross assumptions about the cloud and ground reflectivities. The intensity method used remains with some

undesirable features, as told before, that are significant sensitivity to non-Lambertian behavior of clouds and ground including cloud shadowing, and non-Lambertian behaviour of the surface (for example, the case of the sea glint), and problems with the model in the presence of thin/broken clouds. Under low cloud fraction conditions (< ~0.3), sea glint for example, can cause erroneously high values of retrieved reflectivity and low values of cloud pressure. Over snow/ice scenes, instead, the processing quality flag assigns to cloud fraction a reflectivity equals to 1.

The radiative transfer model assumes that clouds are plane parallel and homogeneous, i.e., it doesn't account for broken, multi-layer or mixed phase clouds. This error is the principal source of noise in comparing satellite measurements with ground-based instruments. The OMI surface UV irradiance represents the spatial average over the OMI footprint.

The main aim of the OMI cloud product is correction for cloud effects in trace gas and aerosol retrievals. From experience, using the TOMS reflectance data, it has been shown by P.K. Bhartia , that the ratios between the TOA reflectances at 340 and 380 nm for a large set of cloudy pixels can be well explained by assuming a Lambertian reflector with albedo of 0.75-0.80 for the clouds, and with varying cloud fraction between 0 and 1. Apparently, a spectrally gray Lambertian reflector suffices to represent the general shape of realistic cloudy spectra. Therefore, in the OMI algorithms clouds are assumed to be Lambertian reflectors with a high albedo (usually 0.8). So, in the case of broken clouds, a pixel is assumed to consist of a clear and a cloudy part. The Lambertian reflector model with high albedo is also called the thick cloud model. It means that all radiance due to clouds in the pixel is assumed to be caused by fractional coverage with a cloud of albedo 0.8. The retrieved cloud fraction is called the effective cloud fraction. From TOMS experience with pixel areas of a few hundred km^2, we know that a pixel-averaged cloud albedo of 0.8 is about the maximum that occurs. Therefore, the retrieved effective cloud fraction for OMI will lie between 0 and 1. For most cases, namely clouds over dark surfaces like ocean (dark in the visible) and vegetation and soil (dark in the UV), the thick cloud model works well. For clouds over bright surfaces like snow and ice, some algorithms need another cloud model, in which the cloud fraction is assumed to be one, but the cloud optical thickness is allowed to vary. This is called the thin cloud model, in which a cloud is assumed to consist of

scattering particles, and the interaction between light transmitted through the cloud and the highly reflective surface is incorporated. In this model the cloud optical thickness (which can be large) is retrieved, and should be used in the cloud correction methods of the trace gas algorithms. The OMI surface UV irradiance algorithm consistently uses this cloud model for both low and high reflecting surfaces.

9.2.1 Cloud cover over the world's top astronomical site and its possible correlation with atmospheric and oceanic circulation

In this paragraph we analyse the thirty years level 3 dataset from Nimbus 7, Earth Probe, Meteor 3 and Aura satellites. Results give us a very interesting view of the cloud cover trend over La Silla, Paranal, Tolonchar, La Palma and Tenerife sites (Figure 9.2) and of some possible correlations with atmospheric and oceanic events as the case of El Nino in the Chilean coasts. Wavelet analysis searching for evidences of precise periodicities is also performed on the base of the results from satellite.

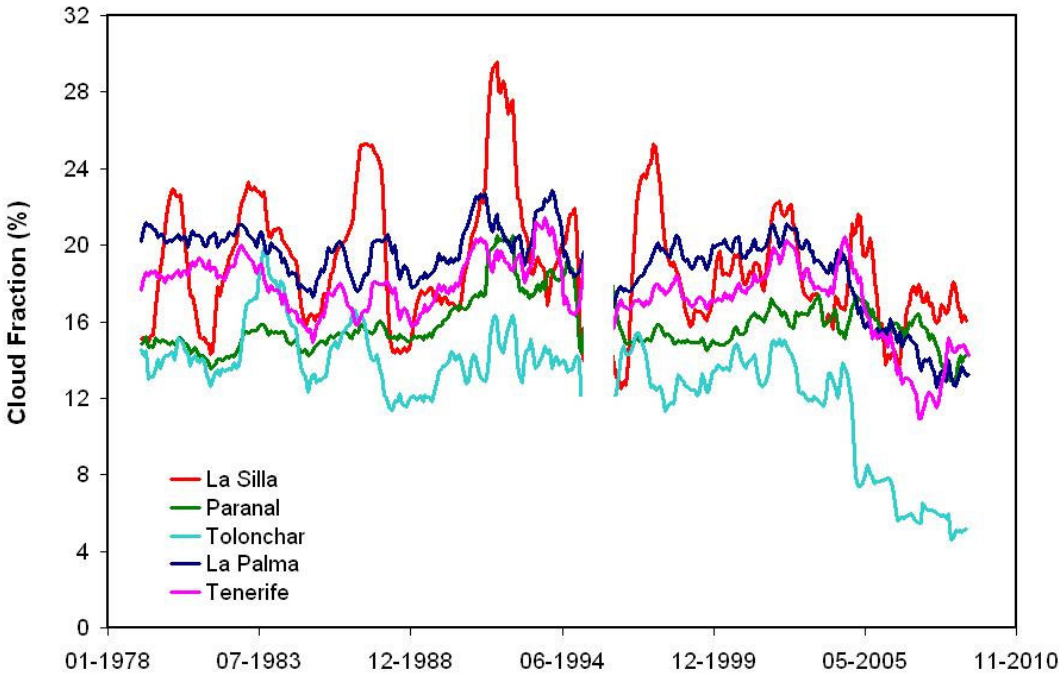

Figure 9.2. Comparison of a thirty –year dataset of satellite cloud cover over four astronomical sites: La Silla (red), Paranal (green), La Palma (blue), Tenerife (pink) and the Tolonchar site (cyan) under evaluation for ELT. Data are represented as 12-month running average.

Figure 9.2 shows that cloud fraction monthly average of all sites together is limited into a 12-30 % range. If we look separately each site we conclude some interesting features.

La Silla (red line) for example, is that site that shows the most marked peaks in cloudiness with a quite regular periodicity that at first sight appears in each 3-4 years. While during the period 1978-1997, La silla had the larger fraction of clouds, a change in the cloud fraction oscillation from 1998, has adjusted this site to the other sites mean trend. Over the whole 30-year, La silla has kept constant its mean cloud fraction level except for a sligth increase in 1992-1993 and for the presentday decresing trend. *Paranal* (green line) shows a low and constant cloud fraction. It appears as the site with the most homogeneous behaviour over these last thirty years as the cloud fraction monthly mean values are consolidate to 16% level except for the little peak during 1992-1994 and the light nowadays decreasing trend. In comparison with La Silla, Paranal has up to 10% less cloudiness in average per month and moreover it does not show large periodicities or oscillation with time.

Tolonchar (cyan line) in figure 9.2 is the site with the persistent lower monthly mean cloud fraction among all the areas here taken in exam (about 13% in average). Its trend appears more similar to La Silla than to Paranal, because it shows peaks analogous occurrences as in La Silla also if with a damped variability. The most interesting feature for Tolonchar, is the strong decreasing trend from the end of 2004 until presentday that need of further investigations as we will see later on.

La Palma (blue line) mantains a quite low cloud fraction (about 20% in mean), perfectly comparable with Chilean observatories, or better from one hand it seems a sort of running average with a high step of La Silla peaked values because it follows in a very strict way La Silla long period trend; from the other it runs side by side with Paranal monthly mean cloud values, except for the 1978-1983 period in which the difference was slightly greater and except for the last four years where La Palma shows a major decrease in cloud fraction respect to Paranal trend. In our opinion this feature appears very interesting because in spite of the distance, the completely different geographical location, and orography, on long-term trend La Palma seems to have some common features with Paranal and in long term mean with La Silla too. This fact could bring to some hypothesis on global scale atmospheric circulation but they are not our aim, however the information stored here is that on long term average the increasing or decreasing trend in cloud fraction is followed side by side from sites on different hemispheres at thousands chilometers of distance.

Tenerife (pink line) shows exactly the same features pointed out for La Palma, the only one additional information being a difference of about 3% in cloud fraction average respect to La Palma.

To understand the reason of the Tolonchar large cloud cover reduction and of nowadays decreasing trend, clearly evident in all the astronomical sites, we perform a test to evaluate the homogeneity of our 30-year satellite datasets. Our suspect is that this decrease in cloud fraction could be due to an instrumental change. To confirm our hypothesis we use the very simple cumulative values (CV) test. For each site we calculate the cloud fraction cumulative values day by day and we compare the resulting cumulative series one with the other. If one site changes respect to another one, this CV test, will show a change in level with a slope variation. The ideal situation would be a 30-year period sole slope also during different instrumental satellite passages. Instead if some changes in slope occur at the interface of two different satellites, it means that a discontinuity, due to the instrumental change is present. In our case the discontinuity can be dictated by different spatial, spectral or vertical resolution, the alghoritm to retrieve cloud fraction being remained the same over the whole analysed period. Looking at the results for the Chilean sites, in Figure 9.3 we observe different slopes for each single cumulative values series.

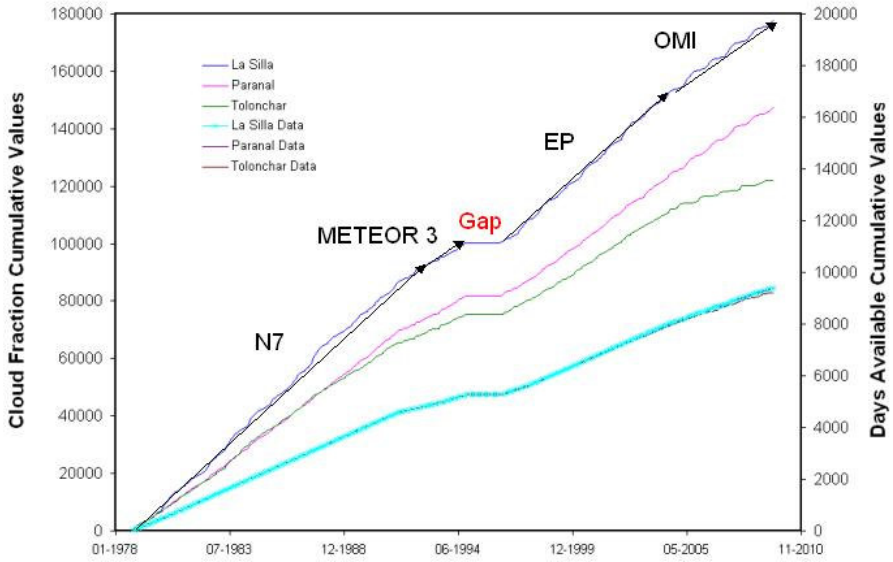

Figure 9.3. Cumulative values test to recognize possible dishomogeneity in 30-year satellite dataset. A discontinuity is detected by the test as a change in slope, a gap as constant values over time. A comparison is performed among the Chilean site: La Silla (blue), Paranal (pink) and Tolonchar (green).

In the plot we have highlight La Silla dishomogeneities with several back arrows to explain the causes of these discontinuities. La Silla cumulative series is exemplificative of all the other Chilean sites too. We see that the changes in slope occurs when the satellite instrument is changed and it easy to distinguish the chain of satellite in time from these different slopes. However, some additional interesting features for each site are evident, as the equal slope of Nimbus 7 and Earth Probe, a true discontinuity with Meteor 3 and OMI passage. To detect if all the sites were subjected to the same discontinuities, we must look at the angle between the previous and the subsequent slope in each series, if this angle is the same for each site it means that the dicontinuity has the same source, otherwise if this angle in comparison with the other sites changes differently in value or in time, it means that additional factors are involved into the discontinuity. This is for example the case of Tolonchar during OMI satellite data usage. The same analysis was performed for Canarian observatories too with the same results (see Figure 9.4).

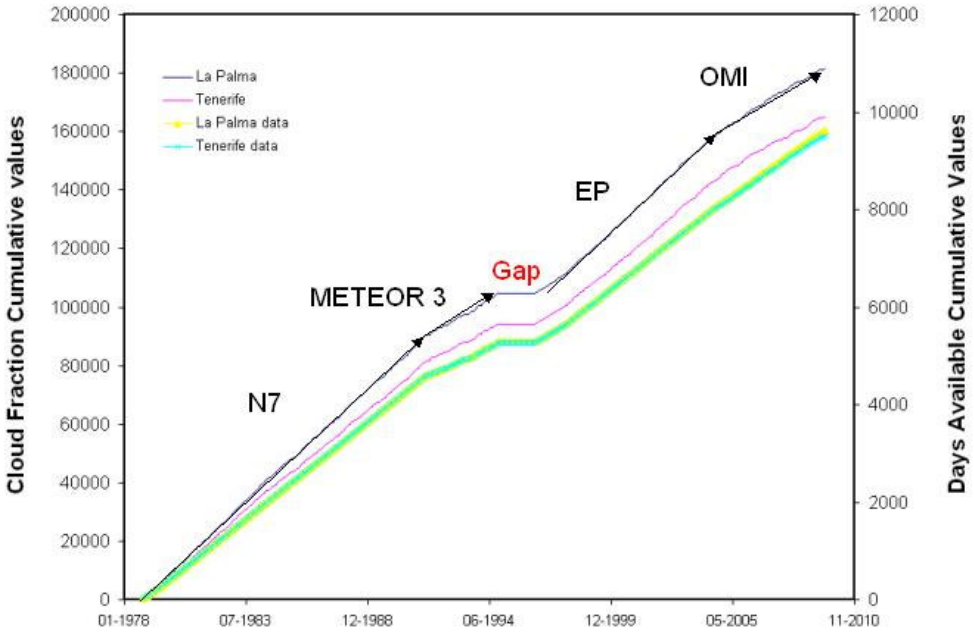

Figure 9.4. Cumulative values test to recognize possible dishomogeneity in 30-year satellite dataset. A discontinuity is detected by the test as a change in slope, a gap as constant values over time. A comparison is performed among the Canarian observatories: La Palma (blue) and Tenerife (pink).

It is necessary to make a further step to know the possible additional dishomogeneity source in Tolonchar since the end of 2004. For this reason we perform a seasonal cloud

cover analysis to eveluate if this discontinuity occurs predominantly during a precise season. In Figure 9.5 we distinguish between summer (red), autumn (orange), winter (blue) and spring (light green) mean cloud fraction. In the graph, from 1978 to 2004, the cloudiness trend has the same seasonal levels, with higher peaks in summer and winter and lower during spring and autumn. However the result retrieved from this plot appears very interesting since the end of 2004. Since this point the seasonal trend over Tolonchar changes completely. The reason must be found in the use of the OMI instrument data as just explained in Figure 9.3. However Figure 9.5 makes clear that OMI works perfectly in comparison with the other instruments during summertime but not in the other seasons. The reason of this satellite seasonal discrimination in cloud coverage retrieval is to search in the orography and geographycal location of Tolonchar.

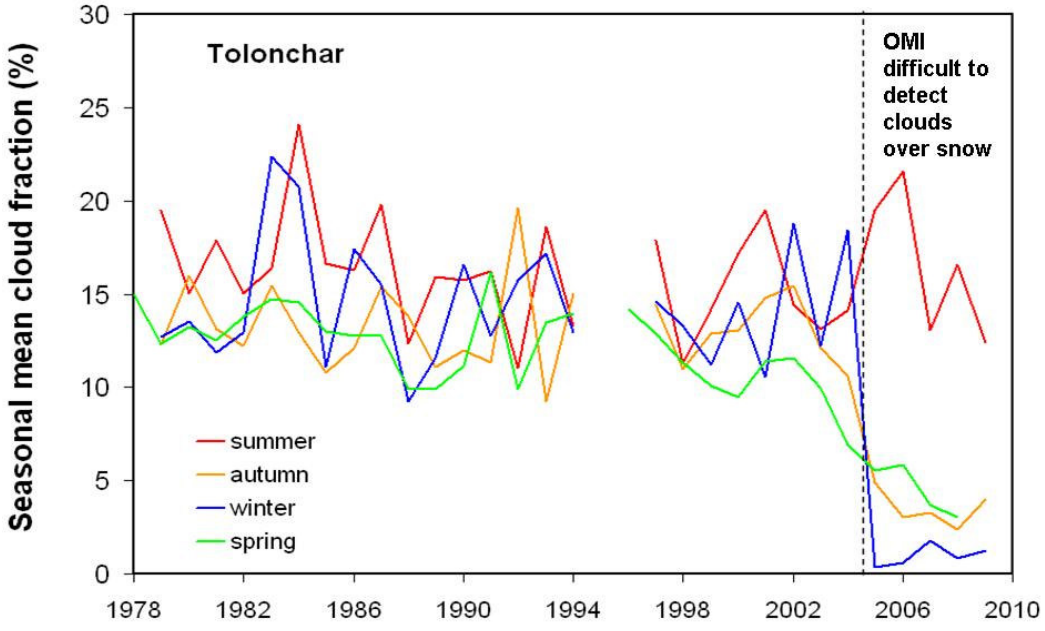

Figure 9.5. Tolonchar seasonal mean cloud cover fraction. Summer (red), autumn (orange), winter (blue) and spring (green). A discontinuity in seasonal trend is evident at the end of 2004 (black dotted line).

Tolonchar, as well as the other Chilean sites, are located in the Atacama desert. Much of Atacama desert extends from the cost up into the Andes mountains and is very high in elevation. The Atacama is actually a pretty cold place, with average daily temperatures ranging between 0°C and 25°C. The annual rainfall that defines it as the driest desert in the world is about 1mm/year. One reason for desertification is that the high atmospheric pressure in this region over the Andes can cause dry, cold air from the upper altitudes.

This dry air has almost no water vapor so it can be easily heated by the sun, causing high ground temperatures with very low humidity.

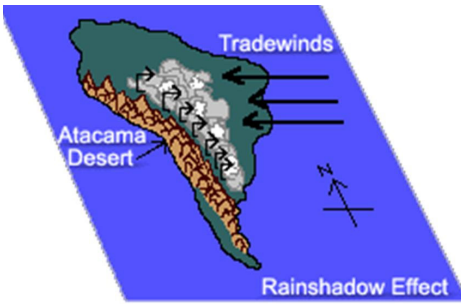

Figure 9.6. The Atacama desert (Chile) and a phenomenon called rainshadow effect that is one of the reason that the Atacama doesn't get enough rainfall.

Another reason that the Atacama doesn't get enough rainfall it is because of a phenomenon called rainshadow. The warm, moist tropical air that blows on the tradewinds from the east, which douse the South American rainforest, get hung-up on the east side of the Andes. The mountains are so high in altitude that the air cools, condenses and rains (or snows) on the mountains. As the air descends the other side of the mountain range it warms, holding in its moisture preventing rain from falling on to the ground below. Even though Atacama gets almost no rainfall, there is water in this arid place under different forms as salt lakes, fog, snow or underground water. To understand the source of OMI lack of data, we evaluate both sources that, for their high reflectivity values, could be flagged as wrong from the satellite or some possible reasons for a real true climatic decrease in cloud cover. Sources for high reflectivity values can be respectively.

Salt lakes: In some lakes in the Andes mountains, such as Atacama, more water is lost through evaporation than is replaced by rainfall so the lakes are drying up. As the water evaporates, the mineral salts in the water become more concentrated, creating very salty water.

Camanchaca: Some locations in the Atacama do receive a marine fog known locally as the Camanchaca, providing sufficient moisture for hypolithic algae, lichens and even some cacti. But in the region that is in the "fog shadow" of the high coastal crest-line, which averages 3,000 metres height for about 100 kilometres South of Antofagasta, the soil has been compared to that of Mars. Most of the precipitation that comes to the Atacama is in the form of fog that blows in from the Pacific. Fog is essentially very low

clouds, consisting of water vapor cooling and beginning to condense. When the air temperature reaches dew point the water vapor in the air condenses to leave little droplets of water behind.

Snow: In the higher elevations when precipitation comes to Atacama snow falls instead of rain. There are small patches of unmelted snow in the mountain tops where it never gets warm enough to melt the snow.

We analyse in detail these possibilities for the Tolonchar area. The very high presence of salt lakes in this area could affect the satellite reflectivity data. The flat area of clay, slit or sand encrusted with salt that forms in arid lands with evaporation is known as a playa. Water evaporating in closed basins precipitates minerals such salts (sodium nitrate and sodium chloride) and borates. However if it was the cause of OMI trend, it would be marked more during summer and less in wintertime due to the higher crystals glint and the higher possibilities of evapontranspiration with summer temperatures. Concerning Camanchaca, Tolonchar is too much into the mainland and to much high to be affected by this phenomenon. Finally the snow presence appears as the more plausible explanation of this OMI lack of data. In fact OMI has difficult to detect clouds presence over snow scenes and this fact brings to a very high number of fill values during the wintertime where snow presence is higher. The satellite works well again in summer. Moreover from the plot 9.5 we can observe that this bias is increasing at present time. This fact could indicate a major snow/ice precence at Tolonchar during these last years 2008 and 2009. We perform a comparative analysis for La Silla and Paranal too to verify if some other similar bias are retrieved using OMI data. In the case of La Silla site (Figure 9.7) we do not observe any evident discontinuity in cloud fraction over the last six years. The explanation is that the satellite has a footprint over a little bit arid area and moreover in its field of view it does not detect ocean scenes that could affect data with higher reflectivity values.

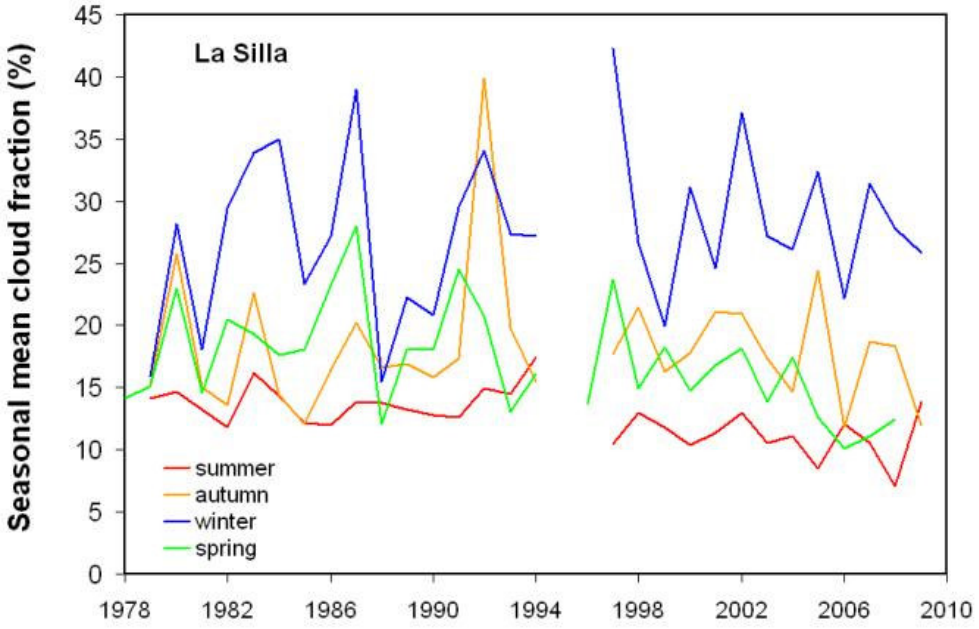

Figure 9.7. La Silla seasonal mean cloud cover fraction. Summer (red), autumn (orange), winter (blue) and spring (green). Practically no discontinuity in seasonal trend is evident at the end of 2004 with the beginning of OMI data use.

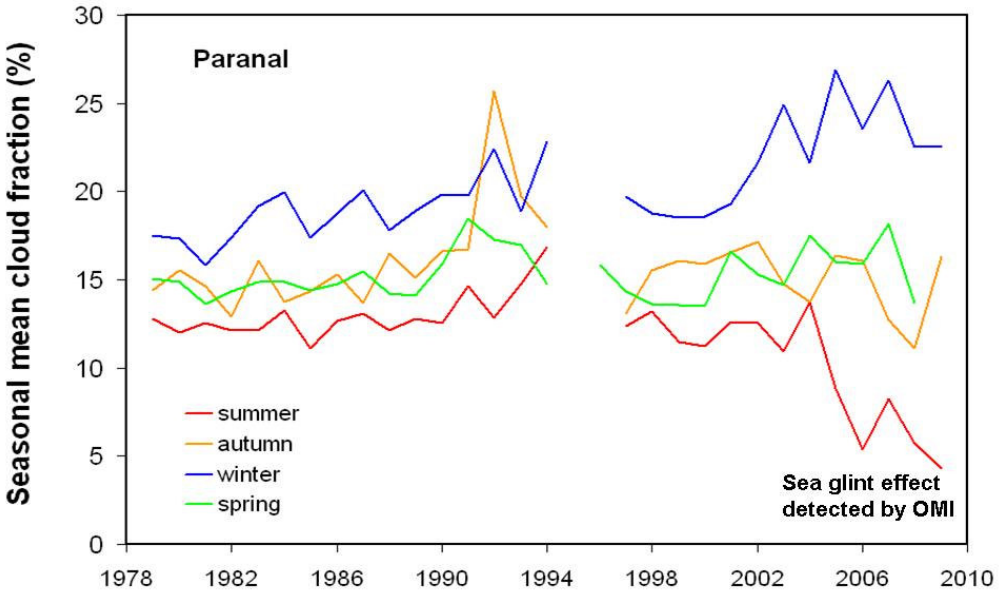

Figure 9.8. Paranal seasonal mean cloud cover fraction. Summer (red), autumn (orange), winter (blue) and spring (green). A discontinuity with the beginning of OMI data use, is seen in summer trend.

For Paranal the situation changes again. In Figure 9.8 we see that with OMI data use, a decrease in cloud dover estimate occurs only during summertime. The explanation is to serach in the satellite field of view that see a large amount of ocean being Paranal near

the Chilean coast. For this reason, in particular during summer, the effect of sea-glint is not trascurable and can enlarge the number of OMI fill values in the dataset.

Concluding our analysis on 30-year cloud cover for the Chilean observatories, we apply the Wavelet analysis to the monthly values for looking at some possible periodicities. In Figure 9.9, for both La Silla and Paranal we show the cloud coverage monthly mean time series data (a), the wavelet power spectrum performed on this dataset (b). The contour levels color in the legend are chosen so that 75%, 50%, 25%, and 5% of the wavelet power is above each level, respectively. The wavelet power spectrum squared variance that helps us to distinguish peaks periodicity over the red noise level (c). In the upper part of the figure, La Silla has a 12-month periodicity that exceeds the red noise level (dotted line) in the variance plot practically constant over the whole 1978-2009 period. Likewise Paranal, shows the same annual periodicity of La Silla with a higher confidence level (more than 75%) during the OMI data use (Figure 9.9). The same analysis performed on Tolonchar does not see this annual periodicity, probably due to the higher rainshadow effect in this area, respect Paranal and La Silla.

In order to search for other periodicities in these series we must remove the yearly trend. The way to make it, is that one to apply the wavelet analysis on the 12-month running average of cloud cover data. The 12-month running averages for cloud cover data were presented at the beginning of this section (Figure 9.2). We performed this approach to all the Chilean sites, finding an interesting result only for La Silla (Figure 9.10). In the graph 9.10 we observe that La Silla data show peaks over the red noise for a period ranging 24-48 months over almost the whole 30-year period. Tolonchar presents this same periodicity (12-24 months) only for the period 1978-1987 This fact gives us the idea of searching for some relationship between the cloud cover in Chilean sites and the occurences of El Nino and La Nina using the Southern Oscillation Index (i.e. the SOI presented in Chapter 6). Performing the Wavelet analysis separately to the Southern Oscillation Index and to the Sea Surface temperature, we obtain the same 24-48 months periodicity, this test supporting our idea.

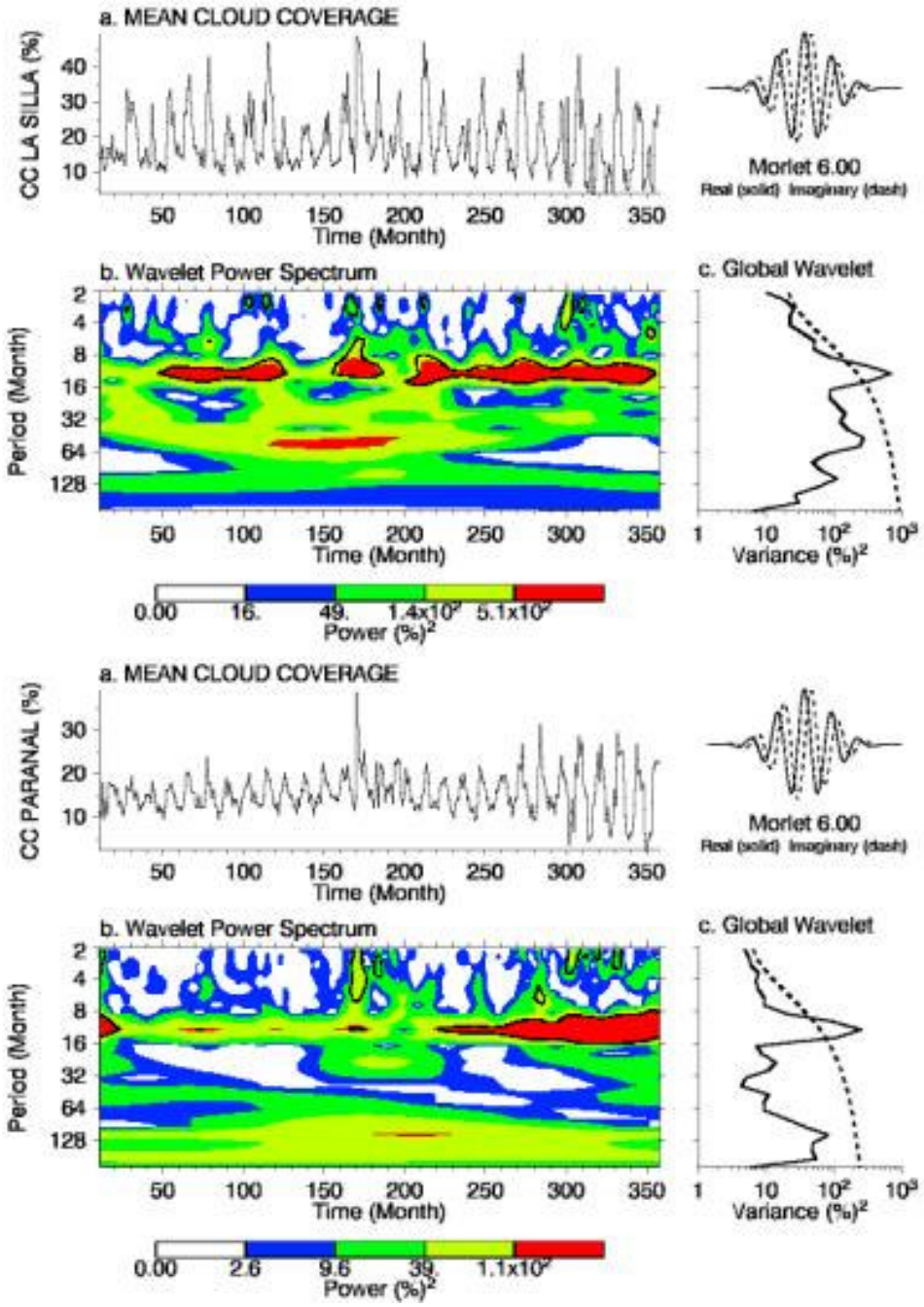

Figure 9.9 La Silla and Paranal cloud coverage monthly mean time series data (a), the wavelet power spectrum (b). The contour levels color in the legend are chosen so that 75%, 50%, 25%, and 5% of the wavelet power is above each level, respectively. Wavelet power spectrum squared variance and the Red Noise level (dashed line) (c).

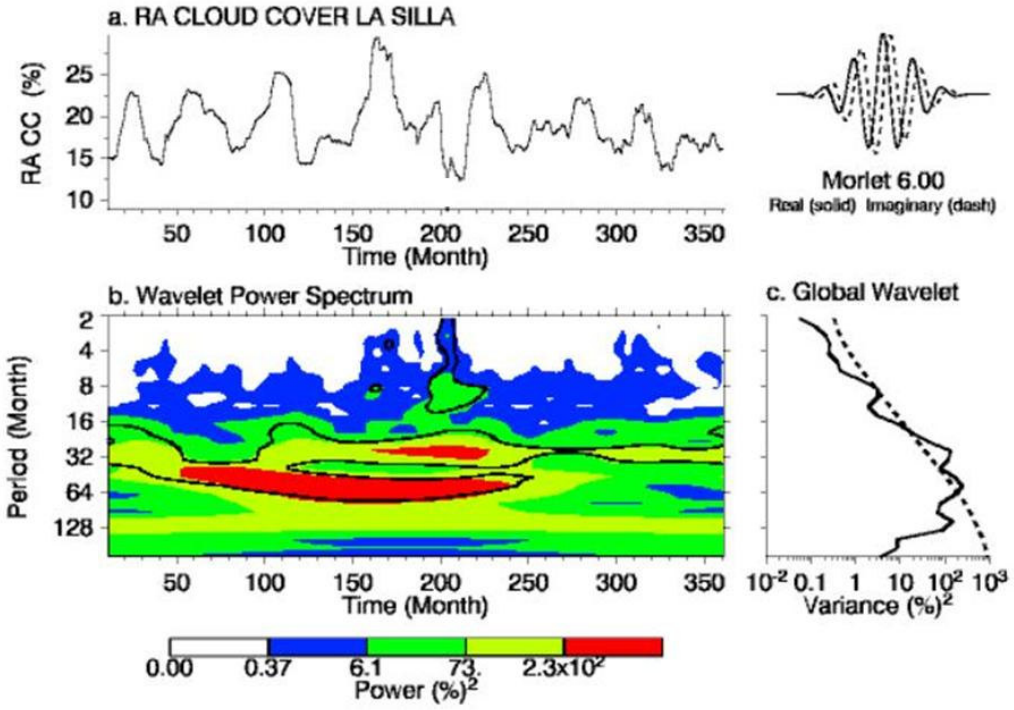

Figure 9.10. La Silla cloud cover running average with 12-month step series data (a), the wavelet power spectrum (b). The contour levels color in the legend are chosen so that 75%, 50%, 25%, and 5% of the wavelet power is above each level, respectively. Wavelet power spectrum squared variance and the Red Noise level (dashed line) (c).

In Figure 9.11. we compare the La Silla 12-month running average cloud fraction (red) over the whole 30-year dataset with the 12-month SOI running average (black). The results show an almost perfect anticorrelation between the increasing in cloud mean fraction and the decreasing in mean SOI and viceversa :

Cloud Fraction (%) = -2.86*SOI +18.03 with a determination coefficient R^2=0.44.

If we remember that negative SOI values are representative of warmer water (El Niño) and positive index to cooler water (La Niña) we understand that when El Niño occurs we have an increase in mean cloud coverage, when La Niña occurs we have instead a decrease. Moreover in this plot we observe that the spread in increasing cloudness (link to El Niño) is stronger (i.e. in mean 7% or more of cloudiness increase) than the spread in decreasing cloudiness due to La Niña phenomenon (i.e. in mean 5% or less of cloudiness decrease). The dependence of Paranal mean cloud cover to El Niño cycles does not show any correlation as already announced by its Wavelet analysis (see Figure 9.12).

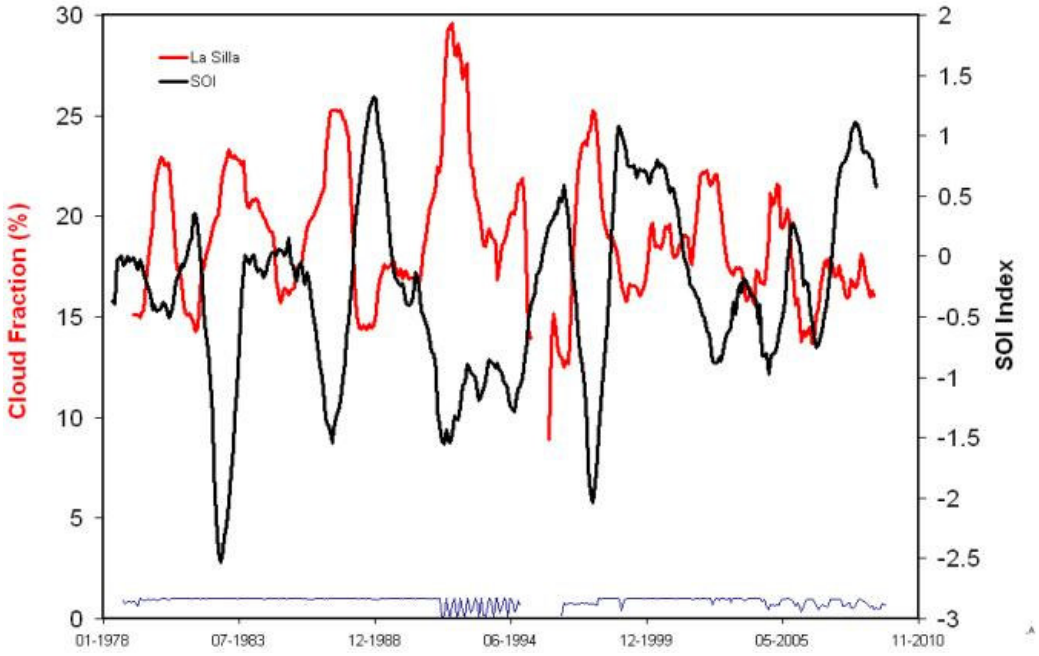

Figure 9.11. La Silla 12-month cloud fraction running average in percentage (red line, main y-axis) and 12-month SOI running average (black line, secondary y-axis). The blue thin line indicates the data coverage.

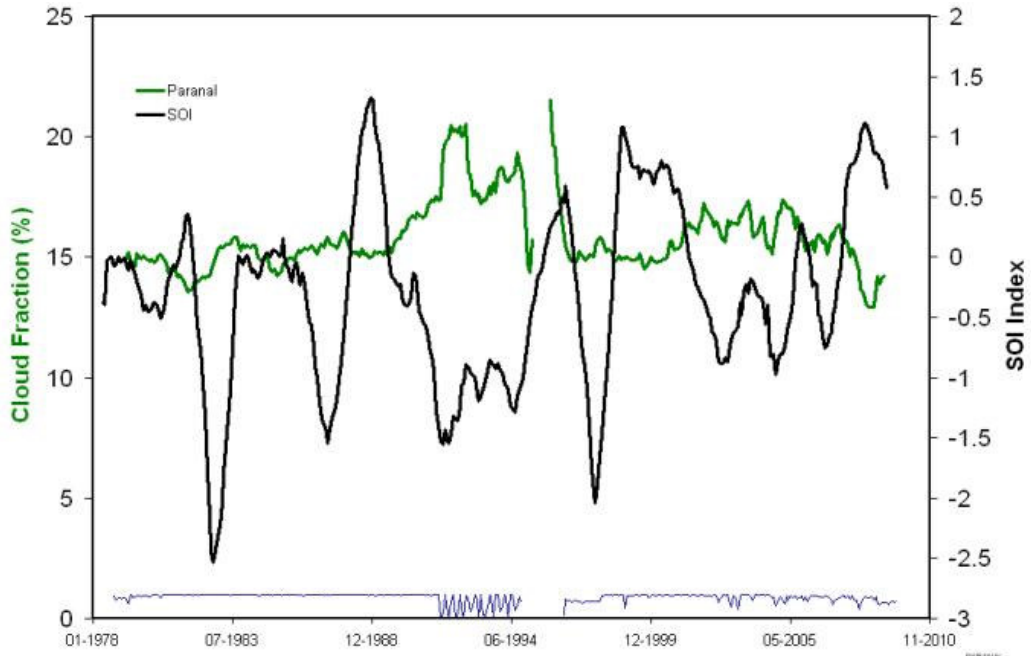

Figure 9.12. Paranal 12-month cloud fraction running average in percentage (green line, main y-axis) and 12-month SOI running average (black line, secondary y-axis). The blue thin line indicates the data coverage.

Paranal shows an almost constant cloud fraction percentage, lightly oscillating around 15% over the last 30-year except for a peaked period occurred in 1992-1994 during a strongest El Niño event that elevated the cloudiness to a 7% highest value than usual.

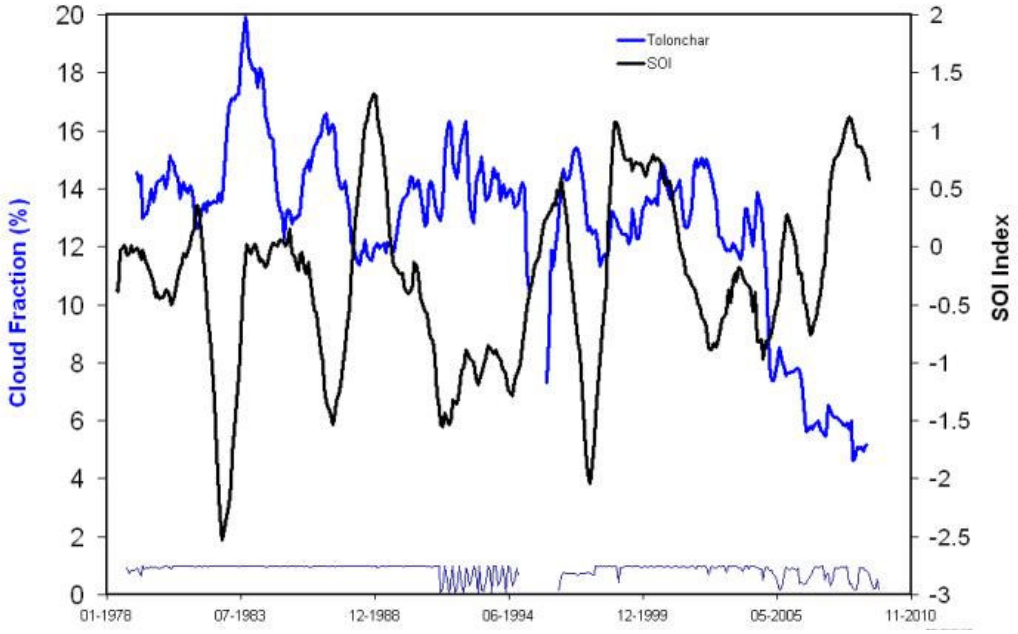

Figure 9.13. Tolonchar 12-month cloud fraction running average in percentage (thick blue line, main y-axis) and 12-month SOI running average (black line, secondary y-axis). The blue thin line indicates the data coverage.

Finally in Figure 9.13. we present the Tolonchar and SOI relationship. As we expect from the Wavelet analysis results, Tolonchar shows a 24-48 month periodicity up to 1988. In the top plot such periodocity is evident with three cycles in which the mean cloud cover appears quite good anticorrelated with the Southern Oscillation index as in the case of La Silla. The mean cloudiness for this area oscillates yearly around 14% value up to 2004 not taking into account the OMI lack of data explained previously. From the above data, the influence of El Niño appears to be changed in this area since 1988. Looking at the only first three clear cycles of the series we observe that the increase in cloudiness was of about 2-3% related to the SOI minimum. A few amount if compared with the changes, clearly linked to El Niño events, that occur in La Silla cloud cover.

9.2.2 Photometric nights pecentage on La Silla and Paranal: comparison between in situ and satellite measurements

Taken advantage from a paper wrote by Marc Sarazin in 10th November 1997 and provided by the NASA Astrophysics Data System we take this work as a starting point to update the plot of monthly fraction photometric nights (Figure 9.14) and to compare

earth-based cloud coverage anomaly with similar values retrieved from satellite for both La Silla and Paranal observatories.

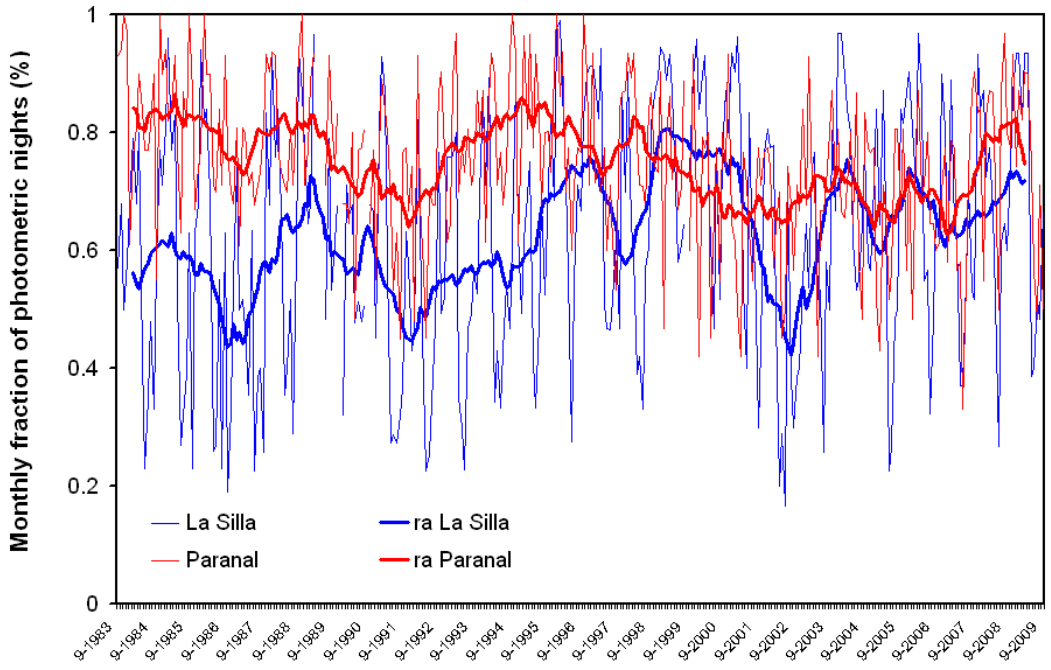

Figure 9.14. Monthly fraction of photometric nights in La Slla (light blue line) and Paranal (light red line). 12-month running average for La Silla data (thick blue line) and 12-month running average for Paranal data (thick red line). Data available from the ESO astroclimate page.

The yearly signal (12-month running average) in Figure 9.14 shows as during the last 27 years, the La Silla mean monthly fraction of photometric nights is changed. If we analyse the difference between Paranal and La Silla this changes are clearest (Figure 9.15). In 1983 to 1996 period, the mean difference of photometric nights in percentage between Paranal and La Silla, was quite substantial oscillating around Paranal 20% photometric nights more than La Silla.

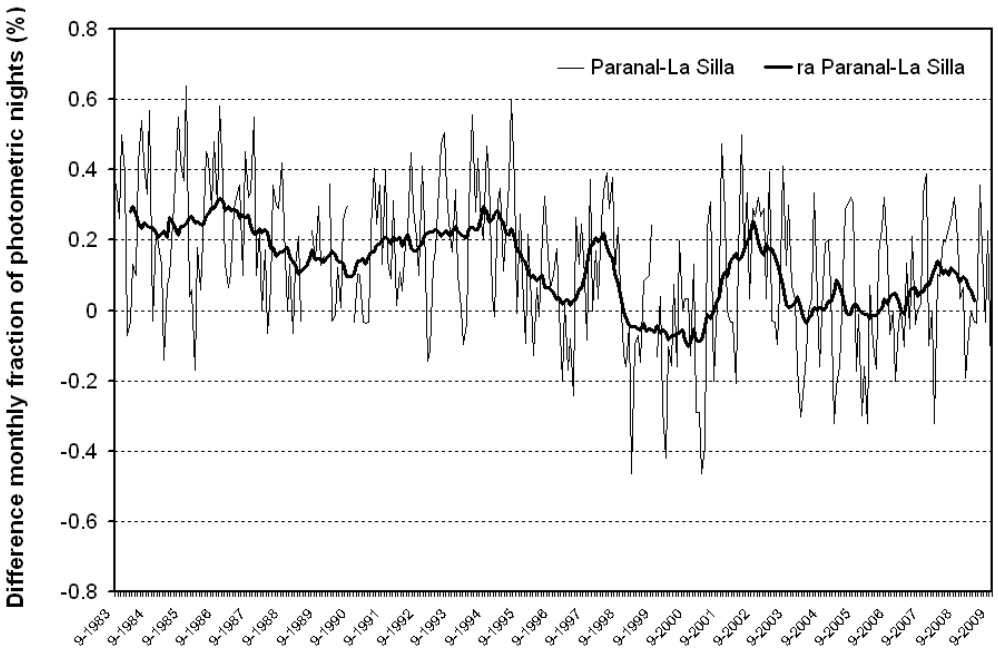

Figure 9.15. Difference in monthly percentages of photometric nights between Paranal and La Silla for the period 1983-2009 (black thin line) and the difference dataset represented by a 12-month running average (black thick line).

However, from 1997 up to 2004, it was observed this difference to oscillate around a 10% lower level. During this period there was a notable improvement in La Silla percentage of photometric nights and contemporary a very little worse in Paranal number of photometric nights. In particular, during the period 1999-2001, the average trend of the Paranal and La silla difference became negative as La Silla reached the same optimal condition for astronomical observations as Paranal. During the years 2003-2007 the two site have persisted in the same mean fraction of photometric nights. However, in these last two years the situation appears quite restored with a return of Paranal fraction of photometric nights of about 5-10% higher respect to La Silla.

In order to analyse the long-term stability of the sky-quality at La Silla and Paranal we compare the data on photometric sky-quality, i.e. the percentage of photometric nights during the twelve months calendar year, calculating the average over consecutive 5-year windows starting from the first complete year available (1984) and ending with the last one (2008). Looking first, at the photometric sky quality at La Silla (Figure 9.16), we observe that the total yearly average over each 5-year windows (as reported in table 9.1) is rather stable with a value of (62% ± 6%)and a seasonal pattern very similar in each

quinquennium with a minimum from May to October and a maximum in photometric nights percentage from November to March.

Table 9.1. La Silla and Paranal yearly average fraction of photometric nights over each 5-year window considered in Figure 9.16.

	1984-1988	**1989-1993**	**1994-1998**	**1999-2003**	**2004-2008**
La Silla	0.57	0.56	0.65	0.65	0.67
Paranal	0.80	0.73	0.80	0.69	0.71

Looking at Figure 9.16, it is interesting to note that the major differences of 1996-2009 respect to the 1983-1995 period highlighted in Figure 9.14 appear here to take place mainly during the second half of the calendar year i.e. from June to December, where the 5-years windows appear to be a little more spread.

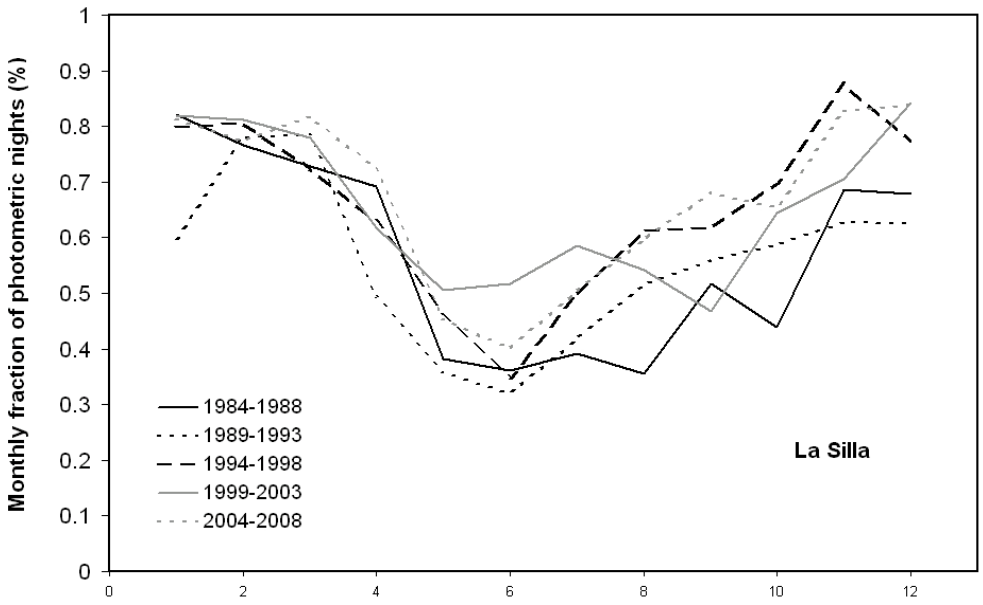

Figure 9.16. Test of possible long-term trend in photometric sky quality at La Silla. Average monthly percentages of photometric nights compared for the 5-year time range: 1984-1988 (blak line), 1989-1993 (black dashed line), 1994-1998 (large dashed line), 1999-2003 (grey line) and 2004-2008 (grey dashed line).

This seasonal pattern is completely in accordance with the La Silla photometric data for the time period: 1965-1972 (dashed curve) and 1983-1988 (full curve) published by Ardeberg et al in 1989 and presented in Figure 9.17.

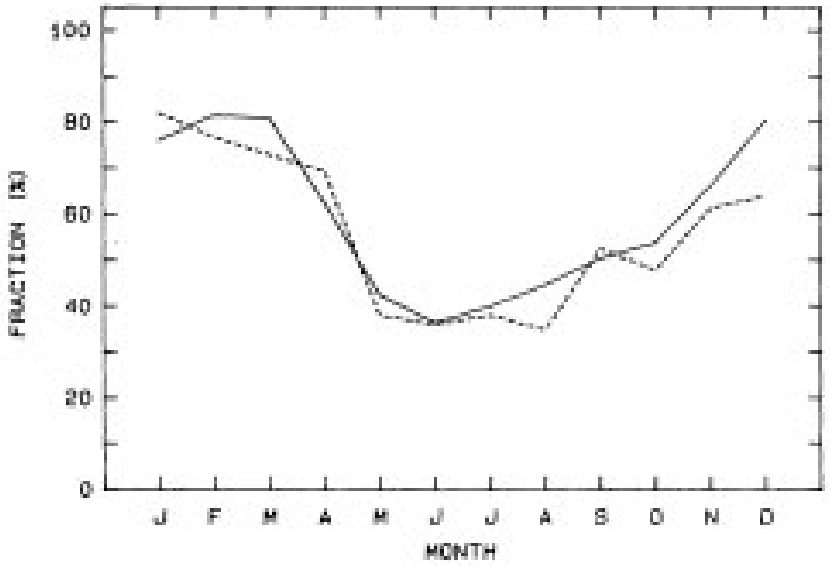

Figure 9.17. Test of possible long-term trend in photometric sky quality at La Silla. Average monthly percentages of photometric nights compared for 1965-1972 (dashed line) and 1983-1988 (black full line).

Moreover, if we analyse the possible long-term trends at La Silla, taking into account the same fraction of photometric nights, respectively on 1983-1995 and 1996-2009 periods, we observe, in figure 9.18, that the two "long" series have the common seasonal trend already observed in Figure 9.16 with a clear gain in monthly fraction of photometric nights in the 1996-2009 period respect to the previous 1983-1995 period. This improvement changes during the course of the year, from a 5% minimum value from February to April to about a 20 % in the months of December and January, settling in mean around a 10% in number of photometric nights per month more than in the past 1983-1995 period.

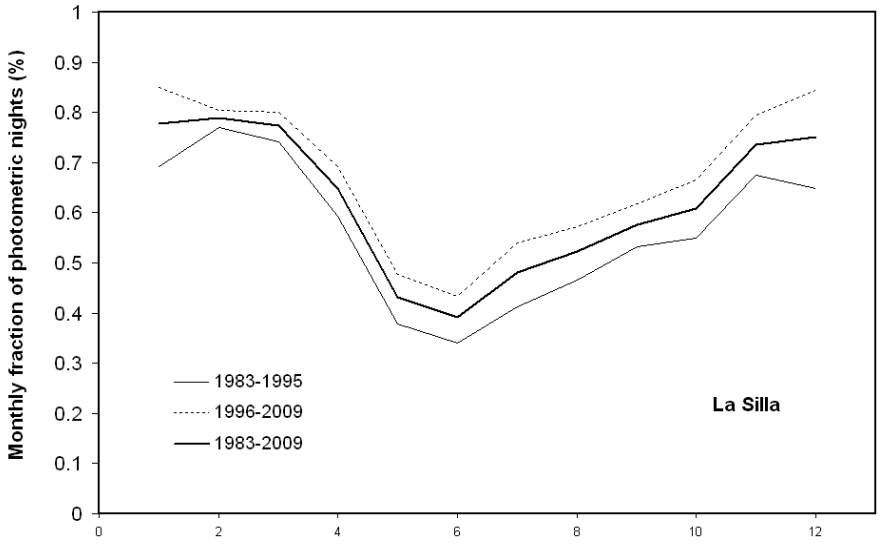

Figure 9.18. Test of possible long-term trend in photometric sky quality at La Silla. Average monthly percentages of photometric nights compared for the 1983-1995 period (blak line), 1996-2009 (black dashed line) and for the whole 27 year dataset (black thick line).

The same analysis on the sky quality monitoring was performed for Paranal too, both over consecutive complete 5-year time windows (see Figure 9.19) and on longer-term trend (1983-1995, 1996-2009) and over the whole 27 years photometric fraction dataset (Figure 9.20).

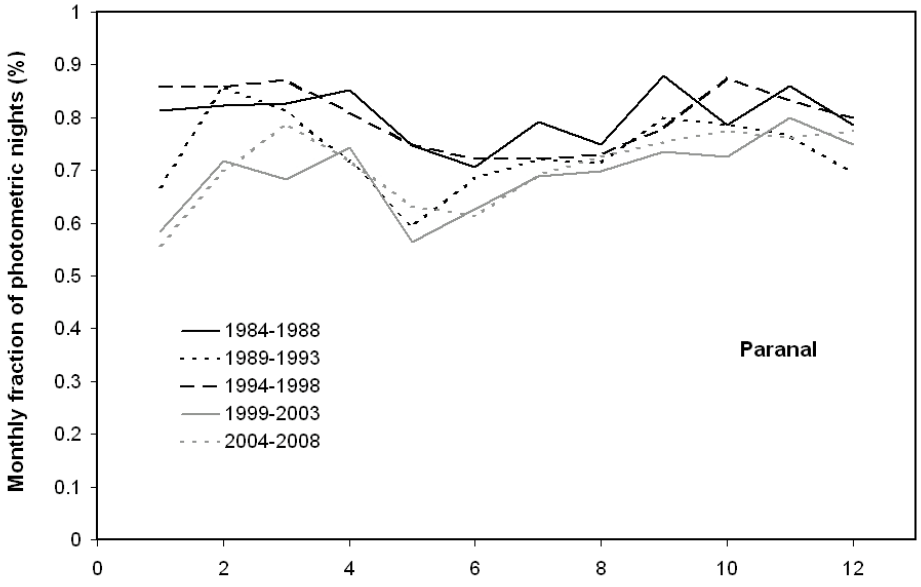

Figure 9.19. Test of possible long-term trend in photometric sky quality at Paranal. Average monthly percentages of photometric nights compared for the 5-year time range: 1984-1988 (blak line), 1989-1993 (black dashed line), 1994-1998 (large dashed line), 1999-2003 (grey line) and 2004-2008 (grey dashed line).

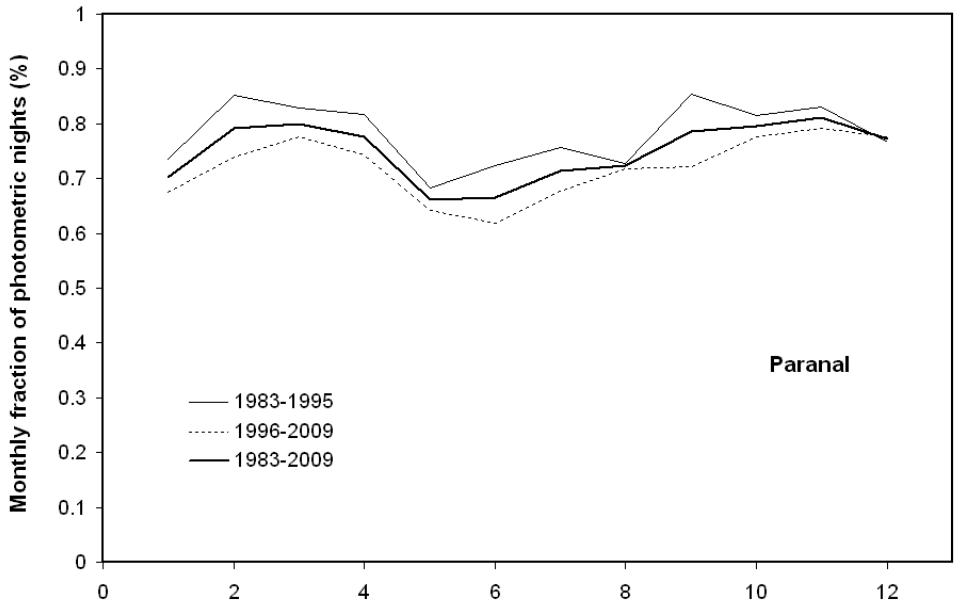

Figure 9.20. Test of possible long-term trend in photometric sky quality at Paranal. Average monthly percentages of photometric nights compared for the 1983-1995 period (blak line), 1996-2009 (black dashed line) and for the whole 27 year dataset (black thick line).

For Paranal the total yearly average is adjusted around a 75%±5% value (see Table 9.1), the seasonal features among the 5-year windows are similar with a light minimum from May to August and a maximum during January, February and March. These data are representative of a certain worsening in number of photometric nights during 1996-2009 period respect to the previous 1983-1995 period. These changes are not homogeneously distributed in the course of the year. They range from a maximum of 10-15% in February, June and September and a minimum with no evidences of change in August and December (Figure 9.20). In this case, however, it is necessary to remember that the parameters that define a photometric night conditions are different for La Silla and Paranal sites, being in this last site more restrictive.

From this analysis it is clear that both La Silla and Paranal have a quite stable situation regards the yearly mean photometric nights percentage with a few oscillating differences in the last 15 year (see Figure 9.14 and Figures 9.18 and 9.20) however, peculiar seasonal trends are evident. In the case of La Silla (Figure 9.16), we observe a quite strong annual difference (about 35%) between maximum and minimum in number of photometric nights, instead for Paranal (Figure 9.19) we observe an almost steady seasonal trend with an interannual photometric nights variation of about 10-15%. In

order to know if some periodicities command these differences, we perform the Wavelet analysis over the monthly fraction of photometric nights both in La Silla and Paranal (Figure 9.21).

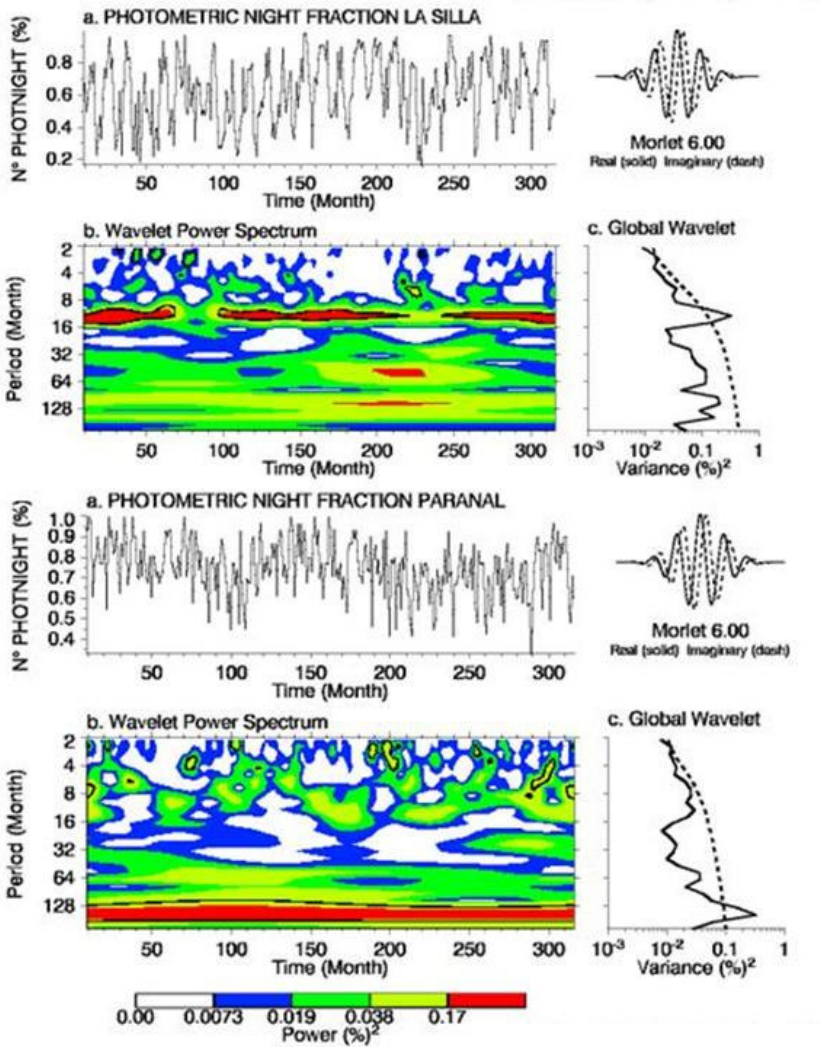

Figure 9.21. La Silla (Top panel) and Paranal (Botton panel) average fraction of available monthly photometric night series data (a), wavelet power spectrum (b). The contour levels color in the legend are chosen so that 75%, 50%, 25%, and 5% of the wavelet power is above each level, respectively. Wavelet power spectrum squared variance and the Red Noise level (dashed line) (c).

From this figure is evident that La Silla has a very high annual periodicity that goes over the red noise while Paranal does not show none significance. This is the first difference that occurs for the fraction of photometric data between these two sites. Another possibility that we explore here is the possible relationship between the cloud cover anomaly and the Southern Oscillation index. We develop the idea presented by Marc Sarazin (1997) to strictly connect SOI series and cloud coverage anomaly

obtained from one hand using photometric nights percentages over the observatories and from the other hand using a similar concept obtained from the satellite cloud cover data elaboration over a 27-year dataset. We start describing the idea presented by Marc Sarazin and then we continue with our other approach.

In Sarazin's opinion we could use both the absolute value and the relative oscillation amplitude of the Southern Oscillation Index to make a prediction concerning the average clear sky statistics for the year to come. Starting from the monthly fraction of phtometric nights we calculate first the average monthly percentage over the whole length of the database (1983-2009), then we calculate the Cloud Cover Anomaly (CCA) over La Silla and Paranal. This value is defined as the relative deviation from the above calculated monthly average conditions in term of number of photometric nights. In Figure 9.22 we show the relative deviation from the monthly average number of photometric nights at La Silla passed with a five –year running average (blue line) and the SOI with the same filter (black line).

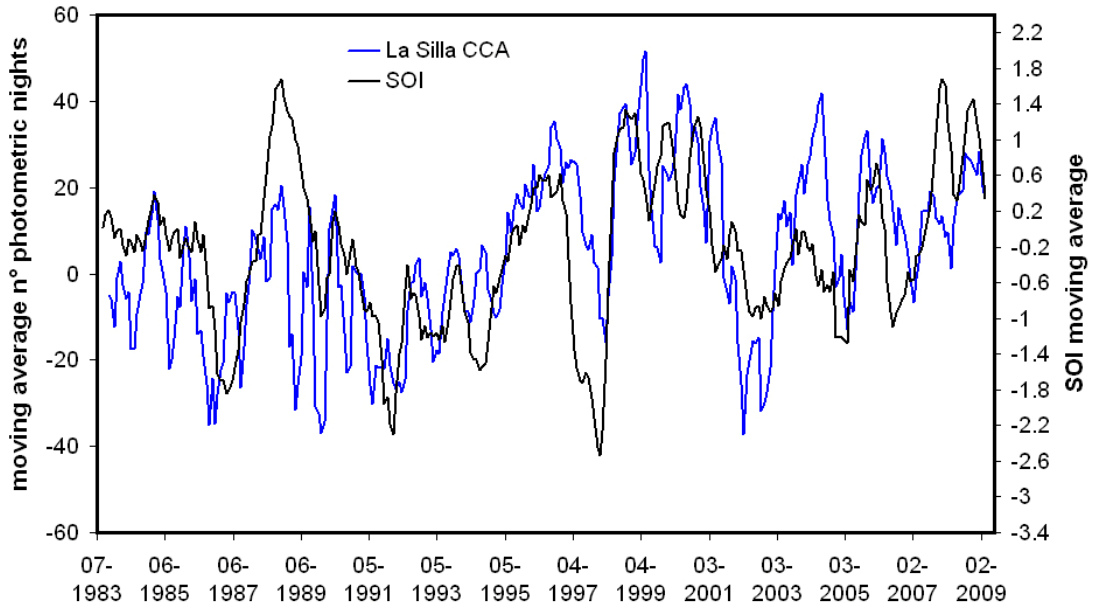

Figure 9.22. Cloud Cover anomaly in La Silla (blue line, main y axis). It is the relative deviation from the monthly average number of photometric nights calculated as a 5-year running average.Southern Oscillation Index 5-year running average (black line, secondary y-axis).

In this plot, the minimum-maximum oscillation in number of photometric nights reaches, has a value of about 70%, a such result means that the difference in number of available photometric nights occuring between a negative SOI peak and a positive one (i.e. between El Nino and La Nina events) can amount to about 150 nights at La Silla. Looking in detail to the plot we see that since 1987 the SOI trend follows well the CCA trend (determination coefficient: $R^2 = 0.26$) confirming our previously results obtained for La Silla (i.e. it exists an anticorrelation between the cloud cover percentage and the SOI).

In Figure 9.23 we show the same analysis relative deviation from the monthly average number of photometric nights at Paranal (red line) with the SOI filter (black line).

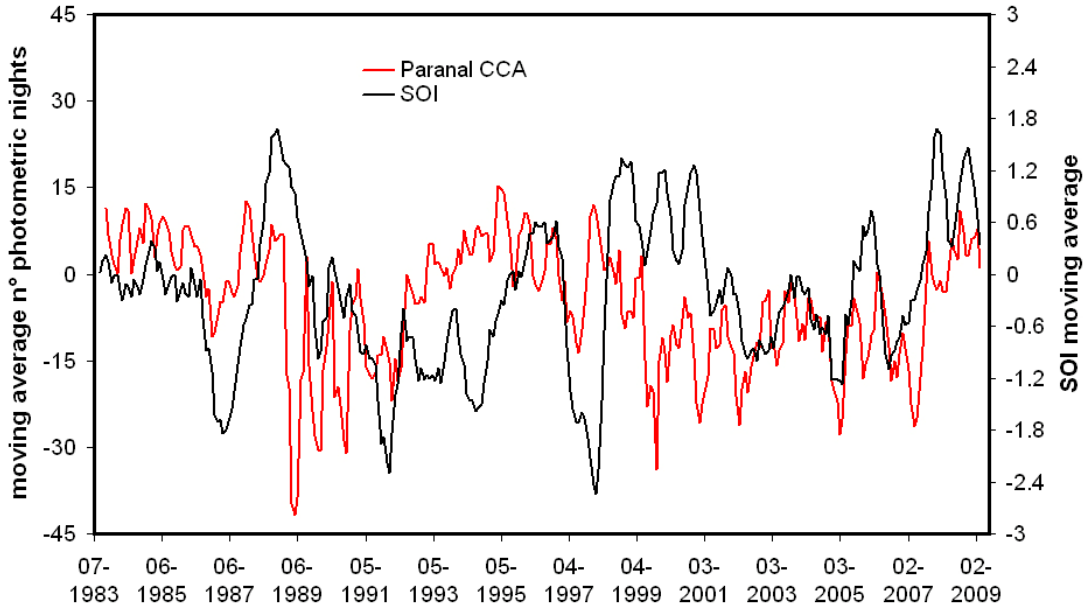

Figure 9.23. Cloud Cover anomaly in Paranal (red line, main y axis). It is the relative deviation from the monthly average number of photometric nights calculated as a 5-year running average.Southern Oscillation Index 5-year running average (black line, secondary y-axis).

In this plot we observe that the (minimum) peak to (maximum) peak variation is less than about 40% that it means a difference in number of available photometric nights during El Nino-La Nina occurences of about 100 nights at Paranal. SOI and CCA in this plot do not show a common trend (determination coefficient: $R^2 = 0.003$) in particular during 1993-2003 period where SOI increases when cloud anomaly decreases and vice-

versa. This fact is quite interesting because the 1993-2003 period is the temporal range where more relevant changes in trend of monthly percentages photometric nights difference between Paranal and La Silla occurred (see Figure 9.15).

If we look at the Wavelet Analysis performed on the series in Figure 9.15 we see that during 1993-2003 there is a light 24-48 month periodicity (with 50% level of significance) that is not present along the rest of the series.

We cover now another step to compare the results obtained until this moment. We make a comparison among the long-term trend in photometric sky quality at La Silla (i.e. average monthly fraction of photometric nights), the long-term trend in satellite mean cloud cover and the long-term seasonal features obtained considering only satellite cloud-free scenes with reflectivity less than 22 % over the same area. The time window chosen to calculate the average is the overlapped period between the in-situ photometric measurements and the satellite data i.e. 1984-1994 and 1997-2008 period (Figure 9.24). In this plot we observe that the series describing the mean fraction of cloud-free scenes (i.e. cloud fraction lower than 22%) has a pronounced minimum in July and increases a lot during December and January (Summertime). From a theorical point of view, the percentage of photometric nights (blue line), should reflect this same feature (pink line). In fact, for both these datasets we observe a pronounced minimum around June-July, as expected. Finally, at the opposite, the green line that represents the monthly mean fraction of cloud cover, shows a maximum in conjunction with the minimum in cloud-free fraction scenes. This kind of approach, tell us that could be possible to obtain the same information, leaving from two different starting points: from one hand the percentage of photometric nights and from the other the percentage of free-cloud scenes (i.e. the percentage of cloud cover lower than a fixed threshold). If these two different ways lead to the same finish, theoretically, it could be possible to use the 35-year cloud cover satellite database to reconstruct over time, the percentage of the number of photometric nights for the top astronomical sites all around the world.

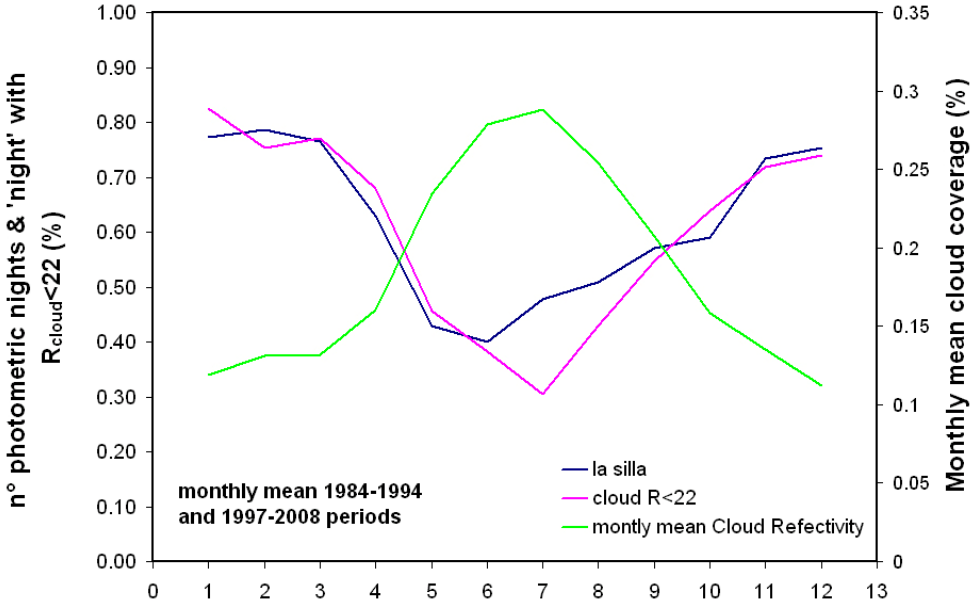

Figure 9.24. Comparison between the annual trend in photometric sky quality (blue line), the annual fraction of low-cloudiness scenes (R<22%) from satellite (pink line) and the mean cloud coverage fraction (green line) from satellite over La Silla.

The same analysis is performed for Paranal too. In Figure 9.25 we observe a situation quite similar to La Silla, with a minimum of free-cloud scenes that agrees with the lower percentage of photometric nights and a mean cloud cover that contemporary shows a maximum. In this plot, although the trends of the percentages of photometric nights and cloud-free scenes is very similar, a certain difference persists that make our hypothesis to reconstruct the past number of photometric nights an hard task. A comparison between in situ photometric data and the cloud fraction values retrieved remote sensing could therefore be hardly comparable due to the large area over which level 3 satellite data are averaged respect to the spatial resolved photometric measurements.

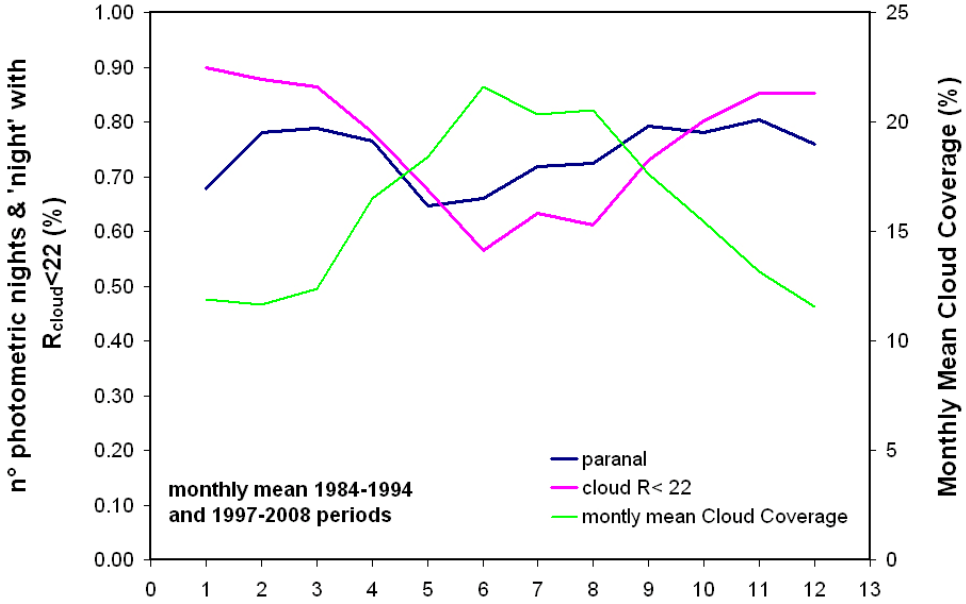

Figure 9.25. Comparison between the annual trend in photometric sky quality (blue line), the annual fraction of low-cloudiness scenes (R<22%) from satellite (pink line) and the mean cloud coverage fraction (green line) from satellite over Paranal.

However, our last aim is that one to try a comparison between the cloud coverage anomaly retrieved using ground-based fraction of photometric nights and a similar theoric value retrieved using satellite cloud fractions. The objective is to analyse the correlation of CCA (in-situ) with the satellite CCA (remote-sensing) so as to assess the usefulness of satellite cloud cover values as a tool to reconstruct a larger time series for photometric data over both, for example, La Silla and Paranal.

The retrieve of remote sensing CCA is completely similar as concept at the CCA given by photometric nights fraction. We calculate first the monthly average of cloud cover over the whole length of the database (1983-2009), then we calculate the satellite Cloud Cover Anomaly (sat CCA) over La Silla and Paranal. This value is defined in the same way of in-situ CCA, as the relative deviation from the above calculated monthly average conditions. The result for La Silla is reported in Figure 9.26. In this plot, at the two series of Figure 9.22, we add the satellite CCA one. Theoretically, the meaning is the same as both CCA and sat CCA show the deviation respect to the long-term mean in percentage. From the plot 9.26 we see that the behaviour of the two CCA series are lightly anti-correlated (determination coefficient: $R^2 = 0.23$) but not comparable in term

of absolute values. However there is a quite good evidence that sat CCA has a similar trend as the Southern Oscillation Index (determination coefficient: $R^2 = 0.29$).

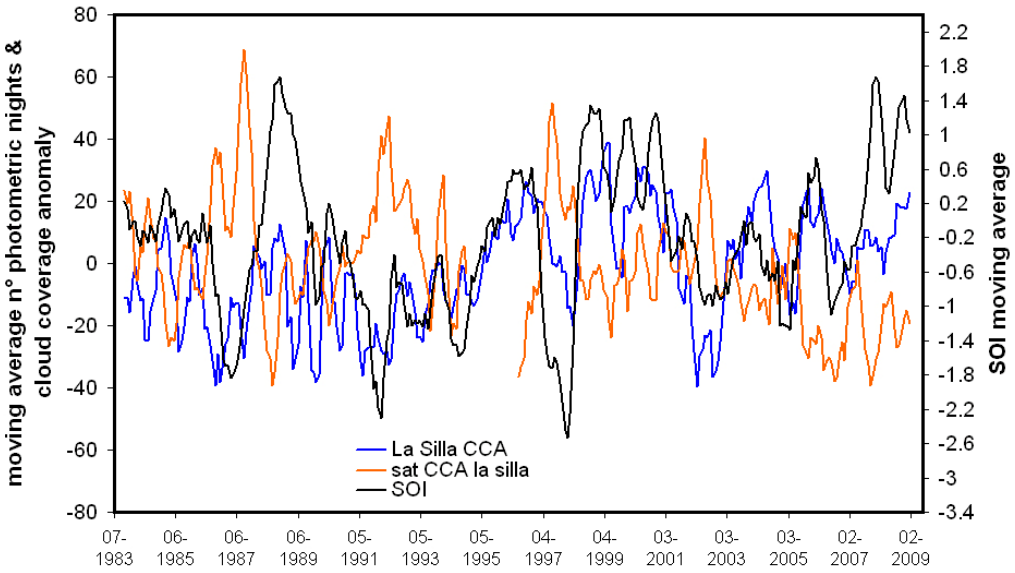

Figure 9.26. Cloud Cover anomaly in La Silla (blue line, main y axis). It is the relative deviation from the monthly average number of photometric nights calculated as a 5-year running average. Southern Oscillation Index 5-year running average (black line, secondary y-axis). Satellite Cloud Cover anomaly over La Silla area (orange line, main y-axis). It is the relative deviation from the monthly average number of cloud fraction calculated as a 5-year running average.

For Paranal the result is a little bit different. In Figure 9.27 we observe that sat CCA series does not run as the in-situ CCA value, being determination coefficient (R^2) equal to 0.02, instead a very weak anti-correlation lasts between the remote sensing CCA and the SOI (determination coefficient: $R^2 = 0.19$). These last two figures support the idea already mentioned, that despite the equal theoretic meaning, variables as satellite cloud cover anomaly and the relative deviation from the monthly average number of photometric nights (CCA), are not easily comparable. The divergence being the different spatial resolution and above all the different height of detection for satellite respect to the observatory quote where the measurements are taken.

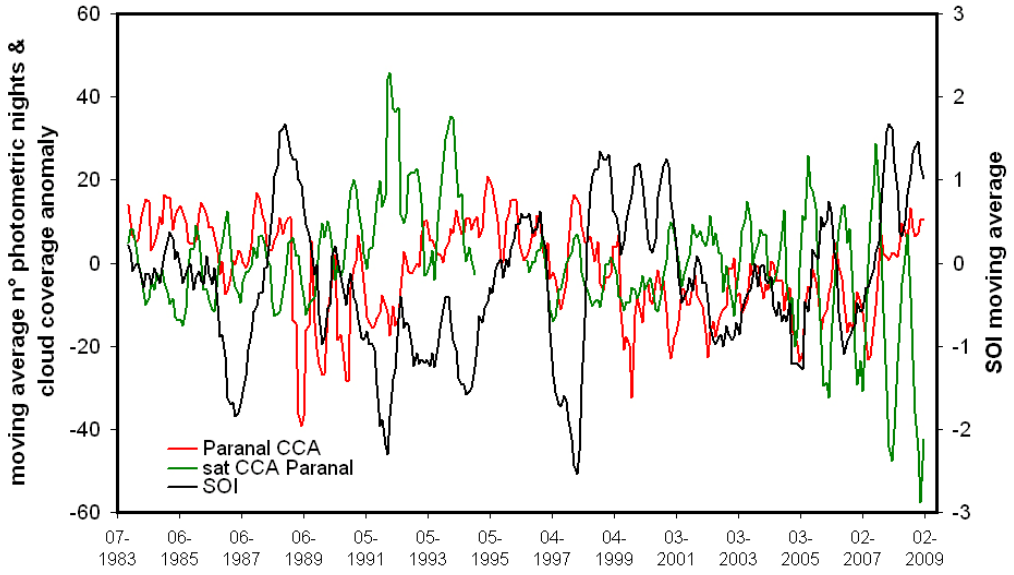

Figure 9.27. Cloud Cover anomaly in Paranal (red line, main y axis). It is the relative deviation from the monthly average number of photometric nights calculated as a 5-year running average. Southern Oscillation Index 5-year running average (black line, secondary y-axis). Satellite Cloud Cover anomaly over Paranal area (green line, main y-axis). It is the relative deviation from the monthly average number of cloud fraction calculated as a 5-year running average.

9.3 Evidences and conclusions

The major evidences found in this chapter are concerning with the cloud climatology both from the climatic point of view of the cloud cover percentage and from an astronomical point of view of the long-term trend of photometric sky quality. We have compared the cloud cover over the world's top astronomical site of La Silla, Paranal, La Palma and Tenerife and we have performed a detailed study to best characterize Tolonchar as a new possible ELT site. The results show that the mean monthly cloud fraction for all these sites is limited in a streap between 12-30% confirming the exceptionality of these sites for their high percentage of clear days. A marked decreasing trend in cloud cover is evident for Tolonchar. A careful analysis for searching the causes of this change over the last six years in this area has been made. The results obtained performing the cumulative values test and seasonal analysis over the three Chilean sites gave us the possibility to identify this change as due to an instrumental bias. In fact the Ozone Monitoring Instrument, looking at the test results and at the seasonal plot, has difficult to detect clouds presence over snow scenes,

increasing a lot the fill values output. The seasonal analysis for Paranal too recognized another OMI instrumental bias due to sea glint effect that afflicts the large satellite field of view.

Statistical tests to search cloud cover periodicities over the 30-year dataset were performed using the Wavelet analysis. Once detrended the annual cycle, the only one statistically significant periodicity was the 24-48 month cycle found for La Silla that is strictly linked to the El Nino-La Nina occurrences. This results was the reason to study more in detail the possible correlation existing between the 12-month (detrended for the annual cycle) cloud fraction running average and the filtered Southern Oscillation Index. The result For La Silla shows an almost perfect anticorrelation between the increasing in cloud mean fraction and the decreasing in mean SOI and viceversa. If we remember that negative SOI values are representative of warmer water (El Niño) and positive index to cooler water (La Niña) we understand that when El Niño occurs we have an increase in mean cloud coverage, when La Niña occurs we have instead a decrease. Moreover in this plot we observe that the spread in increasing cloudness (link to El Niño) is stronger (i.e. in mean 7% or more of cloudiness increase) than the spread in decreasing cloudiness due to La Niña phenomenon (i.e. in mean 5% or less of cloudiness decrease). The other Chilean sites of Paranal and Tolonchar do not show the same strong evidence, the first being no correlated at all and the second being SOI anticorrelated only over about the first 10 years. A second part in data elaboration, as mentioned above, was more related to the photometric nights study.

We started this last analysis with the update of the plot made by ESO astroclimate staff of La Silla and Paranal comparison in term of monthly fraction of photometric nights, enlarging it to a 27-year time series. Starting from this point we have performed autonomously a strict comparison between La Silla and Paranal. We have analysed both the long term trend of one site respect the other and separately we have performed tests to check the stability over time of the photometric sky quality. Sky quality is remained almost the same for both La Silla and Paranal sites, if we compare consecutive 5-year windows in each site. Once changed the long-term window over which to calculate the mean photometric values, in both La Silla and Paranal, the seasonal accordance becomes almost perfect with no long term trends presence. The Wavelet analysis on these results, emphasizes only one clear difference between the two sites that was a high

La Silla annual periodicity in photometric nights variation number respect to Paranal. Finally a last analysis was carried on to compare the cloud coverage anomaly (i.e. relative deviation of the mean number of photometric nights) in-situ measurements, with the satellite Cloud Cover Anomaly (sat CCA) over La Silla and Paranal. This last value being defined as the relative deviation from the above calculated monthly average conditions. The objective of such analysis was to analyse the correlation of CCA (in-situ) with the satellite CCA (remote-sensing) to assess the usefulness of satellite cloud cover values as a tool to reconstruct a larger time series for photometric data over both La Silla and Paranal sites. However the results obtained, although have shown a light anti-correlation (determination coefficient R^2=0.23) between the in situ and remote sensing CCA for La Silla, and between each cloud cover anomaly and the SOI, they pointed out the difficult of a such comparison due mainly to a different spatial resolution and a different height of detection of the satellite respect to the observatory where the measurements were taken.

At last, in order to evaluate the possible difference in cloudiness between the ocean and the innerland and in order to evaluate a possible improvement in CCA and SOI relation, we calculated, at the same latitude, the ratio between the cloud cover percentage over the ocean and the same value over the land. Such analysis was made taking into account two astronomical sites in the inland at a certain distance from the Chilean coasts and representative respectively of the Northern and Southern part of the Country. In Figure 9.28 we observe the ocean-land cloudiness ratio (in percentage) at Tolonchar and La Silla latitudes.

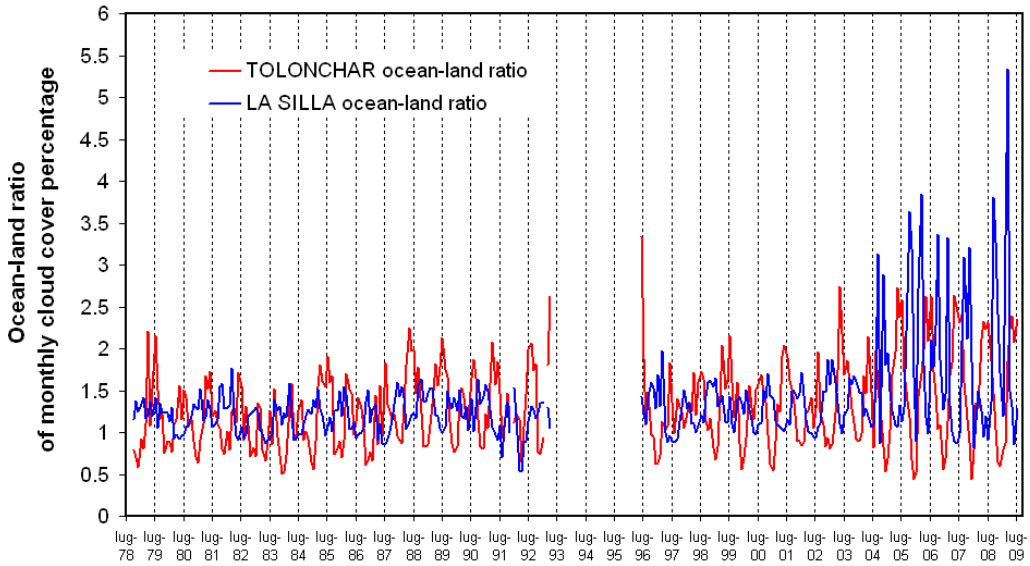

Figure 9.28. Ocean-Land ratio of monthly Cloud Cover percentage at the Tolonchar latitude (Red line) and at La Silla latitude (Blue line).

In this plot, a strong and well defined annual periodicity in the cloud percentage that increases and decreases over the ocean, is clear both for the Northern (Tolonchar) and Southern (La Silla) site. In several years, an opposite tendency in ocean-land cloudiness ratio is evident for Tolonchar respect to La Silla. Since 2004 the OMI bias in cloud cover retrieve is evident. If we analyse, in Figure 9.29, the mean seasonal trends of these ratios, we observe at the Tolonchar latitude, a larger cloud percentage on the ocean respect to the land during the winter and an opposite situation during the summer. Instead, at La Silla latitude we have an opposite tendency: larger cloud presence over the ocean during summer and a lower one in winter.

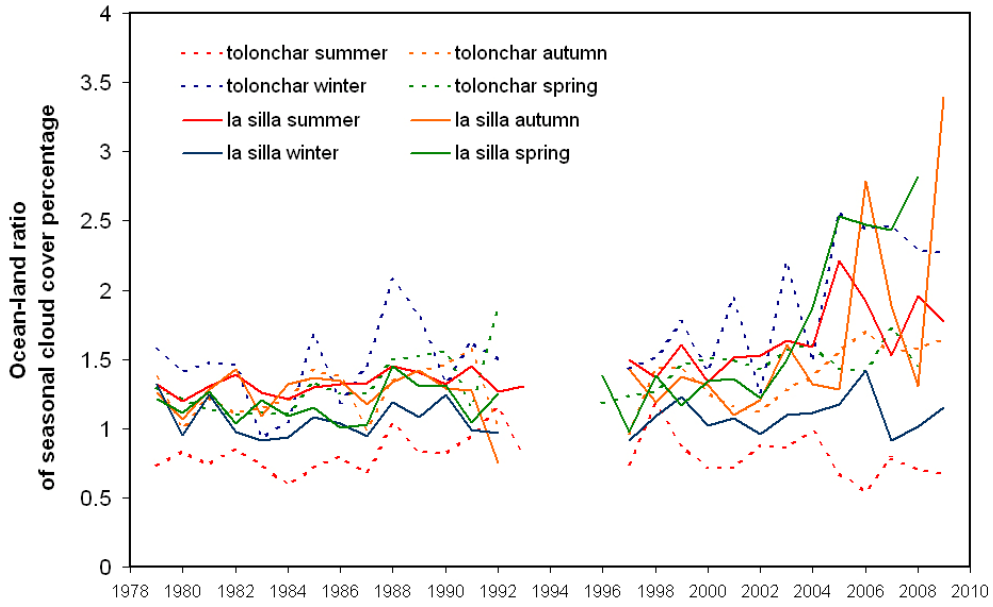

Figure 9.29. Seasonal Ocean-Land ratio of Cloud Cover percentage at the Tolonchar latitude (dotted line) and at La Silla latitude (continue line).

A way to evaluate if these differences in cloud presence, leaving the ocean and going to the inland, change at the same rate in Northern and Southern of Chile is that one to calculate the ocean-land variation in cloud percentage as the ratio between Tolonchar and La Silla (Figure 9.30).

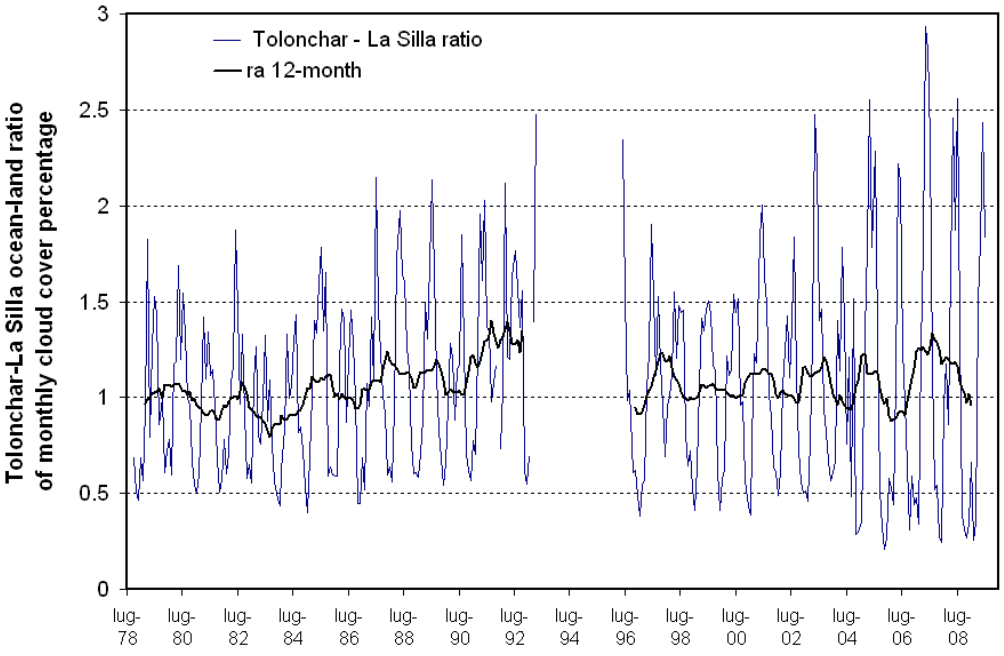

Figure 9.30. Tolonchar-La Silla ratio of the Ocean-Land change in monthly cloud cover percentage.

If this ratio is greater than one, this difference in cloudiness between ocean and land is larger at Tolonchar, otherwise, if lower than one, is larger at La Silla. The figure shows that in average, this difference is larger at Tolonchar, in part due to the more distant location of the site respect the coast. Finally, making a seasonal distinction, in Figure 9.31 we observe that, the Northern and Southern Chile have a similar ocean-inland variation of cloud cover during Spring and Autumn. This difference increases in winter in the Northern part of the Country and decreases in Summer.

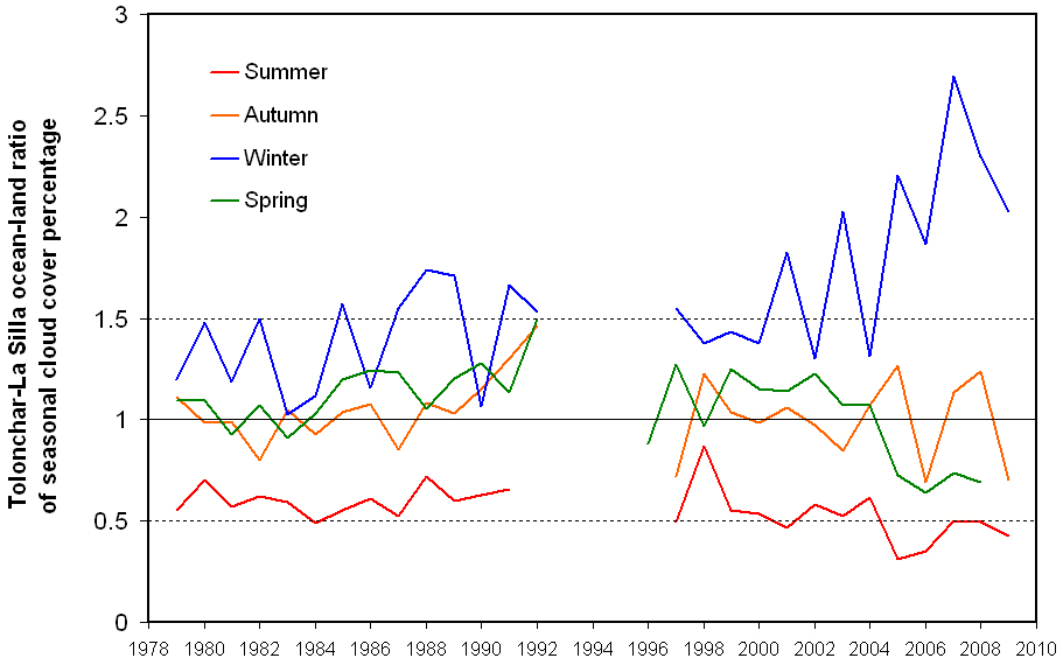

Figure 9.31. Seasonal Tolonchar-La Silla ratio of the Ocean-Land change in cloud cover percentage.

Conclusions

In the part of this thesis concerning '**methodologies of climatic investigations applied to the historical climatology**' we have used both documentary proxy and instrumental observations. The methodology used to analyze documentary proxy has been presented and their potentials and limitations have been stressed out, making attention to improve the calibration and validation approach in data reconstruction respect to the literature. However, this type of data suffer of biases for the difficult in properly calibrating proxy records against instrumental data, for the substantial amount of documentary sources that it is necessary to collect to be sure of the high quality information stored, for the difficult that arises from their chronological interpretations or caused by bias given by the selective perceptions of different observers. However these proxy data based on direct observations of different meteorological parameters (e.g. air temperature, precipitation, or flood events) offer the opportunity to study climate prior to the availability of early instrumental observations. At the end of these constrained steps cover to transform the written documents into a numerical index related to the climatic information, documentary proxy (DP) permit to establish occurrence of extreme events, year-by-year variability, existence of some time periods in which cold or warm situations were repeated, but are not useful to pinpoint long-term trends.

In the same way, a really statistical homogeneous and corrected instrumental time series is only possible through an enduring and long work of collection, validation, homogenization to extract the possible best climatic signal quality from the data. This is the big challenge that we presented in the first part of the thesis the methodology to obtain high quality and statistically robust observations supported by the results obtained performing this careful analysis. This is the only 'reading key' to solve the question if the climate of the 20th-21th century is unusual and to project the present state of the art of climate knowledge into the future. The results obtained in this part of the thesis offer an improvement of both data quality and instrumental data coverage, back in time, up to 360 years ago immediately after the invention of the first meteorological instruments that is a range that covers a time twice as long as the IPCC 2007 span. Added to the reconstructed series based on documentary data is possible to

extend our knowledge on the temporal behaviour of temperature in the Italian and Mediterranean area over the last 500 years, this longer context throws new light especially in relation with the recent global warming. In the last 40 years, in fact, warming is evident over all the Mediterranean stations, in line with the well-known assumption of global warming, however, looking on the long-term time scale, warm periods are not a novelty for the Mediterranean, which was characterized by warming and cooling cycles and the present warming does not much exceed other previous warm periods. This oscillation, coming from data analysis, induces the hypothesis that, although the actual situation presents an increasing temperature in line with the assumption of global warming, in the near future could be no surprising to demonstrate a reversal for the Northern-Italy and for the Padua local area in particular. In fact, if the cycles must continue in the same way as it was in the past, it means that the present situation is approaching a steady turning point with a possible reversal trend different from the scenarios supposed by the nowadays models.

Great attention has been given to the early instrumental observations. In this thesis we have presented the earliest Meteorological Observations (1654-1670), performed for the first meteorological Network (i.e. the Medici Network) at world. These observations carried out by several Galileo's followers have remained unexploited and are presented here for the first time. Their analysis extends back to 1654 our knowledge of past climate. All the series of the Network, either unbroken or fragments, have been recovered, controlled and transformed into modern unit of time and temperature. The small scatter of one with the other shows a good quality of instruments and observational modalities. The two main series, i.e. Florence and Vallombrosa, expressed in terms of anomaly with reference to the 1961-1990 period, show that today the climate in Florence has warmed by +0.09 °C with reference with the Ximenian Observatory in the city centre and 0.45°C with reference with the rural station Firenze Peretola. The warming in Vallombrosa was +1.18 °C partially due to landscape transformation and local business activity. Although the limited knowledge of the local heat island suggests some prudence in drawing conclusions, in Italy this period in the mid of the Little Ice Age appears less cold as generally believed on the ground of proxies.

Beyond this depth study carried on the early thermometers and temperature data born in part thanks the Galileo's and Torricelli's genius and the far-sighted of the Grand Duke

of Tuscany Ferdinand II, another important study is reported here. It extends back to 1716 the long daily temperature series in Padua with the addition of newly recovered data and the transformation of initially obscure indoor readings into outdoor observations in terms of modern units and observational methodology. This long work was justified by the scarcity of information about the early instrumental period and the exceptional contribution they can provide to our knowledge. This study gave us the possibility to check the high quality of the original data, to find the indoor-outdoor transfer function and to fill short gaps. Moreover this instrumental series is particularly interesting for our Padua's astronomical observatory because it is the continuation, back in time, of the temperature series carried out at the specula by Toaldo, Chiminello, Busatta, Conti, Santini and Lorenzoni that were directors of the Padua's astronomical observatory.

From this temperature data we observe that in the 1716-1930 period the climate oscillated following a marked Bruckner cycle (35.8 yr) and a weak Hale cycle (23.9 yr). The climate oscillations were attenuated with progressing time and their amplitude was almost completely damped for the 1930-1980 period, after which the present-day warming started. It is clear that Padua is only one station and cannot be compared with multi-station graphs representative of a wide scale. Nevertheless, it is interesting to see how this station is responding to climate changes and global warming and to compare it with the well-know trend of the Northern Hemisphere produced by IPCC 2007 (Le Treut, 2007). The comparison shows that, after 1860, Padua follows in general what is happening in the Northern Hemisphere, with marked warming after 1980 in spring and summer, but less in winter and autumn. The Padua series, adding some 150 years before the IPCC 2007 report, gives the opportunity to observe the almost regular oscillation that preceded the 1850-2007 period. A wider time scale and the repetition of warmer and colder periods over two-thirds of the series seems to suggest that such cycles might be repeated in the future too. The same has been observed for the Mediterranean Basin (Camuffo et al., 2010). We agree that the problem is very complex and that no general hypotheses can be drawn on the ground of what has happened on a local scale for its limited representative. However, this may be a further, interesting newly open question.

In the second part concerning '**methodologies of climatic investigations applied to the site testing for astronomy**' we have explored the use of other detectors with improved spatial resolution than TOMS (Bertolin, 2005) on board of different satellites that operate in bands of astronomical interest. The selected parameters for this study are the AI provided by Aura/OMI – with visible and UV channels and a spatial resolution from 13 km × 24 km to 24 km ×48 km – and the AOD provided by Terra (from 2000) and Aqua (from 2002) in MODIS with a spatial resolution of 10×10 km. To obtain the best spatial, spectral, radiometric and temporal resolutions, at La Palma site we decided to work with Level 2 data that have the same resolution as the IFOV satellite. The results highlight as OMI instrument detects aerosol presence with more precision than TOMS. We can see that most of the points detected remote sensing fall at lower extinction values below the threshold for dusty nights, suggesting the presence of non-absorbing or weakly absorbing (e.g. carbonaceous) aerosols. From this analysis we obtained the limits for dusty episodes (i.e. calima events) to be near AOD > 0.1 on the AOD scale and AI > 0.6 on AI scale. We also observed that dust episodes measured at ground level, are usually below the threshold for dusty nights on the atmospheric-extinction scale (K_V < 0.15 mag airmass^{-1}), meaning that the presence of calima affects low altitudes, and that only in a few cases reach the Roque de los Muchachos Observatory. We also observed that all clouds detected for their high reflectivity (greater than 15 %) are below the threshold for dusty nights. Similar results have been obtained with the study of Terra and Aqua/MODIS data. Beside the possibility to obtain several general information concerning the cloud and airborne particles presence, currently, the AI and AOD values provided by the NASA satellites alone, are not useful for a careful aerosol site characterization, and in situ data are required to study drainage behaviour, in particular at those astronomical sites with abrupt orography as the ORM case.

Meantime, the analysis of OMI Level 3 data, although with a lower vertical and spatial resolution, has given us several interesting results concerning both the possibility to compare different climatic variables over the area of the top astronomical observatories and to exploit other new area for future astronomical investment project. Thanks a detailed study of the aerosol algorithm performed by Torres, based on aerosol types a-priori assumptions, we were able to define, for each couple of AI and AOD values retrieved from OMI level 3 data, both the SSA and the height of aerosol layer. In order

to best evaluate these results however it was important to perform a study on the site orography to define the site vertical profile from the sea and the mean altitude of the satellite ground footprint in which the level 3 data are averaged. Given all information, it was possible to compare the aerosol load among the different astronomical sites both in term of altitude and typologies. We performed such analysis on four among the top world's sites (i.e. La Silla, Paranal, La Palma and Tenerife) and in particular we tested this methodology to study a new exploitable ELT site: Tolonchar. Concerning La Silla we observed that aerosol are usually found during cloud free days in 2000-8000 m amsl range. In Paranal, airborne particles reach a little bit higher altitude than La Silla (i.e. up to 10 km); from data analysis we observed a few number of particles intrusions but with higher AOD values. In our opinion these high particles with elevated extinction values could be a result of a satellite bias. Paranal in fact is nearest to the ocean than La Silla; the sea glint could therefore affect in major part the retrieve OMI method. For the first time a careful satellite monitoring has been performed on a 6-years database on Tolonchar in order to obtain as information as possible from OMI level 3 data for this area that is actually under evaluation as a possible ELT site. Our results show very important conclusions. Over this area in fact the cloud presence is extremely limited, in mean with a cloud cover 15% lower than Paranal. However, despite this clear information it is difficult to estimate the annual mean number of photometric nights without real in situ measurements. An estimate, considering only cloud cover percentage could range around 280 ± 20 nights but to be reliable it must be supported by stronger in situ evidences. Another important result for Tolonchar it was the detection and the study, for the first time, of the aerosol presence. Aerosol analysis shows regular peaks in AOD extinction due to airborne particles at high elevations. Thanks the possibility to obtain a complete dataset (because the absence of clouds) we are able to estimate the threshold for high extinction events ($AOD > 0.42$) respect to 'normal' aerosol load. Above this threshold (from 5500 m amsl up to stratosphere), airborne particles intrusion could affect observations. In order to search for possible aerosol sources we have looked at the surrounding area and at the local predominant wind direction. We found that the tropospheric aerosol sources are located in several nitrate mines of the zone and on crustal erosion being the main wind direction coming from W-NW, instead the stratospheric source remaining the near active Lascar volcano. Finally

the same analysis with level 3 data was performed also over the Canarian observatories of ORM and Izana, showing that in both sites exist a very efficient inversion layer that above all during winter avoid airborne particles intrusion at the observatories quote, however occasionally in summer, due to the higher Trade wind, some dust episodes reach the astronomical sites.

The major evidences found in Chapter 9 are concerning instead with cloud climatology both from the climatic point of view of the cloud cover percentage and from a more astronomical point of view of the long-term trend of photometric sky quality. We compared the cloud cover over the world's top astronomical site of La Silla, Paranal, La Palma and Tenerife and we performed a detailed study to best characterize Tolonchar also from a cloud climatology point of view. The results show that the mean monthly cloud fraction for all these sites is limited in a band between 12-30% confirming the exceptionality of these sites for their high percentage of clear days. A careful analysis for searching the causes of a marked decreasing trend in cloud cover in Tolonchar over the last five years has been carried out. The results obtained, performing the cumulative values test and seasonal analysis over the three Chilean sites, identified this change as due to an instrumental bias. In fact the Ozone Monitoring Instrument, has difficult to detect clouds presence over snow scenes, increasing a lot the fill values output. From the seasonal analysis for Paranal we recognized another OMI instrumental bias due to sea glint effect that afflicts the large satellite field of view.

Statistical tests to search cloud cover periodicities over the 30-year dataset were performed using the Wavelet analysis. Once de-trended the annual cycle, the only one statistically significant periodicity was the 24-48 month cycle found for La Silla strictly linked to the El Nino-La Nina occurrences. This result was the reason to study more in detail the possible correlation existing between the 12-month (de-trended for the annual cycle) cloud fraction running average and the filtered Southern Oscillation Index. The result For La Silla shows an almost perfect anti-correlation between the increasing in cloud mean fraction and the decreasing in mean SOI and vice-versa. If we remember that negative SOI values are representative of warmer water (El Niño) and positive index to cooler water (La Niña) we understand that when El Niño occurs we have an increase in mean cloud coverage, when La Niña occurs we have instead a decrease. The other Chilean sites of Paranal and Tolonchar do not show the same strong evidence, the

first being no correlated at all and the second being SOI anti-correlated only over about the first 10 years. In the study and data analysis related to the photometric nights we have updated the plot made by ESO astroclimate staff reporting the comparison between La Silla and Paranal in term of monthly fraction of photometric nights. In our new version, this graph covers a 27-year temporal range. Starting from this point we performed autonomously a strict comparison between La Silla and Paranal. We analysed both the sky quality persistence and the long-term trend in number of photometric nights. These analysis reveal that both La Silla and Paranal have a quite stable situation regards the yearly mean photometric nights percentage with a few oscillating differences in the last 15 year (see Figure 9.14) and a peculiar seasonal trend. La Silla (Figure 9.16) has a quite strong annual difference (about 35%) between maximum and minimum in number of photometric nights exhibiting a high annual periodicity with an yearly mean around 227 ± 20 nights; Paranal (Figure 9.19) has instead an almost steady seasonal trend with an interannual photometric nights variation of about 10-15%, assesting the yearly mean around 274 ± 11 nights. Having demonstrated that the difference in number of photometric nights occurring between a negative SOI peak and a positive one can amount to about 150 nights at La Silla and about 100 nights at Paranal, a last analysis was carried out to compare the cloud coverage anomaly (i.e. relative deviation of the mean number of photometric nights) in-situ measurements, with the satellite Cloud Cover Anomaly (sat CCA) over both these area. The objective of such analysis is to analyse the correlation of CCA (in-situ) with the satellite CCA (remote-sensing) in order to assess the usefulness of satellite cloud cover values as a tool to reconstruct a larger time series for photometric data over both La Silla and Paranal sites. In the case of La Silla (Figure 9.26) we observe that the behaviour of the two CCA series are lightly anti-correlated (determination coefficient: $R^2 = 0.23$) but not comparable in term of absolute values. However there is a quite good evidence that sat CCA has a similar trend as the Southern Oscillation Index (determination coefficient: $R^2 = 0.29$). The difficult lies mainly in the different height of detection for satellite respect to the observatory where the measurements were taken and in the different spatial resolution between in situ and remote sensing data.

Figure List

1.1 A painting representation of Venice lagoon frozen over (Winter 1709)
1.2 Tree rings
1.3 Ice core
1.4 Retreat of Jakobshavn glacier calving front (Greenland)
1.5 Worldwide map of daily coverage surface observations accepted by the WMO
1.6 The present day environmental satellite orbiting around the Earth
1.7 Series of NOAA overlapping satellites
1.8 Northern Hemisphere surface temperature reconstruction since A.D. 900
1.9 NH temperature variation during the last 1.3 kyr. IPCC WG1 (2007)

2.1 Time distribution of CNR-ISAC Padua group documentary sources data bank
2.2 Climatic, astronomic, catastrophic and plague items in Middle Age chronicles

3.1 Quantificable advancements thanks to the EU Millennium project
3.2 Schematic view of the general methodology used to reconstruct past climates
3.3 Extreme freezing events on the Venice Lagoon
3.4 Winter temperature anomaly reconstruction (Northern-Central Italy since 1000 A.D.)
3.5 Completeness check of our documentary data bank
3.6 Linear regression to predict temperature from proxy values
3.7 Climatic fluctuations subdivided by classes to obtain indexes
3.8 Difference in climatic signal reconstruction using DP and IO
3.9 The Mediterranean basin taken in exam in the case study
3.10 Temperature anomaly over the last 500-years in the Mediterranean basin (MB)
3.11 Annual temperature anomaly from IO in the MB and Northern Hemisphere (NH)
3.12 Power Spectrum analysis of yearly temperature for the MB

4.1 Sunspot number during the last 400 years
4.2 Raw thermometer readings as retrieved from original registers (Bologna 1716 – 1774)
4.3 Example of bias due to large isolated error
4.4 A schematic view of the nowadays introduction of ‘heating-island’ bias.
4.5 Thermoscope invented by Galileo in 1593 (Benedetto Castelli, 1638)
4.6 Different Florentine Thermometers of the Cimento’s Academy (1657-1667)
4.7 The spirit-in-glass little Florentine thermometer (LFT)
4.8 Five late calibration of the Little Florentine Thermometer (LFT).
4.9 Two letters with meteorological observations from Vallombrosa

4.10 Map of the eleven stations of the Medici Network
4.11 Cloister of the monastery of St. Mary of Angels, Florence
4.12 Different dating stile in the Italian dukedoms during the 17th century.
4.13 Comparison among the temperature series of Medici stations (1654 – 1658)
4.14 Florence daily temperature series (1654-1670)
4.15 Vallombrosa daily temperature series (1654-1670)
4.16 Cross comparison between the individual series of the Medici Network
4.17 Florence daily temperature anomaly series (1654-1670)
4.18 Vallombrosa daily temperature anonaly series (1654-1670)
4.19 (a) Comparison between the Florence and the Central England (CE) series; (b) between Vallombrosa and CE series

5.1 The Amontons thermometer
5.2 Scheme of the Amontons' thermometer
5.3 Sampling time performed by Giovanni Poleni for his outdoor readings (1716-1718)
5.4 Mean daily outdoor temperature observed by Poleni in Padua (1716-1718)
5.5 Daily temperature anomaly for the period 1716-1718 in Padua
5.6 Daily temperature cycle in January and July, Padua, period 1980-2007
5.7 Outdoor temperature for Padua in the 1725-1764 period
5.8 Outdoor temperature anomaly for Padua in the 1725-1764 period
5.9 Outdoor and indoor readings by Poleni and Morgagni in February 1740
5.10 Outdoor monthly temperature for the period 1716-1769 in Padua
5.11 Outdoor monthly temperature anomaly for the 1716-1769 period in Padua
5.12 Outdoor seasonal temperature anomaly for the Padua series (1716-2007)
5.13 Yearly temperature anomaly for the Padua series (1716-2007) and the NH, IPCC 2007
5.14 Power Spectrum analysis of yearly temperature for the Padua series

6.1 The atmosphere representation
6.2 Layer of air column
6.3 Height distribution of gases in diffusive equilibrium
6.4 Vertical distribution of temperature.
6.5 Representation of light from a point source travelling through the atmosphere
6.6 Representation of Kolmogorov cascade theory.
6.7 Comparison of monthly mean seeing at Paranal and La Silla (Chile)
6.8 Seeing value at Paranal and La Silla in comparison with RNSO index
6.9 Cross-section of the Pacific Ocean, along the equator when does not occur El Niño events
6.10 Cross-section of the Pacific Ocean, along the equator when occur El Niño events
6.11 Correlation of SOI with monthly average seeing at Paranal before and after seeing worsening
6.12 Photometric nights fraction at Paranal and La Silla in comparison with the El Nino SOI

6.13 Total number of dark hours per year versus latitude
6.14 Annual variation of inversion layer height scale in Canary Islands
6.15 Seasonal dust transport over the Atlantic
6.16 Monthly averaged wind velocity at different pressure levels at ORM

7.1 Aerosol size distribution
7.2 Aerosol elimination processes
7.3 Different contribution to the total atmospheric extinction
7.4 Extinction coefficients depending with wavelength
7.5 K(V) versus K(B) correlation coefficient
7.6 Atmospheric extinceasured at the CAMC telescope at ORM, La Palma, Canary Islands
7.7 Values of extinction efficiency
7.8 Size distribution in continental aerosol
7.9 Solar radiation change
7.10 Plane parallel atmosphere assumption

8.1 OMI measurement scheme
8.2 The NASA A-Train
8.3 Example of the separation of aerosol types using the aerosol indices
8.4 Rayleigh atmosphere with several surface components of reflectance at TOA
8.5 Frequency of extinction over ORM during winter and summer
8.6 AI from EP/TOMS and Aura/OMI during time at ORM
8.7 AOT from Terra/MODIS and Aqua/MODIS during time at ORM
8.8 AI from OMI and AOD from MODIS under dusty conditions at ORM
8.9 AI (Aura/OMI) and KV correlation at ORM
8.10 La Palma orography profile
8.11 AOD (Terra/MODIS) and KV correlation at ORM
8.12 AOD (Aqua/MODIS) and KV correlation at ORM
8.13 Look up tables of the OMIAERUV alghoritm
8.14 La Silla orography profile
8.15 La Silla vertical distribution of aerosol particles properties
8.16 Height of aerosol during seasonal intrusion at La Silla
8.17 La Silla height of aerosol layer mean tendency
8.18 Paranal orography profile
8.19 Paranal vertical distribution of aerosol particles properties
8.20 Height of aerosol during seasonal intrusion at Paranal
8.21 Paranal height of aerosol layer mean tendency
8.22 Tolonchar orography profile

8.23 30-days RA of aerosol content in free cloud days over Tolonchar area
8.24 Tolonchar vertical distribution of aerosol particles properties
8.25 Nitrate mines in Northern Chile near Tolonchar site
8.26 Cumulative counts of wind direction for Chajnantar site
8.27 Height of aerosol during seasonal intrusion at Tolonchar
8.28 Tolonchar height of aerosol layer mean tendency
8.29 La Palma orography profile
8.30 La Palma vertical distribution of aerosol particles properties
8.31 Height of aerosol during seasonal intrusion at La Palma
8.32 Monthly mean atmospheric extinction over a 25-year period at ORM
8.33 Tenerife orography profile
8.34 Tenerife vertical distribution of aerosol particles properties
8.35 Height of aerosol during seasonal intrusion at Tenerife

9.1 Radiative transfer with and without clouds
9.2 Comparison of 30-yr cloud cover data over La Silla, Paranal, La Palma, Tenerife and Tolonchar
9.3 Cumulative values test to recognize dishomogeneity in 30-yr satellite dataset for La Silla, Paranal and Tolonchar
9.4 Cumulative values test to recognize dishomogeneity in 30-yr satellite dataset for La Palma and Tenerife
9.5 Tolonchar seasonal mean cloud cover fraction
9.6 The phenomenon called rainshadow effect in the Atacama desert
9.7 La Silla seasonal mean cloud cover fraction
9.8 Paranal seasonal mean cloud cover fraction
9.9 Wavelet analysis for La Silla and Paranal cloud cover monthly values
9.10 Wavelet analysis for La Silla cloud cover 12-month RA values
9.11 La Silla 12-month cloud fraction RA values
9.12 Paranal 12-month cloud fraction RA values
9.13 Tolonchar 12-month cloud fraction RA values
9.14 Monthly fraction of photometric nights in La Silla and Paranal
9.15 Paranal-La Silla difference in monthly percentages of photometric nights
9.16 Test of possible long-term trend in photometric sky quality at La Silla (5-yr steps)
9.17 Test of possible long-term trend in photometric sky quality at La Silla (7-yr steps)
9.18 Test of possible long-term trend in photometric sky quality at La Silla (12-yr steps)
9.19 Test of possible long-term trend in photometric sky quality at Paranal (5-yr steps)
9.20 Test of possible long-term trend in photometric sky quality at Paranal (12-yr steps)
9.21 Wavelet analysis of the average fraction of monthly photometric nights in La Silla and Paranal
9.22 La Silla Cloud Cover Anomaly in correlation with the SOI
9.23 Paranal Cloud Cover Anomaly in correlation with the SOI

9.24 Comparison between the annual percentage of photometric nights, fraction of cloud cover and satellite retrieved cover fraction over La Silla

9.25 Comparison between the annual percentage of photometric nights, fraction of cloud cover and satellite retrieved cover fraction over Paranal

9.26 Cloud Cover Anomaly from photometric and satellite data in comparison with SOI over La Silla

9.27 Cloud Cover Anomaly from photometric and satellite data in comparison with SOI over Paranal

9.28 Ocean-Land ratio of monthly Cloud Cover percentage at Tolonchar and La Silla latitudes.

9.29 Seasonal Ocean-Land ratio of Cloud Cover percentage at the Tolonchar and at La Silla latitudes.

9.30 Tolonchar-La Silla ratio of the Ocean-Land change in monthly cloud cover percentage

9.31 Seasonal Tolonchar-La Silla ratio of the Ocean-Land change in cloud cover percentage.

Table List

1.1 Records of Northern Hemisphere temperature. IPCC-WG1 2007

3.1 Temperature indexing from qualitative descriptions of Documentary Proxy
3.2 Documentary proxy classification in terms of Standard Deviation
3.3 Instrumental Series produced within Millennium European project

4.1 Five late calibration of the Little Florentine Thermometer (LFT)
4.2 Stations active in the Medici Network
4.3 Gaps filled in the Florence and Vallombrosa series

5.1 Estimated error for each sub-period of the early Padua series

6.1 Straight line slope referred to wavelength

7.1 Optical depth values due to Rayleigh scattering at different wavelengths

8.1 Overview of instruments on board satellites

9.1 La Silla and Paranal yearly average fraction of photometric nights

Acronymous List

AMSL: Above Mean Sea Level
ABV: Alcohol by Volume
AD: Annus Domini
ADEOS: Advanced Earth Observing Satellite
AE: Atmospheric Extinction
AEMET: Agencia Estatal de Meteorologıa
AEROCE: Atmosphere/Ocean Chemistry Experiment
AERONET: Aerosol Robotic NETwork
AI: Aerosol Index
ALMA: Atacama Large Millimeter Array
AO: Adaptive Optics
AOD: Aerosol Optical Depth
AOT: Aerosol Optical Thickness
AQUA: Earth Observing System Post Meridian (PM)
ATLID: ATmospheric LIDAR
AURA: Earth Observing System Chemistry mission
AVHRR: Advanced Very High Resolution Radiometer
BL: Boundary Layer
BUV: Backscattered UV
CALIPSO: Cloud-Aerosol Lidar and Infrared Pathfinder Satellite
CAMC: Carlsberg Automatic Meridian Circle Telescope
CCA: Cloud Cover Anomaly
CCD: Charge Coupled Device
CCN: Cloud Condensation Nuclei
CE: Central England
CNR: National Research Council
CSIC: Consejo Superior de Investigaciones Cient´ıficas
CU: Cutigliano
CV: Cumulative Value
DB: Data Bank
DIMM: Differential Image Motion Monitor
DISC: Data and Information Services Center
DJF: December-January-February
DP: Documentary Proxy
ELT: Extremely Large Telescopes
ENE: East Northeast
ENSO: El Nino Southern Oscillation
ENVISAT: ENVironmental SATellite
EOS: Earth Observing System
EP: Earth Probe
ERS: European Remote Sensing Satellite
ESA: European Space Agency
ESO: European Southern Observatory
ET: Equation of Time
EU: EUropean
FL: Florence
FOV: Field of View
FR: France
FTP: File Transfer Protocol
FWHM: Full Width at Half Maximum
GES: Goddard Earth Sciences
GIOVANNI: GES-DISC Interactive Online Visualization ANd aNalysis Infrastructure
GMT: Greenwich Mean Time

GOME: Global Ozone Monitoring Experiment
GR: Greece
GSFC: Goddard Space Flight Center
GW: Global Warming
HDF: Hierarchical Data Format
HIRDLS: High Resolution Dynamics Limb Sounder
IAC: Instituto de Astrofisica de Canarias
ICoD/DREAM: Dust loading model forecast from Insular Coastal Dynamics
IFOV: Instantaneous Field of View
IMSS: Institute and Museum of the History of Science
INM: Instituto Nacional de Meteorologıa
INTA: Instituto Nacional de Tecnica Aerospacial
IO: Instrumental Observations
IPCC: Intergovernmental Panel on Climate Change
IR: Infrared
ISAC: Institute of Atmospheric Sciences and Climate
IT: Italy
IYA: International Year of Astronomy
JJA: June-July-August
L2: Level 2 data
L3: Level 3 data
LFT: Little Florentine Thermometer
LIA: Little Ice Age
KV: atmospheric extinction coefficient in V-band
LIDAR: Light Detection And Ranging
MAM: March-April-May
MASS: Multi-Aperture Scintillation Sensor
MFRSR: MultiFilter Rotating Shadowband Radiometer
MIR: Middle IR
MLS: Microwave Limb Sounder
MML: Maritime Mixing Layer
MODIS: Moderate-Resolution Imaging Spectroradiometer
MSG: Meteosat Second Generation
MSL: Mean Sea Level
MWP:Medieval Warm Period
N7: Nimbus-7
NAAPS: Navy Aerosol Analysis and Prediction System
NAO: North Atlantic Oscillation
NASA: National Aeronautics and Space Administration
NH: Northern Hemisphere
NIR: Near-infrared
NNE: North Northeast
NNW: North Northwest
NOAA: National Oceanic and Atmospheric Administration
OAI: Izana Atmospheric Observatory
OMI: Ozone Monitoring Instrument
OMIAERUV: Ozone Monitoring Instrument Aerosol Ultra Violet
OMTO3: OMI Total column Ozone
ORM: Roque de Los Muchachos Observatory
OT: Teide Observatory
PM: Particulate Matter
PSF: Point Spread Function
PT: Portugal
PWV: Precipitable Water Vapour
RA: Running Average
SCIAMACHY: Scanning Imaging Absorption SpectroMeter Atmospheric Chartography
SCIDAR: SCIntillation Detection and Raging
SD: Standard Deviation

SE: Standard Error
SEVIRI: Spinning Enhanced Visible and InfraRed Imager
SLODAR: SLOpe Detection and Raging
SNHTss: Standard Normal homogeneity Test of single shift
SODAR: Sonic Detection And Ranging
SOI: Southern Oscillation Index
SON: Septemper-October-November
SP: Spain
SSA: Single Scattering Albedo
SSS: Single-Star SCIDAR
STAR: Satellite Application and Research
TE: Transfer Equation
TERRA: Earth Observing System Anti Meridian (AM)
TES: Tropospheric Emission Spectrometer
TIROS: Television IR Observation Satellite
TL: Troposphere Layer
TOA: Top of Atmosphere
TOMS: Total Ozone Mapping Spectrometer
TOVS: TIROS Operational Vertical Sounder
UV: Ultraviolet
VA: Vallombrosa
VIS: Visible
VLT: Very Large Telescope
VOC: Volatile Organic Compound
WMO: World Meteorological Organisation
WG: Working Group
WNW: West Northwest

Acknowledgments

I thank heartily Prof. Dario Camuffo and Prof. Sergio Ortolani for their kindness and availability during these years and for their important advices and helps. Thanks go to Prof. Valentina Zitelli for the time devote to me.

Thanks to my own family and my family in law for the support that give me day by day.

Thanks to the kind cooperation of Dr. Silvia Enzi, Prof. Adriana Bernardi and of the dears collegues Dr. Antonio della Valle and Dr. Francesca Becherini.

My PhD grant was supported by the EU, project Millennium (Contract 017008-2) carried out at the Institute of Atmospheric Sciences and Climate (ISAC) of the National Research Council (CNR) in Padua, Italy. Previous EU contracts mentioned in the text are ADVICE (ENV4-CT95-0129) and IMPROVE (ENV4-CT97-0511). This thesis has been possible thanks to the exquisite cooperation of colleagues and Institutions who have facilitated the research of data and metadata, or have kindly supplied data. The following instrumental data are due to the courtesy of: Florence (1889-2007): Prof. GP. Maracchi and Dr. A. Crisci, CNR-IBIMET, Florence; Vallombrosa (1872-2007): Dr. M. Sulli, Istituto Sperimentale per la Selvicoltura, Florence; Locorotondo (1884-2007): Prof. L. Ruggiero, University of Lecce; Palermo (1791-2007): Prof G. Micela, Prof. V. Iuliano and Dr. D. Randazzo, Astronomical Observatory "G.S.Vaiana", Palermo; Erice (1565-1915): Dr. M. Colacino, CNR-ISAC, Rome; Bologna series (1813-2007): Dr. T. Nanni, Dr. M. Brunetti, CNR-ISAC, Bologna. For the archival research, data recovery and any other kind of help, special thanks are due to: Historical Archive of the Astronomical Observatory (INAF), Padua: Dr V. Zanini and Dr L. Pigatto; University Library, Padova: Dr L. Prosdocimi; Library of the Astronomy Department, Bologna University: Dr R. Stasi; National Central Library, Florence (BNCF): Dr. P. Pirolo and Dr S. Pelle; Institute and Museum of History of Science (IMSS), Florence: Prof. P. Galluzzi, Dr. A. Lenzi, Dr. G. Strano, Dr. A. Saviori; Library of the Vallombrosa Abbey: Father P.D. Spotorno; Ximenian Observatory, Florence: Prof. E. Borchi; Italian Corps of Foresters (GFS), Office for the Biodiversity, Vallombrosa: Mrs L. Persia; Naples: Capodimonte Astronomical Observatory (INAF). Most of Portuguese data

collection in the archives and the analysis referring to 18th century has been carried out by João Paulo Taborda (University of Évora). Thanks are due to João Carlos-Garcia and Sandra Oliveira (University of Lisbon). Finally, for useful suggestions and discussions Dr. D. Wheeler, University of Sunderland, Dr V. Cantù and Dr D. Vergari. Dr. P. Pirolo and Dr. S. Pelle, National Central Library (BNCF), Florence; Prof. P. Galluzzi, Dr. A. Lenzi, Dr. G. Strano, Dr. A. Saviori, Institute and Museum of History of Science (IMSS), Florence; Father U. Fossa, Library of Camaldoli Abbey; Mrs L. Persia, Italian Corps of Foresters (GFS), Office for the Biodiversity, Vallombrosa; Father Prof. E. Borchi, Ximenian Observatory, Florence and Dr. D. Vergari, University of Florence. Thanks to the valuable contribution of Drs F. Zardini, C. Cocheo, G. Sturaro and R. Gambicchia.

The IPCC 2007 Northern Hemisphere data used in this thesis are available for downloading at www.cru.uea.ac.uk/cru/data/temperature/#datdow. Our deepest thanks to the TOMS, OMI and MODIS groups from NASA GSFC for AI and AOD measurements, and to the Carlsberg Meridian Circle of the Isaac Newton Group on La Palma for the coefficient-extinction data. Our acknowledgments go to the main directorate of Quality and Environmental Evaluation of the Environment Ministry, the Superior CSIC and the INM of the Environment Ministry for the information on the atmospheric pollution produced by airborne aerosols in Spain. This study is part of the site characterization work developed by the Sky Quality Group of the IAC and has been carried out within the framework of the European Project OPTICON and under Proposal FP6 for Site Selection for the European ELT. Thanks to the always exquisite cooperation go in particular to Antonia Varela and Casiana Muñoz-Tuñón.

Many thanks at last but not least goes to the NASA helpdesk for their careful and quick help. Data used in this thesis were produced with the Giovanni online data system, developed and maintained by the NASA GES DISC.

Bibliography

Alcoforado, M.J., Nunes, M.F. and J.C. Garcia. 2000. Temperature and precipitation reconstruction in Southern Portugal during the late Maunder Minimum (AD 1675-1715). The Holocene 10 (3) : 333-340.

Alexanderson, H. and A. Moberg. 1997. Homogenization of Swedish temperature data. Part 1: homogeneity test for linear trends. International Journal of Climatology 17 : 25–34.

Alexandre, P. 1987. Le climat en Europe au Moyen Age. Contribution à l'histoire des variations climatiques de 1000 à 1425, d'après les sources narratives de l'Europe occidentale. Ecole des Hautes Etudes en Sciences Sociales, Paris

Amontons, G. 1695. Remarques et experiences physiques sur la construction d'une nouvelle clepsydre, sur les baromètres et hygromètres, Jombert, Paris.

Amontons, G. 1699. Moyen de substituer commodément l'action du Feu à la force des Hommes et des Cheveaux pour mouvoir des Machines. Mémoires de l'Académie Royale des Sciences, Paris, pp.112-126.

Amontons, G. 1702. Discours sur quelques propriétés de l'air, et le moyen d'en connaître la température dans tous les climats de la Terre. Mémoires de l'Académie Royale des Sciences, Paris, pp. 155–174.

Antinori, V. 1841. Notizie istoriche relative all'Accademia del Cimento. Tipografia Galileiana, Florence.

Antinori, V. 1858. Archivio Meteorologico Centrale Italiano, Società Tipografica sulle Logge del Grano, Florence.

Ardeberg, A., Lindgren, H. and I. Lundström. 1990. La Silla and Paranal: a comparison of photometric qualities. Astron. Astrophys. 230 : 518-526.

Baiada, E. 1986. Da Beccari a Ranuzzi: la meteorologia nell'Accademia Bolognese nel XVIII secolo. In: R. Finzi (ed.) Le meteore ed il frumento: Clima, agricoltura, meteorologia a Bologna nel '700. Bologna: Il Mulino, pp.99-261

Barriendos, M. 1997. Climatic variations in the Iberian Peninsula during the late Maunder Minimum (AD 1675-1715): an analysis of data from rogation ceremonies. The Holocene 7(1) : 105-111.

Barriendos, M. 2005. Climate and Culture in Spain. Religious Responses to extreme Climatic Events in the Hispanic Kingdoms (16th-19th). In: Behringer W, Lehmann H, Pfister C (ed.) Kulturelle Konsequenzen der "Kleinen Eiszeit". Göttingen, Vandenhoeck and Ruprecht.

Barriendos, M. and M.C. Llasat. 2003. The Case of the `Maldá' Anomaly in the Western Mediterranean Basin (AD 1760–1800): An Example of a Strong Climatic Variability. Climatic Change 61 : 191-216.

Barriendos, M., Martín-Vide, J., Peña, J.C. and R. Rodríguez. 2002. Daily Meteorological Observations in Cádiz - San Fernando. Analysis of the Documentary Sources and the Instrumental Data Content (1786-1996). Climatic Change 53 : 151-170.

Bartolo, S. 1679. Thermologia Aragonia, Naples.

Bergström, H. and A. Moberg. 2002. Daily Air Temperature and Pressure Series for Uppsala (1722–1998). Clim. Change 53(1-3).

Bertolin, C. 2005. Utilizzo dei dati di Earth Probe per lo studio dell'estinzione atmosferica dovuta ad aerosol. Astronomy Degree Thesis, University of Padua, 185 p.

Boffito, G. 1926. I Benedettini di Vallombrosa nella storia della Meteorologia. Meteorologia Pratica 6 : 243-246.

Borchi, E. and R. Macii. 2009. Meteorologia a Firenze. Nascita ed evoluzione. Pagnini Ed., Firenze.

Boyle, R. 1662. New Experiments Physico-Mechanical, Touching the Spring of the Air and its Effects. Second Edition. H. Hall, Oxford.

Bradley, R.S. 1999. Climatic variability in sixteenth-century Europe and its social dimension - Preface. Clim. Change 43(1) : 1–2.

Braganza, K., Karoly, D. J., Hirst, A. C., Mann, M. E., Stott, P. A., Stouffer, R. J.and S. F. B. Tett. 2003. Simple indices of global climate variability and change: Part I, variability and correlation structure. Clim. Dyn. 20 : 491– 502.

Brázdil, R. 2002. Patterns of climate in Central Europe since Viking times. In: Wefer G., Berger, W.H., Behre, K.E. and E. Jansen (eds.), Climate Development and History in the North Atlantic Realm,

Springer-Verlag, Berlin, Heidelberg, New York, Barcelona, Hong Kong, London, Milan, Paris, Tokyo, 355-368.

Brázdil, R., Pfister, C.,Wanner, H., Von Storch, H. and J. Luterbacher. 2005. Historical Climatology In Europe – The State-of-the-art. Climatic Change 70 : 363–430.

Briffa, K.R. et al. 2001. Low-frequency temperature variations from a northern tree ring density network. J. Geophys. Res. 106(D3) : 2929– 2941.

Brunetti, M., Buffoni, L., Lo Vecchio, G., Maugeri, M. and T. Nanni. 2001. Tre secoli di Meteorologia a Bologna. ISAO-CNR, Bologna; Istituto di Fisica Generale Applicata-Università di Milano; Osservatorio Astronomico di Milano-Brera. CUSL, Milan

Camuffo, D. 1984. Analysis of the Series of Precipitation at Padova, Italy. Climatic Change 6 : 57-77.

Camuffo, D. 2002a. History of the long series of the air temperature in Padova (1725-today). Climatic Change 53 (1-3) : 7-76.

Camuffo, D. 2002b. Calibration and instrumental errors in early measurements of air temperature. Climatic Change 53 (1-3) : 297-330.

Camuffo, D. 2002c. Errors in early temperature series arising from changes in style of measuring time, sampling schedule and number of observations. Climatic Change 53 (1-3) : 331-354.

Camuffo, D. and C. Bertolin. 2010a.Recovery of the Early Period of Long Instrumental Time Series of Air Temperature in Padua, Italy (1716-2007). Physics and Chemistry of the Earth (in print)

Camuffo, D. and C. Bertolin. 2010b. The dawn of Meteorology in Italy and the earliest Meteorological Observations (1654-1670). The Holocene (Submitted).

Camuffo, D. and S. Enzi. 1992a. Critical Analysis of Archive Sources for Historical Climatology of Northern Italy. In: Frenzel B (ed.) European Climate Reconstructed from Historical Documents: Methods and Results. Paleoclimate Research, Special Issue 7, Fischer Verlag, Stuttgart.

Camuffo, D. and S. Enzi. 1992b. Reconstructing the Climate of Northern Italy from Archive Sources. In: Bradley R.S., Jones P.D. (eds.) Climate since 1500 A.D.. Routledge, London.

Camuffo, D. and S. Enzi. 1994. The Climate of Italy from 1675 to 1715. In: Frenzel B (ed.): Climatic Trends and Anomalies in Europe 1675-1715. Paleoclimate Research, Special Issue 8, Fischer Verlag, Stuttgart.

Camuffo D, and P. Jones (eds). 2002. Improved Understanding of Past Climatic Variability from Early Daily European Instrumental Sources. Kluwer Academic Publishers, Dordrecht, Boston, London.

Camuffo, D. and G. Sturaro. 2004. Use of proxy-documentary and instrumental data to assess the risk factors leading to sea flooding in Venice. Global and Planetary Change 40 : 93-103.

Camuffo, D., Cocheo, C. and S. Enzi. (2000b) Seasonality of instability phenomena (hailstorms and thunderstorms) in Padova, Northern Italy, from archive and instrumental sources from AD 1300 to 1989. The Holocene 10 (5) : 651-658.

Camuffo, D., Cocheo, C. and G. Sturaro. 2006. 'Corrections of systematic errors, data homogenisation and climatic analysis of the Padova pressure series (1725–1999)', Climatic Change, 79 : 493–514.

Camuffo, D., Bertolin, C., Jones, P., Cornes, R. and E. Garnier. 2009. The earliest daily barometric pressure readings in Italy: Pisa, 1657-8 and Modena, 1694 and the circulation index over Europe, 1694. The Holocene 20 (3) : 1-13, doi: 10.1177/0959683609351900 http://hol.sagepub.com

Camuffo, D., Bertolin, C., Barriendos, M., Dominguez, F., Cocheo, C., Enzi, S., Sghedoni, M., della Valle, A., Garnier, E., Alcoforado, M.J., Xoplaki, E., Luterbacher, J., Diodato, N., Maugeri, M., Nunes, M. F. and R. Rodriguez. 2010. 500 year temperature reconstruction in the Mediterranean Basin. Climatic Change (Accepted).

Cantù, V. 1985. Alla ricerca di documenti sul clima del passato. Accademie e Biblioteche d'Italia 53 (36 n.s./2) : 103-110.

Castelli, B. 1638. Letter to Monsignor Ferdinand Cesarini, dated 20 September 1638. In Bucciantini, M. (ed.), Carteggio di Benedetto Castelli, Archivio della corrispondenza degli scienziati italiani, Olschki, Florence (1988), 313 p.

Cavendish, H., Heberden, A-A., Deluc, M. and P. Horsley. 1777a. The report of the Committee of the Royal Society to consider of the Best Method of Adjusting the Fixed Points of Thermometers; and the Precautions Necessary to be Used in Making Experiments with these Instruments. Philosophical Transactions 67 : 816–857.

Chinnici, I., Foderà Serio, G. and L. Granata. 2000. Duecento anni di meteorologia all'Osservatorio Astronomico di Palermo. Osservatorio Astronomico G.S. Vaiana, Palermo

Chuine, I., Yiou, P., Viovy, N., Seguin, B., Daux, V. and E. Le Roy Ladurine. 2004. Grape ripening as a past climate indicator. Nature 432 : 289-290.

Cocheo, C. and D. Camuffo. 2002. Corrections of systematic errors and data homogenisation in the Padova series (1725 – today). Climatic Change 53(1-3) : 77-100.

Conrad, V. and L.W.Pollack. 1950. Methods in Climatology. Harvard University Press.

Cook, E.R., Esper, J. and R.D. D'Arrigo. 2004. Extra-tropical Northern Hemisphere land temperature variability over the past 1000 years. Quat. Sci. Rev. 23 (20–22) : 2063–2074.

Cotte, L. 1774. Traité de Météorologie: contenant 1. l'histoire des observations météorologiques, 2. un traité des météores, 3. l'histoire & la description du baromètre, du thermomètre & des autres instruments météorologiques, 4. les tables des observations météorologiques & botanicométéorologiques, 5. les résultats des tables & des observations, 6. la méthode pour faire les observations météorologiques, Imprimérie Royale, Paris, p. 635.

Crisci, A., Zozzini, B., Maracchi, G. and F. Meneguzzo. 1998. La serie storica delle temperature medie mensili di Firenze. Proceeding: "Due secoli di osservazioni meteorologiche a Mantova, aspetti scientifici e storici", Mantova 22 ottobre 1998, 143-158.

Crivelli, G. 1744. Elementi di Fisica, Simone Occhi, Venice.

Crowley, T.J. and T.S. Lowery. 2000. How warm was the medieval warm period? Ambio 29(1) : 51–54.

Cyrillus, N. 1731-1732. An Account of an Extraordinary Eruption of Mount Vesuvius in the Month of March, in the Year 1730, Extracted from the Meteorological Diary of That Year at Naples, Communicated by Nichol. Cyrillus, M. D. R. S. S. Philosophical Transactions 37 : 336-338.

D'Arrigo, R., Wilson, R. and G. Jacoby. 2006. On the long-term context for late twentieth century warming. J. Geophys. Res. 111 (D3), doi:10.1029/ 2005JD006352.

Delisle, J. N. 1734. Unpublished letter presented to the Académie Royale, Paris, and read by Mr Godin the 3rd and 10th February, as mentioned in the Registers of the Academy.

Della Porta, G.B. 1584: Magiae Naturalis Libri XX. Horatium Salvianum, Neaples.

Delworth, T.L. and M.E. Mann. 2000. Observed and simulated multidecadal variability in the Northern Hemisphere. Clim. Dyn. 16(9) : 661–676.

Dominguez-Castro, F., Santisteban, J.I., Barriendos, M. and R. Mediavilla. 2008. Seasonal reconstruction of drought episodes for central Spain from rogation ceremonies recorded at Toledo Cathedral from 1506 to 1900: a methodological approach. Global and Planetary Changes 63 : 230-242.

Enzi, S. and D. Camuffo. 1995. Documentary sources of the sea surges in Venice from A.D. 787 to A.D. 1867. Natural Hazards 12: 225-287.

Esper, J., Cook, E.R. and F.H. Schweingruber. 2002. Low-frequency signals in long tree-ring chronologies for reconstructing past temperature variability. Science 295 (5563) : 2250–2253.

Fahrenheit, D. G. 1724. Experimenta et observationes de congelatione acquae in vacuo factae. Philosophical Transactions 33 : 78–84.

Falvey, M. and R. D. Garreaud. 2009. Regional cooling in a warming world: Recent temperature trends in the southeast Pacific and along the west coast of subtropical South America (1979–2006). J. Geophys. Res., 114, D04102, doi:10.1029/2008JD010519.

Font-Tullot, I. 1956. The weather in the Canary Island (in Spanish). Madrid, Servicio Nacional de Meteorologia, Publ. Ser. A 26.

Frank, D., Büntgen, U., Böhm, R., Maugeri, M. and J. Esper. 2007. Warmer early instrumental measurements versus colder reconstructed temperatures: shooting at a moving target, Quaternary Science Reviews 26 : 3298-3310.

Frisinger, H. H. 1983. The History of Meteorology: to 1800, American Meteorological Society, Boston, p. 147.

Gallego, D., Garcia-Herrera, R., Calvo, N. and P. Ribera. 2007. A new meteorological record for Cádiz (Spain) 1806-1852: Implications for climatic reconstructions. Journal of Geophysical Research 112 (D12108).

Gandolfo, C. and M. Sulli. 1970. Vallombrosa 1872-1989: serie ultracentenaria di misure di precipitazioni e di temperatura in ambiente forestale. Annali Istituto Sperimentale Selvicoltura, Florence 21 : 147-181.

Garcıa-Lorenzo, B., Fuensalida, J. J., Munoz-Tunon, C. and E. Mendizabal. 2005. Astronomical site ranking based on tropospheric wind statistics. MNRAS 356 : 849-858.

Garnier, E. 2007. La ville face aux caprices du fleuve XVIe-XVIIIe siècle. Histoire Urbaine 18 : 41-60.

Giorgi, A.1592. Spiritali di Herone Alessandrino ridotti in lingua volgare da Alkessandro Giorgi da Urbino. Ragusi, Urbino.

Guerrero et al. 1998. Extinction over the Canarian Observatories: the limited influence of the Saharan dust. New Astronomy Reviews 42 : 529.

Hegerl, G.C., Crowley, T.J., Hyde, W.T. and D.J. Frame. 2006. Climate sensitivity constrained by temperature reconstructions over the past seven centuries. Nature 440 : 1029–1032.

Hellmann, G. 1908. The Dawn of Meteorology. Quarterly Journal Royal Meteorological Society 34 (148) : 227-232.

Hemmer, J.J. 1783. Descriptio instrumentorum meteorologicorum, tam eorum, quam Societas distribuit, quam quibus praeter haec Manheimii utitur. Ephemerides Societatis Meteorologicae Palatinae, Tomus 1 : 57-90.

Herman, J.R., Bhartia, P.K., Torres, O., Hsu, C., Seftor, C. and E. Celarier. 1997. Global distribution of UV-absorbing aerosols from Nimbus 7/TOMS data. Geophys. Res. 102 (D14) : 16911-16922.

Hsu, C., Herman, J.R., Bhartia, P.K., Seftor, C., Thompson, A.M., Gleason, J.F., Eck, T.F. and B.N. Holben. 1996. Geophys. Res. Lett. 23 (7) : 745-748.

Huang, S.P., Pollack, H.N. and P.Y. Shen. 2000. Temperature trends over the past five centuries reconstructed from borehole temperatures. Nature 403 (6771) : 756–758.

Jimenez, A., Gonzalez Jorge, H. and M.C. Rabello-Soares.1998. Diurnal Atmospheric Extinction over Teide Observatory (Tenerife, Canary Islands). Astronomy and Astrophysics Suppl. Ser. 129 : 413-423.

Jones, P.D. and M. E. Mann. 2004. Climate over past millennia. Rev Geophys 42 (2), RG2002, doi:10.1029/2003RG000143.

Jones, P.D. and A. Moberg. 2003. Hemispheric and large-scale surface air temperature variations: an extensive revision and an update to 2001. Journal of Climate 16 : 206–223.

Jones, P.D., Briffa, K.R., and T.J. Osborn. 2003. Changes in the Northern Hemisphere annual cycle: Implications for paleoclimatology. J. Geophys. Res. 108 (D18) : 4588, doi:10.1029/2003JD003695.

Jones, P.D., Osborn, T.J. and K.R. Briffa. 1997. Estimating sampling errors in large-scale temperature averages. J. Clim. 10 (10) : 2548–2568.

Jones, P.D., Osborn, T.J. and K.R. Briffa. 2001. The evolution of climate over the last millennium. Science 292 (5517) : 662–667.

Jones, P.D., Briffa, K.R., Barnett, T.P. and S.F.B. Tett. 1998. High resolution palaeoclimatic records for the last millennium: interpretation, integration and comparison with General Circulation Model control-run temperatures. The Holocene 8 (4) : 455–471.

Jurin, J. 1723. Invitatio ad observationes Meteorologicas communi consilio instituendas a Jacobo Jurin M.D. Soc. Reg. Secr. et Colleg. Med. Lond. Socio. Philosophical Transactions 379 : 422-427.

King, D.L. 1985. Atmospheric Extinction at the Roque de los Muchachos Observatory, La Palma, RGO/La Palma technical note, no. 31.

Koelemeijer,R.B.A., de Haan, J.F. and P. Stammes. 2003. A database of spectral surface refelectivity in the range 335-772 nm derived from 5.5 years of GOME observations. Journal of Geophysical Research 108 (D2), D24070, doi: 10.1029/2003GL018931.

Kolmogorov, A.N. 1941. Mathematics and its applications in Tikhomirov, V.M. ed., Selected works of A.N. Kolmogorov (Soviet series), Klewer Academic press (1991).

Legrand, J.P. and M. Le Goff. 1992. Les observations météorologiques de Louis Morin. Monographie n°6, Météorologie Nationale, Paris

Leijonhufvud, L., Wilson, R., Moberg, A., Söderberg, J., Retsö, D. and U. Söderlind. 2009. Five centuries of Stockholm winter/spring temperatures reconstructed from documentary evidence and instrumental observations. Climatic Change. doi: 10.1007/s10584-009-9650-y.

.Le Treut, H., Somerville, R., Cubasch, U., Ding, Y., Mauritzen, C., Mokssit, A., Peterson, T. and M. Prather. 2007. Historical Overview of Climate Change. In: Climate Change 2007: The Physical Science Basis. Contribution of Working Group I to the Fourth Assessment Report of the Intergovernmental Panel on Climate Change [Solomon, S., Qin, D., Manning, M., Chen, Z., Marquis, M., Averyt, K.B., Tignor, M. and H.L. Miller (eds.)]. Cambridge University Press, Cambridge, United Kingdom and New York, NY, USA.

Libri, G. 1830. Mémoire sur la determination de l'échelle du thermometer de l'Académie del Cimento. Annales de Chemie et de Physique 45 (2) : 354-361.

Luterbacher, J., Dietrich, D., Xoplaky, E., Grosjean, M. and H. Wanner. 2004. European seasonal and annual temperature variability, trends, and extremes since 1500. Science 303 : 1499-1503.

Magalotti, L. 1667. Saggi di naturali esperienze fatte nell'Accademia del Cimento. Nuova stamperia di Gio. Filippo Cecchi, Florence.

Maheras, P., Alcoforado, M.J. and S. Guika. 1994. Les saisons, les années et les périodes sèches et humides au Portugal durant la dernière période séculaire. Publications de l'Association Internationale de Climatologie 6 : 191-199.

Maheras, P., Alcoforado, M.J., Guika, S. and M. Vafiadis. 1995. Relations entre les périodes sèches et humides et les indices de circulation au Portugal, durant le dernière période séculaire. Publications de l'Association Internationale de Climatologie 7 : 241-248.

Manley, G. 1974. Central England Temperatures: monthly means 1659 to 1973. Quarterly Journal Royal Meteorological Society 100 : 389-405.

Mann, M.E. and P.D. Jones. 2003. Global surface temperatures over the past two millennia. Geophys. Res. Lett. 30 (15) : 1820, doi:10.1029/ 2003GL017814.

Mann, M.E., Bradley, R.S. and M.K. Hughes. 1998. Global-scale temperature patterns and climate forcing over the past six centuries. Nature 392 (6678) : 779–787.

Mann, M.E., Bradley, R.S. and M.K. Hughes. 1999. Northern hemisphere temperatures during the past millennium: Inferences, uncertainties, and limitations. Geophys. Res. Lett. 26 (6) : 759–762.

Mann, M.E., Rutherford, S., Bradley, R.S., Hughes, M.K., and F.T. Keimig. 2003. Optimal Surface Temperature Reconstructions Using Terrestrial Borehole Data, Journal of Geophysical Research, 108 (D7), doi:10.1029/2002JD002532.

Mann, M.E., Rutherford, S., Wahl, E. and C.M. Ammann, 2005b: Testing the fi delity of methods used in 'proxy-based' reconstructions of past climate. J. Clim. 18 (20) : 4097–4107.

Maracchi, G.P. 1991. A brief history of meteorology in Florence from the beginnings to the present. CIESIA-IATA, Florence

Marsenne, M. 1647. Nuove Osservazioni, Vol.III, 216, Parigi.

Martín-Vide, J. and M. Barriendos. 1995. The use of rogation ceremony records in climatic reconstruction: a case study from Catalonia (Spain). Climatic Change 30 (2) : 201-221.

Maugeri, M., Buffoni, L., Delmonte, B. and A. Fassina. 2002. Daily Milan Temperature and Pressure Series (1763–1998): Completing and Homogenising the Data. Climatic Change 53 : 119-149.

Micela, G., Granata, L. and V. Iuliano. 2001. Due secoli di Pioggia a Palermo. Osservatorio Astronomico di Palermo. G.S. Vaiana and University of Palermo, Palermo

Middleton, K.W.E. 1966. A history of the Thermometer and its use in Meteorology. Hopkins, Baltimore.

Moberg, A., Sonechkin, D.M., Holmgren, K., Datsenko, N.M. and W. Karlén. 2005: Highly variable Northern Hemisphere temperatures reconstructed from low and high-resolution proxy data. Nature 433 : 613-617, doi:10.1038/nature03265.

Murdin, P. 1986. Geology and meteorology of Saharan dust. RGO/La Palma technical note, 41.

Newton, I. (published anonymous). 1701. Scala graduum caloris. Philosophical Transactions 22 : 824–829.

Oerlemans, J. 2005. Extracting a climate signal from 169 glacier records. Science 308 (5722) : 675–677.

Owen, T. W., Gallo, K. P., Elvidge, C. D. and K. E. Baugh. 1998. Using DMSPOLS light frequency data to categorize urban environments associated with U.S. climate observing stations. Intl. J. Remote Sensing 19 **:** 3451–3456.

Parker, D. and B. Horton. 2005. Uncertainties in central England temperature 1878–2003 and some improvements to the maximum and minimum series. International Journal of Climatology 25 : 173–188.

Peterson, T.C. and R.S. Vose.1997. An overview of the Global Historical Climatology Network temperature data base. Bull. Amer. Meteor. Soc. 78 (12) : 2837-2849.

Peterson, T.C., Easterling, D.R., Karl, T.R. Groisman, P., Auer, I., Böhm, R., Plummer, N., Nicholis, N., Torok, S., Vincent, L., Tuomenvirta, H., Salinger, J., Førland, E.J., Hanseen-Bauer, I., Alexandersson, H., Jones, P. and D. Parker. 1998. Homogeneity adjustments of in situ atmospheric climate data : a review. Int. J. Climatol. 18 : 1493-1517.

Pfister, C., Luterbacher, J., Schwarz-Zanetti, G. and M. Wegmann. 1998. Winter air temperature variations in Western Europe during the early and high Middle Ages (AD 750–1300). Holocene 8 : 535–552.

Pfister, C., Brazdil, R., Glaser, R., Barriendos, M., Camuffo, D., Deutsch, M., Dobrovolny, P., Enzi, S., Guidoboni, E., Kotyza, O., Militzer, S., Racz, L. and F.S. Rodrigo. 1999. Documentary Evidence on Climate in the Sixteenth-Century Europe. Climatic Change 43 (1) : 55-110.

Piervitali, E. and M. Colacino. 2001. Evidence of drought in Western Sicily during the period 1565-1915 from Liturgical Offices. Climatic Change 49 : 225-238.

Poleni, G. 1709. Johannis Poleni Miscellanea hoc est: I Dissertatio de Barometris et Termometris; II Machinae Aritmeticae, eiusque Descriptio; III, De Sectionibus Conicis Parallelorum in Horologiis Solaribus Tractatus, Aloysium Pavinum, Venice.

Poleni, G. 1716–1725. Unpublished manuscripta, Mss. It., CL. IV, N.631, 5354, Marciana Library, Venice.

Poleni, G. 1740. Ioannis Poleni ad nobilissimum virum comitem Alexandrum de Pompeiis patricium veronensem Epistola, qua nonnullae observationes astronomicae et meteorologicae continentur. Commentaria Academiae Scientificae Petropolitanae Tom. VIII : 439-452.

Raspopov, O. M., Shumilov, O. I., Kasatkina, E. A., Turunen, E. and M. Lindholm. 2000. The Solar Cycle and Terrestrial Climate. Proc. 1st Solar & Space Weather Euroconference; Santa Cruz de Tenerife, Tenerife, Spain, 25-29 September 2000 (ESA SP-463).

Renaldini, C. 1681. Philosophia rationalis, naturalis atque moralis, Frambotti, Padua.

Rivosecchi, I. 1975. Osservazioni e strumenti di meteorologia. Vol. I, CNR IFA, DP 5, Rome.

Rodrigo, F.S. 2002. Changes in climate variability and seasonal rainfall extremes: a case study from San Fernando (Spain), 1821–2000. Theor Appl Climatol 72 : 193–207.

Rodrigo, F.S. and M. Barriendos. 2008. Reconstruction of seasonal and annual rainfall variability in the Iberian Peninsula (16th – 20th Centuries) from documentary data. Global and Planetary Changes 63 : 256-274.

Romero, P. M. and E. Cuevas. 2002. Proc. 3ra. Asamblea Hispano Portuguesa de Geodesia y Geofisica, Valencia

Rossow, W.B. and L.C. Garder. 1993. Cloud detection using satellite measurements of infrared and visible radiances for ISCCP. J. Climate 6 : 2341-2369.

Rutherford, S., Mann, M.E., Delworth, T.L. and R.J. Stouffer. 2003. Climate field reconstruction under stationary and nonstationary forcing. J. Clim. 16 (3) : 462–479.

Rutherford, S., Mann, M. E., Osborn, T. J., Bradley, R. S., Briffa, K. R., Hughes, M. K. and P. D. Jones. 2005. Proxy-based Northern Hemisphere surface temperature reconstructions: Sensitivity to method, predictor network, target season, and target domain. J. Clim. 18 : 2308– 2329.

Sagredo, G.F. 1612. Letter to Galileo, dated 30 June 1612. Manoscritti Galileiani, Carteggio Galileiano, Mss. Gal., P. VI, T. VIII, car. 18 - 20. Biblioteca Centrale Nazionale di Firenze, Florence.

Santorio, S. 1612. Commentaria in Artem Medicam, pars 3. Coll. 229, Giac. Antonio Somasco, Venice.

Sarazin, M. 1997. A cloudy night again? Blame El Nino! A study of the impact of El Nino on the cloud cover above ESO Observatories in Chile. ESO Messenger, November 10.

Sarazin, M. and T. Sadibekova. 2005: Site consideration for the next generation of optical arrays: mid-latitudes sites versus antartica. Bulletin de la Société Royale des sciences de Liège 74 : 5-6.

Schmidt, G.A., Shindell, D.T., Miller, R.L., Mann, M.E. and D. Rind. 2004. General circulation modelling of Holocene climate variability. Quaternary Sci. Rev. 23 : 2167-2181 , doi:10.1016/j.quascirev.2004.08.005.

Schouw, J.F. 1839. Tableau du climat de la vegetation de l'Italie. Résultat de deux voyages en ce pays dans les années 1817-1819 et 1829-1830. Vol.1. Tableau de la temperature et des pluies de l'Italie. Librairie Gyldendal, Imprimerie de Bianco Luno, Copenhagen.

Shindell, D.T., Schmidt, G.A., Mann, M.E. and G. Faluvegi, 2004: Dynamic winter climate response to large tropical volcanic eruptions since 1600. J. Geophys. Res. 109 (D05104), doi:10.1029/2003JD004151.

Shindell, D.T., Schmidt, G.A., Miller, R.L. and M.E. Mann. 2003. Volcanic and Solar Forcing of climate change during the preindustrial era. J.Climate 16 : 4094-4107.

Shindell, D.T., Schmidt, G.A., Mann, M.E., Rind, D. and A. Waple. 2001. Solar Forcing of regional climate change during the Mauder Minimum. Science 294 : 2149-2152.

Slonosky, V. 2002. Wet winters, dry summers? Three centuries of precipitation data from Paris. Geophys Res Lett 29 : 1895–1898

Taborda, J.P., Alcoforado, M.J. and J.C. Garcia. 2004. O Clima no Sul de Portugal no século XVIII. Reconstituição a partir de fontes descritivas e instrumentais. Geo-Ecologia, 2, Centro de Estudos Geográficos, Lisboa

Targioni Tozzetti, G. 1780. Notizie degli aggrandimenti delle Scienze Fisiche accaduti in Toscana nel corso di anni LX del secolo XVII. Tomo I. Bouchard, Florence.

Taton, R. 1961. Histoire générale des Sciences, Vol. II, Presses Universitaires de France, Paris, pp. 533–545.

Toaldo, G. 1770, 1781. Saggio Meteorologico della vera influenza degli Astri, delle Stagioni e mutazioni di Tempo, (1770: 1st edition, 1781: 2nd edition), Manfrè, Stamperia del Seminario, Padova.

Toaldo, G. 1775. 'Emendazione de' barometri e de' termometri', Giornale d'Agricoltura, Venice. Item, 1803, posth. in Completa raccolta di opuscoli, osservazioni e notizie diverse contenute nei giornali Astro Meteorologici dall'anno 1773 sino all'anno 1798 del fu Sig. Abate G. Toaldo coll'aggiunta di alcune altre sue produzioni meteorologiche e pubblicate e inedite, Tomo IV, Andreola, Venice, pp. 48–120.

Torres, C., Cuevas, E., and J. C. Guerra. 2003. Proc. 1er. Encuentro sobre Meteorologia y Atmosfera de Canarias, ISBN 84-8320-251-4, ed. Centro de Publicaciones, Secretaria Gral. Tecnica, Ministerio del Medio Ambiente, Puerto de la Cruz, Tenerife, p. 74.

Torres, O., Herman, J.R., Bhartia, P.K. and A. Sinyuk. 2002. Aerosol properties from EP-TOMS near UV Observations. Adv. Space Res. 29 (11).

Torres, O., Bhartia, P.K., Herman. J.R., Ahmad, Z. and J. Gleason. 1998. Derivation of aerosol properties from satellite measurements of backscattered ultraviolet radiation: Theoretical basis. Journal of geophysical research 103 (D14) : 17099 – 17110.

Varela, A. M., Bertolin, C., Muñoz-Tuñón, C., Ortolani, S. and J. J. Fuensalida. 2008. Astronomical site selection: on the use of satellite data for aerosol content monitoring. MNRAS 391 (2) : 507-520.

Vergari, D. 2006. Contributo alla storia della meteorologia a Firenze. Le osservazioni meteorologiche fiorentine fra il 1751 e il 1813. Annali di Storia di Firenze, 1 : 99-120.

Vittori, O. and A. Mestitz. 1981. Calibration of the Florentine Little Thermometer. Endeavour 5(3) : 113-118.

Viviani, V. 1717 (posthumous). Racconto istorico della vita di Galileo. Manuscripts in Biblioteca Centrale Nazionale di Firenze. Reprinted in A. Favaro (Ed.,), 1907, "Opere di Galileo" Vol. XIX pp. 597-632, Barbera, Florence.

Wei, A.M. 1990. Time series analysis. Addison-Wesley, Edwood City, CA.

Wheeler, D., Garcia-Herrera, R. and F. Koek. 2006. CLIWOC. Climatoloical database for the world's oceans 1750 to 1850. Results of a research project (European Comission, Brussels). Luxemburg. http://www.ucm.es/info/cliwoc/.